Oxidative Medicine and Cellular Longevity

How Oxidative Stress Impacts the Male Reproductive System and Its Diseases

Lead Guest Editor: Shoulong Deng
Guest Editors: Kun Yu, Yi Fang, and Keren Cheng

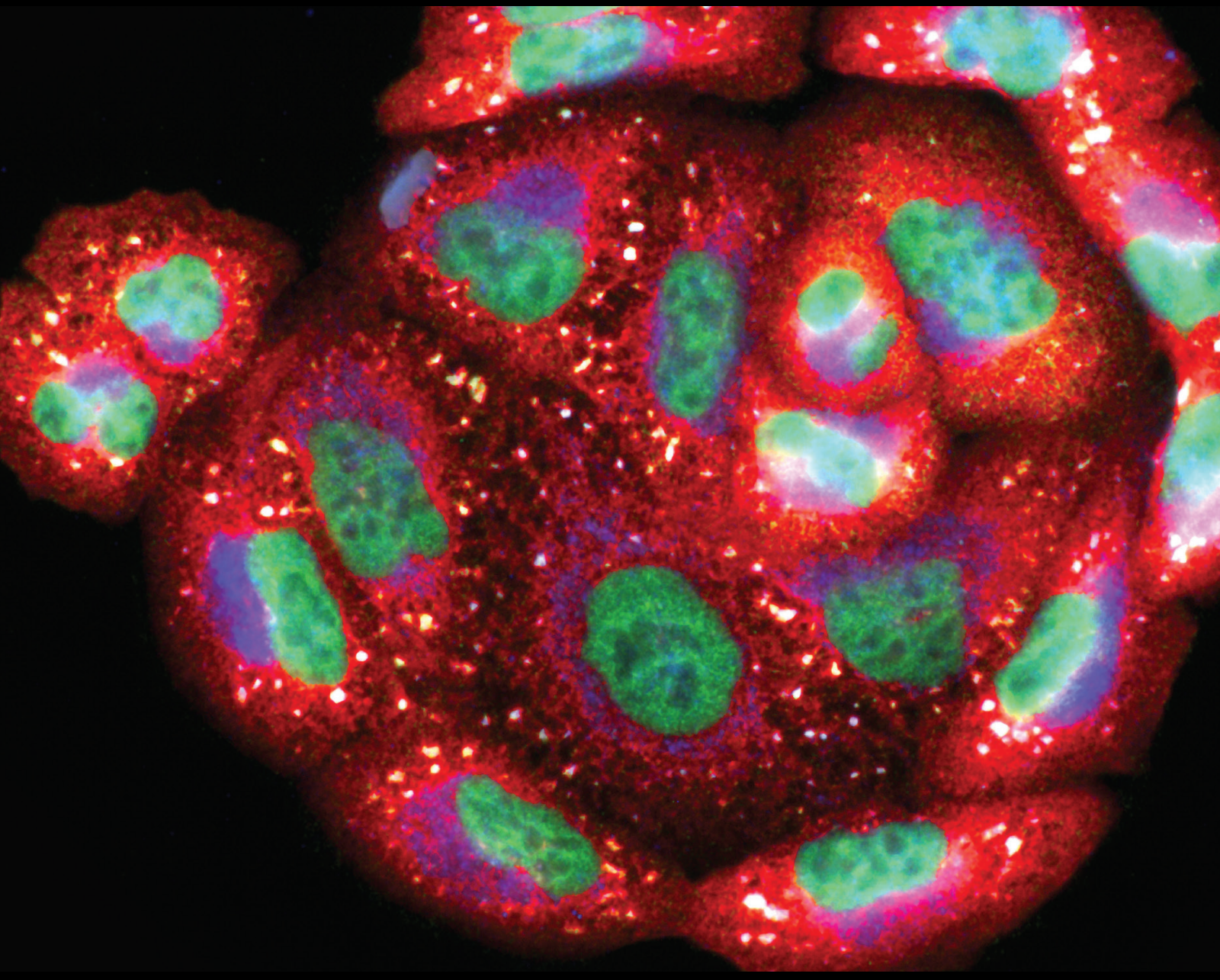

How Oxidative Stress Impacts the Male Reproductive System and Its Diseases

Oxidative Medicine and Cellular Longevity

How Oxidative Stress Impacts the Male Reproductive System and Its Diseases

Lead Guest Editor: Shoulong Deng
Guest Editors: Kun Yu, Yi Fang, and Keren Cheng

Contents

Hindawi
Oxidative Medicine and Cellular Longevity
Volume 2021, Article ID 5561395, 12 pages
https://doi.org/10.1155/2021/5561395

Research Article

Genetic Association in the Maintenance of the Mitochondrial Microenvironment and Sperm Capacity

Hwang I. S. Thomas,[1,2,3] **Ying-Shiuan Chen**,[4] **Ching-Han Hung**,[4,5] **Dilip Bhargava Sreerangaraja Urs**,[6] **Tien-Ling Liao**,[4] **Yen-Chun Lai**,[4] **Katerina Komrskova**,[7,8] **Pavla Postlerová**,[7,9] **Yung-Feng Lin**,[4,6] **and Shu-Huei Kao**[4,6,10]

[1]*Division of Urology, Department of Surgery, Shin Kong Wu Ho-Su Memorial Hospital, Taipei, Taiwan*
[2]*Department of Urology, College of Medicine, Taipei Medical University, Taipei, Taiwan*
[3]*Department of Urology, School of Medicine, Fu-Jen Catholic University, New Taipei, Taiwan*
[4]*School of Medical Laboratory Science and Biotechnology, College of Medical Science and Technology, Taipei Medical University, Taipei, Taiwan*
[5]*Department of Gynecology and Obstetrics, Taipei City Hospital Ren-Ai Branch, Taipei, Taiwan*
[6]*Ph.D. Program in Medical Biotechnology, College of Medical Science and Technology, Taipei Medical University, Taipei, Taiwan*
[7]*Laboratory of Reproductive Biology, Institute of Biotechnology of the Czech Academy of Sciences (BIOCEV), Vestec, Czech Republic*
[8]*Department of Zoology, Faculty of Science, Charles University, Prague, Czech Republic*
[9]*Department of Veterinary Sciences, Faculty of Agrobiology, Food and Natural Resources, University of Life Sciences Prague, Prague, Czech Republic*
[10]*Center for Reproductive Medicine and Sciences, Taipei Medical University Hospital, Taipei, Taiwan*

Correspondence should be addressed to Shu-Huei Kao; kaosh@tmu.edu.tw

Received 12 February 2021; Revised 3 July 2021; Accepted 8 July 2021; Published 6 September 2021

Academic Editor: Yi Fang

Sperm motility is one of the major determinants of male fertility. Since sperm need a great deal of energy to support their fast movement by active metabolism, they are thus extremely vulnerable to oxidative damage by the reactive oxygen species (ROS) and other free radicals generated as byproducts in the electron transport chain. The present study is aimed at understanding the impact of a mitochondrial oxidizing/reducing microenvironment in the etiopathology of male infertility. We detected the mitochondrial DNA (mtDNA) 4,977 bp deletion in human sperm. We examined the gene mutation of ATP synthase 6 (*ATPase6* m.T8993G) in ATP generation, the gene polymorphisms of uncoupling protein 2 (*UCP2*, G-866A) in the uncoupling of oxidative phosphorylation, the role of genes such as manganese superoxide dismutase (*MnSOD*, C47T) and catalase (*CAT*, C-262T) in the scavenging system in neutralizing reactive oxygen species, and the role of human 8-oxoguanine DNA glycosylase (*hOGG1*, C1245G) in 8-hydroxy-2′-deoxyguanosine (8-OHdG) repair. We found that the sperm with higher motility were found to have a higher mitochondrial membrane potential and mitochondrial bioenergetics. The genotype frequencies of *UCP2* G-866A, *MnSOD* C47T, and *CAT* C-262T were found to be significantly different among the fertile subjects, the infertile subjects with more than 50% motility, and the infertile subjects with less than 50% motility. A higher prevalence of the mtDNA 4,977 bp deletion was found in the subjects with impaired sperm motility and fertility. Furthermore, we found that there were significant differences between the occurrences of the mtDNA 4,977 bp deletion and *MnSOD* (C47T) and *hOGG1* (C1245G). In conclusion, the maintenance of the mitochondrial redox microenvironment and genome integrity is an important issue in sperm motility and fertility.

1. Introduction

Male infertility is a growing problem that affects 30% of infertile human couples due to a decline in sperm counts and rise in testicular and sperm anomalies. The evaluation of male-factor infertility has become more important and informative since new diagnostic techniques and therapeutic options have become available. Poor sperm motility has been considered as one of the major causes of male infertility [1]. It is highly probable that the respiratory dysfunction of mitochondria causes a decline in motility [2]. However, there remains a group of these subfertile men in whom routine semen analysis results are within normal values and who are classified as having unexplained male infertility. The presence of antisperm antibodies, sperm DNA damage, and oxidative stress has been suggested to contribute to unexplained male infertility [3].

In mammalian germ cells, reactive oxygen species (ROS) have been shown to be required for sperm maturation, differentiation, capacitation, acrosomal reaction, zona pellucida binding, and oocyte fusion [4]. Notably, ROS levels in semen are higher in infertile males [5, 6]. Excessive generation of ROS was found to be associated with idiopathic male infertility and sperm apoptosis [7]. In addition to the conventional causes for male infertility, cryptorchidism, infections, obstructive lesions, cystic fibrosis, trauma, and tumors have been identified to be associated with oxidative stress [8, 9]. Oxidative stress is represented as a major cause of male fertility in more than 40% of patients revealing evidences of oxidative attack, resulting in high levels of lipid peroxidation and oxidative DNA damage. Extraordinary levels of deleterious ROS lead to DNA damages and fragmentation, motility impairment, mitochondrial dysfunction, and cell apoptosis in human sperm [10–13]. It is important to point out that the oxidative DNA adduct, 8-hydroxy-2′-deoxyguanosine (8-OHdG) is highly mutagenic and might elicit *de novo* mutations during spermatogenesis [14]. More than 9000 genomic lesions in the human sperm genome have been found as highly vulnerable to oxidative attack in human sperm [15]. Oxidative stress-mediated DNA damage may be the etiology for repeated assisted reproductive technology failures [16, 17].

Mitochondrial ATP generation increases sperm linear motility that might have an impact on the *in vivo* transfer of sperm from the uterus to the oviduct [18]. There is reason to believe that sperm mitochondria are one of the major targets of attack by ROS, and mitochondria in particular have been identified as a major source of ROS through electron leakage from mitochondrial respiratory Complexes I and III [19, 20]. The deleterious ROS are usually disposed of by the coordinated functioning of enzymatic antioxidants, but a certain fraction of them may escape the antioxidant defense system and cause transient or permanent DNA damages [17, 21]. Thus, we hypothesized that redox control in the mitochondrial microenvironment is essential for proper sperm motility and fertility. In this study, we investigated the polymorphisms and allele frequencies of these genes contributing to the maintenance of mitochondrial energy generation and oxidative scavenging capacity (Table 1). We examined the gene mutation of ATP synthase 6 (*ATPase6* m.T8993G) in ATP generation, the gene polymorphisms of uncoupling protein 2 (*UCP2*, G-866A) in the uncoupling of oxidative phosphorylation (OXPHOS), the role of genes such as manganese superoxide dismutase (*MnSOD*, C47T) and catalase (*CAT*, C-262T) in the scavenging system in neutralizing ROS, and the role of human 8-oxoguanine DNA glycosylase (*hOGG1*, C1245G) in 8-OHdG repair. We also analyzed the association between the occurrence of an mtDNA common deletion (4,977 bp deletion) and the polymorphisms of these genes. We found that maintenance of the mitochondrial redox microenvironment is an important issue in genome integrity, sperm motility, and fertility.

2. Materials and Methods

2.1. Semen Collection and Assessment of Sperm Motility Characteristics. We collected 220 semen samples from 58 healthy donors who had normal semen characteristics and from 162 infertile or subfertile males at Hsin Kong Wu Ho-Su Memorial Hospital and Taipei City Hospital Ren-Ai Branch. This study was performed according to the tenets of the Declaration of Helsinki for research involving human subjects. The protocol was approved by the Institutional Review Board/Ethics Committee of Hsin Kong Wu Ho-Su Memorial Hospital and Taipei City Hospital Ren-Ai Branch. After informed patient consent was obtained, the semen samples were collected. All of the semen samples were obtained by masturbation after 3–4 days of abstinence. After liquefaction, the characteristics of sperm motility were examined using a computer-assisted semen analyzer (CASA; HTM-2000 motility analyzer; Hamilton Thorn Research, Danvers, MA). Leukospermia and viscous semen samples were excluded from this study.

2.2. Ficoll-Paque Fractionation and Sperm Preparation. To avoid the contamination of sperm by other types of cells such as lymphocytes and epithelial cells, we removed the contaminant cells with Ficoll-Paque (Pharmacia Biotech AB, Uppsala, Sweden) separation before DNA extraction and flow cytometric analysis. Sperm were separated from seminal plasma by centrifugation at $300 \times g$ for 10 min at 25°C. The sperm pellet was resuspended in phosphate-buffered saline (PBS; Dulbecco Oxoid, UniPath Ltd., Hants, UK; pH 7.3), and the final sperm count was adjusted to $2 \sim 4 \times 10^8$ sperm /ml. An aliquot of the suspension was layered on the top of a tube containing 2 ml of 60% and 80% Percoll gradient in Ham's F10 medium and was incubated at 37°C for 90 min. After incubation, the sperm in the different Percoll gradients were collected and washed with PBS before centrifugation at $300 \times g$ for 10 min.

2.3. Mitochondrial Membrane Potential in the H_2O_2-Treated Human Sperm. To visualize the changes in the sperm mitochondrial membrane potential under oxidative stress, sperm were treated with 100 μM H_2O_2 and then stained for 10 min with 10 μM JC-1 (Molecular Probes, Eugene, OR) at 37°C. The dye at lower mitochondrial concentrations with lower $\Delta\Psi$ forms a green fluorescent monomer with emissions at

Table 1: Characteristics of gene mutations and gene polymorphisms.

Gene	Locus	Reference no.	Position	Function	Characteristics
UCP2	G-866A	rs659366	Promoter	Uncoupling proton gradient	Enhanced UCP2 mRNA expression
MnSOD	C47T	rs4880	Exon 2	$O_2^{\bullet-} \longrightarrow H_2O_2$	Stop translocation of MnSOD at mitochondrial inner membrane, not into matrix
CAT	C-262T	rs1001179	Promoter	$H_2O_2 \longrightarrow H_2O$	Reduced CAT mRNA expression
hOGG1	C1245G	rs1052133	Exon 7	Repair enzyme of 8-OHdG	Reduced hOGG1 enzyme activity
ATPase6	T8993G		mtDNA	Respiratory complex	ATP depletion

530 nm, but at higher concentrations, it forms red fluorescent aggregates with emissions at 590 nm. All analyses were performed by confocal fluorescence microscopy (Leica TCS SP5, Leica Microsystems CMS GmbH, Mannheim, Germany) and flow cytometry (FACScan, Becton Dickson, San Jose, CA). Confocal fluorescent images were captured using the Leica SP5 confocal microscope fitted with an Apochromat 63x/1.4 NA immersion objective and with three lasers (argon, 488 nm; diode, 405 nm). In addition, a minimum of 3×10^4 cells per sample were analyzed by flow cytometry. The relative proportions of cells within different areas of the fluorescence profile were quantified with the LYSYS II software program (Becton Dickson).

2.4. Mitochondrial Bioenergetics. The oxygen consumption from extracellular flux analysis of oxygen consumption of sperm was measured using the Seahorse XF extracellular flux analyzers (Seahorse Bioscience, North Billerica, MA). Fresh 1×10^7 sperm samples were placed in 24-well analysis plates, and the volume was adjusted to 0.5 ml. The oxidative phosphorylation capacity of sperm was analyzed after the condition of sperm was equilibrated for 20 minutes. Three chemicals were sequentially injected into the assay medium including 5 μM oligomycin (Complex V inhibitor) at the time of 32 minutes, 1 μM trifluorocarbonylcyanide phenylhydrazone (FCCP, mitochondrial uncoupler) at the time of 56 minutes, and 3 μM rotenone (Complex I inhibitor) at the time of 88 minutes. Results of sperm oxygen consumption rate (OCR) were calibrated with sperm number in each well and analyzed by the Seahorse XF24 software.

2.5. DNA Extraction from Human Sperm. Before sperm DNA extraction, an aliquot of $3\text{-}5 \times 10^7$ sperm was treated with osmotic shock. Sperm were incubated in 15 ml of 50 mM Tris-HCl buffer (pH 6.8) at 8°C for 20 min to lyse the contaminated cells. Sperm cells, which were resistant to this treatment, were then subjected to DNA extraction according to the method described previously [5]. After digestion at 56°C for 2 h in 1.5 ml lysis buffer, the lysate was extracted once each with phenol, phenol/chloroform, and chloroform in succession. The aqueous layers were pooled and precipitated with isopropanol (1 : 1, *v*/*v*) and one-tenth volume of 3 M sodium acetate (pH 5.6), and incubated at -20°C overnight. The sperm DNA was finally dissolved in 10 mM Tris-HCl buffer (pH 8.5).

2.6. Detection of the 4,977 bp MtDNA Deletion in Human Sperm. We performed PCR to analyze the occurrence of 4,977 bp mtDNA deletion using primer pairs L8150 (8150-8169) and H13845 (13845-13826). The nucleotide sequences of the primer pairs used are listed in Table 2. The desired segment was amplified from approximately 100 ng of each DNA sample in a 50 μl reaction mixture containing 200 μM of each dNTP, 0.6 μM of primers, 1 unit of Taq DNA polymerase (PerkinElmer Life Science, Inc. Boston, MA), 50 mM KCl, 1.5 mM $MgCl_2$, and 10 mM Tris-HCl (pH 8.3). PCR was carried out for 25 cycles in a DNA thermal cycler (Model 9600, PerkinElmer). Amplified nucleotide fragments of 719 bp were separated by electrophoresis on 1.5% agarose gels and detected after staining with 0.5 mg/ml ethidium bromide.

2.7. Immunolocalization of 8-OHdG in Human Sperm. Intracellular localization of 8-OHdG was performed with paraformaldehyde-fixed sperm on slides. After two washes with PBS, sperm were treated with cold methanol for 3–5 minutes, washed with PBS, and then incubated for 1 hour at room temperature with 2% bovine serum albumin to prevent nonspecific binding of antibodies. Sperm then were incubated for 24 hours with anti-8-OHdG mouse monoclonal antibody anti-8-OHdG (SC66036 Santa Cruz® Biotechnology, CA, USA), followed by washing with PBS and treatment with Alexa Fluor® 647 (ab150115, Abcam, Cambridge, UK). To visualize sperm head, cells were stained for 15 minutes with 1 μg/ml DAPI (Molecular Probes, Eugene, OR). This probe shows blue fluorescence.

2.8. Genotyping of the Polymorphisms. The point mutation of *ATPase6* (m.T8993G) and the SNPs of *UCP2* (G-866A, rs659366), *MnSOD* (C47T, rs4880), *CAT* (C-262T, rs1001179), and *hOGG1* (C1245G, rs1052133) were analyzed by polymerase chain reaction (PCR) and restriction fragment length polymorphism (RFLP; MJ Research, MA) analysis. The PCR-RFLP assay consisted of primer pairs for PCR amplification and restriction enzymes for digestion; the size products are shown in Table 2. The genotypes of the PCR products were confirmed by DNA sequence analysis. The primers with desired DNA sequences were chemically

Table 2: Primer sequences and predicted sizes of PCR products in this study.

Gene	Primer sequences	RE	PCR products	PCR-RE products
UCP2 G-866A	F: 5′-CACGCTGCTTCTGCCAGGAC-3′ R: 5′-AGGCGTCAGGAGATGGACCG-3′	MluI	360 bp	G: 290/70 bp A: 360 bp
MnSOD C47T	F: 5′-CAGCCCAGCCTGCGTAGACGG-3′ R: 5′-GCGTTGATGTGAGGTTCCAG-3′	BsaWI	172 bp	T: 88/84 bp C: 172 bp
CAT C-262T	F: 5′-AGAGCCTCGCCCCGCCGGACCG-3′ R: 5′-TAAGAGCTGAGAAAGCATAGCT-3′	SmaI	340 bp	C: 185/155 bp T: 340 bp
hOGG1 C1245G	F: 5′-ACTAGTCTCACCAGCCGTGAC-3′ R: 5′-TGGCCTTTGAGGTAGTCACAG-3′	Fun4HI	293 bp	G: 123/124 bp 169/170 bp C: 293 bp
ATPase6 T8993G	F: 5′-GACTAATCACCACCCAAC-3′ R: 5′-TGTCGTGCAGGTAGAGGCTT-3′	Ava I	551 bp	T: 551 bp G: 345/206 bp
mtDNA Δ4977	L8150: 5′-CCGGGGGTATACTACGGTCA-3′ H13845: 5′-GTCTAGGGCTGTTAGAAGTC-3′		719 bp	

Δ4977: 4977 bp deletion; RE: restriction endonuclease.

synthesized by Roche Molecular Systems Inc. (Branchburg, NJ, USA).

2.9. Statistical Analysis. The significance of the correlations among the gene polymorphisms, sperm motility, and fertility was determined with the Chi-squared test using IBM SPSS Statistics 19 (IBM. Armonk, NY). p values less than 0.05 were considered significant.

3. Results

3.1. Oxidative Stress Affects the Mitochondrial Membrane Potential ($\Delta\psi m$) of Human Sperm. Following Percoll fractionation, three sperm fractions were obtained according to their motility and categorized into the 80% Percoll fraction (80%), 60% Percoll fraction (60%), and the residual fraction (R). The JC-1 aggregate staining of the mitochondria was visualized in the sperm from the 80% Percoll fraction (Figure 1(a)). The results showed a significant positive correlation between the changes in membrane potential and sperm motility ($n = 35$, $p < 0.01$). The sperm with higher motility were found to have a higher $\Delta\psi m$ (Figures 1(a) and 1(b)). Treatment of H_2O_2 was found to decrease the $\Delta\psi m$ of sperm in all three fractions (Figure 1(b)).

3.2. Oxidative Stress Decreased Sperm Bioenergetics. Data in Figure 2(a) represent the time course of the OCR analysis under the basal condition, followed by the sequential injections of 5 μM oligomycin (ATP synthase inhibitor), 3 μM FCCP (mitochondrial uncoupler), and 1 μM rotenone (mitochondrial respiratory Complex I inhibitor). The basal, ATP-linked, and maximal OCR were measured in the Percoll-fractionated sperm with and without H_2O_2 treatment. The lower basal OCR, ATP-related OCR, and maximal OCR occurred in the sperm with poor motility (Figure 2(b)). Treatment of H_2O_2 was found to significantly impair mitochondrial bioenergetics and uncoupled mitochondrial respiration.

3.3. Mitochondrial DNA Deletion and 8-OHdG Accumulate in the Sperm with Poor Motility. To test whether the mtDNA 4,977 bp deletion accumulates in the sperm with poor motility and infertility, we analyzed the occurrence of the 4,977 bp deletion in 216 sperm samples. We obtained the 719 bp PCR products from the flanking region of the 4,977 bp deleted mtDNA from the individuals with poor sperm motility (Figure 3(a)) and the 450 bp PCR products from the mtDNA *ND1* gene as the mtDNA control. We further identified the nucleotide sequences of the deleted mtDNA in the junction site showing the 13-nucleotide direct repeat (5′-ACCTCC CTCACCA-3′) on the heavy strand of the mtDNA (Figure 3(b)). In addition, we detected the oxidative DNA adducts (8-OHdG) using anti-8-OHdG antibody conjugated with Alexa Fluor® 647 with the red fluorescent signals. The major signals of 8-OHdG were identified in the sperm midpiece from the 80% Percoll gradient. However, 8-OHdG signals were found in both the sperm head and midpiece from the 60% Percoll gradient (Figure 4).

3.4. Screening of Gene Polymorphisms Involved in Free Radical Scavenging and Mitochondrial Bioenergetics in Human Sperm. To clarify the associations of sperm capacity and gene mutation (*ATPase6* (m.T8993G) and SNPs of *UCP2* (G-866A, rs659366), *MnSOD* (C47T, rs4880), *CAT* (C-262T, rs1001179), and *hOGG1* (C1245G, rs1052133)), a total of 216 sperm samples were categorized into three groups, i.e., fertile subjects (control group), infertile subjects with more than 50% motility, and infertile subjects with less than 50% motility. The genotype frequencies of *UCP2* G-866A, *MnSOD* C47T, and *CAT* C-262T were found to be significantly different among the fertile subjects (control group), infertile subjects with more than 50% motility, and infertile subjects with less than 50% motility (Table 3). In addition, there were significant differences in the allele frequencies of the *UCP2*-866 G allele (GG and GA, $p = 0.007$) and *MnSOD* 47T allele (TT and TC, $p = 0.042$) among the three groups.

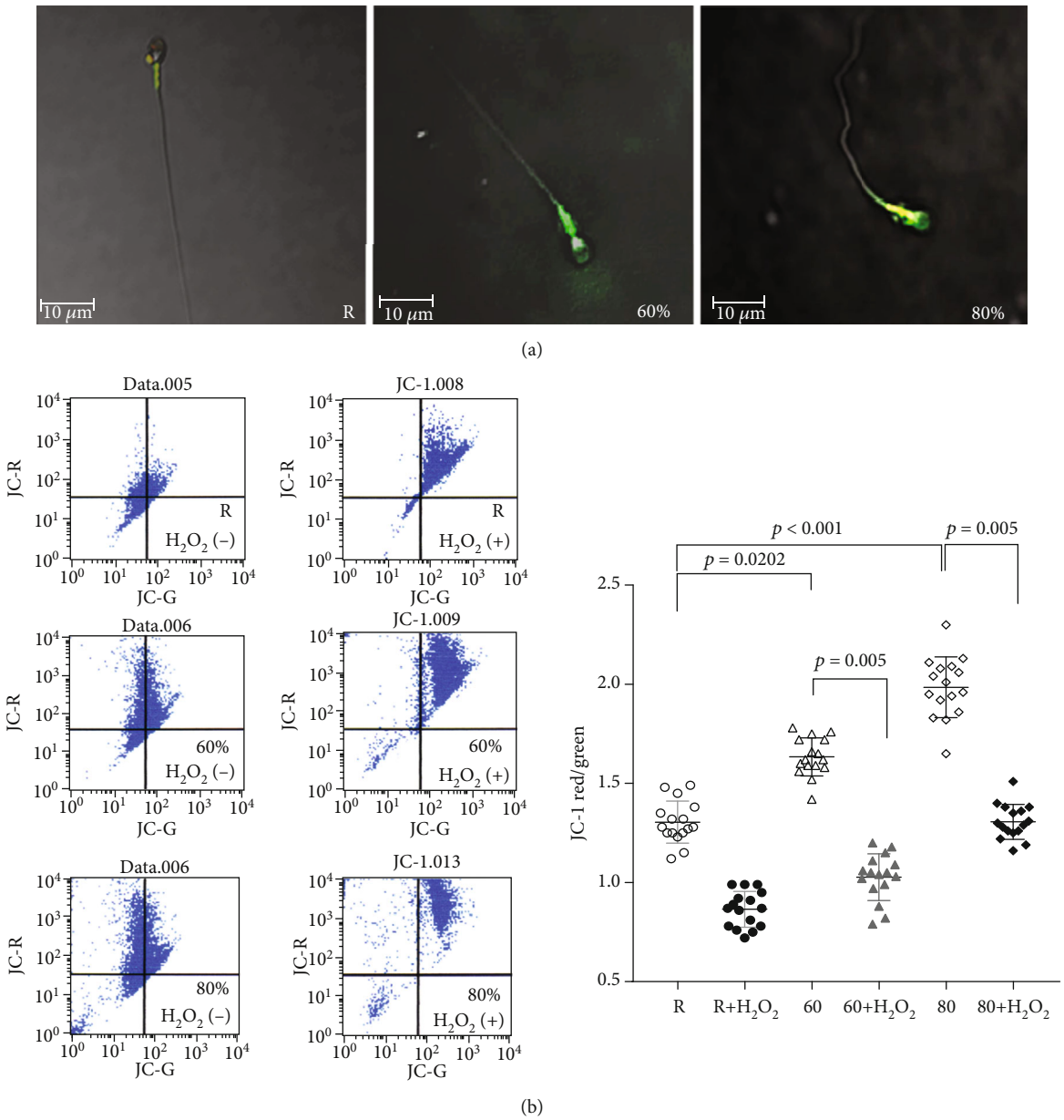

Figure 1: Oxidative insult affects the mitochondrial membrane potential ($\Delta\psi m$) of human sperm. By using JC-1, we analyzed the changes in the mitochondrial membrane potential of the Percoll-fractionated human sperm by flow cytometry and confocal microscopy. Three sperm fractions were obtained according to their motility and categorized into the 80% Percoll fraction (80%), 60% Percoll fraction (60%), and the residual fractions (R). (a) Fluorescent images of the JC-1-stained human sperm. Illustration of JC-1 accumulating preferentially in the mitochondria, existing as a green fluorescent monomer at low membrane potentials and as red-orange fluorescent aggregates at high membrane potentials. The JC-1 aggregate staining of the mitochondria was visualized in the sperm from the 80% Percoll fraction. (b) Dot plot of the mitochondrial membrane potential of human sperm by flow cytometry was represented. Flow data were assessed and expressed as the ratio of red fluorescent intensity versus green fluorescent intensity. The good motile sperm were demonstrated to harbor a higher $\Delta\psi m$. All three sperm fractions exposed to hydrogen peroxide lost their $\Delta\psi m$. Data are presented as the mean ± standard deviation (SD). $^{**}p < 0.01$ compared with the control group.

3.5. Analyzing the Association of the Occurrence of the MtDNA 4,977 bp Deletion and Gene Polymorphisms Involved in the Free Radical Scavenger System and Mitochondrial Bioenergetics. The impaired sperm motility and fertility group had a higher prevalence of the mtDNA 4,977 bp deletion (Table 4). The higher occurrence of the mtDNA 4,977 bp deletion was found in the sperm of the infertile groups ($p = 0.047$). The occurrence of the mtDNA 4,977 bp deletion was 3.7%, 26.7%, and 16.7% in the fertile subjects (control group), infertile subjects with more than 50% motility, and infertile subjects with less than 50% motility, respectively. In addition, there were significant

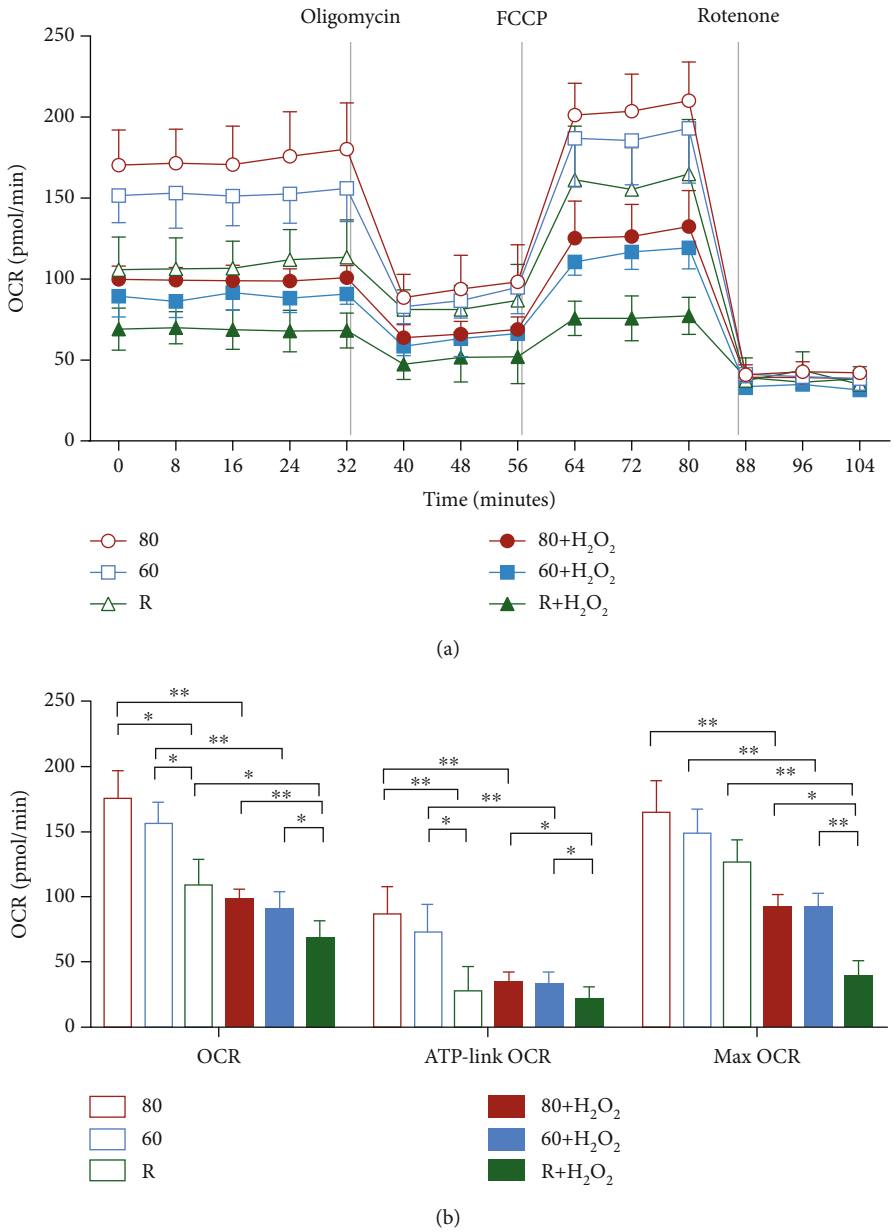

Figure 2: Oxidative stress reduced mitochondrial bioenergetics of human sperm. (a) Mitochondrial respiration as indicators of cellular bioenergetics were assessed using a Seahorse XF24 metabolic flux analyzer. Representative data shows the real-time oxygen consumption rate (OCR) of 1×10^7 sperm with or without H_2O_2 treatment. Dotted lines indicate time of sequential addition of 5 μM oligomycin (the ATP synthase inhibitor), 3 μM FCCP (mitochondria uncoupler), and 1 μM rotenone (mitochondrial respiratory complex inhibitors), respectively. (b) Sperm with lower motility exhibited significant decreases in basal OCR, ATP-linked OCR, and maximal OCR. Results are presented as mean ± standard deviation (SD) ($n = 4$) ($^*p < 0.05$, $^{**}p < 0.01$, and $^{***}p < 0.001$).

differences between the occurrence of the mtDNA 4,977 bp deletion and the gene polymorphisms of *MnSOD* (C47T, $p = 0.042$) and *hOGG1* (C1245G, $p = 0.021$; Table 5).

4. Discussion

ATP synthesis from the mitochondrial OXPHOS system and glycolysis is essential for human sperm motility [22, 23]. Most studies have concentrated on analyzing mitochondrial respiration to determine whether OXPHOS is crucial for ATP production in sperm [12, 23]. Some studies have shown that sperm motility was inhibited by respiratory inhibitors such as rotenone, potassium cyanide, and oligomycin [24, 25], and stimulated by respiratory substrates (e.g., malate, pyruvate, and lactate) and ADP [26, 27]. These results indicated that proper function of the mitochondrial respiratory enzyme complexes and a tight coupling between respiration and phosphorylation is essential for sperm motility. In addition, a significant decrease in sperm respiratory function was found in asthenozoospermic patients [2]. In addition to its involvement in ATP synthesis, sperm mitochondria may serve as intracellular calcium stores and regulate calcium

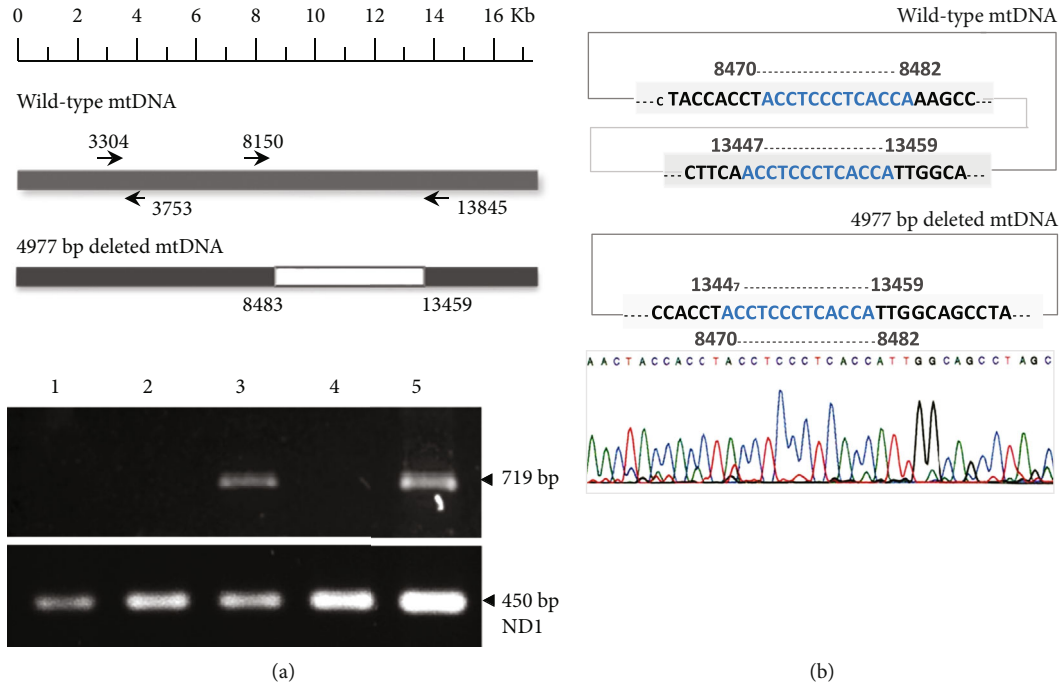

Figure 3: Mitochondrial DNA (mtDNA) deletions in human sperm. (a) An agarose gel electrophoretogram of the PCR products amplified from the mtDNA with the specific 4,977 bp deletion in human sperm using primer-pair L8150-H13845. Lanes 3 and 5 indicate the PCR products of 719 bp amplified from the 4,977 bp deleted mtDNA. Lane 3 was from the infertile subjects with motility scores of 30%. Lane 5 was from the infertile subjects with motility scores of 60%. Lanes 1, 2, and 4 were generated from the normal subjects. The lower gel of the PCR products was amplified from the *ND1* gene using the primer-pair L3304-H3753 for control. (b) Schematic illustration of the nucleotide sequence flanking the junction site at the 5′-end of the 4,977 bp deletion on the heavy strand of the mtDNA in human sperm.

signaling, ROS signaling, and apoptosis [28]. These observations suggested that mitochondria play a key role in the maintenance of sperm motility and fertility [28, 29].

The mitochondrial membrane potential ($\Delta\Psi m$) is a potential marker of mitochondrial function and sensitive index of cell damage because it is easily influenced by environmental stress, which is normally associated with the respiratory chain and OXPHOS system. Several studies have substantiated a potential role of $\Delta\Psi m$ in the determination of sperm fertilizability in ejaculated human sperm [30]. The sperm with high $\Delta\Psi m$ represent a subpopulation of sperm with high fertility performance because they have better membrane integrity and higher motility, i.e., they easily undergo a Ca^{2+} ionophore- (A23187-) induced acrosome reaction [30]. In the present study, a significant positive correlation was found between the changes in the mitochondrial membrane potential and human sperm motility. The sperm with better motility were found to have higher $\Delta\Psi m$ (Figures 1). Recently, studies showed that a metabolic assay platform by Seahorse Metabolic Analyzer reveals oxygen consumption rates (OCR) of sperm in real time [31, 32]. Sperm with the best performance had a higher OCR than those that were less motile or immotile [31]. Sperm with higher ratios of oxygen consumption/lactate excretion rate were able to generate higher ATP contents, achieving higher swimming velocities [32]. Comparing to conventional momentary analysis (as in computer-assisted semen analysis), measuring metabolic activity and respiratory capacity of sperm can be an important indicator for sperm quality and their migration success. We found the sperm with higher motility represented higher basal OCR, ATP-linked OCR, and maximal OCR. Here, we found that the treatment with H_2O_2 caused dissipation of $\Delta\Psi m$ and bioenergetics in all three sperm groups (Figures 1(b) and 2(b)), suggesting that sperm are susceptible to H_2O_2 attack.

Mitochondrial uncoupling is a condition that uncouples proton entry to the mitochondria from ATP synthesis and attenuates the mitochondrial membrane potential. UCPs are a family of inner mitochondrial membrane proteins that are thought to maintain a balance between the energy supply and cell demand in defending cells against ROS production [33, 34]. *UCP2*-866G (rs659366) was found to have higher efficiency of UCP2 expression and promoter activity than -866A. *UCP2* G-866A has been linked to a predisposition to diabetes, obesity, and inflammation [33, 35]. In the present study, the genetic alteration in the *UCP2* G-866A allele was shown to significantly influence sperm fertility and motility.

Upregulation of the enzymes that can neutralize ROS would then be conceivably able to offer at least some protection from the damaging effects. MnSOD converts superoxide to hydrogen peroxide and quenches the free radicals generated by the electron transport chain [36]. A study showed that seminal SOD activity was shown to be positively associated with sperm concentrations and overall motility [37]. Meanwhile, the infertile men with *SOD2* rs4880 CC variants showed a low level of SOD activity compared with that of TT patients [37]. In addition, MnSOD Val16Ala (rs4880) variant genotypes were associated with a significantly higher risk of

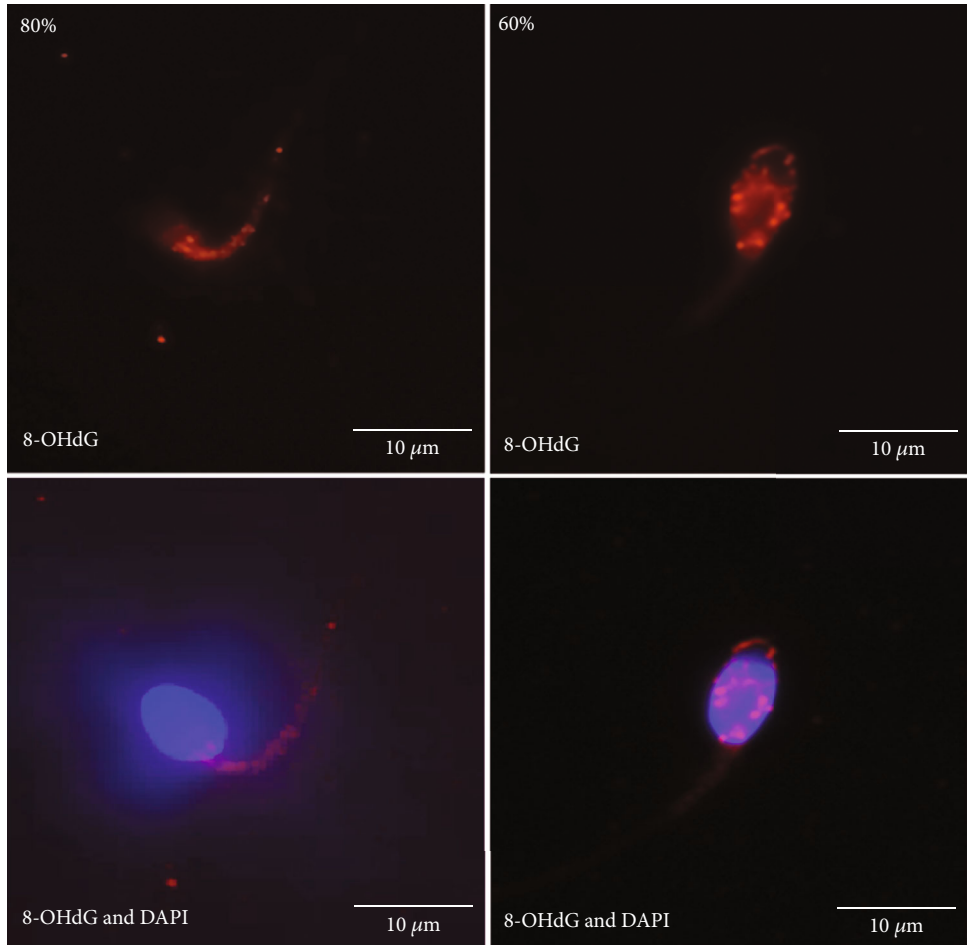

Figure 4: Visualization of 8-OHdG in human sperm. By staining with an anti-8-OHdG antibody conjugated with Alexa Fluor® 647 with the red fluorescent signals, 8-OHdG was identified in the sperm midpiece from the sperm in 80% Percoll gradient. 8-OHdG was found in both the sperm head and midpiece from the sperm in 60% Percoll gradient. The blue fluorescent staining by DAPI was used for labeling the sperm head.

Table 3: Genotype frequencies of the gene polymorphisms on human male fertility and sperm motility.

Gene	Locus	Reference number	Group		No.	Genotype frequency (%)			p value
			Fertility	Motility					
			Normal		54	GG (46.3)	GA (46.3)	AA (7.4)	0.019
UCP2	G-866A	rs659366	Infertile	>50%	111	GG (36.9)	GA (38.8)	AA (24.3)	
			Infertile	<50%	51	GG (25.5)	GA (27.4)	AA (47.1)	
			Normal		54	TT (68.5)	TC (18.5)	CC (13.0)	0.017
MnSOD	C47T	rs4880	Infertile	>50%	111	TT (41.5)	TC (39.6)	CC (18.9)	
			Infertile	<50%	51	TT (35.3)	TC (39.2)	CC (25.4)	
			Normal		54	CC (79.6)	TC (13.0)	TT (7.4)	0.091
CAT	C-262T	rs1001179	Infertile	>50%	111	CC (71.2)	TC (17.1)	TT (11.7)	
			Infertile	<50%	51	CC (62.7)	TC (21.6)	TT (15.7)	
			Normal		54	CC (38.9)	CG (44.4)	GG (16.7)	0.403
hOGG1	C1245G	rs1052133	Infertile	>50%	111	CC (32.4)	CG (48.6)	GG (19.0)	
			Infertile	<50%	51	CC (29.4)	CG (49.0)	GG (21.6)	

male infertility [38]. *SOD2* (MnSOD gene) contains the C47T single-nucleotide polymorphism, which results in a Val16Ala amino acid substitution. The C47T results in a valine to alanine substitution in the mitochondrial targeting sequence, leading to an effect on cellular allocation of MnSOD within the mitochondria. The Val allele is partially arrested in the

Table 4: Allelic frequencies of the gene polymorphisms and mutation frequencies of mitochondrial DNA on human male fertility and sperm motility.

Gene	Locus	Group		No.	Frequency (%)	p value
		Fertility	Motility			
UCP2	nDNA	Normal		54	GG + GA (92.6)	0.007
	G-866A	Infertile	>50%	111	GG + GA (75.7)	
		Infertile	<50%	51	GG + GA (52.9)	
MnSOD	nDNA	Normal		54	TT + CT (31.5)	0.042
	C47T	Infertile	>50%	111	TT + CT (58.6)	
		Infertile	<50%	51	TT + CT (64.8)	
CAT	nDNA	Normal		54	TT + CT (20.4)	0250
	C-262T	Infertile	>50%	111	TT + CT (28.8)	
		Infertile	<50%	51	TT + CT (37.3)	
hOGG1	nDNA	Normal		54	GG + CG (61.1)	0.081
	C1245G	Infertile	>50%	111	GG + CG (67.6)	
		Infertile	<50%	51	GG + CG (70.6)	
ATPase6	mtDNA	Normal		54	T8993G (1.8)	0.247
	T8993G	Infertile	>50%	111	T8993G (1.8)	
		Infertile	<50%	51	T8993G (1.9)	
Δ4977	mtDNA	Normal		54	Δ4977 (3.7)	0.047
	np8483-13459	Infertile	>50%	111	Δ4977 (24.3)	
		Infertile	<50%	51	Δ4977 (17.6)	

nDNA: nuclear DNA; mtDNA: mitochondrial DNA; Δ4977: 4977 bp mtDNA deletion.

Table 5: Genotype frequencies of the gene polymorphisms in the mtDNA 4,977 bp deletion.

Gene	Locus	Group	No.	Genotype frequency (%)			p value
UCP2	G-866A	Δ4977(-)	178	GG (41.0)	GA (38.8)	AA (20.2)	0.019
		Δ4977(+)	38	GG (15.8)	GA (34.2)	AA (50.0)	
MnSOD	C47T	Δ4977(-)	178	CC (52.8)	CT (34.3)	TT (12.9)	0.017
		Δ4977(+)	38	CC (18.4)	CT (34.2)	TT (47.4)	
CAT	C-262T	Δ4977(-)	178	CC (74.7)	TC (15.7)	TT (9.6)	0.326
		Δ4977(+)	38	CC (55.3)	TC (23.7)	TT (21.0)	
hOGG1	C1245G	Δ4977(-)	178	CC (39.3)	CG (51.7)	GG (9.0)	0.021
		Δ4977(+)	38	CC (5.3)	CG (28.9)	GG (65.8)	

inner mitochondrial membrane, leading to decreased active MnSOD within the mitochondrial matrix [39]. Our results showed that *SOD2* C47T was found to be significantly different among the fertile subjects (control group), infertile subjects with more than 50% motility, and infertile subjects with less than 50% motility.

In addition to MnSOD, catalase contributes to the conversion of H_2O_2 to H_2O and O_2. A study showed that catalase activities in asthenozoospermic subjects were significantly lower than normozoospermic males [40]. The *CAT* C-262T (rs1001179) polymorphism in the promoter region of the human catalase gene has been associated with lower transcription factor binding and lower catalase expression [41]. In the present study, a higher prevalence of -262T/T and -262C/T genotype frequencies and higher -262T allele frequencies were found in the infertile subjects with less than 50% motility, but without a statistically significant difference among the three groups. This result was consistent with the findings of Sabouhi et al. They showed that the catalase C-262T polymorphism indicates that the CAT -262T/T genotype confers less susceptibility to male infertility [42].

Oxidative stress and related DNA damage in human sperm is important for sperm motility and fertility [10, 43]. The localization of oxidative lesions also differed depending on the genotoxic agent. 8-Hydroxy-2′-deoxyguanosine (8-OHdG) is one of the most abundant oxidative DNA products after H_2O_2 treatment [44, 45]. Increased 8-OHdG levels have been identified as influencing pregnancy outcomes [46] and are associated with male pathophysiology such as varicocele [47]. If not repaired, the mutagenic 8-OHdG is associated with DNA fragmentation and may cause structural and functional defects of sperm and may lead to male infertility [11, 15, 48]. Oxidative DNA damage is associated with dysregulation of the acrosome network formation [48] and the impairment of telomere interaction and chromatin condensation [11]. Furthermore, oxidation of the DNA bases in sperm

could be a risk factor of de novo mutation transmission to the embryo leading to developmental anomalies and de novo mutations in childhood [15, 43]. The 8-oxoguanine repairs specific enzyme 8-oxoguanine DNA glycosylase (hOGG1) through the base excision repair mechanism. A shift from serine (Ser) to cysteine (Cys) substitution at codon 326, as *hOGG1* C1245G (rs1052133), has been shown to reduce repair activity [49]. The 1245G allele is less effective in repair than the 1245C allele in *hOGG1*. It is known that oxidative damage to mtDNA can cause mitochondrial dysfunction and trigger apoptosis, which may be associated with the accumulation of 8-oxodG. Human OGG1 is also located in the mitochondria (mtOGG1) and has been reported to be associated with mitochondrial function [50]. It has been noted that mtOGG1 suppression was sufficient to diminish mitochondrial respiration and cellular growth rates, and forced expression of mtOGG1 was reversed in those activities [50]. Here, we found that there were no significant differences among the three sperm groups. However, the *OGG1* 1245G allele is associated with the occurrence of the mtDNA 4,977 bp deletion.

In addition to serving as the major intracellular compartment of oxidative metabolism, mitochondria also contain their own genomes. Loss of mtDNA integrity has also been identified in the patients with infertility or subfertility [51–54]. Large-scale deletions of mtDNA have been associated with poor sperm motility [12, 52, 53]. The mtDNA 4,977 bp deletion, also known as mtDNA common deletion, is the most frequent and common mtDNA mutation associated with oxidative damage. In this study, the *SOD2* C47T polymorphism was significantly associated with the occurrence of the mtDNA 4,977 bp deletion. In addition to the mtDNA deletion, male infertility-related single-nucleotide mutations have been reported in eight mtDNA genes, including *ND4*, *COXI*, *COXII*, *COXIII*, *ATPase6*, *ATPase8*, *Cytb*, and *16S rRNA* [55–57]. These single-nucleotide mutations in the mitochondrial genome are associated with poor semen parameters and represent a very important factor affecting sperm maturation, sperm motility, and fertility [58]. In the present study, no association was observed in the mtDNA T8993G mutation among the three sperm groups.

On the basis of our findings, we concluded that mtDNA integrity and energy maintenance may serve as a useful indicator of sperm quality. Our findings also strongly support the hypothesis that the mitochondrial oxidizing microenvironment contributes to the etiopathology of male infertility.

Data Availability

Data available on request.

Conflicts of Interest

The authors declare that they have no conflicts of interest.

Acknowledgments

This study was supported by the Shin Kong Wu Ho-Su Memorial Hospital (SKH-TMU-95-11), the Ministry of Health of the Czech Republic (grant number: NU20-03-00309), the project "BIOCEV—Biotechnology and Biomedicine Centre of the Academy of Sciences and Charles University" (CZ.1.05/1.1.00/02.0109), and the institutional support of the Institute of Biotechnology (RVO: 86652036). The instruments were provided by the Core Facility Center, Office of Research and Development of Taipei Medical University.

Supplementary Materials

Supplementary Table 1: description of patient characteristics. *(Supplementary Materials)*

References

[1] B. Hafez, L. Goff, and S. Hafez, "Recent advances in andrology research: physiopathology and clinical application to fertility and infertility," *Archives of Andrology*, vol. 39, no. 3, pp. 173–195, 1997.

[2] A. Ferramosca, R. Focarelli, P. Piomboni, L. Coppola, and V. Zara, "Oxygen uptake by mitochondria in demembranated human spermatozoa: a reliable tool for the evaluation of sperm respiratory efficiency," *International Journal of Andrology*, vol. 31, no. 3, pp. 337–345, 2008.

[3] A. Hamada, S. C. Esteves, M. Nizza, and A. Agarwal, "Unexplained male infertility: diagnosis and management," *International Braz J Urol*, vol. 38, no. 5, pp. 576–594, 2012.

[4] J. Erenpreiss, M. Bungum, M. Spano, S. Elzanaty, J. Orbidans, and A. Giwercman, "Intra-individual variation in sperm chromatin structure assay parameters in men from infertile couples: clinical implications," *Human Reproduction*, vol. 21, no. 8, pp. 2061–2064, 2006.

[5] S. H. Kao, H. T. Chao, H. W. Chen, T. I. Hwang, T. L. Liao, and Y. H. Wei, "Increase of oxidative stress in human sperm with lower motility," *Fertility and Sterility*, vol. 89, no. 5, pp. 1183–1190, 2008.

[6] R. Mahfouz, R. Sharma, A. Thiyagarajan et al., "Semen characteristics and sperm DNA fragmentation in infertile men with low and high levels of seminal reactive oxygen species," *Fertility and Sterility*, vol. 94, no. 6, pp. 2141–2146, 2010.

[7] M. Cocuzza, S. C. Sikka, K. S. Athayde, and A. Agarwal, "Clinical relevance of oxidative stress and sperm chromatin damage in male infertility: an evidence based analysis," *International Braz J Urol*, vol. 33, no. 5, pp. 603–621, 2007.

[8] A. Agarwal, K. Makker, and R. Sharma, "Clinical relevance of oxidative stress in male factor infertility: an update," *American Journal of Reproductive Immunology*, vol. 59, no. 1, pp. 2–11, 2008.

[9] R. Z. Mahfouz, S. S. du Plessis, N. Aziz, R. Sharma, E. Sabanegh, and A. Agarwal, "Sperm viability, apoptosis, and intracellular reactive oxygen species levels in human spermatozoa before and after induction of oxidative stress," *Fertility and Sterility*, vol. 93, no. 3, pp. 814–821, 2010.

[10] R. J. Aitken and G. N. De Iuliis, "On the possible origins of DNA damage in human spermatozoa," *Molecular Human Reproduction*, vol. 16, no. 1, pp. 3–13, 2010.

[11] B. Berby, C. Bichara, A. Rives-Feraille et al., "Oxidative stress is associated with telomere interaction impairment and chromatin condensation defects in spermatozoa of infertile males," *Antioxidants (Basel)*, vol. 10, no. 4, 2021.

[12] J. C. St John, R. P. Jokhi, and C. L. Barratt, "The impact of mitochondrial genetics on male infertility," *International Journal of Andrology*, vol. 28, no. 2, pp. 65–73, 2005.

[13] M. Dobrakowski, S. Kasperczyk, S. Horak, D. Chyra-Jach, E. Birkner, and A. Kasperczyk, "Oxidative stress and motility impairment in the semen of fertile males," *Andrologia*, vol. 49, no. 10, 2017.

[14] R. J. Aitken and M. A. Baker, "The role of genetics and oxidative stress in the etiology of male infertility—a unifying hypothesis?," *Front Endocrinol (Lausanne)*, vol. 11, 2020.

[15] M. J. Xavier, B. Nixon, S. D. Roman, R. J. Scott, J. R. Drevet, and R. J. Aitken, "Paternal impacts on development: identification of genomic regions vulnerable to oxidative DNA damage in human spermatozoa," *Human Reproduction*, vol. 34, no. 10, pp. 1876–1890, 2019.

[16] C. Wright, S. Milne, and H. Leeson, "Sperm DNA damage caused by oxidative stress: modifiable clinical, lifestyle and nutritional factors in male infertility," *Reproductive Biomedicine Online*, vol. 28, no. 6, pp. 684–703, 2014.

[17] R. J. Aitken, K. T. Jones, and S. A. Robertson, "Reactive oxygen species and sperm function—in sickness and in health," *Journal of Andrology*, vol. 33, no. 6, pp. 1096–1106, 2012.

[18] Z. Zhu, T. Kawai, T. Umehara, S. A. M. Hoque, W. Zeng, and M. Shimada, "Negative effects of ROS generated during linear sperm motility on gene expression and ATP generation in boar sperm mitochondria," *Free Radical Biology & Medicine*, vol. 141, pp. 159–171, 2019.

[19] J. H. Schofield and Z. T. Schafer, "Mitochondrial reactive oxygen species and mitophagy: a complex and nuanced relationship," *Antioxidants & Redox Signaling*, vol. 34, no. 7, pp. 517–530, 2021.

[20] A. J. Koppers, G. N. De Iuliis, J. M. Finnie, E. A. McLaughlin, and R. J. Aitken, "Significance of mitochondrial reactive oxygen species in the generation of oxidative stress in spermatozoa," *The Journal of Clinical Endocrinology and Metabolism*, vol. 93, no. 8, pp. 3199–3207, 2008.

[21] T. Finkel, "Signal transduction by reactive oxygen species," *The Journal of Cell Biology*, vol. 194, no. 1, pp. 7–15, 2011.

[22] A. C. Williams and W. C. Ford, "The role of glucose in supporting motility and capacitation in human spermatozoa," *Journal of Andrology*, vol. 22, no. 4, pp. 680–695, 2001.

[23] J. M. Nascimento, L. Z. Shi, J. Tam et al., "Comparison of glycolysis and oxidative phosphorylation as energy sources for mammalian sperm motility, using the combination of fluorescence imaging, laser tweezers, and real-time automated tracking and trapping," *Journal of Cellular Physiology*, vol. 217, no. 3, pp. 745–751, 2008.

[24] L. Ramió-Lluch, M. Yeste, J. M. Fernández-Novell et al., "Oligomycin A-induced inhibition of mitochondrial ATP-synthase activity suppresses boar sperm motility and in vitro capacitation achievement without modifying overall sperm energy levels," *Reproduction, Fertility, and Development*, vol. 26, no. 6, pp. 883–897, 2014.

[25] B. J. Rogers, M. Ueno, and R. Yanagimachi, "Inhibition of hamster sperm acrosome reaction and fertilization by oligomycin, antimycin A, and rotenone," *The Journal of Experimental Zoology*, vol. 199, no. 1, pp. 129–135, 1977.

[26] J. A. Grootegoed, R. Jansen, and H. J. Van der Molen, "The role of glucose, pyruvate and lactate in ATP production by rat spermatocytes and spermatids," *Biochimica et Biophysica Acta*, vol. 767, no. 2, pp. 248–256, 1984.

[27] M. Nakamura, S. Okinaga, and K. Arai, "Metabolism of pachytene primary spermatocytes from rat testes: pyruvate maintenance of adenosine triphosphate level," *Biology of Reproduction*, vol. 30, no. 5, pp. 1187–1197, 1984.

[28] A. Amaral, B. Lourenco, M. Marques, and J. Ramalho-Santos, "Mitochondria functionality and sperm quality," *Reproduction*, vol. 146, no. 5, pp. R163–R174, 2013.

[29] A. Ferramosca, S. P. Provenzano, L. Coppola, and V. Zara, "Mitochondrial respiratory efficiency is positively correlated with human sperm motility," *Urology*, vol. 79, no. 4, pp. 809–814, 2012.

[30] A. Amaral and J. Ramalho-Santos, "Assessment of mitochondrial potential: implications for the correct monitoring of human sperm function," *International Journal of Andrology*, vol. 33, no. 1, pp. e180–e186, 2010.

[31] V. Magdanz, S. Boryshpolets, C. Ridzewski, B. Eckel, and K. Reinhardt, "The motility-based swim-up technique separates bull sperm based on differences in metabolic rates and tail length," *PLoS One*, vol. 14, no. 10, p. e0223576, 2019.

[32] M. Tourmente, P. Villar-Moya, E. Rial, and E. R. Roldan, "Differences in ATP generation via glycolysis and oxidative phosphorylation and relationships with sperm motility in mouse species," *The Journal of Biological Chemistry*, vol. 290, no. 33, pp. 20613–20626, 2015.

[33] S. Vogler, R. Goedde, B. Miterski et al., "Association of a common polymorphism in the promoter of UCP2 with susceptibility to multiple sclerosis," *Journal of Molecular Medicine*, vol. 83, no. 10, pp. 806–811, 2005.

[34] M. Waldeck-Weiermair, R. Malli, S. Naghdi, M. Trenker, M. J. Kahn, and W. F. Graier, "The contribution of UCP2 and UCP3 to mitochondrial Ca^{2+} uptake is differentially determined by the source of supplied Ca^{2+}," *Cell Calcium*, vol. 47, no. 5, pp. 433–440, 2010.

[35] Y. Emre and T. Nubel, "Uncoupling protein UCP2: when mitochondrial activity meets immunity," *FEBS Letters*, vol. 584, no. 8, pp. 1437–1442, 2010.

[36] S. Lee, E. Tak, J. Lee et al., "Mitochondrial H_2O_2 generated from electron transport chain complex I stimulates muscle differentiation," *Cell Research*, vol. 21, no. 5, pp. 817–834, 2011.

[37] L. Yan, J. Liu, S. Wu, S. Zhang, G. Ji, and A. Gu, "Seminal superoxide dismutase activity and its relationship with semen quality and SOD gene polymorphism," *Journal of Assisted Reproduction and Genetics*, vol. 31, no. 5, pp. 549–554, 2014.

[38] G. Ji, A. Gu, Y. Wang et al., "Genetic variants in antioxidant genes are associated with sperm DNA damage and risk of male infertility in a Chinese population," *Free Radical Biology & Medicine*, vol. 52, no. 4, pp. 775–780, 2012.

[39] A. J. Levine, E. Elkhouly, A. T. Diep, E. R. Lee, H. Frankl, and R. W. Haile, "The MnSOD A16V mitochondrial targeting sequence polymorphism is not associated with increased risk of distal colorectal adenomas: data from a sigmoidoscopy-based case control study," *Cancer Epidemiology, Biomarkers & Prevention*, vol. 11, 10 Part 1, pp. 1140-1141, 2002.

[40] H. Tavilani, M. T. Goodarzi, A. Vaisi-raygani, S. Salimi, and T. Hassanzadeh, "Activity of antioxidant enzymes in seminal plasma and their relationship with lipid peroxidation of spermatozoa," *International Braz J Urol*, vol. 34, no. 4, pp. 485–491, 2008.

[41] L. Forsberg, L. Lyrenas, U. de Faire, and R. Morgenstern, "A common functional C-T substitution polymorphism in the promoter region of the human catalase gene influences

transcription factor binding, reporter gene transcription and is correlated to blood catalase levels," *Free Radical Biology & Medicine*, vol. 30, no. 5, pp. 500–505, 2001.

[42] S. Sabouhi, Z. Salehi, M. H. Bahadori, and M. Mahdavi, "Human catalase gene polymorphism (CAT C-262T) and risk of male infertility," *Andrologia*, vol. 47, no. 1, 2015.

[43] L. Rashki Ghaleno, A. Alizadeh, J. R. Drevet, A. Shahverdi, and M. R. Valojerdi, "Oxidation of sperm DNA and male infertility," *Antioxidants (Basel)*, vol. 10, no. 1, 2021.

[44] A. Valavanidis, T. Vlachogianni, and C. Fiotakis, "8-Hydroxy-2'-deoxyguanosine (8-OHdG): a critical biomarker of oxidative stress and carcinogenesis," *Journal of Environmental Science and Health. Part C, Environmental Carcinogenesis & Ecotoxicology Reviews*, vol. 27, no. 2, pp. 120–139, 2009.

[45] S. Gonzalez-Rojo, C. Fernandez-Diez, M. Lombo, and M. P. Herraez, "Distribution of DNA damage in the human sperm nucleus: implications of the architecture of the sperm head," *Asian Journal of Andrology*, vol. 22, no. 4, pp. 401–408, 2020.

[46] R. J. Aitken and H. W. Bakos, "Should we be measuring DNA damage in human spermatozoa? New light on an old question," *Human Reproduction*, vol. 36, no. 5, pp. 1175–1185, 2021.

[47] A. Agarwal, S. Baskaran, M. K. Panner Selvam et al., "Scientific landscape of oxidative stress in male reproductive research: a scientometric study," *Free Radical Biology & Medicine*, vol. 156, pp. 36–44, 2020.

[48] S. W. Kim, B. Kim, J. Mok, E. S. Kim, and J. Park, "Dysregulation of the acrosome formation network by 8-oxoguanine (8-oxoG) in infertile sperm: a case report with advanced techniques," *International Journal of Molecular Sciences*, vol. 22, no. 11, 2021.

[49] T. Kohno, K. Shinmura, M. Tosaka et al., "Genetic polymorphisms and alternative splicing of the hOGG1 gene, that is involved in the repair of 8-hydroxyguanine in damaged DNA," *Oncogene*, vol. 16, no. 25, pp. 3219–3225, 1998.

[50] Y. K. Lee, H. G. Youn, H. J. Wang, and G. Yoon, "Decreased mitochondrial OGG1 expression is linked to mitochondrial defects and delayed hepatoma cell growth," *Molecules and Cells*, vol. 35, no. 6, pp. 489–497, 2013.

[51] P. Lestienne, P. Reynier, M. F. Chretien, I. Penisson-Besnier, Y. Malthiery, and V. Rohmer, "Oligoasthenospermia associated with multiple mitochondrial DNA rearrangements," *Molecular Human Reproduction*, vol. 3, no. 9, pp. 811–814, 1997.

[52] S. H. Kao, H. T. Chao, and Y. H. Wei, "Multiple deletions of mitochondrial DNA are associated with the decline of motility and fertility of human spermatozoa," *Molecular Human Reproduction*, vol. 4, no. 7, pp. 657–666, 1998.

[53] M. O'Connell, N. McClure, and S. E. Lewis, "Mitochondrial DNA deletions and nuclear DNA fragmentation in testicular and epididymal human sperm," *Human Reproduction*, vol. 17, no. 6, pp. 1565–1570, 2002.

[54] E. Carra, D. Sangiorgi, F. Gattuccio, and A. M. Rinaldi, "Male infertility and mitochondrial DNA," *Biochemical and Biophysical Research Communications*, vol. 322, no. 1, pp. 333–339, 2004.

[55] S. Baklouti-Gargouri, M. Ghorbel, A. Ben Mahmoud et al., "Mitochondrial DNA mutations and polymorphisms in asthenospermic infertile men," *Molecular Biology Reports*, vol. 40, no. 8, pp. 4705–4712, 2013.

[56] D. Selvi Rani, A. Vanniarajan, N. J. Gupta, B. Chakravarty, L. Singh, and K. Thangaraj, "A novel missense mutation C11994T in the mitochondrial ND4 gene as a cause of low sperm motility in the Indian subcontinent," *Fertility and Sterility*, vol. 86, no. 6, pp. 1783–1785, 2006.

[57] A. J. Holyoake, I. L. Sin, P. S. Benny, and F. Y. Sin, "Association of a novel human mtDNA ATPase6 mutation with immature sperm cells," *Andrologia*, vol. 31, no. 6, pp. 339–345, 1999.

[58] M. B. Shamsi, R. Kumar, A. Bhatt et al., "Mitochondrial DNA mutations in etiopathogenesis of male infertility," *Indian Journal of Urology*, vol. 24, no. 2, pp. 150–154, 2008.

Hindawi
Oxidative Medicine and Cellular Longevity
Volume 2021, Article ID 5596090, 32 pages
https://doi.org/10.1155/2021/5596090

Research Article

Long-Term Administration of Abacavir and Etravirine Impairs Semen Quality and Alters Redox System and Bone Metabolism in Growing Male Wistar Rats

Agnieszka Matuszewska,[1] **Beata Nowak**,[1] **Wojciech Niżański**,[2] **Maria Eberhardt**,[2] **Kinga Domrazek**,[2,3] **Anna Nikodem**,[4] **Benita Wiatrak**,[1] **Krzysztof Zduniak**,[5] **Kamil Olejnik**,[5] **Anna Merwid-Ląd**,[1] **Tomasz Tomkalski**,[6] **Diana Jędrzejuk**,[7] **Ewa Szeląg**,[8] **Marzenna Podhorska-Okołów**,[9] **Aleksandra Piotrowska**,[10] **Izabela Jęśkowiak**,[1] **Agata Heinrich**,[1] **Maria Rutkowska**,[1] **Wojciech Dziewiszek**,[1] **Tomasz Sozański**,[1] **Joanna Kwiatkowska**,[1] **Paulina Jawień**,[1] **Marek Bolanowski**,[7] **and Adam Szeląg**[1]

[1]*Department of Pharmacology, Wrocław Medical University, Wrocław 50-367, Poland*
[2]*Department of Reproduction and Clinic of Farm Animals, Wrocław University of Environmental and Life Sciences, Wrocław 50-375, Poland*
[3]*Department of Small Animal Diseases and Clinic, Lab of Small Animal Reproduction, Institute of Veterinary Medicine, Warsaw University of Life Sciences, Warsaw 02-787, Poland*
[4]*Department of Mechanics, Materials and Biomedical Engineering, Wrocław University of Science and Technology, Wrocław 50-370, Poland*
[5]*Department of Pathology, Wrocław Medical University, Wrocław 50-367, Poland*
[6]*Department of Endocrinology, Diabetology and Internal Medicine, Tadeusz Marciniak Lower Silesia Specialist Hospital-Centre for Medical Emergency, Wrocław 54-049, Poland*
[7]*Department of Endocrinology, Diabetes and Isotope Therapy, Wrocław Medical University, Wrocław 50-367, Poland*
[8]*Department of Maxillofacial Orthopaedics and Orthodontics, Wrocław Medical University, Wrocław 50-425, Poland*
[9]*Department of Ultrastructure Research, Wrocław Medical University, Wrocław 50-367, Poland*
[10]*Department of Histology and Embryology, Department of Human Morphology and Embryology, Wrocław Medical University, Wrocław 50-367, Poland*

Correspondence should be addressed to Agnieszka Matuszewska; agnieszka.matuszewska@umed.wroc.pl

Received 10 February 2021; Revised 24 May 2021; Accepted 5 July 2021; Published 31 July 2021

Academic Editor: Yi Fang

Highly active antiretroviral therapy (HAART) is used in HIV-infected patients. Alongside the prolongation of patients' life, adverse side effects associated with long-term therapy are becoming an increasing problem. Therefore, optimizing of HAART is extremely important. The study is aimed at evaluating the toxicity of abacavir and etravirine in monotherapy on the reproductive system, liver, kidneys, and bones in young, sexually mature, male rats. Thirty-six 8-week-old male Wistar rats randomized into three 12-animal groups received either normal saline (control), abacavir 60 mg/kg (AB group), or etravirine 40 mg/kg (ET group) once daily for 16 weeks. Semen morphology, oxide–redox state parameters (MDA, SOD, catalase, GPx, glutathione, GSH/GSSG ratio) in tissue homogenates (testes, liver, kidneys), and serum samples were studied. In bones, microcomputed tomography and a four-point bending test were performed. Total sperm count, sperm concentration, motility, and sperm morphology did not differ significantly in AB or ET groups compared to the control. In the flow cytometry of semen, an increased percentage of cells with denatured DNA was noticed for both tested drugs. However, no significant changes of oxide–redox state in testicular

homogenates were found, except of increased SOD activity in the AB-receiving group. Additionally, ET significantly altered catalase and GPx in the liver and SOD activity in kidneys. Abacavir decreased catalase in the liver and GSH levels in kidneys. AB caused significant changes to bone microarchitecture (bone volume fraction, trabecular number, connectivity density, total porosity) and increased Young's modulus. Etravirine had a greater impact on macrometric parameters of bones (tibial index, mid-tibial diameter, femur length). After 4 weeks in the ET group, a lower 1,25-dihydroxyvitamin D_3 serum concentration was found. The results showed that abacavir and etravirine disturb oxidative stress. An increase in the percentage of sperms with chromatin damage suggests decreased fertility in rats receiving the studied drugs. Both drugs affected bone formation in growing rats. Additionally, etravirine disturbed vitamin D metabolism.

1. Introduction

According to the World Health Organization (WHO) statistics, there are about 37.9 million people infected with the human immunodeficiency virus (HIV). Despite increased public awareness, many awareness-raising campaigns, and better health education, there are about 1.7 million new HIV cases every year [1]. Antiretroviral therapy made it possible to decrease the viral load below the sensitivity limit of diagnostic tests, caused an increase in the level of CD4 lymphocytes, and reduced the incidence of opportunistic infections and the development of full-blown acquired immunodeficiency syndrome (AIDS). As a consequence, mortality in HIV patients has decreased significantly [2–4]. However, drug-induced side effects associated with long-term antiretroviral therapy are becoming a growing concern [2, 3, 5]. HIV therapy involves highly active antiretroviral therapy (HAART), meaning that patients are treated with drug combinations. The identification of the numerous adverse effects of a single drug becomes problematic.

The proposed mechanism of toxic action of HAART on testes, sperm, bones, liver, kidneys, and other tissues is complex and not fully understood. In hepatotoxicity, e.g., hypersensitivity with acute hepatic necrosis, metabolic-host mediated injury, or mitochondrial toxicity are postulated. Kidney injury may depend on the action on organic anion transporters in proximal tubules and the accumulation of active drugs in this structure. In many tissues, the imbalance of oxidative stress parameters (pro- and antioxidants) with the resultant oxidation of biomolecules is an important trigger mechanism leading to tissue damage and dysfunction [6–8].

Widespread access to antiretroviral therapy has led many perinatally HIV-infected children to reach adolescence and adulthood [9, 10]. They become sexually active and make decisions about their reproductive health. It is estimated that about 75% of persons who are infected with HIV are in the reproductive period of life [11]. The reproductive system, especially of males, is overly sensitive to many xenobiotics. Drugs are given in a long-term schedule [6]. Iyer et al. reported that HIV status and HAART administration were associated with subfertility both in males and females [12]. In males, HAART was found to impair semen quality [13]. Kehl et al. detected a lower ejaculate volume as well as less slow progressive and more abnormally shaped spermatozoa in HAART-receiving patients [13]. Other authors reported altered mitochondrial DNA and intensified oxidative stress in HAART-receiving males that negatively impact testicular functions [14]. Concentrations of antiretroviral drugs in the seminal plasma vary between drugs. They are the highest for nucleoside analogues and lowest for protease inhibitors. Abacavir and etravirine reach a high concentration in the seminal plasma [15, 16] as they easily cross the blood-testis barrier [16, 17]. On one hand, a high concentration of an antiretroviral drug in the seminal plasma is favorable, because the drug may suppress viral replication in semen and prevent the sexual transmission of the infection. On the other hand, a higher concentration of the drug in testes increases the risk of gonadal toxicity. Most men and women with HIV desire to have children [18]. Therefore, it is extremely important to investigate the effect of drugs given for a long time to young patients on the reproductive system and fertility.

Osteoporosis is a generalized disease of bones with disorders of bone microarchitecture and low bone mass, leading to increased bone fragility [19]. Osteoporosis is a silent disease with a long-lasting symptomless period, and the first clinical symptom is often an osteoporotic fracture [20]. Osteoporotic fractures may be spontaneous or follow a minor trauma. Spine, hip, distal forearm, or rib fractures are the most characteristic for patients with osteoporosis [21, 22]. The occurrence of a bone fracture indicates the advanced stage of the disease, decreases the quality of life, and is the cause of disability and premature death [20, 23]. Therefore, not only the prophylaxis of osteoporosis and osteoporotic fractures but also the recognition of drugs causing osteoporosis seems to be very important.

In HIV patients, the risk of osteoporosis is 3.7 times higher than in the general population [24]. Many studies also suggest a significantly increased risk of fracture in people with HIV [25, 26], reaching 12.8/1,000 people/year [25]. One of the important factors influencing bone metabolism and properties in HIV-positive patients may include the administration of antiretroviral drugs. Retrospective and prospective studies have shown 2%-6% decreases in bone mineral density (BMD) in the first 2 years after the combined antiretroviral therapy started [27]. In children, a reduction in bone mass gain and a decrease in peak bone mass have been observed, resulting in an increased incidence of osteoporosis and bone fractures later in their lives [28, 29].

Abacavir can be used in children from 4 months of age [30] and etravirine in children from 2 years of age [31]. In vitro studies suggested that abacavir and etravirine may affect bone cell differentiation [32]. As antiretroviral drugs are given to humans as part of HAART, it is impossible to assess the testicular toxicity and the influence of a single drug on bone metabolism in humans. Single antiretroviral agents are used in various HAART schedules and are continuously

updated [33–35]. It means that the HAART schedule is not fixed, but changes over time [33–35]. In order to choose the optimal HAART drug combination, the efficacy of drugs and current knowledge about viral mutation and drug resistance is just as important as the adverse effects [36, 37]. The schedule is also personalized due to comorbidities and the risk of drug-drug interactions so the potential for a single agent to cause selective tissue toxicity (not only for drug combinations) may be very important in terms of making clinical decisions [38, 39].

Rats are very often used as the animal experimental model for the assessment of the impact of drugs on the male reproductive system [40–42], bones [43, 44], and as well as for the evaluation of direct tissue toxicity [45, 46]. Laboratory methods and reagents are available for measurements of hormone levels and immunological studies in rats, ensuring repeatability and facilitating the comparison of results. Rat models allow scientists to eliminate some variations observed in human trials (e.g., possibility for monotherapy, homogenous groups, lack of concomitant diseases, identical environmental conditions, and diet). The study was conducted in 8-week-old, young adult, male rats. Male rats are sexually mature at the age of six weeks because they develop rapidly during infancy [47, 48]. The most active growth of male rats is during the first 8 months of life [49]. Therefore, our study was conducted between the 8^{th} and 24^{th} week of their lives.

The aim of this study was to evaluate the influence of long-term abacavir or etravirine monotherapy on testicular toxicity and bones. As hepato- and nephrotoxicity often limit drug usage, the authors also decided to investigate the effect of these drugs on the liver and kidneys.

2. Materials and Methods

2.1. Ethical Statement and Animals. The study was approved by the Local Ethics Committee for Animal Experiments in Wroclaw at the Ludwik Hirszfeld Institute of Immunology and Experimental Therapy of the Polish Academy of Sciences (Approval No. 38/2019). All animal procedures during the study followed the ethical standards and practices of the institution where the study was conducted [50].

Rats were bred and housed at the Animal Laboratory of the Wroclaw Medical University. During the study, animals were housed two per cage with enrichment products (shelters, aspen gnawing sticks, cardboard rolls) with a 24-hour cycle (controlled 12 hours in the light/12 hours in the dark), at an ambient temperature of 22°C, with ventilation, with free access to water, and standard certified animal feed (Altromin 1324, Germany). The feed contained 0.7% calcium, 0.5% phosphorus, and 600 U.I. vitamin D3/kg.

2.2. Study Design. Thirty-six male 8-week-old Wistar rats were randomly divided into three groups (twelve rats each). The groups were organized as follows:

(i) The control group (group C) received a 0.9% saline solution in a volume of 4 ml/kg

(ii) The AB group received abacavir at a dose of 60 mg/kg (Ziagen, Santa Cruz Biotechnology, USA) suspended in a 0.9% saline solution in a volume of 4 ml/kg

(iii) The ET group received etravirine at a dose of 40 mg/kg (Etravirine, Biosynth Carbosynth, UK) suspended in a 0.9% saline solution in a volume of 4 ml/kg

According to the recommended 3Rs rule [50], to minimize the number of animals in the study, the impact of drugs used in monotherapy was evaluated, not the drug combination. The single dose of abacavir and etravirine for rats was calculated according to the recommendations for converting doses from humans to rats [51] (Table 1). Tested antiretroviral drugs and/or normal saline were administered once daily for 16 weeks intragastrically via a gastric tube.

The study design is presented in Figure 1.

After 4 and 8 weeks of the study, blood samples from the tail vein were taken. Eight hours before their blood was taken, the animals were deprived of the feed. Markers of bone turnover must be assessed after a period of fasting. Additionally, to minimize the impact of calcium and vitamin D-containing food on the evaluation these blood parameters, food deprivation was necessary.

After 16 weeks of the study, the rats were anesthetized by intraperitoneal injections of ketamine (60 mg/kg) and xylazine (10 mg/kg), and blood samples were taken via a cardiac puncture. After that, the rats were euthanized by cervical vertebrae dislocation in deep anesthesia. The epididymis, testes, liver, kidneys, and bones (tibia and femur) were dissected immediately and carefully cleaned of surrounding tissues.

Spermatozoa were collected by epididymal slicing with a scalpel blade according to the method used by Martinez-Pastor et al. [52]. Epididymis was dissected from testicles, cleaned of surrounding tissues, and placed on glass Petri dishes containing 1 ml of the HTF medium (Human Tubal Fluid). Multiple incisions of the epididymal cauda were performed to extract sperm cells from tubules. After slicing, Petri dishes were placed on the heating stage for 10-minute incubation. Subsequently, epididymal tissues were removed, and white fluid containing spermatozoa was analyzed.

The testes, liver, kidneys, right tibia, and right femur were weighed and measured. Then, the right testis, right liver lobe, and right kidney were stored at -80°C and later homogenized as described below. The right tibia and right femur were evaluated densitometrically and with microcomputed tomography (mCT). Then, the biomechanical properties of the right femur were measured using a four-point bending test. The left testis, left liver lobe, left kidney, and left tibia were stored in 10% neutral buffered formalin for histopathological examination.

2.3. Serum Parameters. Blood samples were centrifuged at 4,000 g at 4°C for 10 minutes in the MPW-350R laboratory centrifuge (MPW Med. Instruments, Poland). The obtained serum was frozen at -80°C until the proper measurements were made. For the serum, the following parameters were

Table 1: Conversion of a single dose of the tested anti-retroviral drugs from human to rats.

Drug	Human dose	Corresponding rat dose
Abacavir	8 mg/kg-10 mg/kg	49.6 mg/kg-62 mg/kg
Etravirine	5.7 mg/kg-6.7 mg/kg	35.3 mg/kg-41.5 mg/kg

assessed using purchased ELISA kits in accordance with the manufacturers' instructions: luteinizing hormone (LH), follicle-stimulating hormone (FSH), testosterone, sex hormone-binding globulin (SHBG), inhibin B, estradiol, thyroid-stimulating hormone (TSH), prolactin, aminoterminal propeptide of type I procollagen (PINP), osteoclast-derived tartrate-resistant acid phosphatase form 5b (TRACP), sclerostin, Dickkopf-related protein 1 (DKK1), osteoprotegerin (OPG), 25-hydroxyvitamin D (25-OH-D), 1,25-dihydroxyvitamin D_3 (1,25-$(OH)_2$-D_3), parathormone, and aspartate aminotransferase (AST) (Bioassay Technology Laboratory China: Rat Luteinizing Hormone ELISA kit EA0013Ra, Rat Follicle-stimulating Hormone ELISA kit REF E0182Ra, Rat Testosterone ELISA kit REF E0259Ra, Rat Sex Hormone-binding Globulin ELISA kit E0646Ra, Rat Inhibin B ELISA kit REF E0728Ra, Rat Estradiol ELISA kit REF E0174Ra, Thyroid-Stimulating Hormone ELISA kit REF E0180Ra, Rat Prolactin ELISA kit E0190Ra; Immunodiagnostic Systems Limited UK: Rat/Mouse PINP EIA REF AC-33F, Rat TRAPTM ELISA REF SB-TR102; Cloud-Clone Corp. USA: ELISA kit for Sclerostin SEC864Ra; ELISA kit for Dickkopf Related Protein 1 SEA741Ra, ELISA kit for Osteoprotegerin SEA108Ra; Bioassay Technology Laboratory China: Rat 25-hydroxyvitamin D ELISA kit E1445Ra, Rat 1,25-dihydroxyvitamin D_3 ELISA kit E0000Ra; Cloud-Clone Corp. USA: ELISA kit for Parathyroid Hormone CEA866Ra; ELK Biotechnology China: Rat AST ELISA Kit Cat. ELK5635).

Serum total calcium, inorganic phosphorus, and creatinine levels were determined in a certified laboratory using an Alinity C instrument with Abbott (calcium G75615R01 B7P57P; phosphorus G84652R01 B8P40P; creatinine G75642R02 B7P99P).

2.4. Macrometric Parameters. The testes, liver, kidneys, right tibia, and right femur were weighed using the RADWAG AS 60/220/C/2 (Poland) electronic weighing scale. Based on the obtained measurements, the testicular index, hepatic index, renal index, tibial index, and femoral index were calculated according to the following formulas:

$$\text{Testicular index} = \frac{\text{mass of testes [g]}}{\text{body weight [g]}} \times 100\%, \quad (1)$$

$$\text{Hepatic index} = \frac{\text{liver mass [g]}}{\text{body weight [g]}} \times 100\%, \quad (2)$$

$$\text{Renal index} = \frac{\text{mass of kidneys [g]}}{\text{body weight [g]}} \times 100\%, \quad (3)$$

$$\text{Tibial index} = \frac{\text{tibia mass [g]}}{\text{body weight [g]}} \times 100\%, \quad (4)$$

$$\text{Femoral index} = \frac{\text{femur mass [g]}}{\text{body weight [g]}} \times 100\%. \quad (5)$$

Measurements of bone length were made using the electronic calliper with the 0.01 mm resolution (Pro Sp. z o.o., Poland).

2.5. Semen

2.5.1. Spermatozoa Recovery. The epididymis from eight randomly chosen rats in each group was examined. Spermatozoa were collected by epididymal slicing with a scalpel blade according to the method described by Martinez-Pastor et al. [52]. The epididymis was dissected from testicles, cleaned of surrounding tissues, and placed on glass Petri dishes containing 1 ml of the HTF medium (Human Tubal Fluid). Multiple incisions of the epididymal cauda were performed to extract sperm cells from tubules. After slicing, Petri dishes were placed on the heating stage for 10-minute incubation. Subsequently, epididymal tissues were removed, and white fluid containing spermatozoa was analyzed.

2.5.2. Motility Assessment. Subjective motility was determined immediately after removal of the sliced epididymal tissue. A drop (10 μl) of spermatozoa-rich fluid was placed on a glass slide and covered with a cover slide. The evaluation was performed using the phase-contrast microscope (Nikon Eclipse E200; 200× zoom) with a warm stage by two independent researchers, and the mean value was calculated.

2.5.3. Morphology Evaluation. Morphology was assessed after staining with Giemsa stain according to the modified Watson method [53]. Spermatozoa were classified as normal or possessing one of the abnormalities: proximal droplet (%), distal droplet (%), head abnormalities (%), detached head (%), acrosome abnormalities (%), midpiece defects (%), "Dag-like" defect (%), bent tail (%), and coiled tail (%) [54].

2.5.4. Computer-Assisted Sperm Analysis (CASA). The computer-assisted analysis of sperm concentration was performed using HTM IVOS ver. 12.2 (Hamilton Thorne Biosciences, Beverly, MA, USA). The spermatozoa-rich fluid in the amount of 10 μl was suspended in 40 μl of the HTF extender with 50 μl of IDENT Stain (Hamilton Thorne) and incubated for 5 minutes at 37°C before evaluation. The analysis was carried out using IDENT settings (frames: 60; No. of frames: 40; minimum contrast: 30; minimum cell size: 4; cell size: 13; cell intensity: 75) [55].

2.5.5. Assessment of the Function and Structure of Sperm Cells by Flow Cytometry. Sperm cell functionality was evaluated using fluorescent staining and flow cytometry analysis. Flow cytometric analyses were performed on the Guava EasyCyte 5 (Merck KGaA, Darmstadt, Germany) cytometer. The fluorescent probes used in the study were excited by the Argon ion 488 nm laser. Acquisitions were made using GuavaSoft™ 3.1.1 (Merck KGaA, Darmstadt, Germany). Nonsperm events were gated out based on scatter properties and not

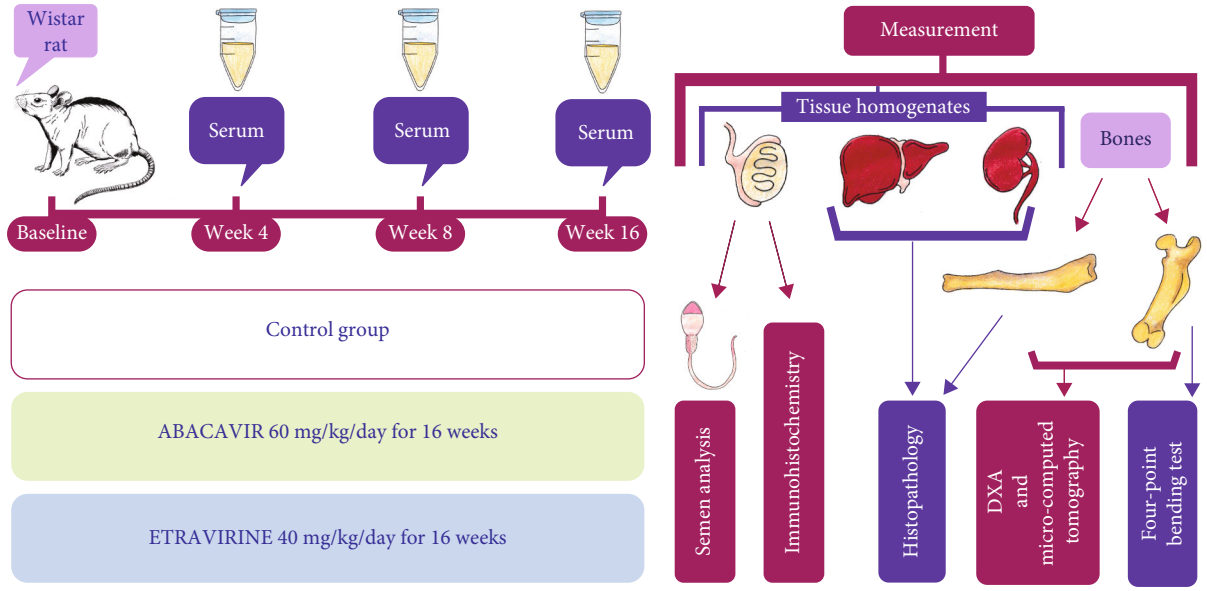

Figure 1: General design of the study.

analyzed. A total of 10,000 events were analyzed for each sample. The following features were assessed: membrane integrity, acrosome integrity, mitochondrial activity, lipid peroxidation, apoptosis and membrane lipid disorder, and chromatin status [55, 56].

The membrane integrity of rat spermatozoa was assessed using SYBR-14 stain combined with propidium iodide (PI) (Life Technologies Ltd., Grand Island, NY, USA). The sperm-rich fluid in the amount of 300 μl was incubated in the dark for 10 minutes with 5 μl of the SYBR-14 working solution (0.1 μl of SYBR14+ 4.9 μl of TRIS III extender). The analysis was performed after 3 minutes of incubation with 3 μl of PI. The spermatozoa with intact membranes emitted green fluorescence. The cells with red fluorescence were classified as dead [56].

Acrosome integrity was assessed by lectin PNA stain from the Arachis hypogaea Alexa Fluor® 488 conjugate (Life Technologies Ltd., Grand Island, NY, USA). Diluted samples were mixed with 10 μl of the PNA working solution (1 μg/ml) and incubated for 5 minutes at room temperature in the dark. Before the analysis, the samples were washed, and 3 μl of PI was added [55].

Mitochondrial activity was determined using the JC-1 dye (Life Technologies Ltd., Grand Island, NY, USA). The spermatozoa-rich fluid in the amount of 500 μl was stained with 0.67 μl of the JC-1 stock solution (3 mM stock solution of JC-1 in DMSO). The samples were incubated for 20 minutes at 37°C in the dark. The sperm cells emitting orange fluorescence were classified as having high mitochondrial activity. The spermatozoa emitting green fluorescence were defined as those with low mitochondrial activity [55].

Lipid peroxidation (LPO) was evaluated by dyeing using the C_{11}-BODIPY$^{581/591}$ fluorescent lipid probe (Life Technologies Ltd., Grand Island, NY, USA). One μl of 2 mM C_{11}-BODIPY$^{581/591}$ in ethanol was added to a diluted sperm-rich fluid and incubated for 30 minutes at 37°C in the dark. Subsequently, centrifugation at 500 × g for 3 minutes was performed, and the sperm pellets were resuspended in 500 μl of the HTF extender. To determine viability, the spermatozoa were stained with PI and incubated for 5 minutes at room temperature. The sperm cells emitting orange fluorescence (nonoxidized state of C_{11}-BODIPY$^{581/591}$) were defined as live cells without LPO [55].

Apoptosis and membrane lipid disorder were evaluated with the YO-PRO-1 dye (25 μM solution in DMSO) (Life Technologies Ltd., Grand Island, NY, USA) [48]. One μl of YO-PRO-1 stain (final concentration: 25 nM) was added to 1 ml of a diluted spermatozoa-rich fluid (500 μl of HTF and 500 μl of spermatozoa solution). After 10-minute incubation, 3 μl of PI was added before cytometric analysis. The cells showing green fluorescence were classified as YO-PRO-1 positive. The spermatozoa that remained unstained were categorized as living population [56].

Chromatin status was established using the acridine orange dye (AO, Life Technologies Ltd., Grand Island, NY, USA). The spermatozoa-rich solution (100 μl) was subjected to brief acid denaturation by adding 200 μl of the lysis solution (Triton X-100 0.1% (v/v), NaCl 0.15 M, HCl 0.08 M, pH 1.4). After 30 seconds, 600 μl of the AO solution (6 μg AO/ml in a buffer: citric acid 0.1 M, Na_2HPO_4 0.2 M, EDTA 1 mM, NaCl 0.15 M, pH 6) was added. The analysis was performed after 3 minutes of incubation. The spermatozoa with high DNA stainability emitted green fluorescence (HDS). The sperm cells emitting red fluorescence were considered a population of cells characterized by a high DNA fragmentation index (DFI) [55].

2.6. Tissue Homogenates

2.6.1. Reproductive Hormones in Tissue Homogenates. In testicular homogenates, testosterone, estradiol, and inhibin B concentrations were evaluated using ELISA kits: Rat

Testosterone ELISA REF E0259Ra, Bioassay Technology Laboratory; Rat Estradiol ELISA Kit REF E0174Ra, Bioassay Technology Laboratory; Rat Inhibin B ELISA kit REF E0728Ra Bioassay Technology Laboratory; China.

2.6.2. Preparation of Tissue Homogenates for Sex Hormone Assessment. To 160 mg of testis tissue, 800 μl of the cooled (-20°C) methanol: propanol (1 : 1) mixture was added. The Pro250 homogenizer (PRO Scientific Inc., Oxford, CT, USA) was used. After homogenization, the samples were centrifuged for 10 minutes at 15,000 × g, and the supernatant was collected.

2.6.3. Redox Status in Tissue Homogenates (Figure 2). Oxide–redox state parameters such as malondialdehyde (MDA), superoxide dismutase (SOD), catalase, glutathione peroxidase (GPx), and glutathione were assessed in homogenates from the testes, liver, and kidneys. The following kits, Rat Malondialdehyde ELISA Kit E0156Ra, Bioassay Technology Laboratory China; Superoxide Dismutase Assay Kit No 706002, Cayman; Catalase Assay Kit No 707002, Cayman; Glutathione Peroxidase Assay Kit No 703102, Cayman; Glutathione Assay Kit No 703002, Cayman; USA, were used.

2.6.4. Preparation of Tissue Homogenates for Redox State Assessment. The MDA concentration was measured in the homogenates that were prepared in the same way as for measurements of reproductive hormones. The oxide–redox state was assessed from the tissues of the liver, kidney, and testes. For all tested parameters, the tissues were prepared in the buffers recommended by the manufacturer at a concentration of 10%. Superoxide dismutase activity was assessed in a tissue solution in the 20 mM HEPES buffer, pH 7.0, supplemented by 1 mM EDTA, 210 mM mannitol, and 70 mM sucrose. Catalase activity was evaluated in the homogenates prepared in 50 mM potassium phosphate, pH 7.0, containing 1 mM EDTA. Glutathione peroxidase activity in the tissues was measured in the 50 mM Tris-HCl, pH 7.5, 5 mM EDTA, and 1 mM DTT solution. The last parameter—glutathione—was analyzed in the same homogenate solution as the one prepared to evaluate catalase activity. In the latter case, after collecting the supernatant, 0.1 g/ml of MPA was added for 5 minutes at room temperature; then, the samples were centrifuged again at >2,000 g for at least two minutes, and the collected supernatant was stored at -20°C until assayed. The other centrifugation supernatants were stored at -80°C until assayed.

2.6.5. Immunohistochemical Examination (IHC) of Testes. Slides were deparaffined and rehydrated, and antigen retrieval was carried out by boiling the sections in EnVision FLEX Target Retrieval Solution pH 9 using a PTLink-20 minutes, 97°C (Dako, Glostrup, Denmark). The visualization of the studied antigen was performed using the EnVision FLEX+, Mouse, High pH System (Dako) according to the manufacturer's instructions. The detection of the minichromosome maintenance 7 protein (MCM-7) antigen (1 : 50, Leica Novocastra, Wetzlar, Germany) and the glutathione antigen (1 : 100, Abcam, Cambridge, UK) was conducted for 20 minutes at room temperature. Then, slides were incubated with secondary antibodies conjugated with horseradish peroxidase (EnVision FLEX/HRP-20 minutes at room temperature). Finally, the sections were counterstained with EnVision FLEX Hematoxylin (Dako) dehydrated in graded ethanol concentrations (70%, 96%, 99.8%) and in xylene and closed in Dako Mounting Medium (Dako). The primary antibody was diluted in the EnVision FLEX Antibody Diluent background-reducing reagent (Dako).

2.6.6. Expression of Minichromosome Maintenance 7 Protein (MCM-7). The IHC of MCM-7 sections of testes was evaluated in a blinded way under the BX-41 light microscope (Olympus, Tokyo, Japan). For the evaluation of MCM-7-positive cells, three fields with the highest number of cells showing a positive reaction were selected. The evaluation was performed by counting brown-labeled nuclei at ×400 magnification. The percentage of positive cells in each field was assessed according to the following formula: (positive cells/all cells) × 100%.

2.6.7. Expression of Glutathione in IHC in Testes. For the evaluation of the cytoplasmic expression of glutathione levels, the semiquantitative method—immunoreactive score (IRS) according to Remmele and Stegner [57–59]—was applied, and samples were evaluated in the blinded way. The scale is based on the percentage of cells showing a positive reaction (0 points—no cells with a positive reaction; 1 point—1-10% cells with a positive reaction; 2 points—11-50%; 3 points—51-80%; 4 points—>80% cells) as well as on the intensity of the reaction color (0—no reaction; 1—weak; 2—moderate; 3—strong). The IRS final score is the result of multiplying the score obtained from the percentage of cells with a positive reaction by the score of the reaction intensity and is in the range of 0-12 [57–59].

2.6.8. Liver and Renal Histology. The liver and kidneys were fixed in 10% neutral buffered formalin. The dehydration process was then performed using graduated concentrations of ethanol and ethanol-xylene. The final solution was pure xylene. The tissue was infiltrated with appropriate purified paraffin. From the fixed liver and kidney tissues in paraffin, slices 4 μm thick were cut with a microtome and standard stained with hematoxylin and eosin. The preparations were assessed under the Olympus BX50 light microscope equipped with the Zeiss Axiocam 208 color microscope camera using Labscope.

2.6.9. Dual-Energy X-Ray Absorptiometry (DXA). The right tibia and right femur were examined densitometrically. The tests were performed on Hologic DXA equipment (Hologic Discovery W 81507, Marlborough, USA) using software for small animals. The scanner was calibrated daily with the phantom supplied by the manufacturer. Bone mineral density (BMD) results were obtained as grams of mineral content per square of bone area (g/cm^2) [60].

2.6.10. Micro-X-Ray Computed Tomography. Structural properties were measured using the SkyScan 1172, Bruker® computed microtomograph. Each sample was registered with a resolution of 9 μm, a voltage of 74 kV at 133 μA, using a

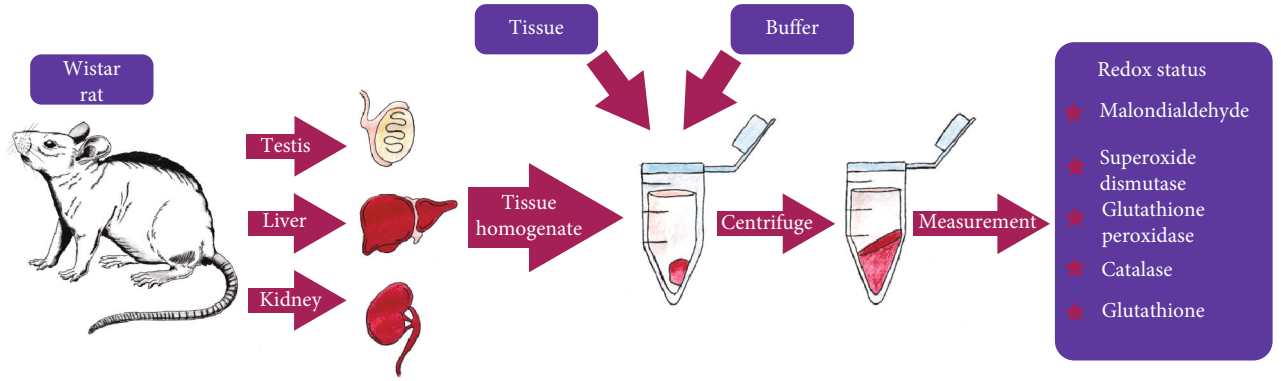

Figure 2: General diagram of tissue homogenate preparation for redox state measurements.

0.5 mm Al filter. 3D structural properties were measured using CTAn (CTAn, Bruker). For each long bone (tibia and femur), measures were taken for 2 areas: the cancellous bone and cortical bone.

Before 3D morphometric analyses, the images were aligned with the major bone axis, and a set of trabecular and cortical regions of interest (ROIs) was selected. The selection of ROIs (Figure 3) was based on the commonly accepted procedure used for small animals [61–63]. It was carried out in the CTAn programme (Bruker®) based on an automated algorithm prepared in accordance with the MCT-003 method note [64]. The growth plate was used as an anatomical referent to determine trabecular and cortical regions used in the estimation of 3D structural properties. To select the location of the trabecular region, an offset of 100 slices from the growth plate towards the metaphysis, where the trabecular ROI starts, was applied. In other words, an offset is a number of cross-sections between the growth plate and the start of the trabecular ROI. From this location, an extent of 400 slices defines the trabecular volume of interest (VOI). At a resolution of 9 μm, this number of slices corresponds to the region of approximately 3.5 mm in height. The next offset of 100 slices separates the trabecular ROI and cortical ROI. For the measurements, the cortical ROI was defined as 100 slices that correspond to approximately 0.9 mm. Within each ROI, the automatic selection of a specific bone was applied, and then the images were segmented using an adaptive global threshold algorithm. The quantitative analysis (CTAn, Bruker®) of the cancellous bone structure considered bone volume fraction (BV/TV), bone surface density (BS/TV), specific bone surface (BS/BV), trabecular thickness (Tb.Th), number (Tb.N) and separation (Tb.Sp) of trabeculae, structure model index (SMI), connectivity density (Conn.D), total porosity (Po.tot), and degree of anisotropy (DA).

For the cortical bone, the analysis involved the determination of average cortical thickness (Ct.Th), total cross-sectional area inside the periosteal envelope (Tt.Ar), cortical bone area (Ct.Ar), and cortical area fraction (Ct.Ar/Tt.Ar).

2.6.11. Bone Histology. The histomorphometric examination of the tibia was performed in line with the 2012 update of the standardized nomenclature, symbols, and units for bone histomorphometry [65].

The left tibiae of the rats were fixed in 10% neutral buffered formalin and later decalcified in the 10% neutral buffered EDTA solution. The EDTA solution was changed once after 24 hours. The metaphyseal and epiphyseal regions of the proximal tibia were harvested, embedded in paraffin, and cut into 5 μm thick slides. The slides were stained using the standard hematoxylin and eosin method and scanned using the Hamamatsu NanoZoomer 2.0 histological slide scanner and NDP.scan SQ 1.0. Finally, each sample was exported to a TIFF file.

The TIFF file was analyzed with ImageJ 1.52. Every image was briefly segmented, and the total trabecular area (B.Ar) and trabecular perimeter (B.Pm) were measured.

The bone volume to tissue volume ratio (BV/TV) was calculated as B.Ar/T.Ar. Next, the bone surface to tissue volume ratio (BS/TV) was calculated as B.Pm/T.Ar×1.2 and the BS/BV ratio as BS/TV×BV/TV. Mean trabecular thickness (Tb. Th) was calculated as 2/BS/BV.

2.6.12. Mechanical Tests. Mechanical properties were assessed using a four-point bending test with the MTS 858 MiniBionix machine (Eden Prairie, MN, USA) (Figure 4). In order to determine bend strength, each femoral epiphysis was fixed in aluminium alloy sleeves and embedded with the Duracryl™ Plus self-polymerised acrylic (SpofaDental, Jicin, Czech Republic). In the four-point bending test, the load was applied to the upper prisms. The spacing of the upper prisms was equal to 54 mm, and the distance between the lower support points was 24 mm. The loading speed during bending was 1 mm/min. The mechanical tests carried out in the four-point bending test led to the determination of three mechanical parameters: Young's modulus, bend strength, and bending stiffness. The values of the mechanical parameters were determined using classical formulas [66].

To calculate Young's modulus, the cross-section area of the femur sample needs to be measured. The area of each sample was determined at the point where the sample broke by finding the smallest ellipse that outlines the sample and calculating its area. The area was calculated using the measurements of the length of the ellipse's axis

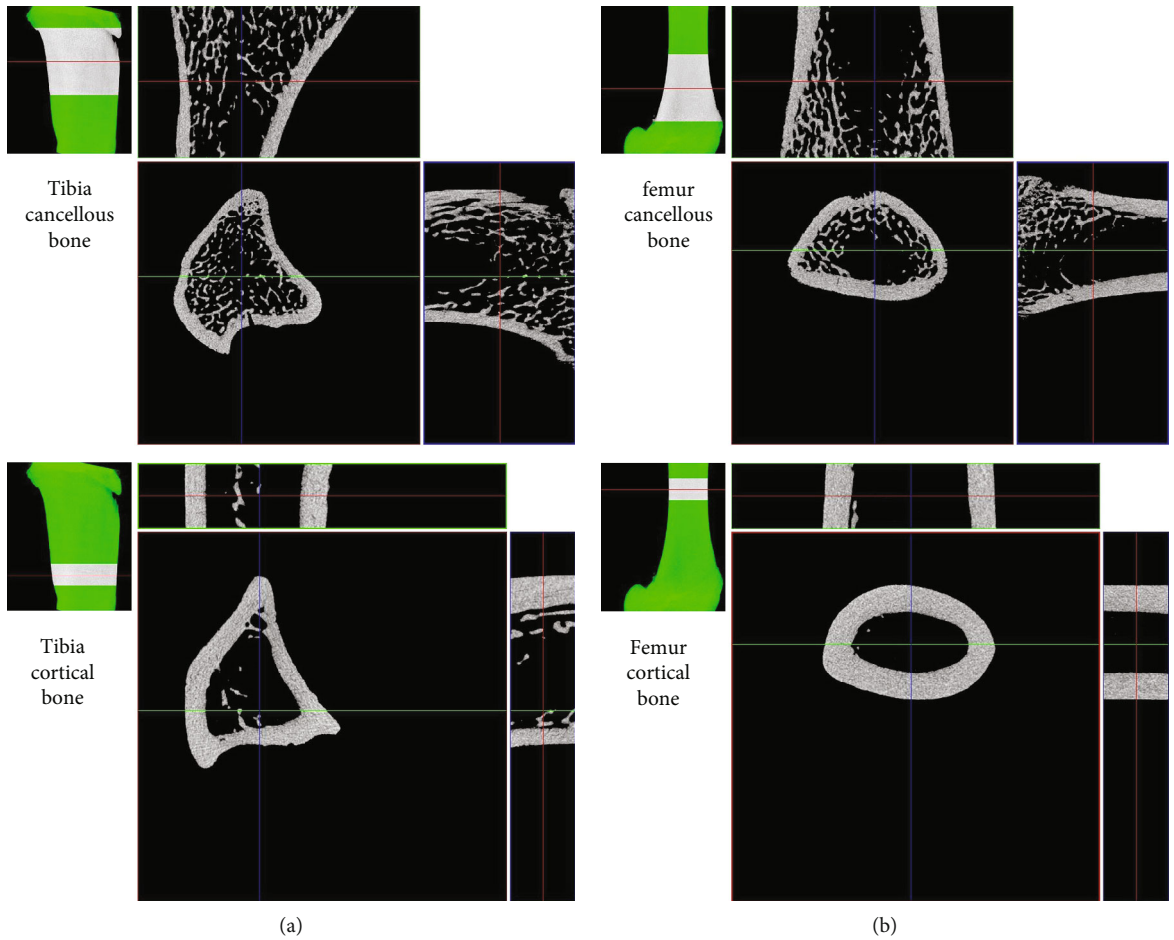

Figure 3: Choice of the region of interest (ROI) for measurements in the cancellous and cortical bone of (a) the proximal metaphysis of the tibia and (b) the distal metaphysis of the femur.

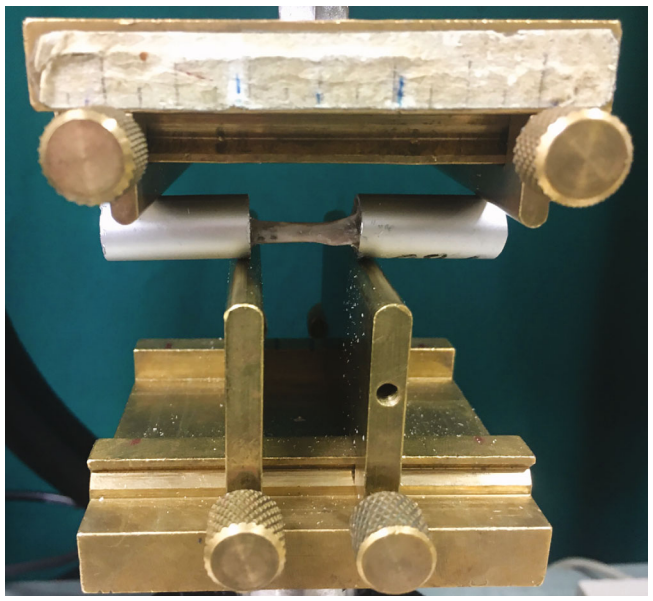

Figure 4: Measuring system for testing the mechanical properties of the femurs in the four-point bending test.

with the Zeiss Stereo Discovery V20, Germany stereo microscope.

2.6.13. Statistical Analysis. Due to the lack of a normal distribution of the results for all examined parameters, the statistical analysis was performed with nonparametric tests (ANOVA Kruskal-Wallis and the appropriate posthoc test). The statistical analysis was performed in Statistica v.13. The significance level was $p \leq 0.05$. All results are presented as the median (lower quartile–upper quartile).

3. Results

3.1. Body Weight. On the first day of the study, the control group, the AB group, and the ET group did not differ significantly in body weight. Similarly, no differences in body weight were observed between the groups during the entire study period (Figure 5).

3.2. Macrometric Parameters. The results are presented in Table 2. The weight of testes and the testicular index as well as the weight of the kidney and the renal index did not differ from the control group in the AB or ET group. The hepatic index was significantly higher in the ET group when

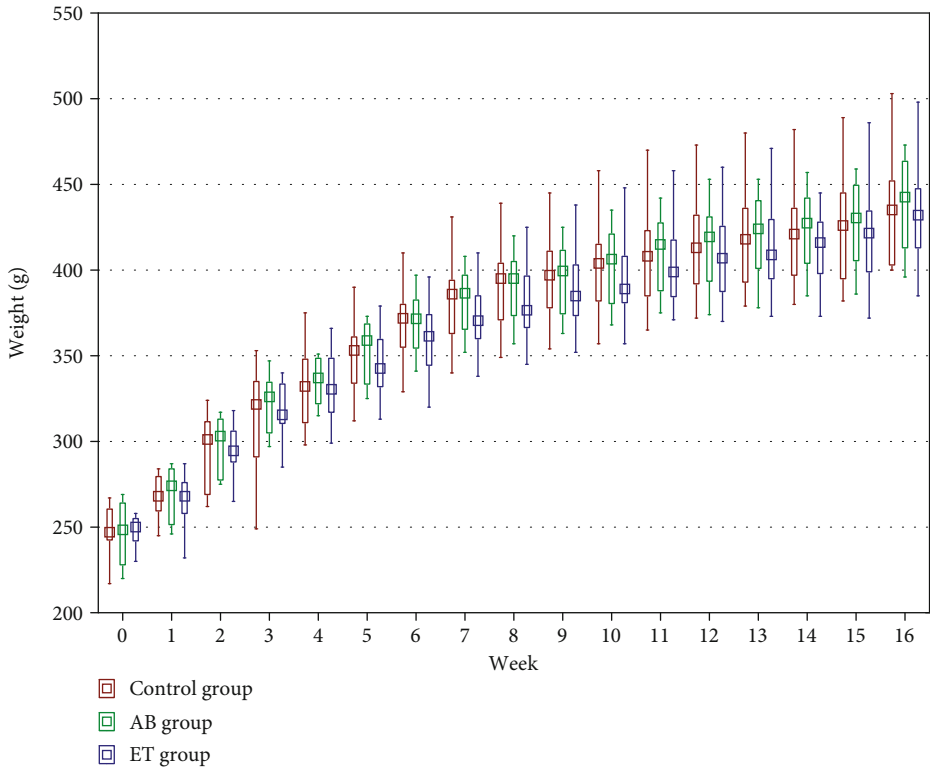

Figure 5: Effect of abacavir and etravirine administration on body weight. No significant difference between the analyzed groups was detected.

Table 2: Effect of 16-week administration of abacavir and etravirine on macrometric parameters (AB group: group receiving abacavir 60 mg/kg for 16 weeks; ET group: group receiving etravirine 40 mg/kg for 16 weeks). Results presented as median (lower quartile–upper quartile); ^AB group vs. control group, $p \leq 0.05$; *ET group vs. control group, $p \leq 0.05$.

	Control group	AB group	ET group
Weight of testis [g]	1.736 (1.459-1.895)	1.742 (1.644-1.854)	1.706 (1.570-1.797)
Testicular index [%]	0.790 (0.677-0.876)	0.775 (0.739-0.857)	0.781 (0.679-0.831)
Weight of liver [g]	10.49 (9.96-11.03)	11.13 (10.75-11.93)	11.21 (10.92-12.00)
Hepatic index [%]	2.405 (2.310-2.503)	2.598 (2.500-2.664)	2.680 (2.469-2.788)*
Weight of kidney [g]	1.275 (1.147-1.425)	1.311 (1.192-1.398)	1.264 (1.207-1.357)
Renal index [%]	0.578 (0.532-0.618)	0.591 (0.571-0.605)	0.599 (0.537-0.645)
Tibia weight [g]	0.787 (0.753-0.841)	0.827 (0.792-0.840)	0.830 (0.820-0.873)
Tibial index [%]	0.183 (0.174-0.192)	0.183 (0.178-0.197)	0.195 (0.184-0.210)*
Tibia length [mm]	41.73 (41.38-42.45)	41.94 (41.74-42.38)	41.82 (41.27-42.52)
Mid-tibial diameter [mm]	2.47 (2.43-2.52)	2.54 (2.41-2.67)	2.61 (2.55-2.66)*
Femur weight [g]	1.151 (1.131-1.173)	1.151 (1.095-1.178)	1.150 (1.096-1.189)
Femoral index [%]	0.265 (0.253-0.271)	0.255 (0.247-0.273)	0.271 (0.255-0.281)
Femur length [mm]	38.24 (37.65-38.62)	37.88 (37.72-38.65)	37.64 (37.34-38.18)*
Mid-femoral diameter [mm]	3.485 (3.36-3.53)	3.505 (3.435-3.630)	3.59 (3.51-3.68)

compared to the control group. At the same time, the weight of the liver did not differ significantly between the AB or ET groups and the control group.

The group receiving etravirine for 16 weeks had a significantly greater tibial index, a greater diameter of the tibia, and a lower femur length than in the control group. In the group receiving abacavir at the end of the study, no differences in bone macrometric parameters were found.

3.3. Reproductive Hormones. The levels of reproductive hormones in serum and testicular homogenates are presented in Table 3. In the group receiving etravirine, only LH serum

Table 3: Effect of 16-week administration of abacavir and etravirine on levels of reproductive hormones in serum and in testicular homogenates (AB group: group receiving abacavir 60 mg/kg for 16 weeks; ET group: group receiving etravirine 40 mg/kg for 16 weeks; LH: luteinising hormone; FSH: follicle-stimulating hormone; SHBG: sex hormone-binding globulin; TSH: thyroid-stimulating hormone. Results presented as median (lower quartile–upper quartile); ^AB group vs. control group, $p \leq 0.05$; *ET group vs. control group, $p \leq 0.05$).

		Control group	AB group	ET group
Week 8 serum	LH [mIU/ml]	4.93 (4.39-5.64)	4.60 (3.52-5.38)	3.99 (3.83-4.48)*
	FSH [mIU/ml]	2.09 (1.95-2.31)	2.05 (1.83-2.23)	2.25 (2.13-2.36)
	Testosterone [ng/l]	104.1 (93.5-109.0)	98.1 (88.4-104.6)	105.7 (94.0-112.7)
	Estradiol [ng/l]	33.6 (32.6-36.3)	33.8 (32.2-36.2)	33.3 (31.4-35.6)
	SHBG [ng/ml]	1.52 (1.26-1.67)	1.26 (1.09-1.67)	1.31 (1.09-1.52)
Week 16 serum	LH [mIU/ml]	4.0 (3.54-4.42)	3.30 (3.13-3.40)	4.12 (3.33-4.25)
	FSH [mIU/ml]	1.94 (1.73-2.08)	1.89 (1.62-2.15)	1.92 (1.51-2.22)
	Testosterone [ng/l]	99.8 (91.0-113.3)	97.6 (88.7-107.3)	100.3 (91.7-104.9)
	Estradiol [ng/l]	31.5 (28.0-35.8)	32.0 (29.5-33.1)	33.0 (30.7-34.6)
	Inhibin B [ng/l]	27.2 (17.7-28.8)	26.8 (22.2-33.7)	26.3 (21.7-29.2)
	SHBG [ng/ml]	1.35 (1.26-1.61)	1.39 (1.22-1.64)	1.24 (1.13-1.51)
	Prolactin [ng/ml]	8.18 (5.82-9.23)	7.62 (6.13-8.07)	6.77 (6.21-8.41)
	TSH [mIU/ml]	1.68 (1.42-2.06)	1.96 (1.56-2.05)	1.76 (1.57-1.95)
Week 16 testicular homogenates	Testosterone [ng/l]	71.1 (68.8-74.1)	76.6 (72.4-84.1)	82.9 (72.7-94.1)
	Estradiol [ng/l]	173.9 (169.0-185.0)	194.4 (164.1-208.7)	192.6 (172.0-205.4)
	Inhibin B [ng/l]	54.6 (43.5-57.1)	59.5 (50.7-64.8)	52.7 (47.0-58.4)

levels were significantly lower after 8 weeks of the study compared to the control group.

3.4. Minichromosome Maintenance 7 Protein. The immunohistochemical examination revealed an increased expression of minichromosome maintenance 7 protein in the ET group compared to the control group (36.4 (35.3-37.8) % vs. 33.7 (32.8-35.5) %, $p \leq 0.05$). No significant difference between the abacavir-receiving animals (31.7 (30.3-34.5) %) and the control group was found. The representative photos of the immunohistochemical evaluation are shown in Figure 6.

3.5. Semen Analysis. The results are presented in Table 4. Neither abacavir nor etravirine administration impacted total sperm count, sperm concentration, subjective motility, or sperm morphology. In the flow cytometry of semen, the percentage of cells with denatured DNA was found to be significantly greater in both study groups (AB and ET) than in the control group.

3.6. Redox Status. In testicular homogenates, significantly higher SOD activity was noticed only in the AB-receiving group compared to the control rats. Etravirine did not affect SOD activity. Catalase and GPx activities and MDA and GSH levels, as well as the GSH/GSSG ratio in both AB and ET groups, were comparable to the control (Figure 7). In the immunohistochemical examination of testicular glutathione expression, no differences were revealed between the studied and control group. Representative slides are shown in Figure 8.

In liver homogenates, catalase activity significantly decreased in both studied groups (AB and ET) compared to the control group. Additionally, etravirine significantly decreased GPx activity at all time points under consideration (Figure 9).

Abacavir decreased GSH levels in kidney homogenates, with the difference being significant at four out of the six analyzed time points. However, it did not affect the GSH/GSSG ratio. Significant differences in the GSSG concentration at single time points for AB and ET (in the 10^{th}, 15^{th} and 25^{th} minutes, respectively) were noticed. In the etravirine-receiving group, SOD activity in the kidney was significantly lower (Figure 10).

3.7. Liver and Renal Histology. There were no histopathological changes in the kidneys and liver in the analyzed preparations. The structure of the glomeruli and renal tubules was normal. Hepatocytes and the portal area (hepatic artery, portal vein, and bile duct) were anatomically normal. Sample images are shown in Figure 11.

3.8. Bone Metabolism. The results are presented in Table 5. A significant decrease in serum PINP, TRACP, and sclerostin levels between week 4 and week 16 was observed in all analyzed groups. Additionally, a decrease in serum DKK1 levels between week 4 and week 16 in the control group and in the ET group was identified. DKK1 levels were not significantly changed between week 4 and week 16 in the AB group. After 16 weeks of the study, the concentration of the Dickkopf-related protein was higher in the AB group than in the control group.

After 4 weeks of the study, the concentration of 1,25-dihydroxyvitamin D_3 in rats receiving etravirine was lower than in the control group. After 16 weeks, creatinine levels were lower in the ET group, whereas aspartate aminotransferase activity was significantly higher in the AB group.

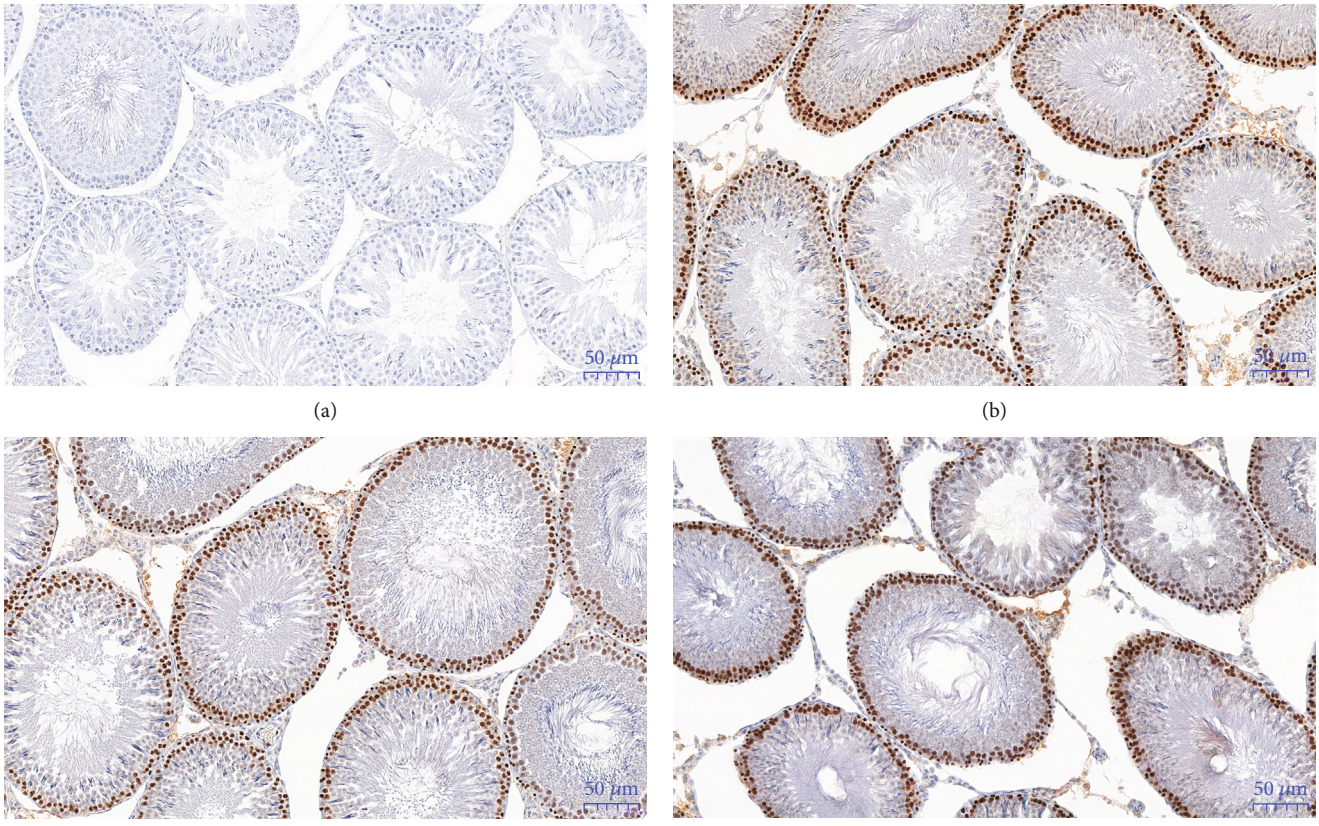

Figure 6: Representative slides of the expression of the MCM-7 protein in the immunohistochemical examination of testes: negative control (a), in the control group (b), the group receiving abacavir (c), and the group receiving etravirine (d). ×20 magnification.

3.9. Bone Mineral Density. The results are presented in Table 6. After 16-week treatment with the analyzed drugs and/or normal saline, no statistically significant differences in tibial or femoral bone mineral density were observed between the groups.

3.10. Bone Histology. The histomorphometric parameters analyzed in longitudinal sections of paraffin-embedded tibiae are presented in Table 7. Bone volume fraction (BV/TV) and the bone surface/tissue volume (BS/TV) ratio were significantly higher in the abacavir-receiving group compared to the control group. No difference in trabecular thickness (Tb.Th) and BS/BV was detected between the AB and control groups. No significant impact of etravirine on tibial histomorphometric parameters was found.

3.11. Micro-X-Ray Computed Tomography. The bone morphology results vary between the tibia and femur. The results of mCT are presented in Table 8. Sample mCT scans are shown in Figure 12. No significant differences were observed for tibial and femoral Ct.Ar between the studied groups. Cortical thickness (Cr.Th) was also comparable between all three groups in both analysed localizations. The analysis of the tibial cancellous bone revealed an increase in bone volume fraction (BV/TV) for the abacavir-receiving group. Additionally, abacavir led to a higher trabecular number (Tb.N) and connectivity density (Conn.D) along with lower total porosity (Po.tot) of the tibial cancellous bone. No significant differences were observed for the femoral cancellous bone between the analyzed groups.

3.12. Mechanical Properties of Femurs. The results are given in Figure 13. In the four-point bending test, increased Young's modulus in abacavir-receiving animals was observed compared to the untreated ones. No effect of etravirine on Young's modulus was found. No statistically significant differences were found between the groups in terms of flexural strength and stiffness.

4. Discussion

Abnormalities in testicular and epididymal morphology, sperm morphology and motility, and oxidative stress disturbances caused by HIV infection and HAART therapy may directly affect male fertility. In animal studies, HAART therapy may influence plasma levels of sex hormones, such as testosterone, prolactin, LH, or FSH [67, 68]. HAART also caused decreased sperm count, motility, viability, and amount of sperm with normal morphology together with atrophy of seminiferous tubules and depletion of spermatogenic cells, especially of secondary spermatocytes [68, 69]. HAART had a negative effect on the frequencies and latencies of various sexual behaviour parameters in male rats

Table 4: Effect of 16-week administration of abacavir and etravirine on semen parameters (AB group: group receiving abacavir 60 mg/kg for 16 weeks; ET group: group receiving etravirine 40 mg/kg for 16 weeks; DFI: DNA fragmentation index; HDS: high DNA stainability. Results presented as median (lower quartile–upper quartile); ^abacavir vs. control group, $p \leq 0.05$; *etravirine vs. control group, $p \leq 0.05$).

		Control group	AB group	ET group
Total sperm count [mln]		58.9 (40.7-87.6)	64.2 (54.4-84.1)	63.8 (42.8-75.6)
Sperm concentration [mln/ml]		73.7 (50.8-109.5)	80.3 (68.0-102.1)	79.8 (53.5-94.6)
Subjective motility [%]		57.5 (55-65)	62.5 (50-65)	62.5 (52.5-65)
Sperm morphology	Morphologically normal [%]	93.0 (87.2-93.2)	88.6 (87.2-92.2)	92.9 (83.6-96.1)
	Proximal droplet [%]	0 (0-0)	0 (0-0)	0 (0-0)
	Distal droplet [%]	0.75 (0-0.75)	0.62 (0.25-1.50)	0.5 (0.37-0.75)
	Head abnormalities [%]	0 (0-0)	0 (0-0.25)	0 (0-0.37)
	Detached head [%]	2.5 (2-3)	2.87 (2.5-3.5)	1.87 (1.0-4.37)
	Acrosome abnormalities [%]	0 (0-0)	0 (0-0)	0 (0-0)
	Midpiece defects [%]	2.25 (1-6.2)	5.5 (2.2-6.2)	2.12 (0.87-7.5)
	"Dag-like" defect [%]	0 (0-0)	0 (0-0)	0 (0-0)
	Bent tail [%]	2 (1-2.7)	1.6 (1.2-3.0)	1.1 (0.37-3.0)
	Coiled tail [%]	0 (0-0)	0 (0-0)	0 (0-0)
Plasma membrane and acrosome integrity	Live cells with intact acrosome [%]	39.7 (33.9-45.2)	42.3 (32.3-44.9)	44.5 (40.8-50.2)
	Live cells with ruptured acrosome [%]	0.23 (0.1-0.23)	0.17 (0.12-0.31)	0.15 (0.12-0.24)
	Dead cells with intact acrosome [%]	58.9 (52.3-63.7)	56.0 (53.5-66.5)	54.0 (47.9-57.2)
	Dead cells with ruptured acrosome [%]	2.09 (1.28-2.19)	1.57 (1.25-2.05)	1.60 (0.87-2.34)
Mitochondrial activity	High mitochondrial activity [%]	6.54 (5.68-7.85)	3.20 (1.71-5.17)	3.25 (1.94-4.72)
	Low mitochondrial activity [%]	93.5 (92.1-94.3)	96.8 (94.8-98.3)	96.7 (95.3-98.0)
Lipid peroxidation	Live without LPO [%]	23.3 (20.0-25.7)	24.7 (22.5-27.3)	24.7 (22.5-27.3)
	Live with LPO [%]	0.06 (0.03-0.21)	0.05 (0.03-0.16)	0.05 (0.03-0.16)
	Dead without LPO [%]	75.7 (73.7-78.2)	74.5 (72.1-76.4)	74.5 (72.1-76.4)
	Dead with LPO [%]	0.79 (0.57-0.82)	0.68 (0.51-1.15)	0.68 (0.51-1.15)
Apoptosis and necrosis	Live cells [%]	42.6 (31.0-44.2)	48.8 (45.7-51.9)	54.3 (41.0-60.3)
	Dead cells [%]	55.1 (54.5-65.5)	48.5 (45.4-51.0)	43.3 (38.4-55.2)
	Apoptotic and necrotic cells [%]	1.64 (1.28-2.09)	1.85 (1.72-2.27)	2.20 (1.33-4.56)
	Apoptotic cells [%]	0.61 (0.07-0.82)	0.75 (0.12-1.25)	0.06 (0.02-0.12)
Chromatin status	DFI [%]	0.85 (0.61-1.00)	1.56 (1.18-2.00)^	1.41 (1.17 – 2.03) *
	HDS [%]	18.5 (10.5-20.5)	8.0 (6.5-12.1)	12.1 (11.6-18.6)

and impaired their fertility with a reduced number of offspring of male HAART-receiving rodents [68, 70].

In the current study, the impact of abacavir and etravirine in male rats on reproductive toxicity was evaluated. The paper assessed the hormonal status in serum after 8 and 16 weeks of drug administration and basic morphological parameters of testes and epididymis, as well as semen morphology and viability, oxidative stress parameters, and antioxidant activity.

After 8 weeks of etravirine administration, a temporary decrease in serum LH levels was observed. After 16 weeks, serum luteinizing hormone levels were lower in the AB group than in the control group. As there was no significant difference in serum testosterone levels between all the analyzed groups, it cannot be excluded that changes in LH levels observed in this study were associated with the pulsative release of LH [71].

Oxidative stress has been reported to be one of the most important causes of male infertility, but not the only one [72]. The pathological concentration of reactive oxygen species (ROS) leads to excessive lipid peroxidation, DNA damage, and cellular apoptosis [73]. In the male reproductive system, the proper balance between oxidative stress and antioxidant systems is particularly important because ROS in low concentrations are necessary for physiological sperm functions such as spermatogenesis, capacitation, acrosome reaction, motility of sperm flagella, or fertilization. Excessive oxidative stress resulting from imbalances between

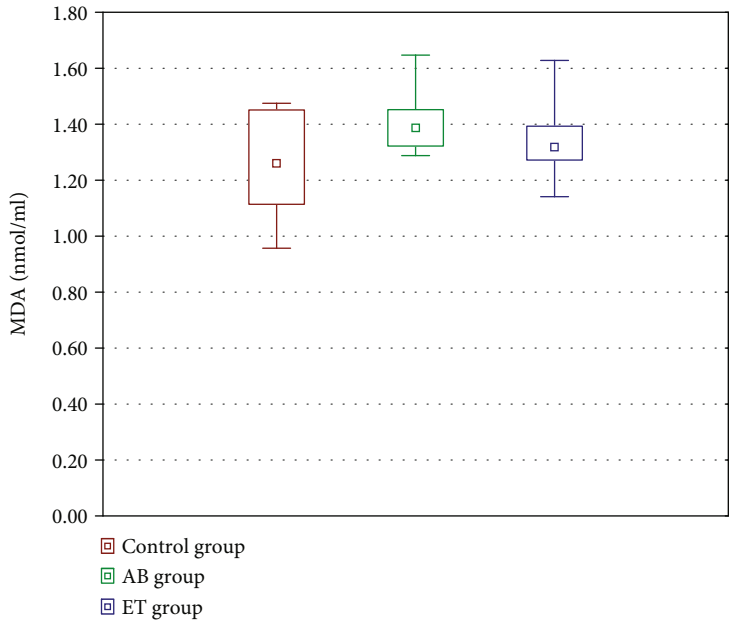

(a)

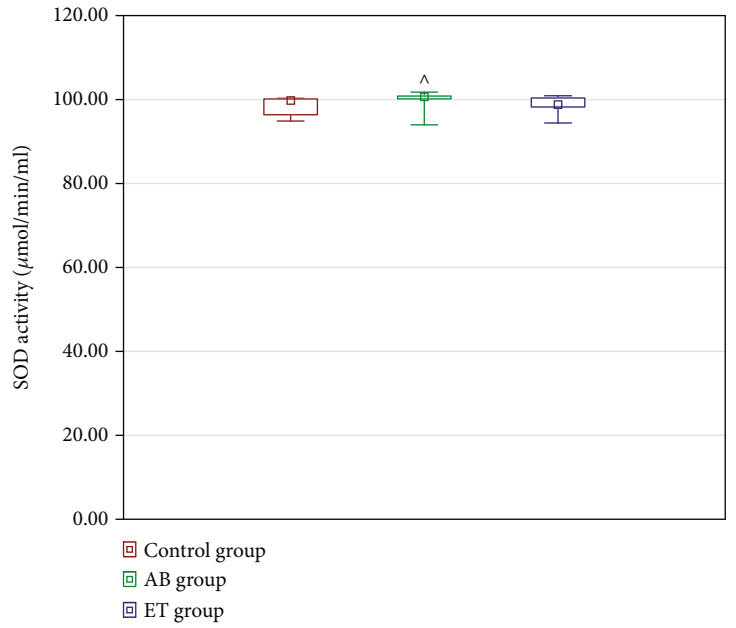

(b)

Figure 7: Continued.

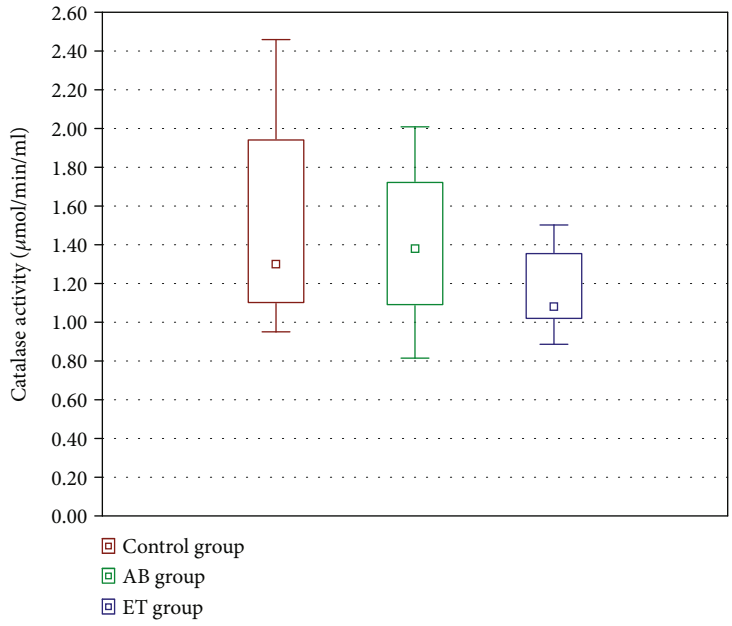

(c)

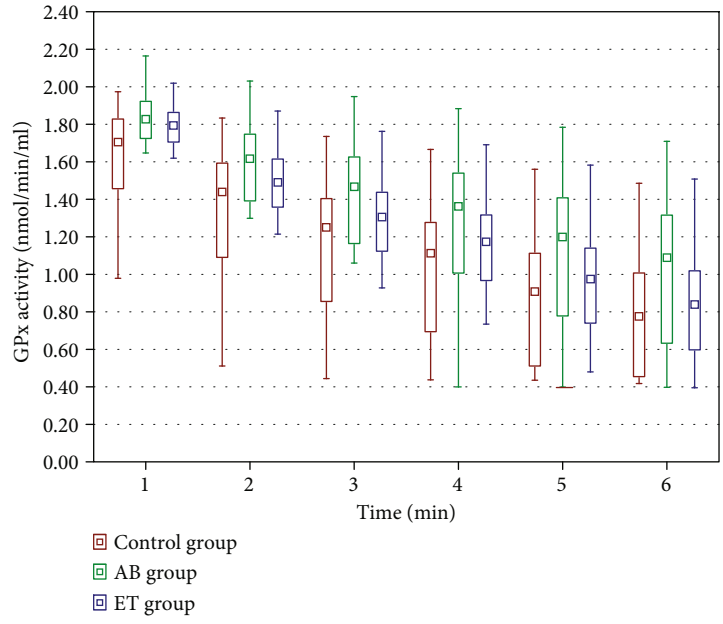

(d)

Figure 7: Continued.

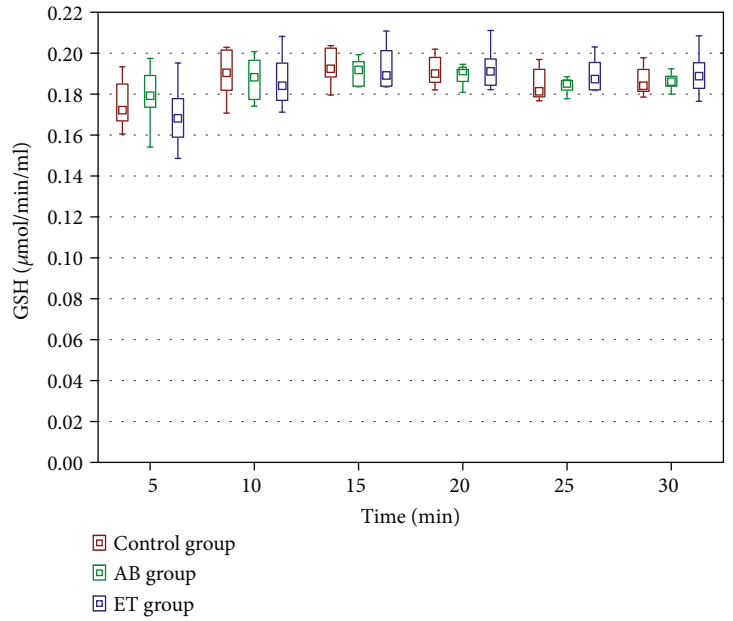

(e)

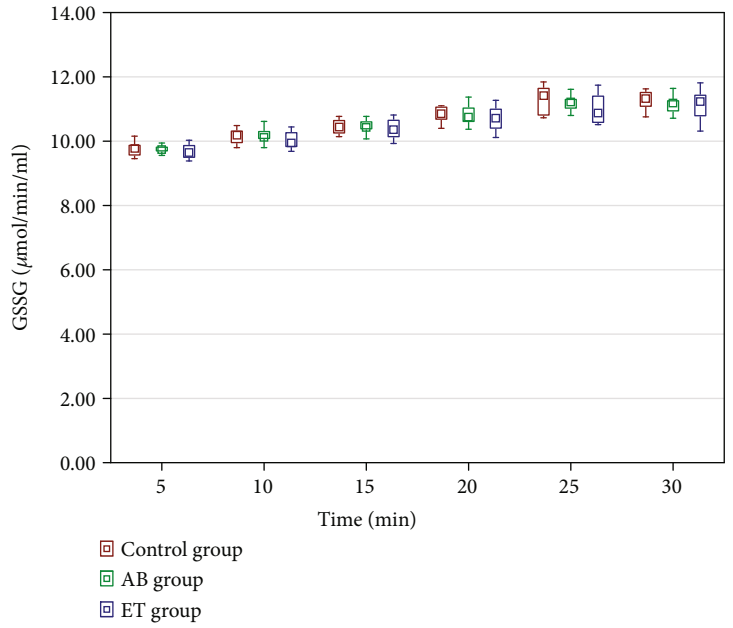

(f)

Figure 7: Continued.

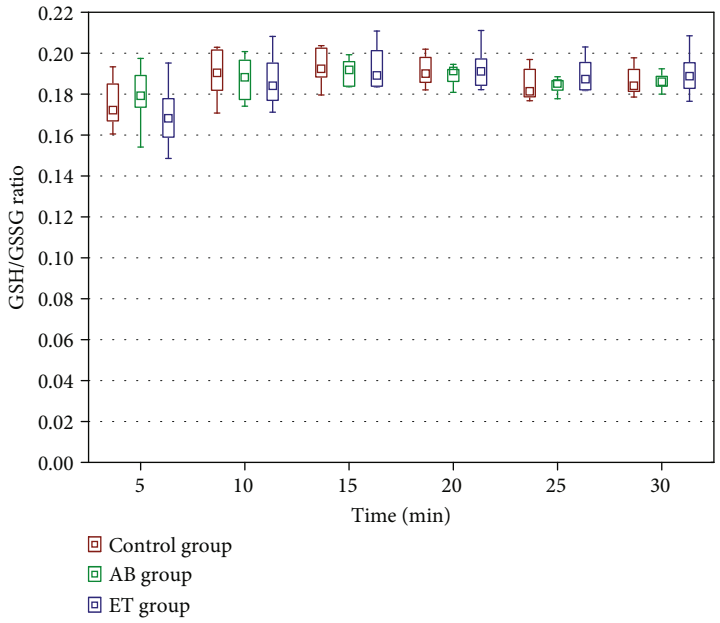

(g)

Figure 7: Effect of 16-week administration of abacavir and etravirine on MDA (a), superoxide dismutase activity (b), catalase activity (c), GPx activity (d), GSH (e), GSSG (f), and GSH/GSSG ratio (g) in testicular homogenates. Results presented as median (lower quartile-upper quartile); ^abacavir vs. control group, $p \leq 0.05$; *etravirine vs. control group, $p \leq 0.05$.

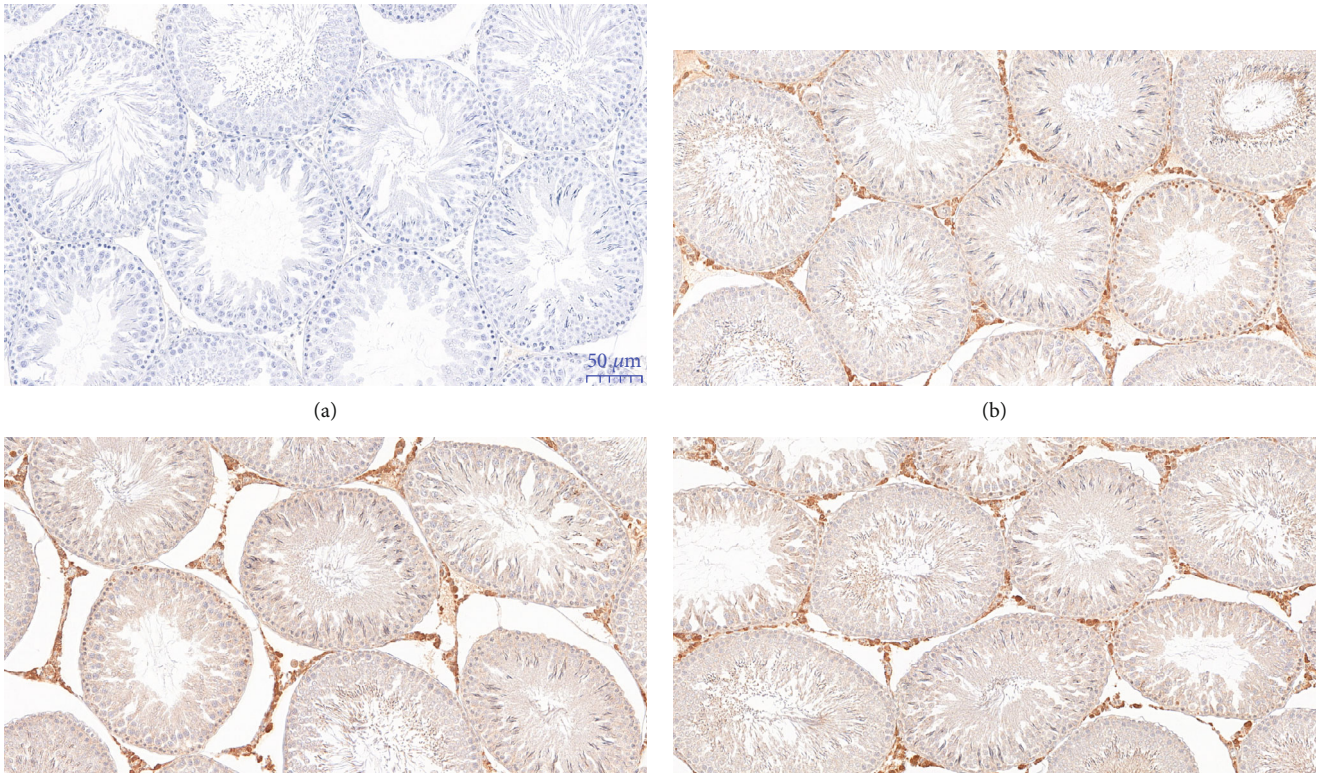

(a) (b)

(c) (d)

Figure 8: Selected cross-sections of testes (immunohistochemistry) for the glutathione expression: negative control (a), in the control group (b), the group receiving abacavir (c), and the group receiving etravirine (d). ×20 magnification.

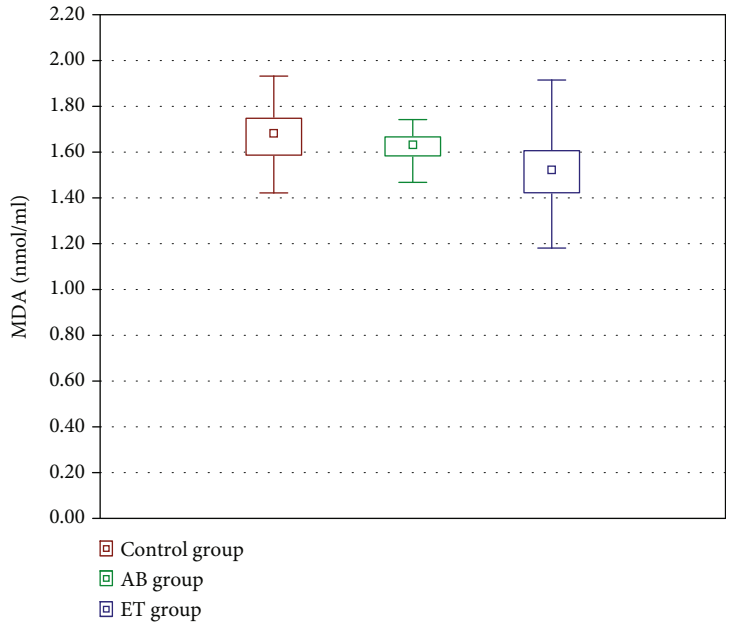

(a)

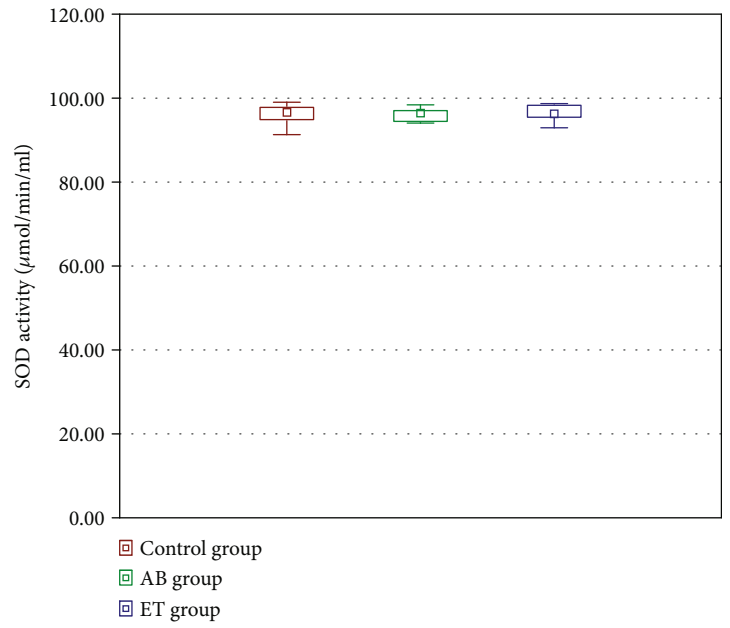

(b)

Figure 9: Continued.

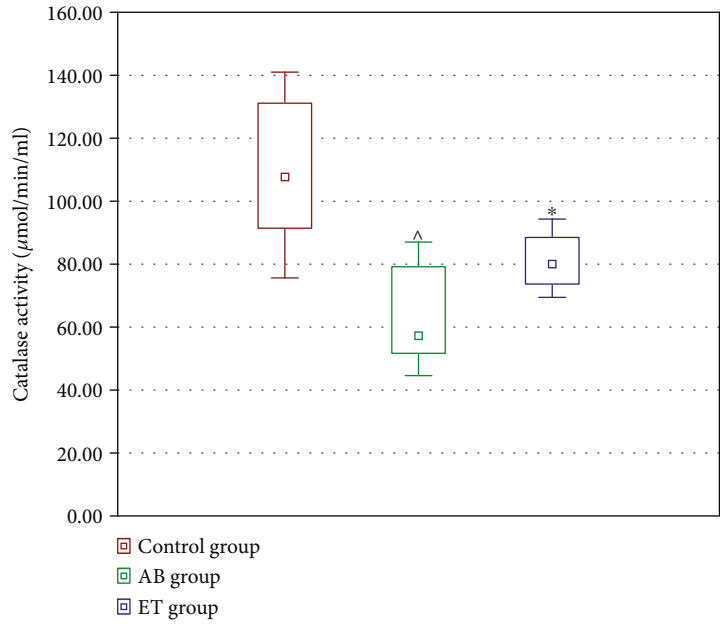

(c)

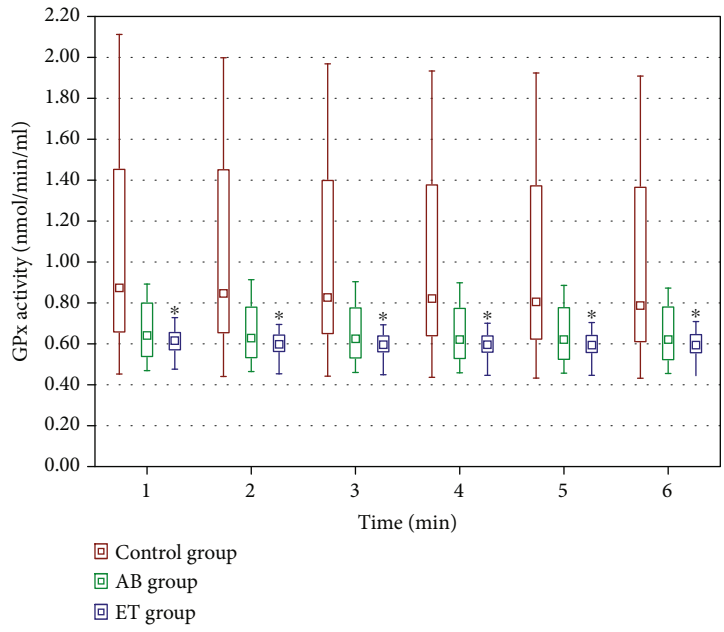

(d)

Figure 9: Continued.

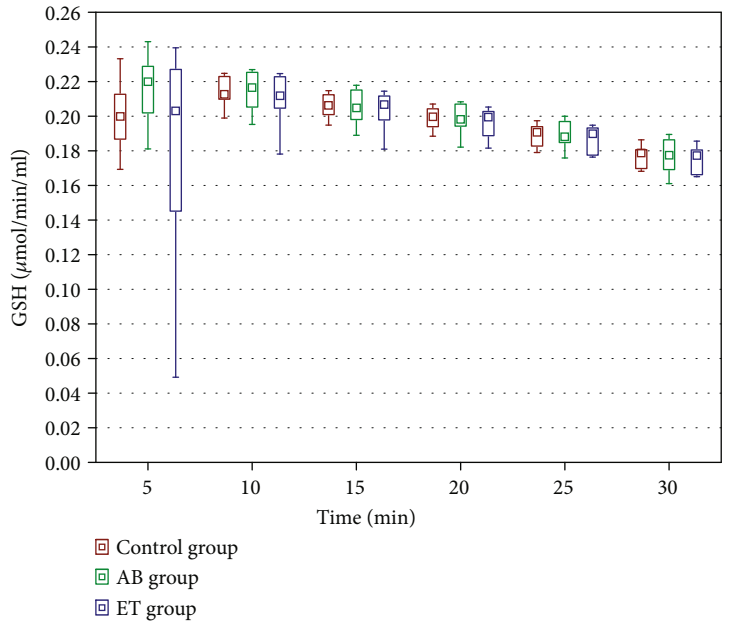

(e)

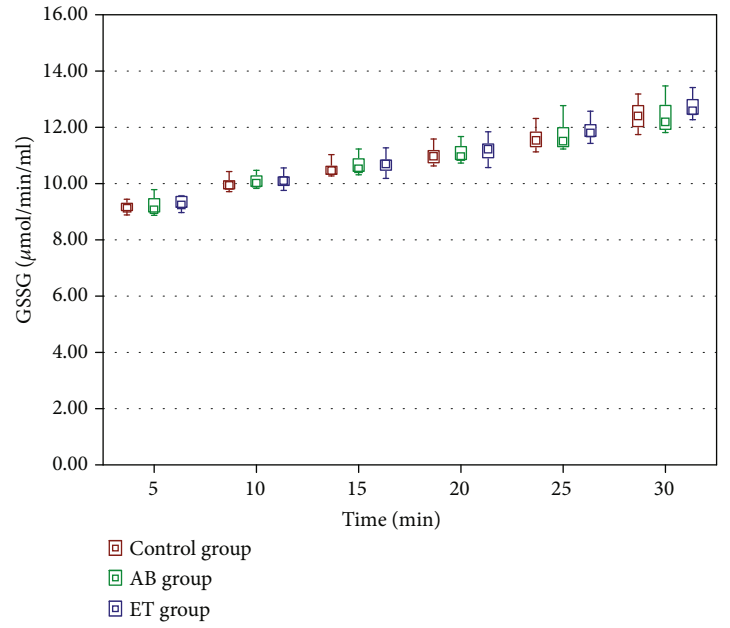

(f)

Figure 9: Continued.

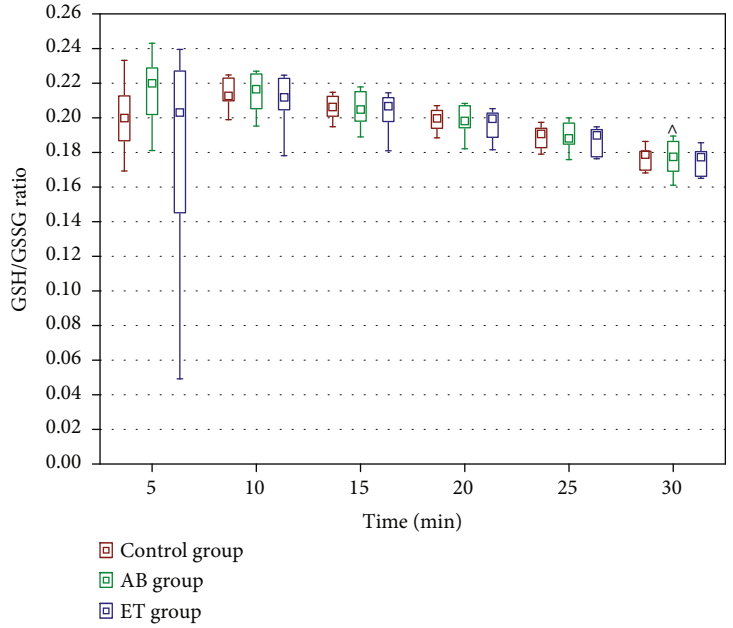

(g)

Figure 9: Effect of 16-week administration of abacavir and etravirine on MDA (a), superoxide dismutase activity (b), catalase activity (c), GPx activity (d), GSH (e), GSSG (f), and GSH/GSSG ratio (g) in homogenates from the liver; results presented as median (lower quartile–upper quartile); ^abacavir vs. control group, $p \leq 0.05$; *etravirine vs. control group, $p \leq 0.05$.

antioxidants and free radicals may be toxic and account for infertility. Plasma membranes in sperm are rich in unsaturated fatty acids, making them very susceptible to peroxidation and damage.

Moreover, spermatozoa contain only little cytoplasm, resulting in insufficient cytoplasmic antioxidant defense [74, 75]. The cells are protected from oxidative stress by an enzymatic (CAT, SOD, GPx) and nonenzymatic (GSH) antioxidant system [72]. SOD converts superoxide anion (O_2^-) to hydrogen peroxide (H_2O_2) and prevents the formation of highly reactive hydroxyl radicals. Hydrogen peroxide is further directly converted to H_2O by catalase or by glutathione peroxidase using the reduced glutathione (GSH) molecule, which is converted to the oxidized glutathione form (GSSG) [76]. MDA is a stable end product of the formation of free radicals and is the main biomarker for oxidative stress analysis and monitoring in various tissues, including testes [75].

Several in vitro studies suggest that antiretroviral drugs may generate ROS. It was found that various nucleoside reverse transcriptase inhibitors (NRTIs) impair the mitochondrial function in HepG2 cells and alter oxidative stress parameters causing, e.g., an increase in MDA levels (zidovudine and tenofovir) and a decrease in the GSH concentration (stavudine) [77]. Efavirenz, the first-generation of nonnucleoside reverse transcriptase inhibitors (NNRTIs), was also found to generate oxidative stress in endothelial cell lines [78, 79]. ROS generation is largely due to interference with mitochondrial function, altered replication of DNA in mitochondria, and inhibition of oxidative phosphorylation processes [80].

In the AB and ET groups, increased DNA instability expressed by an elevated percentage of spermatozoa with denatured DNA was found. In the study of testicular homogenates, abacavir was the only drug to significantly increased activity of SOD, which is one of the first in the enzymatic antioxidant pathway. No other changes in prooxidant (MDA) or enzymatic/nonenzymatic antioxidants were noticed in testes, suggesting that the described changes in DNA instability in spermatozoa are not the direct consequence of oxidative stress generation. It must, however, be stated that oxidative stress parameters in the seminal plasma were not assessed in this study and not affected the redox state in testes, not definitely excluding imbalances between pro- and antioxidants in semen.

Zini et al. reported that male infertility is associated with poor sperm DNA stability [81]. They also noted that if assisted conception is performed, fertilization with DNA-damaged spermatozoa may increase the risk of genetic diseases in children. The doubled percentage of spermatozoa with denatured DNA in abacavir- and etravirine-receiving rats supports the hypothesis that these drugs may impair male fertility due to increasing DNA instability, which should be confirmed in further studies, e.g., one focusing on the fertilization rate.

More pronounced changes in oxidative stress parameters were detected in the liver and kidneys. Etravirine significantly affects SOD activity in kidneys as well as catalase and GPx activities in the liver, suggesting the possible negative impact on the state of antioxidants; still, this does not affect MDA levels—the main prooxidant end product. Similarly, abacavir decreases catalase activity in the liver and GSH levels in rat kidneys without affecting the MDA concentration in both tissues. Both drugs are metabolized in the liver, but different metabolic pathways are important. Abacavir metabolism

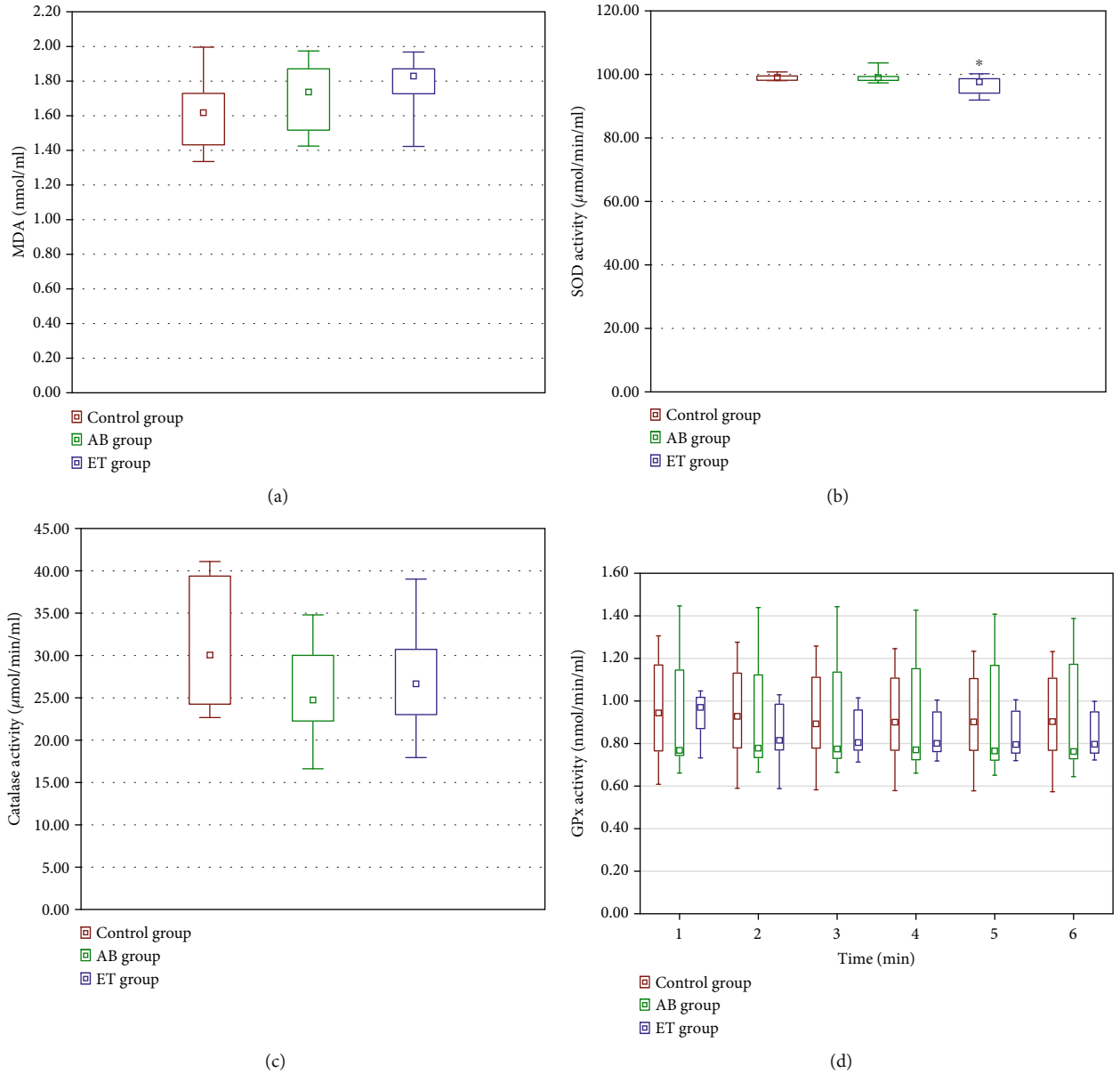

Figure 10: Continued.

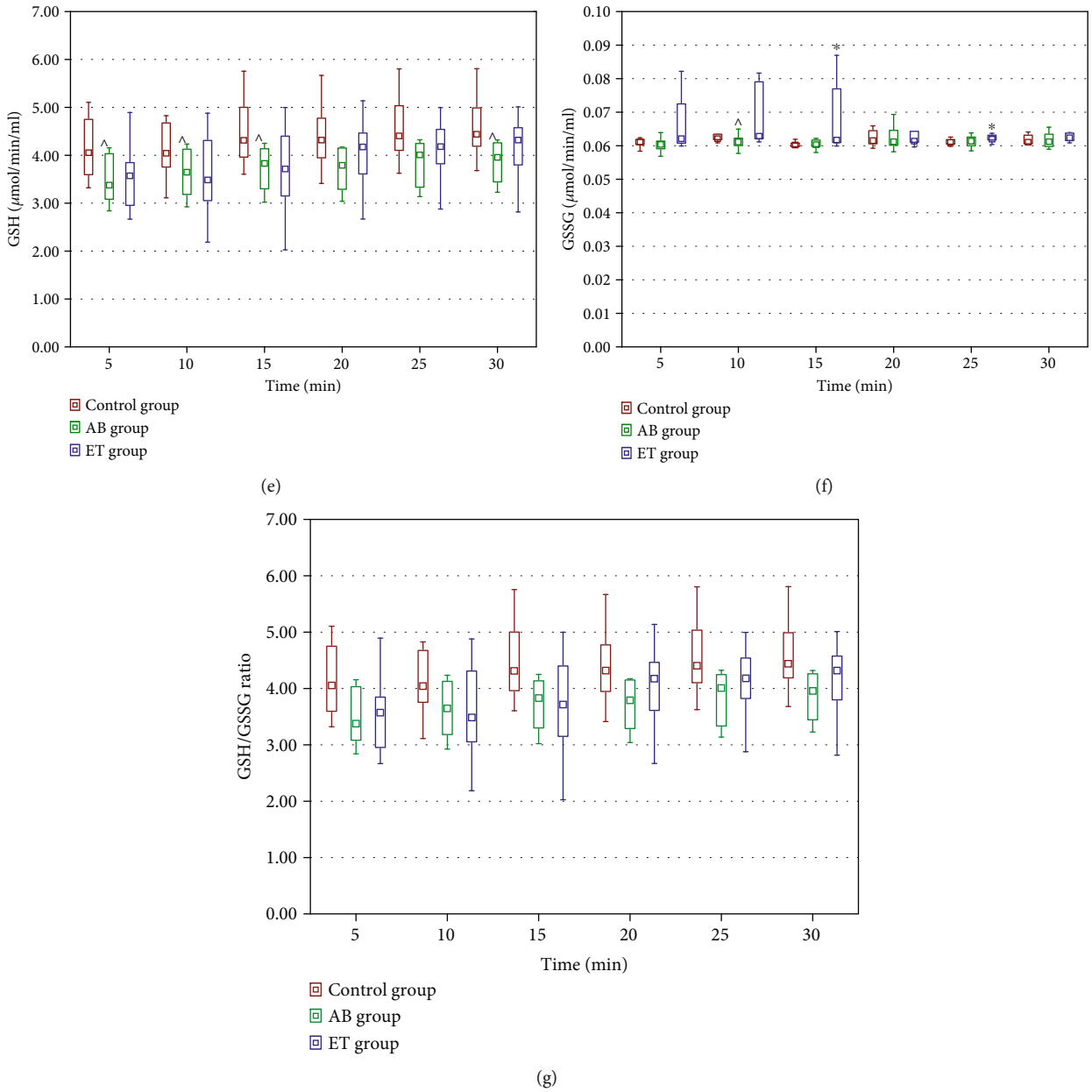

Figure 10: Effect of 16-week administration of abacavir and etravirine on MDA (a), superoxide dismutase activity (b), catalase activity (c), GPx activity (d), GSH (e), GSSG (f), and GSH/GSSG ratio (g) in homogenates from kidneys. Results presented as median (lower quartile–upper quartile); ^abacavir vs. control group, $p \leq 0.05$; *etravirine vs. control group, $p \leq 0.05$.

depends mainly on alcohol dehydrogenase and glucuronidation [82]. Etravirine is metabolized by CYP3A and CYP2C enzymes and later undergoes glucuronidation [83]. It seems that the 16-week abacavir administration affects the liver to a greater extent than etravirine administration, which was also reflected in significantly elevated AST activity in the AB-receiving group and a higher liver index. In the histological assessment, no pathological changes in the structure of livers obtained from both AB and ET groups were described, suggesting that AB causes functional rather than morphological injury.

Despite some alterations in the redox state in kidneys, the morphology of AB or ET administration was not affected, as shown in the histological evaluation. Moreover, serum creatinine levels were not significantly changed in the AB group and even were lowered significantly in the ET group, meaning that both drugs are rather not nephrotoxic. The detected mild decrease in creatinine levels in the ET-receiving animals had no clinical significance as the obtained results were within the normal limits for rats for an enzymatic method of plasma creatinine determination [84].

The lack of significant changes in SOD, CAT, and GPx activities and GSH and MDA concentrations in testes between the groups, but the presence of significant differences in the oxide–redox state between the studied and control groups in the liver and kidney, may result from drug

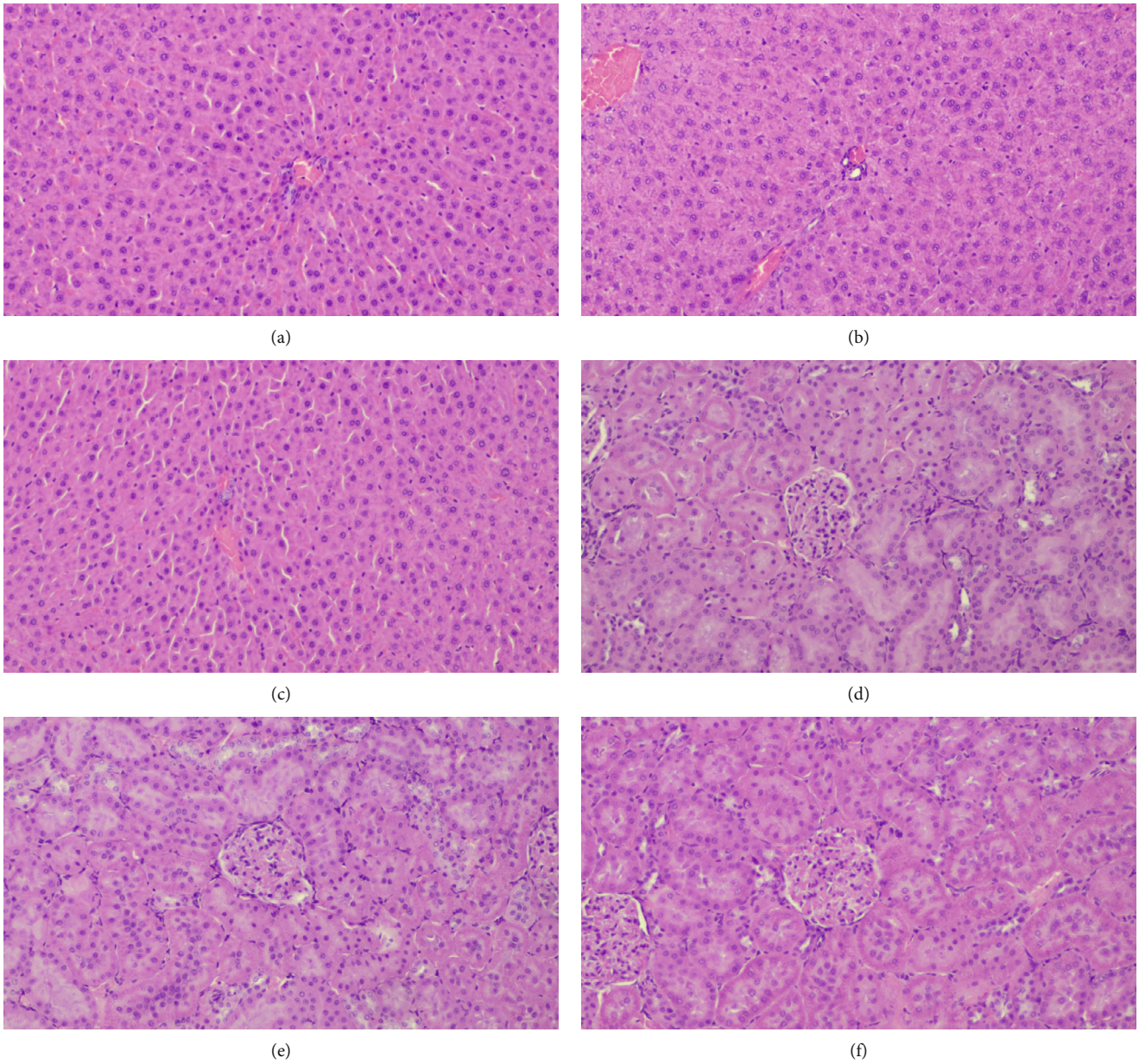

Figure 11: Sample images from the histopathologic examination of the liver (a–c) and kidneys (d–f) in the control group (a, d), the abacavir-receiving group (b, e), and the etravirine-receiving group (c, f).

pharmacokinetics. Drug concentration in plasma and in other body fluids and tissues depends on absorption, biotransformation, distribution, and excretion [85]. Following absorption from the gastrointestinal tract, drugs are transported to the liver by portal circulation to reach general circulation and are distributed to various tissues [86]. However, drug concentrations in tissues may vary greatly and depend on the drug molecular size, degree of protein binding, membrane permeability, presence of specific blood-tissue barriers, and tissue blood flow [87]. The delivery of drugs to the organs is mainly determined by the tissue blood flow. The accumulation of drugs in highly perfused tissues is greater than in tissues with low blood perfusion [85]. It is estimated that the blood flow in the renal cortex is about 700 ml/min/100 g of tissue, in the liver about 100-130 ml/min/100 g of tissue, and in testes only about 9-12 ml/min/100 g of tissue [88–90]. Further, the liver is the main place for drug metabolism, possibly resulting in reactive toxic metabolites [82, 91]. In kidneys, being the most important excreting organ, primary urine is concentrated and, thus, kidneys are exposed to high concentrations of drugs and their metabolites [92]. Studies on abacavir pharmacokinetics in mice that were given a single oral dose of 10 mg/kg confirm that after 15 minutes, the highest concentrations were found in the gallbladder, digestive tract, and kidneys, followed by a decrease below the detectable limit within 16 hours. In pregnant rats given the same oral dose, a high abacavir concentration after 6 hours was found in kidneys and the liver, whereas high abacavir levels in the liver

Table 5: Effect of abacavir and etravirine administration on serum parameters after 4 and 16 weeks (AB group: group receiving abacavir 60 mg/kg for 16 weeks; ET group: group receiving etravirine 40 mg/kg for 16 weeks; PINP: N-terminal propeptide of type I procollagen; TRACP: tartrate-resistant acid phosphatase from 5b; DKK1: Dickkopf-related protein 1; OPG: osteoprotegerin; 25-OH-D: 25-hydroxyvitamin D. Results presented as median (lower quartile-upper quartile); ^AB group vs. control group, $p \leq 0.05$; *ET group vs. control group, $p \leq 0.05$).

		Control group	AB group	ET group
Week 4	PINP [ng/ml]	14.6 (10.9-18.9)	18.1 (11.9-23.0)	12.4 (7.0-17.6)
	TRACP [U/l]	2.4 (1.8-2.8)	2.2 (2.0-2.7)	2.6 (1.9-2.9)
	Sclerostin [pg/ml]	1037.7 (983.6-1336.8)	1101.0 (1008.6-1193.0)	1110.6 (982.8-1182.1)
	DKK1 [ng/ml]	3.9 (3.5-7.7)	5.3 (3.2-6.7)	5.2 (4.4-7.8)
	OPG [pg/ml]	165.5 (154.0-169.5)	150.1 (132.9-163.4)	123.9 (98.7-167.4)
	1,25-dihydroxyvitamin D_3 [nmol/l]	7.9 (6.0-8.2)	6.9 (6.5-7.6)	6.8 (5.4 – 7.6)*
Week 16	PINP [ng/ml]	0.8 (0.5-1.1)	0.7 (0.6-0.8)	0.7 (0.6-0.9)
	TRACP [U/l]	1.3 (0.9-1.5)	1.1 (1.0-1.3)	1.1 (1.0-1.3)
	Sclerostin [pg/ml]	836.3 (726.6-1047.0)	830.7 (559.4-884.6)	859.7 (774.5-1010.1)
	DKK1 [ng/ml]	3.0 (1.9-5.3)	5.4 (3.2-12.5)^	2.7 (2.0-5.5)
	OPG [pg/ml]	79.7 (70.0-96.1)	86.4 (58.9-113.9)	102.9 (73.4-124.5)
	25-OH-D [nmol/l]	2.0 (1.7-2.1)	2.0 (1.8-2.2)	2.0 (1.8-2.2)
	1,25-dihydroxyvitamin D_3 [nmol/l]	6.3 (5.8-9.3)	6.8 (4.5-7.3)	6.6 (5.2-8.1)
	Parathormone [pg/ml]	42.0 (33.7-53.3)	47.0 (41.9-51.5)	49.2 (45.6-52.1)
	Total calcium [mg/dl]	9.3 (9.0-9.6)	9.3 (8.9-9.5)	9.1 (9.0-9.3)
	Inorganic phosphorus [mg/dl]	6.0 (5.0-7.4)	6.2 (5.7-7.6)	5.2 (5.0-6.6)
	Aspartate aminotransferase [U/l]	0.33 (0.25-0.50)	0.51 (0.48-0.75)^	0.39 (0.34-0.55)
	Creatinine [mg/dl]	0.33 (0.29-0.38)	0.33 (0.28-0.35)	0.29 (0.26-0.33)*

Table 6: Effect of 16-week administration of abacavir and etravirine on the bone mineral density (AB group: group receiving abacavir 60 mg/kg for 16 weeks; ET group: group receiving etravirine 40 mg/kg for 16 weeks. Results presented as median (lower quartile–upper quartile).

	Control group	AB group	ET group
Tibial BMD [g/cm^2]	0.223 (0.220-0.234)	0.228 (0.224-0.237)	0.231 (0.226-0.234)
Femoral BMD [g/cm^2]	0.276 (0.265-0.284)	0.272 (0.265-0.279)	0.276 (0.271-0.283)

Table 7: Effect of 16-week administration of abacavir and etravirine on the tibia assessed using histopathological examination (AB group: group receiving abacavir 60 mg/kg for 16 weeks; ET group: group receiving etravirine 40 mg/kg for 16 weeks; BV/TV: bone volume/tissue volume; BS/TV: bone surface/tissue volume; BS/BV: bone surface/bone volume ratio; Tb.Th: trabecular thickness. Results presented as median (lower quartile–upper quartile); ^AB group vs. control group, $p \leq 0.05$).

	Control group	AB group	ET group
BV/TV [%]	18.3 (12.6-21.6)	24.6 (23.3-26.4)^	17.2 (14.4-19.8)
BS/TV [mm^2/mm^3]	7.61 (7.17-9.49)	9.93 (9.68-10.7)^	8.41 (7.09-9.54)
BS/BV [mm^2/mm^3]	47.5 (36.2-53.4)	40.8 (35.7-46.3)	49.1 (41.4-52.6)
Tb.Th [mm]	0.042 (0.037-0.055)	0.049 (0.043-0.0056)	0.041 (0.038-0.048)

were still present after 48 hours [93]. The data obtained from animal pharmacokinetic studies reveal that high etravirine levels were found in the liver and renal cortex compared to the lowest concentrations determined in, e.g., the seminal vesicle [94].

The balance between cell proliferation and apoptosis is important for the maintenance of male fertility [95]. In this study, etravirine increased the MCM-7 protein (proliferation marker) expression in testes, pointing to the imbalance between proliferation and apoptosis. The consequence of increased proliferation may include the formation of functionally immature Sertoli cells [96].

No effect of abacavir on femoral and tibial BMD was demonstrated in this study. These findings are in line with the observations reported by Stelbrink et al. [97]. Their study revealed that a BMD loss was significantly greater (about 6%)

Table 8: Effect of 16-week administration of abacavir and etravirine on the cancellous and cortical bone of the tibia and femur assessed using micro-X-ray computed tomography (AB group: group receiving abacavir 60 mg/kg for 16 weeks; ET group: group receiving etravirine 40 mg/kg for 16 weeks; BV/TV: bone volume fraction; BS/TV: bone surface density; BS/BV: specific bone surface; Tb.Th: trabecular thickness; Tb.N: trabecular number; Tb.Sp: trabecular separation; SMI: structure model index; Conn.D: connectivity density; Po.tot: total porosity; DA: degree of anisotropy; Ct.Th: average cortical thickness; Tt.Ar: total cross-sectional area inside the periosteal envelope; Ct.Ar: cortical bone area; Ct.Ar/Tt.Ar: cortical area fraction. Results presented as median (lower quartile–upper quartile); ^AB group vs. control group, $p \leq 0.05$).

			Control group	AB group	ET group
Tibia	Cancellous bone	BV/TV [%]	13.2 (11.6-14.3)	14.7 (12.7-17.9)^	13.8 (12.7-15.9)
		BS/TV [mm^2/mm^3]	6.1 (4.6-6.6)	6.7 (5.6-7.7)	6.5 (5.8-6.8)
		BS/BV [mm^2/mm^3]	45.0 (43.0-47.9)	43.8 (42.7-46.4)	44.9 (42.6-47.2)
		Tb.Th [mm]	0.083 (0.080-0.087)	0.084 (0.081-0.086)	0.083 (0.080-0.086)
		Tb.N [1/mm]	1.64 (1.23-1.74)	1.80 (1.49-2.11)^	1.75 (1.54-1.87)
		Tb.Sp [mm]	0.52 (0.49-0.77)	0.44 (0.38-0.58)	0.44 (0.41-0.56)
		SMI [-]	2.15 (2.04-2.23)	2.07 (1.95-2.16)	2.01 (1.95-2.22)
		Conn.D [$1/mm^3$]	41.4 (27.4-45.5)	46.3 (35.5-59.8)^	44.5 (38.7-48.2)
		Po.tot [%]	86.8 (85.6-88.3)	85.2 (82.1-87.3)^	86.2 (84.1-87.3)
		DA [-]	1.70 (1.54-1.76)	1.65 (1.62-1.75)	1.68 (1.59-1.76)
Tibia	Cortical bone	Ct.Th [mm]	0.62 (0.61-0.65)	0.63 (0.60-0.64)	0.63 (0.62-0.65)
		Tt.Ar [mm^2]	48.3 (47.8-49.1)	50.7 (48.7-52.4)	51.2 (49.2-53.1)
		Ct.Ar [mm^2]	63.2 (61.3-65.8)	66.2 (62.6-69.4)	64.4 (63.0-69.6)
		Ct.Ar/tt.Ar [%]	1.29 (1.26-1.31)	1.29 (1.26-1.33)	1.28 (1.25-1.36)
Femur	Cancellous bone	BV/TV [%]	18.3 (15.7-19.0)	18.2 (16.4-20.4)	18.7 (16.7-20.3)
		BS/TV [mm^2/mm^3]	7.85 (6.14-8.12)	7.37 (7.11-8.73)	7.83 (7.48-8.46)
		BS/BV [mm^2/mm^3]	42.5 (41.0-44.1)	42.7 (41.8-43.3)	42.9 (41.7-44.8)
		Tb.Th [mm]	0.086 (0.084-0.089)	0.085 (0.083-0.088)	0.085 (0.083-0.087)
		Tb.N [1/mm]	2.16 (1.71-2.22)	2.04 (1.93-2.40)	2.16 (2.02-2.31)
		Tb.Sp [mm]	0.53 (0.49-0.75)	0.56 (0.42-0.68)	0.52 (0.45-0.61)
		SMI [-]	1.76 (1.72-1.81)	1.71 (1.61-1.77)	1.69 (1.65-1.84)
		Conn.D [$1/mm^3$]	75.4 (52.9-80.6)	73.5 (69.6-86.9)	79.5 (71.2-84.3)
		Po.tot [%]	81.7 (81.0-84.3)	81.8 (79.5-83.6)	81.3 (79.7-83.3)
		DA [-]	1.23 (1.22-1.26)	1.21 (1.17-1.25)	1.24 (1.21-1.25)
Femur	Cortical bone	Ct.Th [mm]	0.74 (0.73-0.76)	0.73 (0.70-0.75)	0.72 (0.71-0.74)
		Tt.Ar [mm^2]	47.5 (45.2-48.7)	47.9 (47.0-49.4)	48.6 (47.0-51.0)
		Ct.Ar [mm^2]	56.8 (55.3-57.6)	57.5 (55.8-62.2)	60.0 (56.0-63.4)
		Ct.Ar/tt.Ar [%]	1.20 (1.17-1.22)	1.21 (1.18-1.26)	1.21 (1.18-1.25)

in the tenofovir-emtricitabine group than in the abacavir-lamivudine group [97]. Negredo et al. also reported that introducing abacavir instead of tenofovir into therapy exerted beneficial BMD effects [98]. The histomorphometric analysis of tibial sections yields significantly higher bone volume fraction (BV/TV) and bone surface density (BS/TV) in the abacavir-receiving animals. In microcomputed tomography of the tibial trabecular bone, an increased trabecular number (Tb.N) and connectivity density (Conn.D) associated with lower total porosity in the AB group were also identified. All other microarchitectural parameters determined by mCT analysis were comparable in all three analyzed groups. The four-point bending test revealed increased Young's modulus in the AB group, indicating increased tensile stiffness of the femoral bone in the abacavir-receiving animals. Stiffness and flexural strength were comparable between the analyzed groups. Higher Tb.N and Conn.D may be attributed to the fact that abacavir was reported to activate adenosine A_2 receptors (A_2R) [99]. Medeiro et al. demonstrated that the A_2R agonist inhibited osteoclast differentiation [100]. Based on these reports, it may be hypothesized that abacavir, through the activation of A_2R, may shift the balance between bone resorption and bone formation towards osteogenesis. However, in the in vitro study using the osteosarcoma Saos-2 cell line as a model, it was observed that abacavir inhibited osteoblast differentiation and decreased the ability of the cells to form calcium deposits in the extracellular matrix [32].

Further studies are needed to explain the effect of abacavir on bone metabolism. Bone strength depends not only on bone mineralisation but also on bone geometry and the shape of bones, the microarchitecture of trabecular bones, turnover,

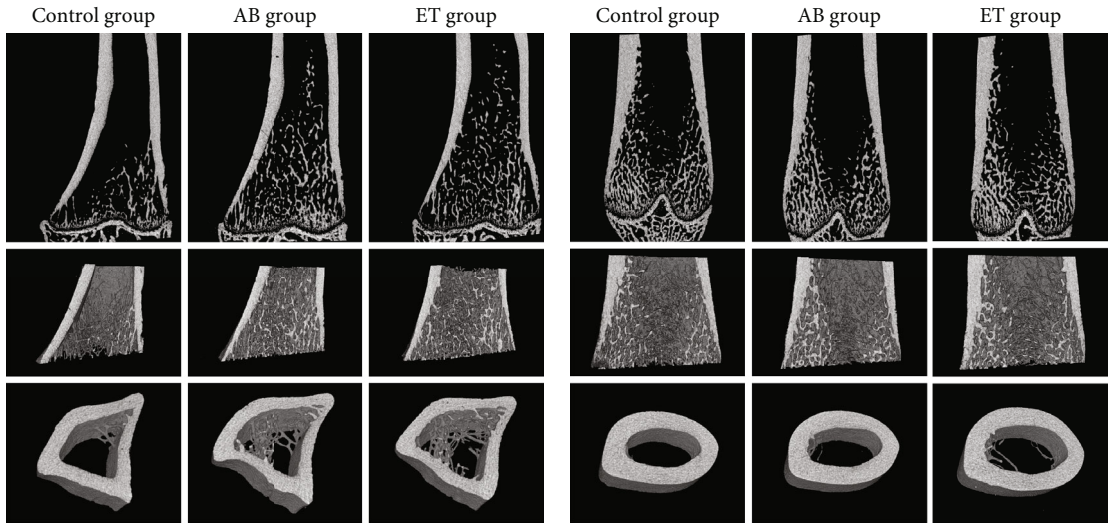

Figure 12: Representative mCT scans of (a) tibial bones and (b) femoral bones.

and collagen in the extracellular matrix. Even though Esposito et al. reported that abacavir impairs the mineralisation and synthesis of type I collagen [32], it did not decrease the mechanical resistance of femoral bones in this study. It is suspected that the increased number and trabeculae and elevated connectivity density detected in mCT counteracted the probable unfavorable impact of abacavir-induced mineralization inhibition on bone mechanical properties.

In this study, serum levels of bone turnover markers were measured twice—in week 4 and in week 16. In week 4, there was no difference in serum levels of PINP, TRACP, sclerostin, and Dickkopf-related protein 1 (DKK1) between the groups under analysis. In week 16, serum levels of PINP, TRACP, and sclerostin remained comparable between all groups. Serum DKK1 levels were elevated in the AB group compared to the control group. No difference in serum DKK1 levels between the control group and the ET group was detected. Lower serum levels of PINP and TRACP observed in the study between week 4 and week 16 resulted from an inhibition of bone turnover associated with growth slowing (Table 6, Figure 3). Sclerostin and DKK1 are both Wnt antagonists. The increase in DKK1 levels in the AB group may lead to slower bone formation and growth retardation if it should persist for a longer time. In the mice model, increased DKK1 levels were associated with osteopenia [101]. However, Ueland et al. found that femoral and spine BMD in postmenopausal women were positively correlated with cortical and trabecular DKK1 levels, respectively. Cortical DKK1 was also positively correlated with volumetric bone density and biomechanical strength [102]. This study also points to better bone parameters in the abacavir-receiving group despite increased serum DKK1 levels, which requires further detailed investigations and measurements of sclerostin or DKK1 levels in bone biopsies.

In this study, femoral and tibial BMDs were comparable between the ET and control groups. Additionally, the present study did not demonstrate any effect of etravirine on bone microarchitecture in neither in bone histomorphometry nor bone mCT examination. These findings are consistent with the results presented by other authors [103, 104], who found no negative impact of the therapy with raltegravir plus etravirine and ritonavir-boosted darunavir plus etravirine on bones. In the present study, etravirine was found to have no effect on bone mechanical properties, supporting the hypothesis that it does not exert a harmful effect on bones in growing rats.

In the study using the osteosarcoma Saos-2 cell line as a model, it was observed that the presence of etravirine in the culture medium increased the number of calcium deposits, pointing to an increase in final osteoblast differentiation and an increase in bone formation [28]. In this study, in the group receiving etravirine for 16 weeks, a higher tibial index and greater mid-tibial diameter were determined. This suggests an increase in bone formation, which is consistent with the in vitro results [32]. In rats, bone turnover is more rapid in the tibia than in the femur, which explains why changes in the tibial index without changes in the femoral index were found in the present study. Even though the tibial index was higher in the ET group than in the control one, PINP levels were comparable between both groups. PINP is a bone formation marker, with its levels being correlated with the formation of matrix collagen in bones. Considering the results reported by Esposito et al. [32] and the results presented in this study, it may be suspected that etravirine increases calcium deposit formation but without promoting the synthesis of collagen in the bone matrix. However, it cannot be excluded that rapid bone turnover in growing rats masked the effect of etravirine on collagen formation. The lack of a statistically significant difference between the ET group and the control group in terms of serum PINP levels (bone formation marker) may result from significant and rapid bone turnover in the growing period, making observations difficult. What is more, concentrations of bone turnover markers in serum reflect the current intensity of bone

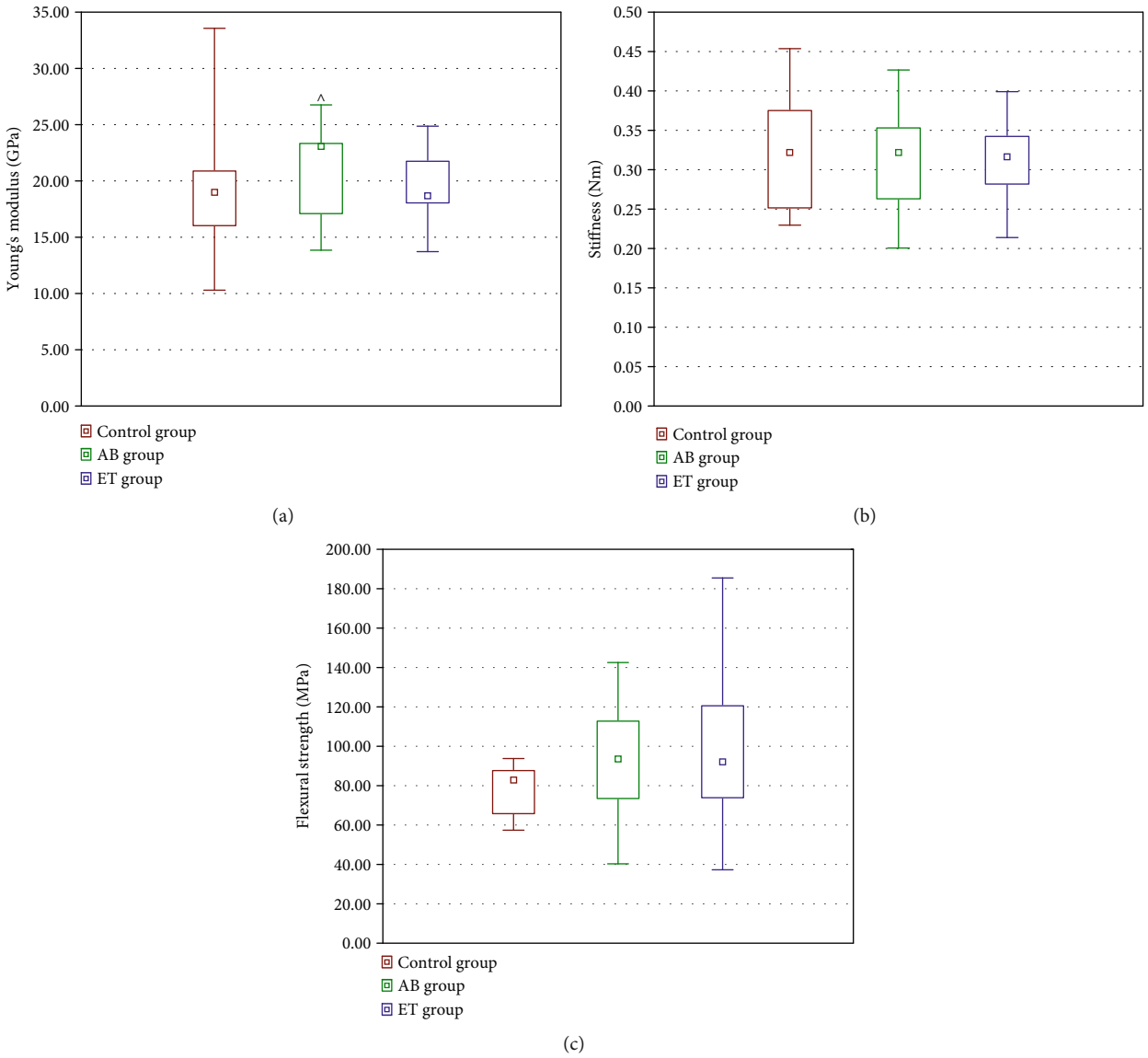

Figure 13: Effect of 16-week administration of abacavir and etravirine on the biomechanical properties of right femurs: Young's modulus (a), stiffness (b), and flexural strength (c). Results presented as median (lower quartile-upper quartile); ^abacavir vs. control group, $p \leq 0.05$.

formation and resorption, but do not confirm the intensity of these processes in a longer period [105].

In the 4th week of this study, a significant decrease in serum 1,25-dihydroxyvitamin D_3 levels was measured in the etravirine-receiving group. Decreased vitamin D concentrations and the impairment of vitamin D metabolic pathways by antiretroviral drugs (especially HIV protease inhibitors and nonnucleoside reverse transcriptase inhibitors) were found by other authors, which were confirmed by both in vitro and in vivo studies [106, 107]. Efavirenz, belonging to the same group as etravirine, was found to increase 25-hydroxyvitamin D catabolism, resulting in increased levels of inactive metabolites [106, 107]. To date, no studies have been conducted to assess the effect of etravirine on BMD. Long-term vitamin D deficiency could lead to bone mineralization disorders and a decrease in bone mineral density. This study assessed vitamin D levels twice—in week 4 and week 16 of the study. It is impossible to predict how long vitamin D deficiency lasted after one random evaluation during the study. Despite transiently decreased vitamin D levels, no differences in bone mineral density, histomorphometric parameters, or mechanical properties of bones were demonstrated between the ET-receiving and control groups. This may be explained by further positive impact of etravirine on bone formation.

5. Conclusions

Abacavir and etravirine doubled the percentage of sperms with denatured DNA, suggesting decreased fertility in animals receiving these drugs. The results of this study indicate that etravirine may decrease serum vitamin D concentration, which dictates the need to monitor vitamin D levels in etravirine-receiving children. However, no harmful effect of

etravirine on bones in growing rats was identified. Abacavir was found to improve bone microarchitecture in growing rats but may affect the liver function.

Abbreviations

AB:	Abacavir
AST:	Aspartate aminotransferase
A_2R:	Adenosine A_2 receptors
BMD:	Bone mineral density
BS:	Bone surface
BS/BV:	Specific bone surface
BS/TV:	Bone surface density
BV:	Bone volume
BV/TV:	Bone volume fraction
CAT:	Catalase
Conn.D:	Connectivity density
Ct.Ar:	Cortical bone area
Ct.Ar/Tt.Ar:	Cortical area fraction
Ct.Th:	Average cortical thickness
DA:	Degree of anisotropy
DFI:	DNA fragmentation
DKK1:	Dickkopf-related protein 1
DXA:	Dual-energy X-ray absorptiometry
ET:	Etravirine
GPx:	Glutathione peroxidase
GSH:	Reduced glutathione
GSSG:	Oxidized glutathione
HDS:	High DNA stainability
IHC:	Immunohistochemical examination
LH:	Luteinising hormone
mCT:	Microcomputed tomography
MDA:	Malondialdehyde
MCM-7:	Minichromosome maintenance 7 protein
PINP:	N-Terminal propeptide of type I procollagen
Po.tot:	Total porosity
PRL:	Prolactin
ROS:	Reactive oxygen species
SHBG:	Sex hormone binding globulin
SMI:	Structure model index
SOD:	Superoxide dismutase
Tb.N:	Trabecular thickness number
Tb.Sp:	Trabecular separation
Tb.Th:	Trabecular thickness
TRACP:	Tartrate-resistant acid phosphatase form 5b
TSH:	Thyroid-stimulating hormone
Tt.Ar:	Total cross-sectional area inside the periosteal envelope
TV:	Tissue volume
$1,25\text{-}(OH)_2\text{-}D_3$:	1,25-Dihydroxyvitamin D_3
25-OH-D:	25-Hydroxyvitamin D.

Data Availability

The data underlying this article will be shared on request to the corresponding author.

Conflicts of Interest

The authors declare no conflict of interest regarding the publication of this paper.

Acknowledgments

This study was funded by the Wroclaw Medical University [grant number SUB.A080.19.024].

References

[1] World Health Organization, *Progress report on HIV, viral hepatitis and sexually transmitted infections, 2019*, Who, 2019.

[2] H. B. Andrade, C. R. Shinotsuka, I. R. F. da Silva et al., "Highly active antiretroviral therapy for critically ill HIV patients: a systematic review and meta-analysis," *PLoS One*, vol. 12, no. 10, article e0186968, 2017.

[3] M. Melku, G. Abebe, A. Teketel et al., "Immunological status and virological suppression among HIV-infected adults on highly active antiretroviral therapy," *Environmental Health and Preventive Medicine*, vol. 25, no. 1, p. 43, 2020.

[4] J. Cohen, A. Beaubrun, R. Bashyal, A. Huang, J. Li, and O. Baser, "Real-world adherence and persistence for newly-prescribed HIV treatment: single versus multiple tablet regimen comparison among US medicaid beneficiaries," *AIDS Research and Therapy*, vol. 17, no. 1, p. 12, 2020.

[5] T. A. Mega, F. B. Usamo, and G. Z. Negera, "Immunologic response of HIV-infected children to different regimens of antiretroviral therapy: a retrospective observational study," *AIDS Research and Treatment*, vol. 2020, Article ID 6415432, 8 pages, 2020.

[6] O. Awodele, T. D. Popoola, O. Idowu, B. M. Bashua, N. A. Awolola, and W. O. Okunowo, "Investigations into the risk of reproductive toxicity following exposure to highly active anti-retroviral drugs in rodents," *The Tokai Journal of Experimental and Clinical Medicine*, vol. 43, no. 2, pp. 54–63, 2018.

[7] M. A. Hamed, G. O. Aremu, and R. E. Akhigbe, "Concomitant administration of HAART aggravates anti-Koch-induced oxidative hepatorenal damage via dysregulation of glutathione and elevation of uric acid production," *Biomedicine & Pharmacotherapy*, vol. 137, article 111309, 2021.

[8] K. N. Althoff, M. Smit, P. Reiss, and A. C. Justice, "HIV and ageing: improving quantity and quality of life," *Current Opinion in HIV and AIDS*, vol. 11, no. 5, pp. 527–536, 2016.

[9] J. C. Beghin, J. C. Yombi, J. Ruelle, and D. Van der Linden, "Moving forward with treatment options for HIV-infected children," *Expert Opinion on Pharmacotherapy*, vol. 19, no. 1, pp. 27–37, 2018.

[10] G. N. Sanjeeva, M. Sahana, H. B. Pavithra et al., "Transition of children with perinatally acquired HIV-infection into adulthood: social outcome and quality of life," *Indian Journal of Pediatrics*, vol. 86, no. 3, pp. 233–240, 2019.

[11] A. E. Semprini and S. Fiore, "HIV and reproduction," *Current Opinion in Obstetrics & Gynecology*, vol. 16, no. 3, pp. 257–262, 2004.

[12] J. R. Iyer, A. Van Rie, S. A. Haberlen et al., "Subfertility among HIV-affected couples in a safer conception cohort in South Africa," *American journal of obstetrics and gynecology*, vol. 221, no. 1, pp. 48.e1–48.e18, 2019.

[13] S. Kehl, M. Weigel, D. Müller, M. Gentili, A. Hornemann, and M. Sütterlin, "HIV-infection and modern antiretroviral therapy impair sperm quality," *Archives of Gynecology and Obstetrics*, vol. 284, no. 1, pp. 229–233, 2011.

[14] O. O. Ogedengbe, E. C. S. Naidu, and O. O. Azu, "Antiretroviral therapy and alcohol interactions: X-raying testicular and seminal parameters under the HAART era," *European Journal of Drug Metabolism and Pharmacokinetics*, vol. 43, no. 2, pp. 121–135, 2018.

[15] L. J. Else, S. Taylor, D. J. Back, and S. H. Khoo, "Pharmacokinetics of antiretroviral drugs in anatomical sanctuary sites: the male and female genital tract," *Antiviral Therapy*, vol. 16, no. 8, pp. 1149–1167, 2011.

[16] K. C. Brown, K. B. Patterson, S. H. Jennings et al., "Single-and multiple-dose pharmacokinetics of darunavir plus ritonavir and etravirine in semen and rectal tissue of HIV-negative men," *Journal of Acquired Immune Deficiency Syndromes*, vol. 61, no. 2, pp. 138–144, 2012.

[17] R. M. E. van Praag, R. P. G. van Heeswijk, S. Jurriaans, J. M. A. Lange, R. M. W. Hoetelmans, and J. M. Prins, "Penetration of the nucleoside analogue abacavir into the genital tract of men infected with human immunodeficiency virus type 1," *Clinical infectious diseases*, vol. 33, no. 8, pp. e91–e92, 2001.

[18] V. Savasi, M. Oneta, A. Laoreti et al., "Effects of antiretroviral therapy on sperm DNA integrity of HIV-1-infected men," *American Journal of Men's Health*, vol. 12, no. 6, pp. 1835–1842, 2018.

[19] E. M. Curtis, R. J. Moon, N. C. Harvey, and C. Cooper, "The impact of fragility fracture and approaches to osteoporosis risk assessment worldwide," *Bone*, vol. 104, pp. 29–38, 2017.

[20] T. Sozen, L. Ozisik, and N. Calik Basaran, "An overview and management of osteoporosis," *European journal of rheumatology*, vol. 4, no. 1, pp. 46–56, 2017.

[21] R. Liu, A. Chao, K. Wang, and J. Wu, "Incidence and risk factors of medical complications and direct medical costs after osteoporotic fracture among patients in China," *Archives of Osteoporosis*, vol. 13, no. 1, p. 12, 2018.

[22] D. Martinez-Laguna, A. Soria-Castro, C. Carbonell-Abella et al., "Validacion de las fracturas por fragilidad en la historia clinica informatizada de atencion primaria: un estudio poblacional," *Reumatología Clínica*, vol. 15, no. 5, pp. e1–e4, 2019.

[23] R. Rizzoli, "Postmenopausal osteoporosis: Assessment and management," *Best Practice & Research. Clinical Endocrinology & Metabolism*, vol. 32, no. 5, pp. 739–757, 2018.

[24] A. Calmy, C. A. Fux, R. Norris et al., "Low bone mineral density, renal dysfunction, and fracture risk in HIV infection: a cross-sectional study," *The Journal of Infectious Diseases*, vol. 200, no. 11, pp. 1746–1754, 2009.

[25] M. O. Premaor and J. E. Compston, "People living with HIV and fracture risk," *Osteoporosis International*, vol. 31, no. 9, pp. 1633–1644, 2020.

[26] A. Richterman and P. E. Sax, "Antiretroviral therapy in older people with HIV," *Current Opinion in HIV and AIDS*, vol. 15, no. 2, pp. 118–125, 2020.

[27] G. A. McComsey, D. Kitch, E. S. Daar et al., "Bone mineral density and fractures in antiretroviral-naive persons randomized to receive abacavir-lamivudine or tenofovir disoproxil fumarate-emtricitabine along with efavirenz or atazanavir-ritonavir: AIDS Clinical Trials Group A5224s, a substudy of ACTG A5202," *The Journal of Infectious Diseases*, vol. 203, no. 12, pp. 1791–1801, 2011.

[28] C. M. Gordon, B. S. Zemel, T. A. L. Wren et al., "The Determinants of Peak Bone Mass," *The Journal of pediatrics*, vol. 180, pp. 261–269, 2017.

[29] C. M. Weaver, C. M. Gordon, K. F. Janz et al., "The National Osteoporosis Foundation's position statement on peak bone mass development and lifestyle factors: a systematic review and implementation recommendations," *Osteoporosis International*, vol. 27, no. 4, article 3440, pp. 1281–1386, 2016.

[30] European Medicines Agency, "Ziagen: EPAR - Product Information," 2021, https://www.ema.europa.eu/documents/product-information/ziagen-epar-product-information_en.pdf.

[31] European Medicines Agency, "Intelence: EPAR - Product Information," 2021, https://www.ema.europa.eu/en/documents/product-information/intelence-epar-product-information_en.pdf.

[32] V. Esposito, A. Perna, A. Lucariello et al., "Different impact of antiretroviral drugs on bone differentiation in an in vitro model," *Journal of Cellular Biochemistry*, vol. 116, no. 10, pp. 2188–2194, 2015.

[33] L. Ryom, A. Cotter, R. de Miguel et al., "2019 update of the European AIDS clinical society guidelines for treatment of people living with HIV version 10.0," *HIV Medicine*, vol. 21, no. 10, pp. 617–624, 2020.

[34] AIDS and Hepatitis C Professional Group, Society of Infectious Diseases, Chinese Medical Association, and Chinese Center for Disease Control and Prevention, "Chinese guidelines for diagnosis and treatment of HIV/AIDS 2018," *Zhonghua Nei Ke Za Zhi*, vol. 57, no. 12, pp. 867–884, 2018.

[35] M. S. Saag, R. T. Gandhi, J. F. Hoy et al., "Antiretroviral drugs for treatment and prevention of HIV infection in adults: 2020 recommendations of the international antiviral society-USA panel," *Jama*, vol. 324, no. 16, pp. 1651–1669, 2020.

[36] M. G. Atta, S. De Seigneux, and G. M. Lucas, "Clinical pharmacology in HIV therapy," *Clinical Journal of the American Society of Nephrology*, vol. 14, no. 3, pp. 435–444, 2019.

[37] J. T. García and J. Bascuñana, "Safety and tolerability: current challenges to antiretroviral therapy for the long-term management of HIV infection," *AIDS Reviews*, vol. 18, pp. 127–137, 2016.

[38] E. Huesgen, K. E. DeSear, E. F. Egelund, R. Smith, B. Max, and J. Janelle, "A HAART-breaking review of alternative antiretroviral administration: practical considerations with crushing and enteral tube scenarios," *Pharmacotherapy*, vol. 36, no. 11, pp. 1145–1165, 2016.

[39] S. de Castro and M. J. Camarasa, "Polypharmacology in HIV inhibition: can a drug with simultaneous action against two relevant targets be an alternative to combination therapy?," *European Journal of Medicinal Chemistry*, vol. 150, pp. 206–227, 2018.

[40] M. G. Paulis, E. M. Hafez, and N. F. El-Tahawy, "Toxicity and postwithdrawal effects of ketamine on the reproductive function of male albino rats: hormonal, histological, and immunohistochemical study," *Human & Experimental Toxicology*, vol. 39, no. 8, pp. 1054–1065, 2020.

[41] H. A. A. Aly, "Testicular toxicity of gentamicin in adult rats: ameliorative effect of lycopene," *Human & Experimental Toxicology*, vol. 38, no. 11, pp. 1302–1313, 2019.

[42] S. G. Felemban, M. A. Aldubayan, A. H. Alhowail, and I. S. Almami, "Vitamin B17 Ameliorates Methotrexate-Induced Reproductive Toxicity, Oxidative Stress, and Testicular

Injury in Male Rats," *Oxidative Medicine and Cellular Longevity*, vol. 2020, Article ID 4372719, 11 pages, 2020.

[43] P. P. Lelovas, T. T. Xanthos, S. E. Thoma, G. P. Lyritis, and I. A. Dontas, "The laboratory rat as an animal model for osteoporosis research," *Comparative Medicine*, vol. 58, no. 5, pp. 424–430, 2008.

[44] J. Folwarczna, N. Konarek, K. Freier, D. Karbowniczek, P. Londzin, and A. Janas, "Effects of loratadine, a histamine H_1 receptor antagonist, on the skeletal system of young male rats," *Drug Design, Development and Therapy*, vol. 13, pp. 3357–3367, 2019.

[45] K. Rjiba-Touati, I. Amara, M. Bousabbeh et al., "Recombinant human erythropoietin prevents etoposide- and methotrexate-induced toxicity in kidney and liver tissues via the regulation of oxidative damage and genotoxicity in Wistar rats," *Human & Experimental Toxicology*, vol. 37, no. 8, pp. 848–858, 2018.

[46] M. S. Hareedy, E. A. Ahmed, and M. F. Ali, "Montelukast modifies simvastatin-induced myopathy and hepatotoxicity," *Drug Development Research*, vol. 80, no. 7, pp. 1000–1009, 2019.

[47] N. A. Andreollo, E. F. Santosdos, M. R. Araújo, and L. R. Lopes, "Idade dos ratos versus idade humana: qual é a relação?," *Arquivos Brasileiros de Cirurgia Digestiva*, vol. 25, no. 1, pp. 49–51, 2012.

[48] P. Sengupta, "The laboratory rat: relating its age with human's," *International Journal of Preventive Medicine*, vol. 4, no. 6, pp. 624–630, 2013.

[49] W. S. Jee and W. Yao, "Overview: animal models of osteopenia and osteoporosis," *Journal of Musculoskeletal & Neuronal Interactions*, vol. 1, no. 3, pp. 193–207, 2001.

[50] "Directive 2010/63/EU of the European Parliament and of the Council of 22 September 2010 on the protection of animals used for scientific purposes 2010," 2010.

[51] A. Nair and S. Jacob, "A simple practice guide for dose conversion between animals and human," *Journal of basic and clinical pharmacy*, vol. 7, no. 2, pp. 27–31, 2016.

[52] F. Martinez-Pastor, V. Garcia-Macias, M. Alvarez et al., "Comparison of two methods for obtaining spermatozoa from the cauda epididymis of Iberian red deer," *Theriogenology*, vol. 65, no. 3, pp. 471–485, 2006.

[53] W. Nizański, G. J. Dejneka, M. Klimowicz, and A. Dubiel, "Ocena wybranych właściwości plemników najądrzowych kota domowego i ich konserwacja w niskich temperaturach," *Medycyna Weterynaryjna*, vol. 61, pp. 173–178, 2005.

[54] M. Polit, S. Prochowska, and W. Niżański, "Comparison of the characteristics of chinchilla epidydimal semen after collection, storage at 5°C and cryopreservation," *Reproduction in Domestic Animals*, vol. 53, pp. 29–36, 2018.

[55] A. Partyka, O. Rodak, J. Bajzert, J. Kochan, and W. Nizański, "The effect of L-carnitine, hypotaurine, and taurine supplementation on the quality of cryopreserved chicken semen," *BioMed Research International*, vol. 2017, Article ID 7279341, 8 pages, 2017.

[56] W. Niżański, A. Partyka, and T. Rijsselaere, "Use of fluorescent stainings and flow cytometry for canine semen assessment," *Reproduction in Domestic Animals*, vol. 47, pp. 215–221, 2012.

[57] W. Remmele and H. E. Stegner, "Vorschlag zur einheitlichen Definition eines Immunreaktiven Score (IRS) für den immunhistochemischen Ostrogenrezeptor-Nachweis (ER-ICA) im Mammakarzinomgewebe," *Pathologe*, vol. 8, no. 3, pp. 138–140, 1987.

[58] D. Kaemmerer, L. Peter, A. Lupp et al., "Comparing of IRS and Her2 as immunohistochemical scoring schemes in gastroenteropancreatic neuroendocrine tumors," *International Journal of Clinical and Experimental Pathology*, vol. 5, no. 3, pp. 187–194, 2012.

[59] Ł. Zadka, M. J. Kulus, K. Kurnol et al., "The expression of IL10RA in colorectal cancer and its correlation with the proliferation index and the clinical stage of the disease," *Cytokine*, vol. 110, pp. 116–125, 2018.

[60] Hologic, "Hologic osteoporosis assessment. HL7 Results interface specification," 2017, http://www.hologic.ca/sites/default/files/HL7%20Results%20Interface%20%28MAN-03662%29%20English%20Rev%20002%2004-17_0.pdf.

[61] G. M. Campbell and A. Sophocleous, "Quantitative analysis of bone and soft tissue by micro-computed tomography: applications to ex vivo and in vivo studies," *BoneKEy reports*, vol. 3, pp. 1–12, 2014.

[62] K. Verdelis, L. Lukashova, E. Atti et al., "MicroCT morphometry analysis of mouse cancellous bone: Intra- and intersystem reproducibility," *Bone*, vol. 49, no. 3, pp. 580–587, 2011.

[63] M. L. Bouxsein, S. K. Boyd, B. A. Christiansen, R. E. Guldberg, K. J. Jepsen, and R. Müller, "Guidelines for assessment of bone microstructure in rodents using micro–computed tomography," *Journal of Bone and Mineral Research*, vol. 25, no. 7, pp. 1468–1486, 2010.

[64] Bruker microCT, *Method for ex-vivo micro-CT analysis of mouse bone (proximal tibia , distal femur)*, Method Note MCT-003, 2008.

[65] D. W. Dempster, J. E. Compston, M. K. Drezner et al., "Standardized nomenclature, symbols, and units for bone histomorphometry: a 2012 update of the report of the ASBMR Histomorphometry nomenclature committee," *Journal of Bone and Mineral Research*, vol. 28, no. 1, pp. 2–17, 2013.

[66] C. H. Turner and D. B. Burr, "Basic biomechanical measurements of bone: a tutorial," *Bone*, vol. 14, no. 4, pp. 595–608, 1993.

[67] O. O. Ogedengbe, A. I. Jegede, I. O. Onanuga et al., "Adjuvant potential of virgin coconut oil extract on antiretroviral therapy- induced testicular toxicity: an ultrastructural study," *Andrologia*, vol. 50, no. 3, 2018.

[68] R. E. Akhigbe, M. A. Hamed, and A. F. Odetayo, "HAART and anti-Koch's impair sexual competence, sperm quality and offspring quality when used singly and in combination in male Wistar rats," *Andrologia*, vol. 53, no. 2, article e13951, 2021.

[69] A. I. Jegede, U. Offor, I. O. Onanuga, E. C. S. Naidu, and O. O. Azu, "Effect of co-administration ofHypoxis hemerocallideaextract and antiretroviral therapy (HAART) on the histomorphology and seminal parameters in Sprague Dawley rats," *Andrologia*, vol. 49, no. 2, 2017.

[70] C. K. Onwuamah, O. C. Ezechi, E. C. Herbertson, R. A. Audu, I. A. O. Ujah, and P. G. C. Odeigah, "Foetal loss and enhanced fertility observed in mice treated with zidovudine or nevirapine," *PLoS One*, vol. 9, no. 9, article e107899, 2014.

[71] A. E. Herbison, "The gonadotropin-releasing hormone pulse generator," *Endocrinology*, vol. 159, no. 11, pp. 3723–3736, 2018.

[72] R. J. Aitken and S. D. Roman, "Antioxidant systems and oxidative stress in the testes," *Oxidative Medicine and Cellular Longevity*, vol. 1, no. 1, 24 pages, 2008.

[73] N. Rubio-Riquelme, N. Huerta-Retamal, M. J. Gómez-Torres, and R. M. Martínez-Espinosa, "Catalase as a molecular target for male infertility diagnosis and monitoring: an overview," *Antioxidants*, vol. 9, no. 1, pp. 78–118, 2020.

[74] P. Nguyen-Powanda and B. Robaire, "Oxidative stress and reproductive function in the aging male," *Biology (Basel)*, vol. 9, no. 9, pp. 282–315, 2020.

[75] S. Dutta, A. Majzoub, and A. Agarwal, "Oxidative stress and sperm function: a systematic review on evaluation and management," *Arab Journal of Urology*, vol. 17, no. 2, pp. 87–97, 2019.

[76] T. T. Turner and J. J. Lysiak, "Oxidative stress: a common factor in testicular dysfunction," *Journal of Andrology*, vol. 29, no. 5, pp. 488–498, 2008.

[77] S. Nagiah, A. Phulukdaree, and A. Chuturgoon, "Mitochondrial and oxidative stress response in HepG2 cells following acute and prolonged exposure to antiretroviral drugs," *Journal of Cellular Biochemistry*, vol. 116, no. 9, pp. 1939–1946, 2015.

[78] A. R. Eckard and S. Mora, "Bone health in HIV-infected children and adolescents," *Current Opinion in HIV and AIDS*, vol. 11, pp. 294–300, 2016.

[79] M. Weiß, B. Kost, I. Renner-Müller, E. Wolf, I. Mylonas, and A. Brüning, "Efavirenz causes oxidative stress, endoplasmic reticulum stress, and autophagy in endothelial cells," *Cardiovascular Toxicology*, vol. 16, no. 1, pp. 90–99, 2016.

[80] A. V. Ivanov, V. T. Valuev-Elliston, O. N. Ivanova et al., "Oxidative stress during HIV infection: mechanisms and consequences," *Oxidative Medicine and Cellular Longevity*, vol. 2016, Article ID 8910396, 18 pages, 2016.

[81] A. Zini, R. Bielecki, D. Phang, and M. T. Zenzes, "Correlations between two markers of sperm DNA integrity, DNA denaturation and DNA fragmentation, in fertile and infertile men," *Fertility and Sterility*, vol. 75, no. 4, pp. 674–677, 2001.

[82] C. Charneira, A. L. A. Godinho, M. C. Oliveira et al., "Reactive aldehyde metabolites from the anti-HIV drug abacavir: amino acid adducts as possible factors in abacavir toxicity," *Chemical Research in Toxicology*, vol. 24, no. 12, pp. 2129–2141, 2011.

[83] J. P. Havens, A. T. Podany, K. K. Scarsi, and C. V. Fletcher, "Clinical pharmacokinetics and pharmacodynamics of etravirine: an updated review," *Clinical Pharmacokinetics*, vol. 59, no. 2, pp. 137–154, 2020.

[84] A. Keppler, N. Gretz, R. Schmidt et al., "Plasma creatinine determination in mice and rats: an enzymatic method compares favorably with a high-performance liquid chromatography assay," *Kidney International*, vol. 71, no. 1, pp. 74–78, 2007.

[85] N. H. G. Holford, "Pharmacokinetics & pharmacodynamics: rational dosing & the time course of drug action," in *Basic & Clinical Pharmacology*, B. G. Katzung and T. W. Vanderah, Eds., McGraw-Hill, 15e edition, 2021.

[86] L. A. Bauer, "Clinical pharmacokinetic and pharmacodynamic concepts," in *Applied Clinical Pharmacokinetics*, McGraw-Hill, 3e edition, 2014.

[87] I. L. O. Buxton, "Pharmacokinetics: the dynamics of drug absorption, distribution, metabolism, and elimination," in *The Pharmacological Basis of Therapeutics*, L. L. Brunton, R. Hilal-Dandan, and B. C. Knollmann, Eds., Goodman & Gilman's, 13e edition, 2018.

[88] R. J. Roman, "Renal Blood Flow," in *Laser-Doppler blood flowmetry*, A. P. Shepherd and P. Å. Öberg, Eds., vol. 107 of Developments in Cardiovascular Medicine, pp. 289–304, Springer, Boston, Springer, Boston, MA, 1990.

[89] K. PTW and K. GB, "Importance of hepatic flows in liver transplantation," *Journal of Hepatology and Gastrointestinal disorders*, vol. 2, no. 2, pp. 15–17, 2016.

[90] K. E. Barrett, S. M. Barman, H. L. Brooks, and J. X.-J. Yuan, "Function of the male reproductive system," *Ganong's Review of Medical Physiology*, vol. 26e, 2021.

[91] E. Klieser, C. Mayr, T. Kiesslich et al., "The crosstalk of miRNA and oxidative stress in the liver: from physiology to pathology and clinical implications," *International Journal of Molecular Sciences*, vol. 20, no. 21, p. 5266, 2019.

[92] X. Yang and L. Han, "Roles of renal drug transporter in drug disposition and renal toxicity," *Advances in Experimental Medicine and Biology*, vol. 1141, pp. 341–360, 2019.

[93] European Medicines Agency Committee for Medicinal Products for Human Use (CHMP), *Assessment report*, Triumeq, 2014, International non-proprietary name: dolutegravir / abacavir / lamivudine. Procedure No. EMEA/H/C/002754/0000, https://www.ema.europa.eu/en/documents/assessment-report/triumeq-epar-public-assessment-report_en.pdf.

[94] *CHMP Assessment report for Intelence*, European Medicines Agency Evaluation of Medicines for Human Use, 2008.

[95] G. H. Campolina-Silva, R. A. Hess, and C. A. Oliveira, "Seasonal variation of cell proliferation and apoptosis in the efferent ductules and epididymis of the Neotropical bat *Artibeus lituratus* (Chiroptera, Phyllostomidae)," *General and Comparative Endocrinology*, vol. 273, pp. 3–10, 2019.

[96] R. M. Sharpe, C. Mckinnell, C. Kivlin, and J. S. Fisher, "Proliferation and functional maturation of Sertoli cells, and their relevance to disorders of testis function in adulthood," *Reproduction*, vol. 125, no. 6, pp. 769–784, 2003.

[97] H. J. Stellbrink, C. Orkin, J. R. Arribas et al., "Comparison of changes in bone density and turnover with abacavir-lamivudine versus tenofovir-emtricitabine in HIV-infected adults: 48-week results from the ASSERT study," *Clinical Infectious Diseases*, vol. 51, no. 8, pp. 963–972, 2010.

[98] E. Negredo, P. Domingo, N. Pérez-Álvarez et al., "Improvement in bone mineral density after switching from tenofovir to abacavir in HIV-1-infected patients with low bone mineral density: two-centre randomized pilot study (OsteoTDF study)," *The Journal of Antimicrobial Chemotherapy*, vol. 69, no. 12, pp. 3368–3371, 2014.

[99] R. W. S. Li, C. Yang, S. W. Chan et al., "Relaxation effect of abacavir on rat basilar arteries," *PloS one*, vol. 10, no. 4, article e0123043, 2015.

[100] A. Mediero, F. M. Kara, T. Wilder, and B. N. Cronstein, "Adenosine A_{2A} Receptor Ligation Inhibits Osteoclast Formation," *The American Journal of Pathology*, vol. 180, no. 2, pp. 775–786, 2012.

[101] J. Li, I. Sarosi, R. C. Cattley et al., "*Dkk1* -mediated inhibition of Wnt signaling in bone results in osteopenia," *Bone*, vol. 39, no. 4, pp. 754–766, 2006.

[102] T. Ueland, L. Stilgren, and J. Bollerslev, "Bone matrix levels of dickkopf and sclerostin are positively correlated with bone mass and strength in postmenopausal osteoporosis,"

International Journal of Molecular Sciences, vol. 20, no. 12, p. 2896, 2019.

[103] L. Calza, E. Magistrelli, V. Colangeli et al., "Dual raltegravir-etravirine combination as maintenance regimen in virologically suppressed HIV-1-infected patients," *AIDS Research and Human Retroviruses*, vol. 33, no. 7, pp. 632–638, 2017.

[104] L. A. Battalora, B. Young, and E. T. Overton, "Bones, fractures, antiretroviral therapy and HIV," *Current Infectious Disease Reports*, vol. 16, no. 2, p. 393, 2014.

[105] J. Jürimäe, "Interpretation and application of bone turnover markers in children and adolescents," *Current Opinion in Pediatrics*, vol. 22, no. 4, pp. 494–500, 2010.

[106] M. R. Pinzone, M. di Rosa, M. Malaguarnera et al., "Vitamin D deficiency in HIV infection: an underestimated and undertreated epidemic," *European Review for Medical and Pharmacological Sciences*, vol. 17, no. 9, pp. 1218–1232, 2013.

[107] P. Mansueto, A. Seidita, G. Vitale, S. Gangemi, C. Iaria, and A. Cascio, "Vitamin D deficiency in HIV infection: not only a bone disorder," *BioMed Research International*, vol. 2015, Article ID 735615, 18 pages, 2015.

Hindawi
Oxidative Medicine and Cellular Longevity
Volume 2021, Article ID 5570331, 22 pages
https://doi.org/10.1155/2021/5570331

Research Article

Effect of Omega-3 or Omega-6 Dietary Supplementation on Testicular Steroidogenesis, Adipokine Network, Cytokines, and Oxidative Stress in Adult Male Rats

Amira Moustafa

Department of Physiology, Faculty of Veterinary Medicine, Zagazig University, 44519 Zagazig, Egypt

Correspondence should be addressed to Amira Moustafa; amiramostafa@zu.edu.eg

Received 2 March 2021; Revised 15 May 2021; Accepted 9 June 2021; Published 29 June 2021

Academic Editor: Yi Fang

This study was undertaken to elucidate the effect of omega-3 and omega-6 supplementation on the levels of different adipokines and cytokines, as well as the antioxidant system, in relation to male reproductive hormones and testicular functions. Adult male Sprague-Dawley rats were daily gavaged with either physiological saline (control group), sunflower oil (omega 6 group; 1 mL/kg body weight), or fish oil (omega-3 group; 1000 mg/kg body weight) for 12 weeks. The administration of omega-3 or omega-6 resulted in decreased serum concentrations of kisspeptin 1, gonadotropin-releasing hormone, luteinizing hormone, follicle-stimulating hormone, and testosterone. In addition, it downregulated the mRNA expression levels of steroidogenic genes. The intratesticular levels of apelin, adiponectin, and irisin were elevated while chemerin, leptin, resistin, vaspin, and visfatin were declined following the administration of either omega-3 or omega-6. The testicular concentration of interleukin 10 was increased while interleukin 1 beta, interleukin 6, tumor necrosis factor α, and nuclear factor kappa B were decreased after consumption of omega-3 or omega-6. In the testes, the levels of superoxide dismutase, catalase, glutathione peroxidase 1, and the total antioxidant capacity were improved. In conclusion, the administration of omega-3 or omega-6 adversely affects the process of steroidogenesis but improves the antioxidant and anti-inflammatory status of the reproductive system via modulating the levels of testicular adipokines.

1. Introduction

Based on their chemical nature, polyunsaturated fatty acids (PUFAs) are categorized into three groups: omega-3, omega-6, and omega-9. Linoleic acid, which is plentiful in vegetable oils such as sunflower oil, is the primary dietary source of omega-6 PUFA [1], and eicosapentaenoic acid (EPA) and docosahexaenoic acid (DHA) omega-3 PUFAs can be directly obtained from fish oils. Although diets rich in PUFAs are supposedly healthier, most people consume a higher amount of omega-6 PUFAs than required for normal physiological functioning, primarily as linoleic acid [2]. In particular, the Western diet is relatively low in omega-3 PUFAs and abundant in omega-6 PUFAs [3]. In both humans and animals, decreasing the consumption of omega-6 and increasing the intake of omega-3 are encouraged for better health [3]. Omega-3 fatty acids derived from fish oil have been shown to decrease inflammation, improve cardiac function [4], promote lipid degradation [5], and prevent neurological and psychiatric disorders [6]. Oxidative stress represents the imbalance between reactive oxygen species (ROS) production and the antioxidant defense mechanism. Spermatozoa are rich in mitochondria and are highly susceptible to ROS, and excess ROS production has been reported as a primary cause of male infertility [7]. Omega-3 PUFAs have been shown to enhance antioxidant enzyme activity and protect cells from excess ROS [8].

Adipokines work as autocrine, paracrine, and endocrine signaling molecules [9] that connect obesity and infertility. Adipokines are secreted primarily from adipose tissue, as well as lymphocytes, fibroblasts, and macrophages [10, 11]. Adipokines and their receptors are namely expressed in testicular cells: Sertoli cells, Leydig cells, and spermatozoa [12]. Moreover, several adipokines such as adiponectin,

leptin, visfatin, chemerin, resistin, progranulin, and vaspin have been revealed in semen [13]. The expression of adipokines genes in the brain and pituitaries [14] suggests that adipokines could centrally act on the hypothalamus-pituitary axis and regulate reproductive functions.

In males, hypothalamic neurons secrete gonadotropin-releasing hormone (GnRH) that triggers the release of follicle-stimulating hormone (FSH) and luteinizing hormone (LH) from the pituitary gland, which in turn regulate testicular steroidogenesis and spermatogenesis [15]. In Leydig cells, testosterone is biosynthesized from cholesterol by a series of steroidogenic enzymes. First, the steroidogenic acute regulatory protein (StAR) mediates the process of importation of cholesterol into the mitochondria. In the mitochondria, cholesterol side-chain cleavage enzyme (CYP11A1) converts cholesterol into pregnenolone, which is then converted to progesterone by 3β-hydroxysteroid dehydrogenase (3β-HSD) [16]. 17α-hydroxylase/17, 20-lyase (CYP17A1), converts progesterone into androstenedione, which is converted to testosterone by 17β-hydroxysteroid dehydrogenase (17β-HSD), and testosterone is converted to estradiol by aromatase cytochrome P450 (CYP19) [16]. Thus, the synthesis of sex steroid hormones and the resultant male fertility could be influenced by the activity and/or expression of testicular steroidogenic enzymes.

The hormonal interaction between adipose tissue and the gonads is complex. Understanding the contribution of adipokines in testicular functions is of special interest, and little is known about the effect of omega-3 and omega-6 supplementation on testicular adipokines, particularly their potential effects on spermatogenesis and steroidogenesis. Therefore, the present study is aimed at assessing adipokines (leptin, adiponectin, chemerin, apelin, visfatin, vaspin, resistin, and irisin) in testicular tissues, examining the mRNA expression of steroidogenic genes, and determining the anti-inflammatory and antioxidant potentials of omega-3 and omega-6.

2. Materials and Methods

2.1. Tested Compounds. Omega-3 plus capsules were purchased from the SEDICO Company (Cairo, Egypt) and were 1000 mg fish oil soft gel capsules containing 13% EPA and 9% DHA.

Sunflower oil was purchased from Arma Oils Co. (10th of Ramadan City, Egypt) and contained a higher concentration of linoleic acid (polyunsaturated omega-6; 59%) than oleic acid (monounsaturated omega-9; 30%) [17].

2.2. Animal Experiment. Thirty adult Sprague-Dawley male rats (body weight, 300–330 g) were purchased from the animal research center (Faculty of Veterinary Medicine, Zagazig University). Rats were housed with two rats per cage under a light-dark cycle of 12 : 12 h in a controlled room with a constant temperature of 22°C and 50% humidity. Rats were acclimatized to the housing conditions for two weeks prior to the experiment, and pellet food and water were supplied ad libitum. Rats were randomly assigned to the control group ($n = 10$), the sunflower oil group ($n = 10$), or the omega-3 group ($n = 10$). For 12 weeks, rats were administered the following by oral gavage each day (between 8:00 and 9:00 a.m.): (1) physiological saline (1 mL/kg body weight/d; the control group); (2) sunflower oil, rich in omega-6 PUFAs [1] (1 mL/kg body weight/d; the sunflower group); and (3) omega-3 capsules, rich in omega-3 PUFAs [18] (1000 mg/kg body weight/d; the omega-3 group). Bodyweight and food intake were measured weekly. The amount of oils and saline were readjusted with the increase in body weight.

The study was approved by the Institutional Animal Care and Use Committee of the Faculty of Veterinary Medicine, Zagazig University (Permit Number: ZU-IACUC/2/F/103/2020).

2.3. Sample Collection. Rats were sacrificed by rapid decapitation [19] after overnight fasting, and trunk blood was collected and centrifuged at 4000 rpm for 15 minutes at 4°C. Then, the serum was separated and stored at −20°C until analysis. The testicular homogenates for cytokines, adipokines, and hormone measurements were prepared by suspending the testes in ice-cold phosphate buffer (0.1 M, 7.4), disrupting the tissues by a homogenizer, and centrifugation at 3000 rpm for 20 min. The supernatants were aliquoted and used for different measurements. For histological and immunohistochemical examinations, the testes, epididymides, prostate glands, and seminal vesicles were excised, weighed, and fixed in 10% neutral buffered formalin solution. For histological examination, the testicular sections were stained with hematoxylin and eosin (H&E). Part of the testes was rapidly excised, weighed, snap-frozen in liquid nitrogen, and stored at −80°C for gene expression.

2.4. Analysis of Semen Quality. The cauda epididymides were immediately excised after sacrifice. The tissues were sliced with a scalpel several times in a Petri dish containing 2 mL normal saline at 37°C to release spermatozoa, and the percentage of sperm motility was assessed using a light microscope (×40) as described previously [20–22]. Semen samples were diluted five times (v/v) with normal saline containing a few drops of formalin (40%) to kill the spermatozoa, and sperm was counted using a hemocytometer [23]. Morphological abnormalities of the sperm were identified, and the results were expressed as percentages [24].

2.5. Measurement of Hormones. The enzyme-linked immunosorbent assay (ELISA; Cusabio Biotech Co., Wuhan, China) was used to determine the concentrations of kisspeptin 1 (CSB-E13434r), FSH (CSB-E06869r), LH (CSB-E12654r), and testosterone (CSB-E05100r) according to the manufacturer's protocol. The analytical sensitivities of these assays for kisspeptin 1, FSH, LH, and testosterone were 0.039 ng/mL, 0.07 mIU/mL, 0.15 mlU/mL, and 0.06 ng/mL, respectively. The intra-assay and interassay coefficients of variation were below 10%.

GnRH, prolactin, and 17β estradiol (E2) concentrations were estimated using an ELISA kit (MyBioSource Inc., San Diego, CA, USA; Cat No. MBS268023, MBS2512489, and MBS263466, respectively) according to the manufacturer's instructions. The analytical sensitivities of this assay for

GnRH, prolactin, and E2 were 5.0 pg/mL, 0.469 ng/mL, and 5.0 pg/mL, respectively. The coefficients of variation were less than 8%. The absorbance was measured at 450 nm using a *DNM-9602* microplate reader (PERLONG, Beijing, China).

The testicular concentration of prostaglandin F2 alpha (PGF2α) was estimated using a rat ELISA kit from MyBioSource Inc. (San Diego, CA, USA; Cat No. MBS764597), and prostaglandin E2 (PGE2) was assessed by ELISA kit from LifeSpan BioScience, Inc. (WA, USA; Cat No. LS-F27545) according to the manufacturer's protocol at an absorbance of 450 nm. The analytical sensitivities of these assays for PGF2α and PGE2 were <4.688 pg/mL and 0.1 ng/mL, respectively. The intra- and interassay coefficients of variation were <8% and <10%, respectively.

2.6. Measurement of Testicular Adipokines and Cytokines. Rat ELISA kits (Cusabio Biotech Co., Wuhan, China) were used to measure the concentrations of testicular adipokines, namely adiponectin (Cat No. CSB-E07271r), apelin (Cat No. CSB-E13435r), leptin (Cat No. CSB-E07433r), resistin (Cat No. CSB-E06885r), vaspin (Cat No. CSB-E09813r), and visfatin (Cat No. CSB-E08941r), following the manufacturer's instructions (analytic sensitivities: 0.039 ng/mL, 0.078 ng/mL, 0.068 ng/mL, 31.25 pg/mL, 7.8 pg/mL, and 0.78 ng/mL, respectively). The intra-assay and interassay precisions were <8% and <10%, respectively.

Chemerin concentrations were estimated using a rat ELISA kit (MyBioSource Inc., San Diego, CA, USA; Cat No. MBS760975), and testicular irisin levels were measured using another ELISA kit (Wuhan Fine Biotech Co. Ltd., China; Cat No. ER1486) according to the manufacturer's protocol (analytical sensitivities, 18.75 pg/mL and 0.469 ng/mL, respectively). A microplate reader (DNM-9602, PERLONG, Beijing, China) was used to measure the absorbance at 450 nm.

The level of the proinflammatory cytokine interleukin 1 beta (IL-1B) was assessed using an ELISA kit (MyBioSource Inc., San Diego, CA, USA; Cat No. MBS825017) with a sensitivity of 15 pg/mL. Rat ELISA kits (Cusabio Biotech Co., Wuhan, China) were used to measure the intratesticular concentrations of interleukin 6 (IL-6; Cat No. CSB-E04640r), interleukin-10 (IL-10; Cat No. CSB-E04595r), tumor necrosis factor-α (TNF-α; Cat No. CSB-E11987r), and nuclear factor kappa B (NF-κB; Cat No. CSB-E13148r) according to the manufacturer's instructions (analytical sensitivities, 0.078 pg/mL, 0.78 pg/mL, 1.56 pg/mL, and 0.39 pg/mL, respectively). The intra-assay and interassay precisions were below 8% and 10%, respectively.

2.7. Serum Lipid Analysis. Serum concentrations of free fatty acids were assessed by a rat ELISA kit (Cusabio Biotech Co., Wuhan, China; Cat No. CSB-E08770r) with a sensitivity of 4 ng/mL. Serum triglycerides, cholesterol, HDL-cholesterol, LDL-cholesterol, and VLDL-cholesterol concentrations were determined using the Reactivos Spinreact colorimetric assay kits (Barcelona, Spain) according to the manufacturer's instructions.

2.8. Spermatozoa Lipid Analysis. Spermatozoa were separated by centrifuging semen at 1000 g for 15 min. seminal plasma was carefully removed, filtered, and stored at −80°C until use. The remaining pellet was washed three times with phosphate-buffered saline (PBS), then resuspended in 0.5 mL PBS, homogenized, and sonicated. The concentrations of total lipids, triglycerides, and cholesterol were assessed using the Reactivos Spinreact colorimetric assay kits (Barcelona, Spain) following the manufacturer's instructions. Phospholipids were measured calorimetrically at 570 nm using an ELISA kit (Abnova, Taipei, Taiwan; Cat No. KA1635) according to the manufacturer's protocol. The levels of arachidonic acid were estimated using a quantitative ELISA kit (Creative Diagnostics, New York, USA; Cat No. DEIA-Bj2354) at 450 nm according to the manufacturer's instructions.

2.9. Analysis of Fructose, α-Glucosidase, and Acid Phosphatase in Seminal Plasma. Fructose concentrations in the seminal plasma were measured spectrophotometrically using an assay kit (Sigma Chemical Company, St. Louis, MO, USA), and the absorbance values were read at 340 nm wavelength. Alpha-glucosidase was estimated using a rat ELISA kit (Cusabio Biotech Co., Wuhan, China; Cat No. CSB-E09906r), and the concentrations of acid phosphatase were determined using another ELISA kit (Reagent Genie, Dublin, Ireland) following the manufacturer's protocol. The intra-assay and interassay precisions were below 8% and 10%, respectively.

2.10. Immunohistochemistry of the Androgen Receptor. The specimens of testes, seminal vesicles, prostate glands, and epididymides were fixed in 10% neutral buffered formalin solution, and the paraffin sections were prepared [25]. An UltraVision LP large volume detection system (Thermo Fisher Scientific, Fremont, USA; Cat No. TP-060-HL) was used for the detection of immunohistochemical expression and the localization of androgen receptor in the target tissues. The tissue slices (4 μm thick) were deparaffinized and rehydrated, and endogenous peroxidase activity was blocked using hydrogen peroxide (H_2O_2; 3% solution in methanol) for 10 min. Antigen retrieval was performed by heating the tissue sections in 10 mM citrate buffer (pH, 6.0) for 5 min, followed by cooling at room temperature for 20 min. After rinsing three times in PBS, the nonspecific background staining was blocked by incubating the tissue slices with Ultra V Block for 5 minutes at room temperature. Then, the tissue slices were incubated overnight at 4°C with a rabbit polyclonal antibody against androgen receptor (200 μg/mL; Thermo Fisher Scientific, Fermont, USA; Cat No. RB-9030-R7). The slices were rinsed in PBS, incubated with a biotinylated goat anti-polyvalent for 10 minutes at room temperature, followed by incubation with streptavidin peroxidase for another 10 minutes at room temperature. 3,3′-Diaminobenzidine (DAB; Quartett Immunodiagnostika GmbH, Berlin, Germany) was used as a chromogen, and sections were counterstained with hematoxylin. Negative control slides were incubated without the primary antibody. The mean intensity of the brown staining was obtained from five

Table 1: Specific primers used for the analysis of different gene expressions.

Gene	GenBank accession no.	Primer sequences (5′-3′)	Orientation	Product size (bp)
STAR	NM_031558.3	CACAGTCATCACCCATGAGC	Forward	166
		AGCTCTGATGACACCGCTTT	Reverse	
CYP17A1	NM_012753	CTCTGGGCACTGCATCAC	Forward	114
		CAAGTAACTCTGCGTGGGT	Reverse	
CYP19	NM_017085	GCCTGTCGTGGACTTGGT	Forward	142
		GGTAAATTCATTGGGCTTGG	Reverse	
3β-HSD	M38178	TGTGCCAGCCTTCATCTAC	Forward	145
		CTTCTCGGCCATCCTTTT	Reverse	
17β-HSD	NM_054007	GACCGCCGATGAGTTTGT	Forward	140
		TTTGGGTGGTGCTGCTGT	Reverse	
CYP11A1	J05156	CTTTGGTGCAGGTGGCTAG	Forward	115
		CGGAAGTGCGTGGTGTTT	Reverse	
GAPDH	NM_017008.4	GTGCCAGCCTCGTCTCATAG	Forward	122
		CGTTGATGGCAACAATGTCCA	Reverse	

[1]Steroidogenic acute regulatory protein (StAR); 17α-hydroxylase/17, 20-lyase (CYP17A1); aromatase cytochrome P450 (CYP19); 3β-hydroxysteroid dehydrogenase (3β-HSD); 17β-hydroxysteroid dehydrogenase (17β-HSD); cholesterol side-chain cleavage enzyme (CYP11A1); glyceraldehyde 3-phosphate dehydrogenase (*GAPDH*).

random fields in each slide using the ImageJ Fiji software version 1.53f. The formula $FI = 255 - i$ was used to calculate the final DAB intensity, where FI is the final DAB intensity, 255 is the maximum intensity for 8-bit images, and i is the mean DAB intensity obtained from the software [26].

2.11. RNA Extraction and cDNA Synthesis. Total RNA was extracted from the testes of all groups using TRIzol (Invitrogen; Thermo Fisher Scientific, Inc.) according to the manufacturer's instructions as previously indicated [20, 22]. The NanoDrop ND-1000 spectrophotometer (NanoDrop Technologies, Wilmington, Delaware, USA) was used to determine the concentration and purity of the total RNA. A HiSenScript™ RH (-) cDNA synthesis kit (iNtRON Biotechnology Co., South Korea) was utilized to reverse-transcribe the total RNA into cDNA following the manufacturer's protocol. Then, the reaction mixtures were incubated in a Veriti 96-well thermal cycler (Applied Biosystems, Foster City, CA) for 60 minutes at 45°C, followed by 10 minutes at 85°C.

2.12. Real-Time Polymerase Chain Reaction. A Stratagene Mx3005P system (Agilent Technologies, Santa Clara, CA, USA) and RbTaq™ qPCR 2X premix (SYBR green with low ROX; Enzynomics, Daejeon, Korea) were used to perform real-time reverse transcription-polymerase chain reaction (RT-PCR) following the manufacturer's instructions. The expression levels of the target mRNAs were quantified relative to the level of the GAPDH (housekeeping gene). The oligonucleotide primer sequences [27] (Eurofins Genomics, Ebersberg, Germany) are listed in Table 1.

2.13. Measurement of the Testicular Levels of the Antioxidant Enzymes and Lipid Peroxidation. The testicular levels of catalase (CAT), glutathione peroxidase 1 (GPx1), and ROS were determined using rat ELISA kits (MyBioSource Inc., San Diego, CA, USA; Cat No. MBS2600683, MBS451149, and MBS164653, respectively) according to the manufacturer protocol (sensitivities: 0.06 ng/mL, 0.63 ng/mL, and 2.49 U/mL, respectively). The intra-assay and interassay coefficients of variation were <8% and 10%, respectively. The levels of hydrogen peroxide (H_2O_2) and total antioxidant capacity (TAC) were measured using ELISA kits (Cell Biolabs, Inc., OxiSelect™, San Diego, CA, USA; Cat No. STA-844 and STA-360, respectively). The absorbance was measured at 540 nm and 490 nm, respectively, using a DNM-9602 microplate reader (PERLONG, Beijing, China). The concentrations of superoxide dismutase (SOD) were estimated using rat ELISA kits according to the manufacturer's instructions (Cusabio Biotech Co., Wuhan, China; Cat No. CSB-E08555r) with a sensitivity of 1.95 U/mL. The lipid peroxidation marker malondialdehyde (MDA) was determined using a colorimetric assay kit (Elabscience, Inc., Texas, USA; Cat No.E-BC-K025-S) with an analytic sensitivity of 0.38 nmol/mL according to the manufacturer's instructions.

2.14. Data Analysis. Data are illustrated as the means ± the standard error of the means and were analyzed using one-way analysis of variance. Post hoc multiple comparisons were performed using Tukey's test. The statistical significance was set at $P < 0.05$.

3. Results

3.1. Effect of Omega-3 and Sunflower Oil on Body Weight and Sperm Parameters. The omega-3 group exhibited significantly less body weight gain than the other two groups (Figure 1(a); $P < 0.01$). Neither omega-3 nor sunflower oil administration affected the sperm cell concentration or sperm motility (Figures 1(b) and 1(c), respectively), but both significantly increased the number of morphologically

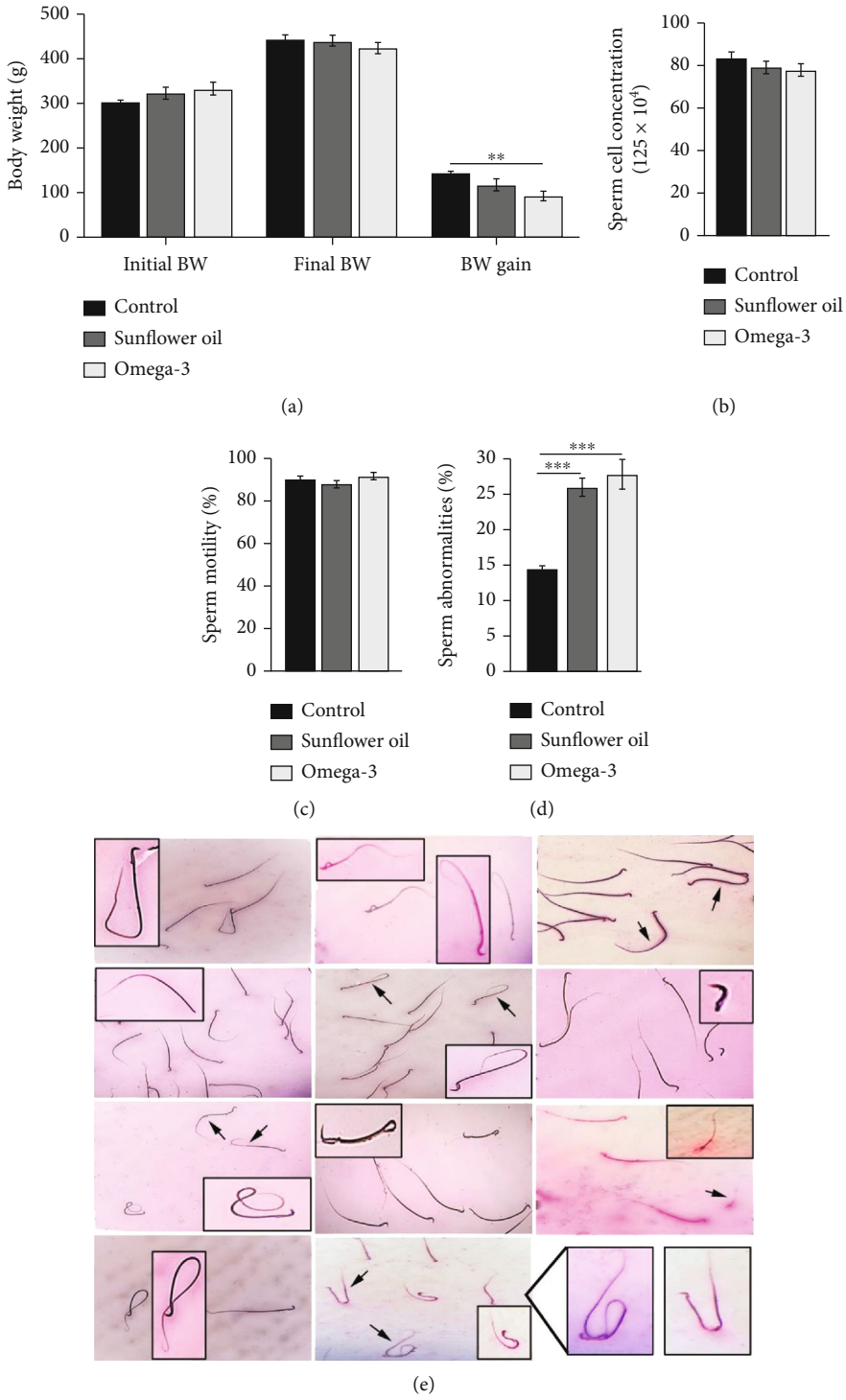

Figure 1: Changes in bodyweight and sperm parameters. (a) Changes in initial and final body weight and body weight gain (g) in the control, sunflower oil, and omega-3 groups. (b–d) Sperm count, motility (%), and abnormalities (%), respectively, in the control, sunflower oil, and omega-3 groups. Data are mean ± SEM ($n = 10$/group). $^{**}P < 0.01$ and $^{***}P < 0.001$ by Tukey's multiple comparison post hoc test. (e) Photomicrographs of sperm abnormalities including: tail abnormalities, bent neck, detached head and tail, and amorphous head.

abnormal sperms (Figure 1(d); $P < 0.01$). The observed sperm abnormalities included tail abnormalities (looped tail, curved tail, coiled tail, and detached tail), head abnormalities (amorphous head and detached head), and bent neck (Figure 1(e)).

3.2. Effect of Omega-3 and Sunflower Oil on Serum and Sperm Lipid Profile. Serum levels of total cholesterol, free fatty acids, LDL, and HDL revealed no significant changes among different groups (Figures 2(a), 2(c), 2(d), and 2(e)). However, the levels of triglycerides and VLDL were

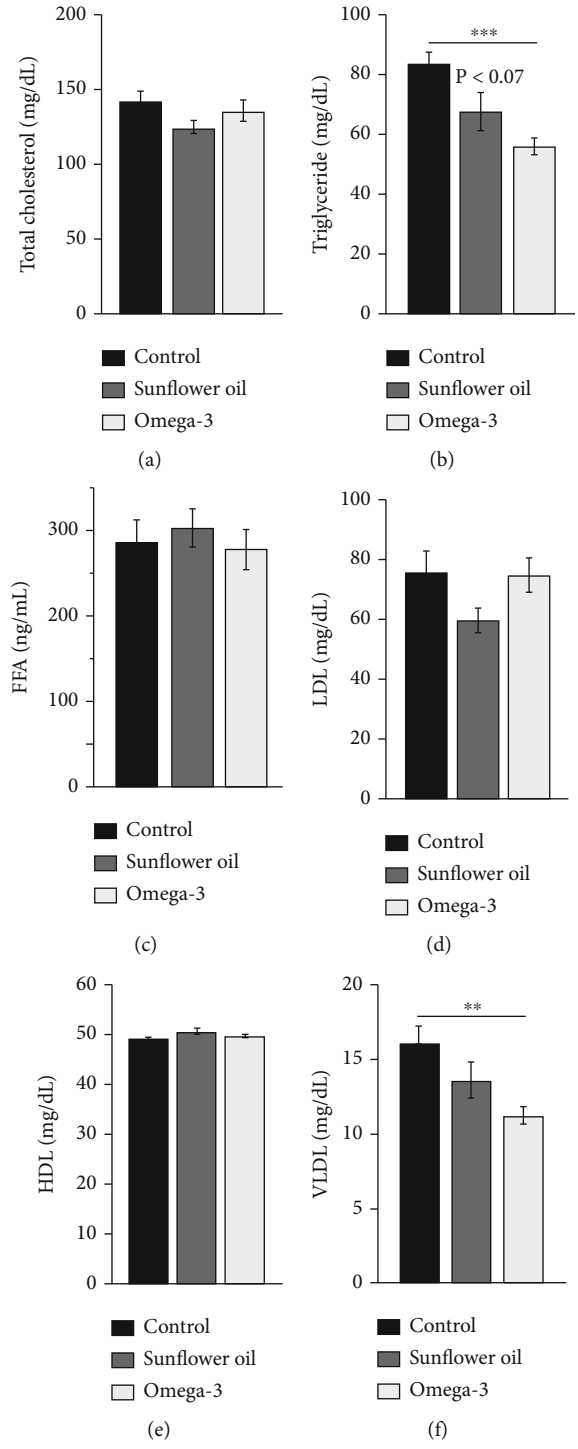

Figure 2: Changes in serum lipid profile. (a) Total cholesterol (mg/dL), (b) triglyceride (mg/dL), (c) free fatty acids (FFA, ng/mL), (d) low-density lipoprotein (LDL, mg/dL), (e) high-density lipoprotein (HDL, mg/dL), and (F) very low-density lipoprotein (VLDL, mg/dL) in the control, sunflower oil, and omega-3 groups. Data are expressed as mean ± SEM ($n = 10$/group). $^{**}P < 0.01$ and $^{***}P < 0.001$ by Tukey's multiple comparison post hoc test.

significantly declined following omega-3 administration (Figures 2(b) and 2(f); $P < 0.001$ and $P < 0.01$, respectively). In the sunflower oil group, triglycerides and VLDL concentrations tended to decrease, but the results remained insignificant (Figures 2(b) and 2(f)).

Sperm concentrations of arachidonic acid were significantly decreased in both omega-3 and sunflower oil groups compared with the control group (Figure 3(a); $P < 0.001$) and sharply reduced in the sunflower oil group compared with the omega-3 group (Figure 3(a); $P < 0.001$). Sperm

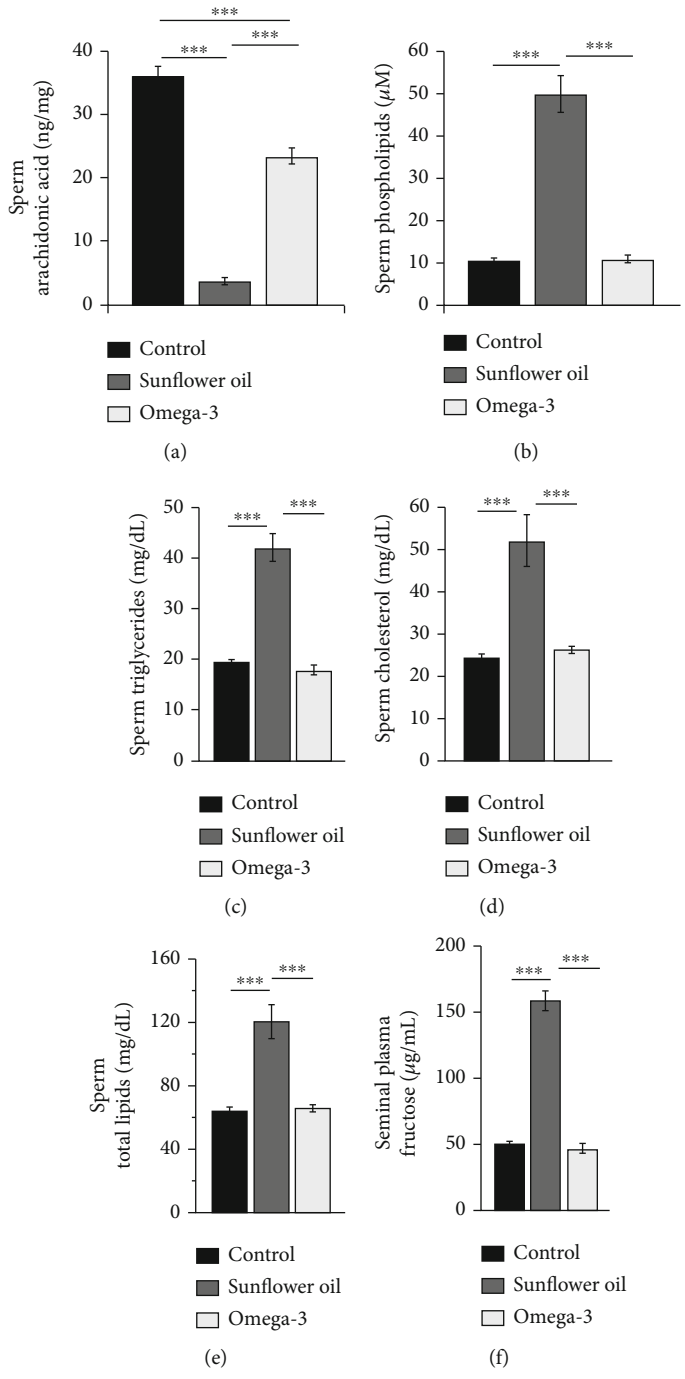

Figure 3: Continued.

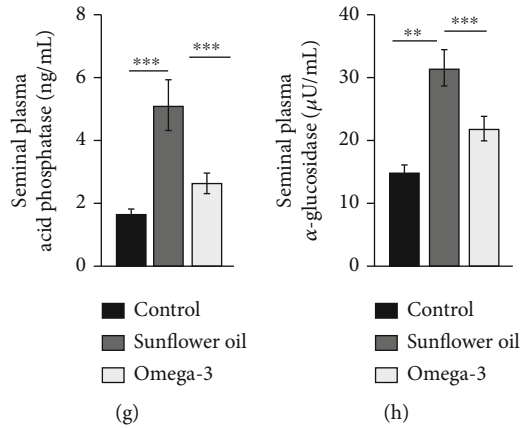

FIGURE 3: Changes in spermatozoa lipid composition and seminal plasma biochemistry. Spermatozoa lipid contents, namely, (a) arachidonic acid (ng/mg), (b) phospholipids (μM), (c) triglycerides (mg/dL), (d) cholesterol (mg/dL), and (e) total lipids (mg/dL) in the control, sunflower oil, and omega-3 groups. Seminal plasma levels of (f) fructose (μg/mL), (g) acid phosphatase (ng/mL), and (h) α-glucosidase (μU/mL) in the control, sunflower oil, and omega-3 groups. Data are presented as mean ± SEM ($n = 10$/group). $^{**}P < 0.01$ and $^{***}P < 0.001$ by Tukey's multiple comparison post hoc test.

levels of phospholipids, triglycerides, cholesterol, and total lipids were significantly elevated following sunflower oil administration compared with the control and omega-3 groups (Figures 3(b)–3(e); $P < 0.001$).

3.3. Effect of Omega-3 and Sunflower Oil on the Levels of Seminal Plasma Fructose, α-Glucosidase, and Acid Phosphatase. The levels of fructose (seminal vesicles), α-glucosidase (epididymides), and acid phosphatase (prostate glands) in seminal plasma were significantly increased in the sunflower oil group compared with the control and omega-3 groups (Figures 3(f)–3(h); $P < 0.001$).

3.4. Effect of Omega-3 and Sunflower Oil on Serum and Testicular Levels of Reproductive Hormones. Serum concentrations of kisspeptin, GnRH, LH, FSH, and testosterone were significantly reduced in the omega-3 and sunflower oil groups compared with the control group (Figures 4(a)–4(e); $P < 0.001$ and $P < 0.01$, respectively). The levels of prolactin and E2 were augmented in the omega-3 or sunflower oil groups compared with the control group (Figures 4(f) and 4(g); $P < 0.001$). However, the sunflower oil group showed a much higher E2 than the omega-3 group (Figure 4(g); $P < 0.001$).

The intratesticular concentrations of testosterone were significantly reduced in the sunflower oil and omega-3 group compared with the control group (Figure 4(h); $P < 0.001$), and such inhibition was significantly higher in the omega-3 group than in the sunflower oil group (Figure 4(h); $P < 0.001$). Moreover, the intratesticular levels of E2 were significantly reduced in the sunflower oil and omega-3 groups compared with the control group (Figure 4(i); $P < 0.001$), and the reduction was higher in the omega-3 group than in the sunflower oil group (Figure 4(i); $P < 0.001$).

3.5. Effect of Omega-3 and Sunflower Oil on the Steroidogenesis Genes Expression. To investigate the mechanism responsible for the inhibitory effect of sunflower oil and omega-3 on the process of steroidogenesis, RT-PCR was performed to detect the changes in genes regulating steroidogenesis. *STAR* mRNA levels were significantly reduced in the sunflower oil and omega-3 groups (Figure 5(a); $P < 0.05$). In addition, the expression levels of the *CYP11A1* and *3β-HSD* genes were downregulated in the sunflower oil and omega-3 groups (Figures 5(b) and 5(c); $P < 0.01$ and $P < 0.001$). The expression levels of *17β-HSD* mRNA were significantly decreased in both sunflower oil and omega-3 groups (Figure 5(d); $P < 0.05$). The administration of sunflower oil or omega-3 significantly downregulated the mRNA expression levels of *CYP17A1* (Figure 5(e); $P < 0.01$). The expression levels of the *CYP19* gene were significantly decreased by the sunflower oil and omega-3 administration (Figure 5(f); $P < 0.05$ and $P < 0.01$, respectively).

3.6. Effect of Omega-3 and Sunflower Oil on the Immunohistochemical Expression of the Androgen Receptor. In testicular tissues (Figure 6(a)), androgen receptor expression was revealed in the nuclei of spindle-shaped Leydig cells, myoid cells, and Sertoli cells in all examined groups. However, this expression was significantly increased in the omega-3 group compared with the control group (Figure 6(e); $P < 0.05$). No significant difference was noticed between the control group and the sunflower oil group, but the intensity of immunostaining was reduced in the sunflower oil group compared with the omega-3 group (Figure 6(e); $P < 0.001$). Sertoli cells were identified by their large columnar or pyramidal shape and oval nucleus and are attached to the basal lamina of the basement membrane. Leydig cells are characterized by a polyhedral shape with large prominent ovoid nuclei and are present in the connective tissues among the seminiferous tubules. Myoid cells are smooth muscle cells that surround the seminiferous tubules and are characterized by elongated shapes with spindle-shaped nuclei.

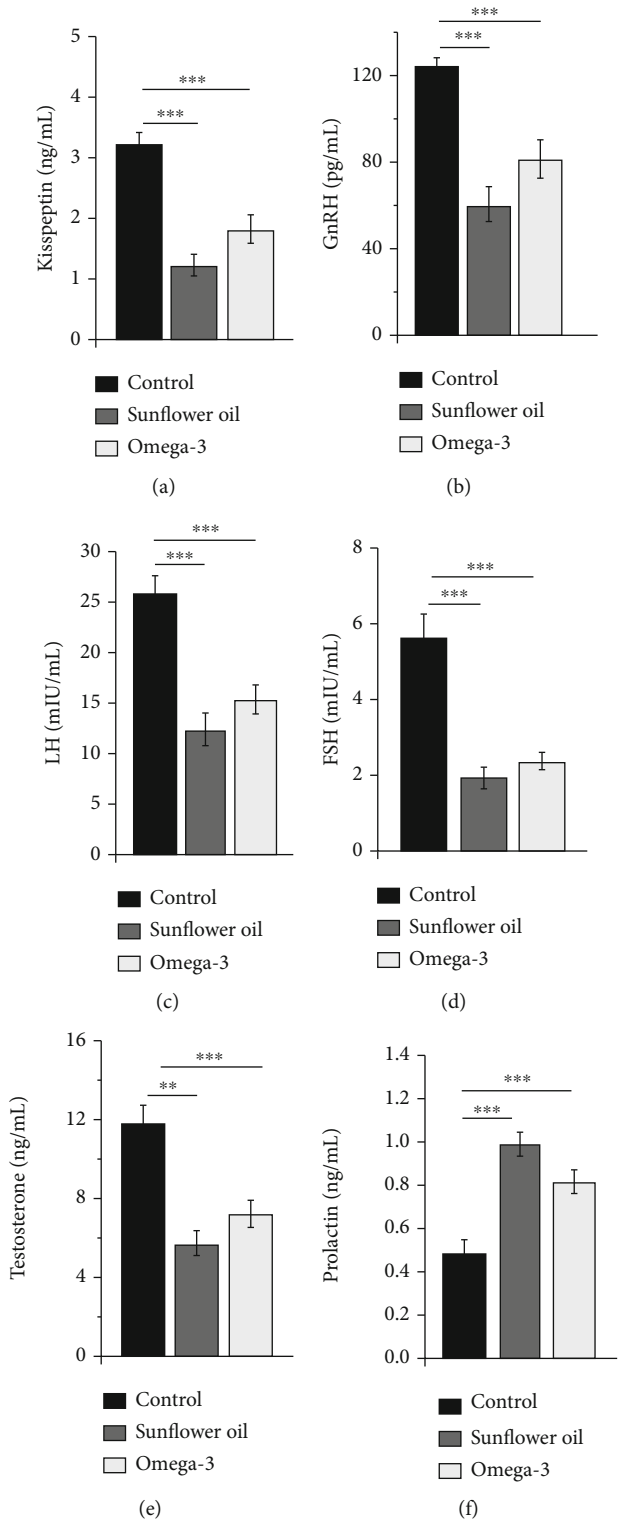

Figure 4: Continued.

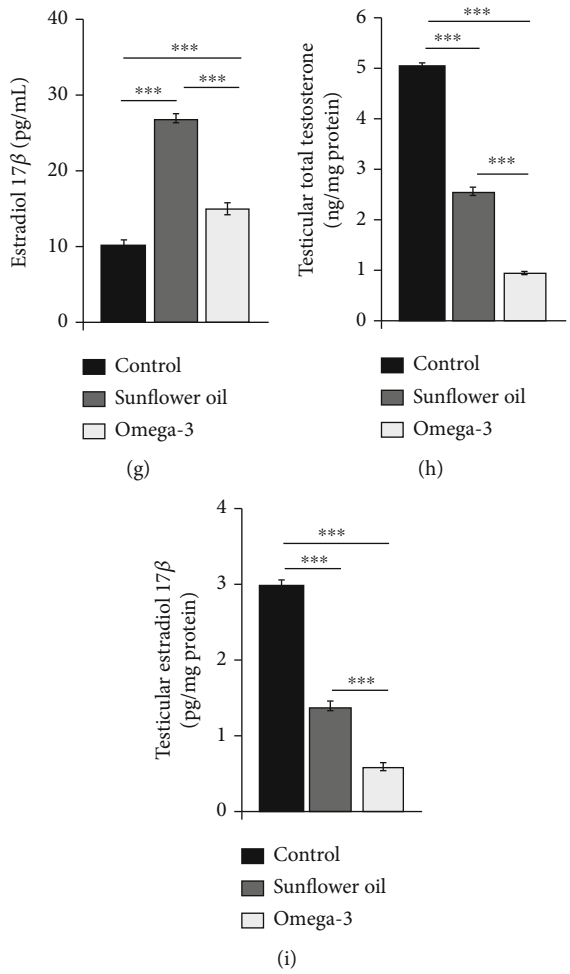

Figure 4: Changes in serum and testicular hormones concentrations. Serum concentrations of (a) kisspeptin (ng/mL), (b) gonadotropin-releasing hormone (GnRH; pg/mL), (c) luteinizing hormone (LH; mIU/mL), (d) follicle-stimulating hormone (FSH; mIU/mL), (e) testosterone (ng/mL), (f) Prolactin (ng/mL), and (g) estradiol 17β (E2; pg/mL) in the control, sunflower oil, and omega-3 groups. Testicular levels of (h) total testosterone (ng/mg) and (i) estradiol 17β (E2; pg/mg) in the control, sunflower oil, and omega-3 groups. Data are shown as mean ± SEM ($n = 10$/group). $^{**}P < 0.01$ and $^{***}P < 0.001$ by Tukey's multiple comparison post hoc test.

The epididymides of all three groups showed androgen receptor staining in the nuclei of interstitial stromal cells, and epithelial cells with robust staining of the latter (Figure 6(b)). The intensity of the androgen receptor staining was augmented in the omega-3 group compared with the control and sunflower oil groups (Figure 6(e); $P < 0.01$ and $P < 0.05$, respectively). The immunohistochemical staining of the androgen receptor in the seminal vesicles was located in the nuclei of the epithelial cells and fibromuscular stroma of all three groups (Figure 6(c)). The nuclear staining intensity was increased in the omega-3 group compared with the control and sunflower oil groups (Figure 6(e); $P < 0.001$ and $P < 0.01$, respectively). In the prostate gland, androgen receptor immunoreactivity was localized to the nuclei of the epithelial cells in all three groups (Figure 6(d)). However, the nuclear staining intensity was significantly decreased in the sunflower oil group compared with the omega-3 group (Figure 6(e); $P < 0.05$). The immunoreactivity of the androgen receptor was undetectable in the control sections of testes, epididymis, seminal vesicle, and prostate, which were incubated without the primary antibody (Figure 6(f)).

3.7. Effect of Omega-3 and Sunflower Oil on the Testicular Levels of Cytokines and Prostaglandins. The testicular levels of NF-κB, TNF-α, IL-1β, and IL-6 were significantly attenuated in the sunflower oil and omega-3 groups compared with the control group (Figures 7(a)–7(d); $P < 0.001$). However, the attenuation was considerably greater in the sunflower oil group than in the omega-3 group (Figures 7(a)–7(d); $P < 0.001$). Compared with the control group, the sunflower oil and omega-3 groups showed a significant increase in the testicular levels of IL-10 (Figure 7(e); $P < 0.001$), with more prominent changes in the omega-3 group than in the sunflower oil group. In the testes, the levels of both PGF2α and PGE2 were significantly diminished in the sunflower oil and omega-3 groups compared with the control group (Figures 7(f) and 7(g); $P < 0.001$), and the reduction was significantly larger in the sunflower oil group than in the omega-3 group (Figures 7(f) and 7(g); $P < 0.001$).

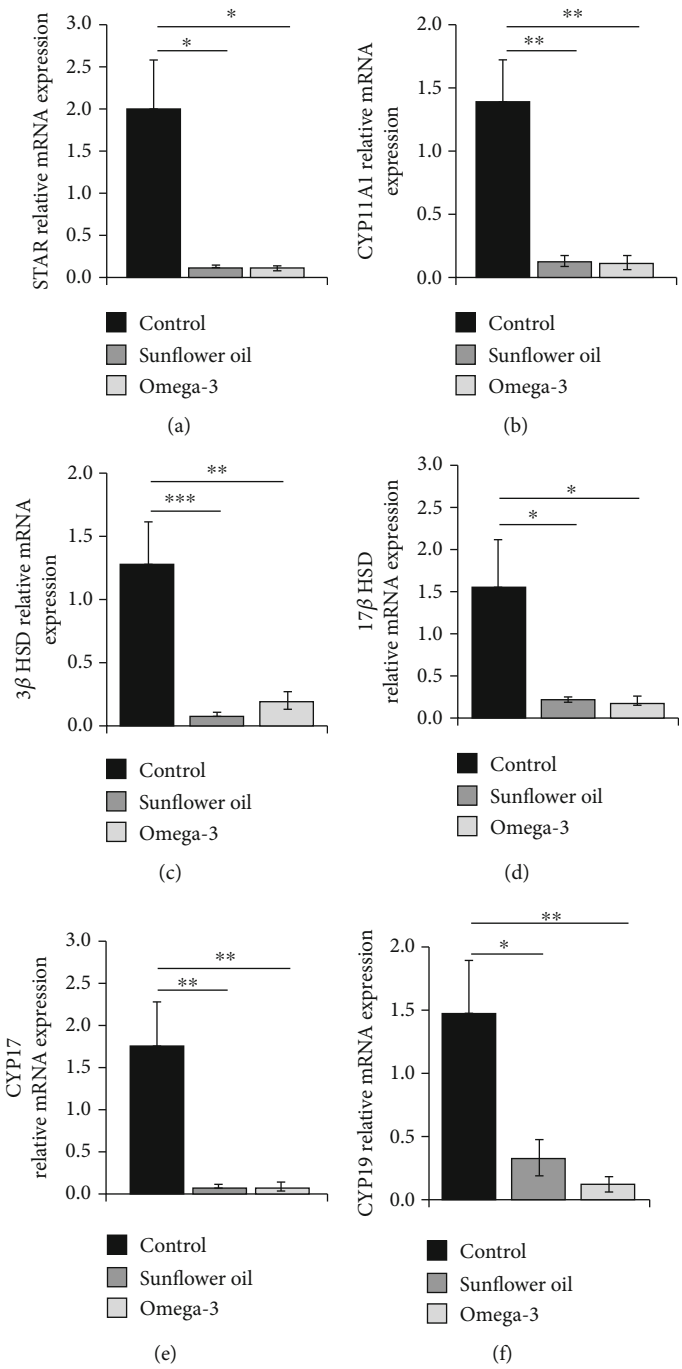

Figure 5: Changes in the expression levels of testicular steroidogenic genes. Relative expression levels of (a) Steroidogenic acute regulatory protein (*StAR*), (b) cholesterol side-chain cleavage enzyme (*CYP11A1*), (c) 3β-hydroxysteroid dehydrogenase (*3β-HSD*), (d) 17β-hydroxysteroid dehydrogenase (*17β-HSD*), (e) 17α-hydroxylase/17, 20-lyase (*CYP17A1*), and (f) cytochrome P450 aromatase (*CYP19*) in the control, sunflower oil, and omega-3 groups. Data are expressed as mean ± SEM. $^{*}P < 0.05$, $^{**}P < 0.01$, and $^{***}P < 0.001$ by Tukey's multiple comparison post hoc test.

3.8. Effect of Omega-3 and Sunflower Oil on the Testicular Concentrations of Adipokines. The testicular levels of adipokines, namely apelin, adiponectin, and irisin, were significantly increased in the sunflower oil and omega-3 groups compared with the control group, and the increment was larger in the sunflower oil group than in the omega-3 group (Figures 8(a)–8(c); $P < 0.001$). However, compared with the control group, the sunflower oil and omega-3 groups had significantly decreased testicular levels of chemerin, leptin, resistin, vaspin, and visfatin, and the reduction was larger in the sunflower oil group than in the omega-3 group (Figures 8(d)–8(h); $P < 0.001$).

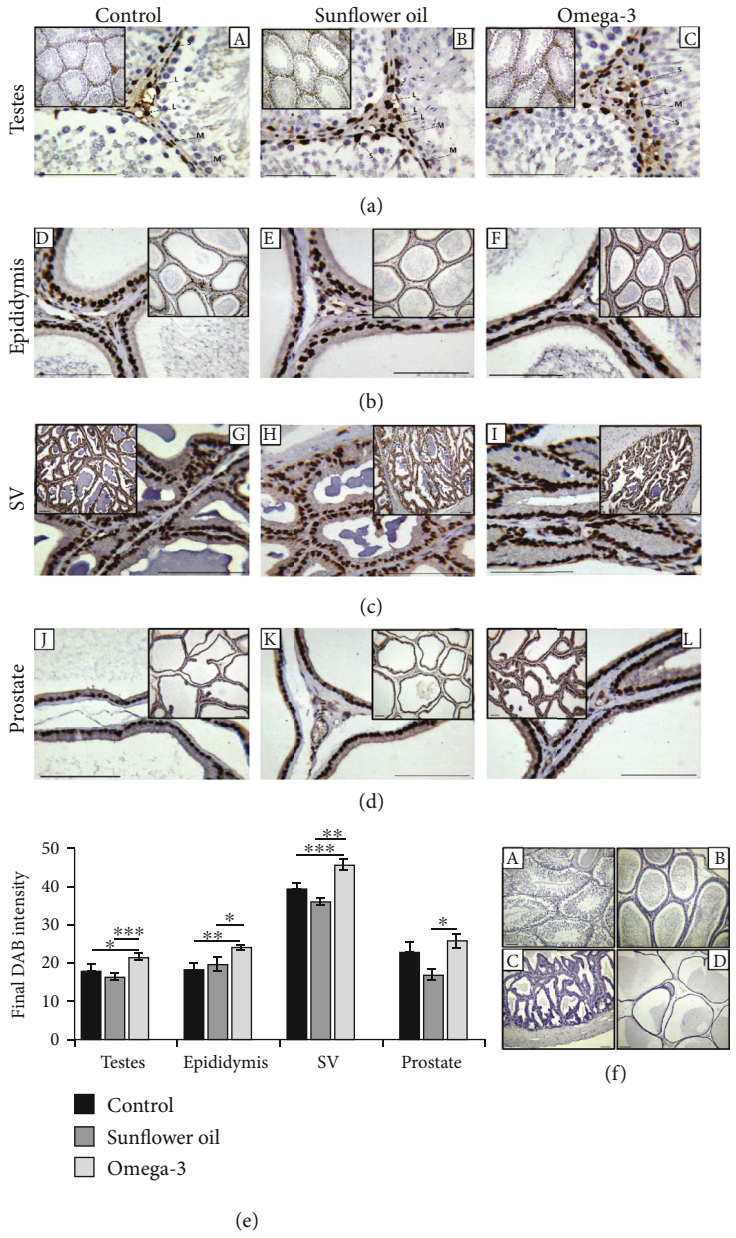

Figure 6: Immunohistochemical staining of androgen receptor in different reproductive tissues. Immunohistochemical distribution of androgen receptor in (a) testes, (b) epididymis, (c) seminal vesicle (SV), and (d) prostate of the control (A, D, G, and J, respectively), sunflower oil (B, E, H, and K, respectively), and omega-3 (C, F, I, and L, respectively) groups. (e) Quantitative analysis of the nuclear immunostaining of androgen receptor in the control, sunflower oil and omega-3 groups. Data are calculated by the ImageJ *Fiji* software and presented as mean ± SEM. $^{*}P < 0.05$, $^{**}P < 0.01$, and $^{***}P < 0.001$ by Tukey's multiple comparison post hoc test. (f) Negative tissue sections of (A) testes, (B) epididymis, (C) seminal vesicle, and (D) prostate. Scale bar = 100 μm.

3.9. Effect of Omega-3 and Sunflower Oil on the Testicular Levels of the Antioxidant Enzymes, ROS, and TAC. The testicular levels of SOD, CAT, GPx, and TAC were significantly elevated in the sunflower oil and omega-3 groups compared with the control group (Figures 9(a)–9(d); $P < 0.001$), with more elevation in the omega-3 group than in the sunflower oil group (Figures 9(a)–9(d); $P < 0.001$). Conversely, the levels of ROS, MDA, and H_2O_2 were lower in both sunflower oil and omega-3 groups than in the control group (Figures 9(e)–9(g); $P < 0.001$), with a greater reduction in the omega-3 group than in the sunflower oil group (Figures 9(e)–9(g); $P < 0.001$).

4. Discussion

Phospholipids and cholesterol are significant elements of human spermatozoa plasma membranes and are necessary for the fluidity, permeability, and capacitation of the membrane [28], and alteration in spermatozoa lipid contents has been linked to male infertility [29]. The results of the present study showed that only sunflower oil administration increases the spermatozoa content of phospholipids, triglycerides, cholesterol, and total lipids, which may be attributed to sunflower oil being rich in linoleic acid. However, the

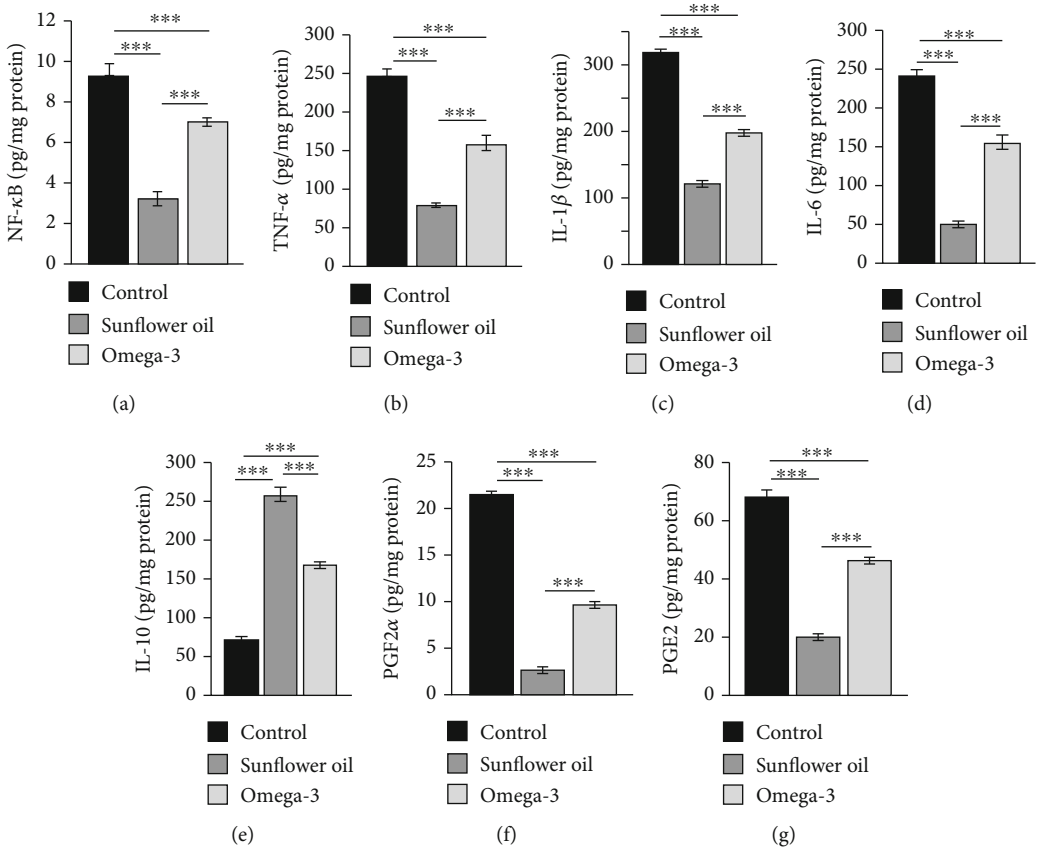

Figure 7: Changes in the testicular levels of cytokines and prostaglandins. Testicular concentrations of (a) NF-κB (pg/mg), (b) tumor necrosis factor alpha (TNF-α; pg/mg), (c) interleukin-1β (IL-1β; pg/mg), (d) interleukin-6 (IL-6; pg/mg), (e) interleukin-10 (IL-10; pg/mg), (f) prostaglandin F2 alpha (PGF2α; pg/mg), and (g) prostaglandin E2 (PGE2; pg/mg) in the control, sunflower oil, and omega-3 groups. Data are shown as mean ± SEM ($n = 10$/group). $^{***}P < 0.001$ by Tukey's multiple comparison post hoc test.

spermatozoa content of arachidonic acid was decreased after the administration of omega-3 or sunflower oil. Increasing the intake of linoleic acid has been demonstrated to increase [30] or decrease the tissue content of arachidonic acid [31, 32] where increased linoleic acid in the diet may compete with arachidonic acid for deacylation into the phospholipids [31–33]. The ingestion of omega-3 PUFAs from fish oil has been shown to reduce the membrane levels of arachidonic acid and decrease concomitantly the potential arachidonic acid synthesis of eicosanoids [34, 35]. The metabolism of arachidonic acid by cyclooxygenases results in the synthesis of 2-series prostaglandins: PGE2, PGI2, PGD2, and PGF2α. In the present study, the administration of omega-3 or sunflower oil for 12 weeks significantly reduced the circulating levels of PGE2 and PGF2α. Fish oil and omega-3 PUFA have been shown to diminish PGE2 production [36, 37], and the administration of 6 g/d DHA abolished endotoxin-stimulated mononuclear cell production of PGE2 [38].

Seminal plasma contains a mixture of various parameters originating from the epididymis and accessory sex glands, which are essential for sperm maturation and fertilization capacity [39]. Fructose is the primary energy source for sperm activity, and a decline in sperm motility and fertilization capability has been associated with low seminal fructose levels [40]. Acid phosphatase has been reported to be linked to semen concentration [41] and the carbohydrate metabolism of spermatozoa [42]. Furthermore, the activity of the seminal plasma α-glucosidase indicates the functional condition of the epididymis [43] and is closely correlated with ejaculate volume, sperm concentration, and acrosome reaction [44]. Decreased levels of fructose and low activity of α-glucosidase have been associated with high levels of omega-3 or omega-6 fatty acids in boar seminal plasma [45]. In the present study, although sunflower oil administration induced increases in the levels of fructose, acid phosphatase, and α-glucosidase in the seminal plasma, indicating a positive impact on the function of the epididymis and accessory glands, particularly the prostate and seminal vesicle, this did not affect semen properties.

Data about the effect of omega-3 and omega-6 PUFAs supplementation on the male reproductive system and semen quality are controversial. In humans, the administration of DHA (1 g/d) and EPA (1 g/d) ameliorated total sperm count, sperm motility, and morphology [46]. Moreover, men supplemented with fish oil exhibited increased testicular size and sperm concentration, along with decreased levels of FSH and LH and elevated free testosterone [47]. Fish oil supplementation has been shown to increase total sperm count, total morphologically normal sperms, and total sperm viability in dogs [48]. However, in boars, fish oil supplementation

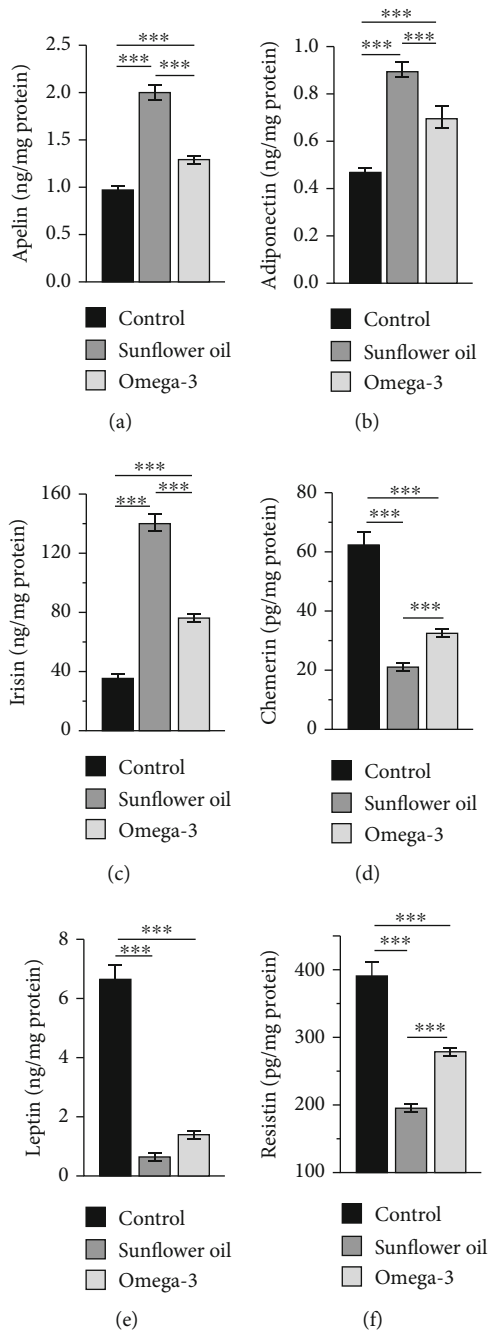

Figure 8: Continued.

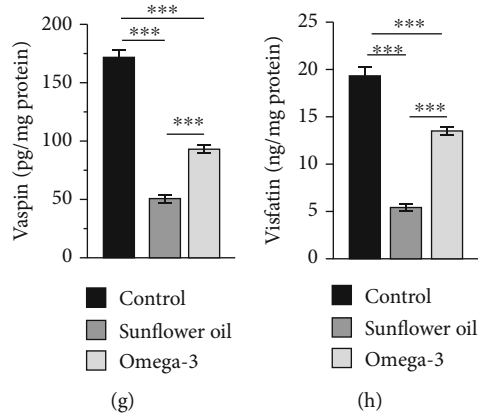

Figure 8: Changes in the testicular levels of different adipokines. Testicular levels of (a) apelin (ng/mg), (b) adiponectin (ng/mg), (c) irisin (ng/mg), (d) chemerin (pg/mg), (e) leptin (ng/mg), (f) resistin (pg/mg), (g) vaspin (pg/mg), and (h) visfatin (ng/mg) in the control, sunflower oil, and omega-3 groups. Data are expressed as mean ± SEM ($n = 10$/group). $^{***}P < 0.001$ by Tukey's multiple comparison post hoc test.

either reduced the number of morphologically abnormal sperms and improved sperm motility [49] or had no effect on semen quality [50, 51]. In this study, the administration of either omega-3 or sunflower oil for 12 weeks has no obvious effect on sperm count or sperm motility but significantly increased the number of morphologically abnormal sperms indicating spermatogenesis failure.

Kisspeptin is a significant stimulus to the secretion of GnRH and gonadotrophins [52, 53], and a reduction in GnRH and gonadotropin secretions, along with a subsequent decrease in testosterone synthesis by Leydig cells, impairs the process of spermatogenesis. In this study, the administration of omega-3 or sunflower oil inhibited the kisspeptin-GnRH signaling cascade, which further decreases LH, FSH, and testosterone production. Testosterone levels have been shown to increase in rats [54] and decrease in humans [55], dogs [48], and boars [56] after fish oil supplementation. The production of testosterone in Leydig cells is controlled by several genes including *STAR*, *CYP11A1*, *3β-HSD*, *CYP17A1*, and *17β-HSD*. The results herein demonstrated downregulation of these genes by sunflower oil or omega-3 administration, indicating steroidogenesis suppression. Steroidogenesis is reduced by omega-6 PUFAs via its direct effects on StAR and cytochrome P450 [40, 57]. By the nonreversible action of aromatase (CYP19), testosterone can be aromatized to E2 [58]. In this study, the downregulation of testicular *CYP19* mRNA levels contributed to decreased intratesticular levels of E2 following sunflower oil and omega-3 administration. However; the serum levels of E2 were significantly increased, indicating an extratesticular conversion of testosterone to E2. It has been reported that E2 stimulates the secretion of prolactin [59, 60] and increases prolactin mRNA levels [61]. Moreover, acute hyperprolactinemia has been shown to suppress the synthesis of testosterone and male fertility via inhibiting the secretion of GnRH [62], which subsequently inhibits LH pulses [63]. Furthermore, chronic treatment with prolactin has been demonstrated to decrease the expression levels of kisspeptin and GnRH in female mice [64]. Therefore, sunflower oil- and omega-3-induced hyperprolactinemia may be attributed to the repression of kisspeptin-GnRH signaling cascade noticed in this study.

The androgen-androgen receptor (AR) signaling cascade has a fundamental role in the function of male reproductive and nonproductive organs. Activation of the AR mediates testosterone effects, and both androgens and estrogens regulate AR expression in adult rats [65, 66]. Castration has been reported to increase AR mRNA levels [67], and testosterone treatment antagonizes the effect of castration [68]. Estrogen treatment has been shown to increase AR content in the medial amygdala [69] and augment AR mRNA content of the anterior pituitary gland [65]. Furthermore, prolactin induces a dose-dependent increase in nuclear AR content and increases AR mRNA levels in the prostate gland [70, 71]. In the present study, both sunflower oil and omega-3 administration induced a decline in the circulating level of testosterone and an increase in the circulating levels of prolactin and E2. This induction may modulate the expression of ARs in reproductive organs, but 4the intensity of the immunohistochemical expression of ARs in the testes, epididymides, and seminal vesicles (but not prostate) was increased only by omega-3 administration. These results suggest that PUFAs have a tissue-specific effect on ARs that relies on the chemical nature of unsaturated fatty acids. Omega-3 PUFAs have been reported to decrease the number of ARs, as well as plasma testosterone concentrations, in Japanese men [55]. Moreover, omega-3 PUFAs, but not omega-6 PUFAs, are capable of blocking the upregulation of AR gene transcription caused by androgen loss [72].

Inflammation and oxidative stress are known to have adverse impacts on the male reproductive system. The plasma membrane of testicular germ cells consists primarily of PUFAs, which render them susceptible to oxidation by free radicals and thus negatively affect spermatogenesis. Antioxidant enzymes play an integral role in maintaining redox equilibrium. The synergistic interactions of the endogenous enzymatic and nonenzymatic antioxidant systems are measured by TAC [73], and elevated TAC indicates a more efficient antioxidant defense system. In the present study, both

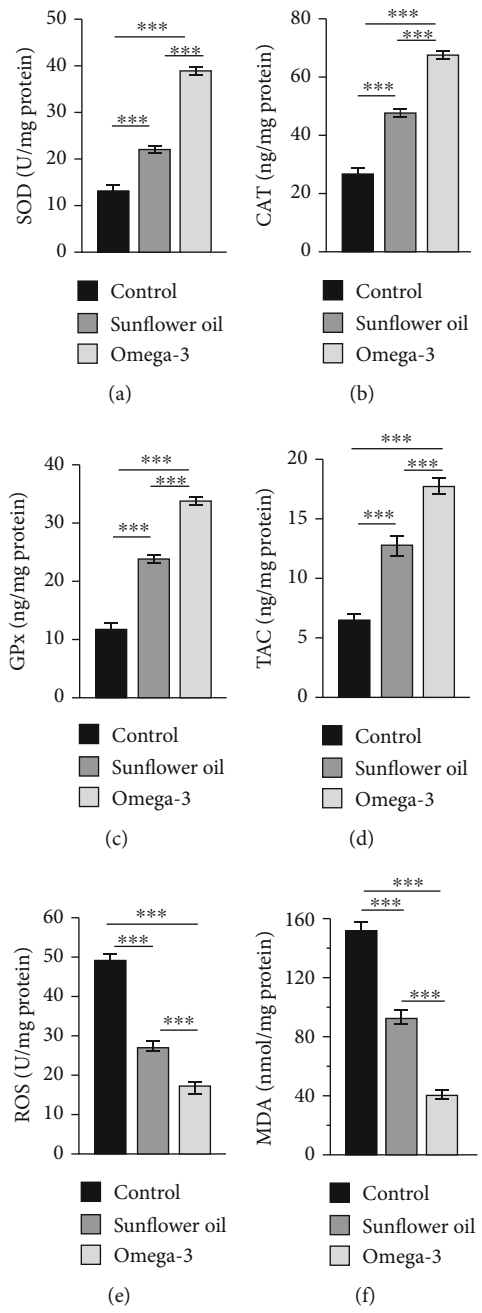

Figure 9: Continued.

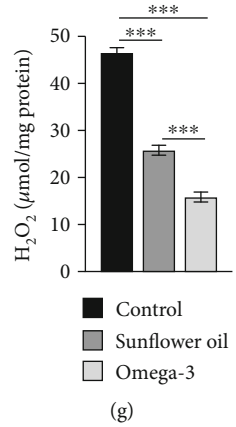

Figure 9: Testicular tissue levels of antioxidant enzymes, total antioxidant capacity, and reactive oxygen species. Testicular tissue levels of (a) superoxide dismutase (SOD; U/mg), (b) catalase (ng/mg), (c) glutathione peroxidase (GPx; ng/mg), (d) total antioxidant capacity (TAC; ng/mg), (e) reactive oxygen species (ROS; U/mg), (f) malondialdehyde (MDA; nmol/mg), and (g) hydrogen peroxide (H_2O_2; μmol/mg) in the control, sunflower oil, and omega-3 groups. Data are expressed as mean ± SEM ($n = 10$/group). $^{***}P < 0.001$ by Tukey's multiple comparison post hoc test.

sunflower oil and omega-3 administration increased TAC and the activity of the antioxidant defense system, particularly SOD, CAT, and GPx, which prevents the accumulation of H_2O_2 and MDA release. A reduction in lipid peroxidation in sperm of dogs [74] and mice [75] has been reported after omega-3 PUFA supplementation. The transcription factor NF-κB functions as a key link between oxidative stress and inflammation [76] and induces various inflammatory genes, such as TNF-α, IL-1β, and IL-6 [77]. ROS is a key factor for activation of NF-κB [78], which has a negative impact on ROS formation [79], and overexpression of ROS-scavenging enzymes as SOD, GPx, and catalase has been reported to abrogate NF-κB induction [78]; TNF-α-mediated production of NF-κB is blunted by CAT [80]. Moreover, H_2O_2 has been demonstrated as a second messenger for the signal-induced activation of NF-κB [81] and exposure to oxidants as H_2O_2 has been shown to stimulate NF-κB production [82]. In this study, the administration of sunflower oil and omega-3 significantly inhibited NF-κB and downstream cytokine production.

The levels and functional activities of adipokines regulate various signaling systems in the target tissues including the hypothalamic-pituitary-gonadal (HPG) axis. Apelin and its receptor are expressed in the HPG axis, and apelin has been reported to induce infertility via suppressing reproductive hormones including LH, FSH, and testosterone [83, 84]. Moreover, apelin has anti-inflammatory effects [85], stimulates antioxidant enzyme expression, and prevents the production of ROS in adipocytes [86]. Therefore, the increased intratesticular levels of apelin found in this study may have partly contributed to sunflower oil- and omega-3-induced decreases in male reproductive hormones and increases in antioxidant enzyme levels. In particular, apelin has been demonstrated to augment the level of serum adiponectin and reduce leptin [87].

Adiponectin acts as a testicular protective mechanism against the effects of proinflammatory mediators on steroidogenesis [88]. The expression of adiponectin and its receptors in the testis has been reported [22, 89, 90]. Leydig cells are the primary intratesticular source of adiponectin [89]. In the present study, the intratesticular levels of adiponectin were significantly increased following sunflower oil and omega-3 administration. Both basal and GnRH-stimulated LH secretion has been shown to be suppressed by adiponectin [91, 92]. However, adiponectin interacts with kisspeptin-expressing neurons and downregulates kisspeptin1 gene expression, decreasing the stimulatory effect of kisspeptin on GnRH neurons [93]. Therefore, the elevated intratesticular adiponectin levels observed in this study following sunflower oil and omega-3 administration may partially contribute to the inhibition of kisspeptin-GnRH-induced LH production. In rats, a negative relationship between serum adiponectin and testosterone level has been reported [94]. Irisin, an adipo-myokine engaged in energy homeostasis, has various metabolic functions. The injection of exogenous irisin has been shown to boost FSH, LH, and testosterone secretion and ameliorate sperm count and motility in male rats [95]. Furthermore, irisin has shown anti-inflammatory effects via reducing the activity of NF-κB and decreasing the levels of proinflammatory cytokines such as TNF-α, IL-1β, and IL-6 [96]. In the present study, sunflower oil and omega-3 administration significantly increased the intratesticular levels of irisin, which may play a role in testicular protection via its potential anti-inflammatory effects.

Leptin has been demonstrated to play a direct role in testicular endocrine function and spermatogenesis [97, 98] through its action on the male pituitary-gonadal axis [98]. Leptin stimulates the release of gonadotropins via activation of kisspeptin-induced GnRH neurons in the hypothalamic premammillary nucleus [99]. In the testes, leptin gene expression has been demonstrated in spermatocytes, spermatozoa, and seminiferous tubules [100–102]. In the seminiferous tubules and epididymides, leptin may augment sperm damage via ROS production [103]. In this study, intratesticular leptin concentrations were markedly decreased after

sunflower oil and omega-3 administration, suggesting a protective mechanism against ROS generation. Sertoli cell-induced nutritional support of spermatogenesis is amended by leptin [104]. Nevertheless, leptin correlates with reduced sperm motility in seminal plasma [11].

Resistin is a novel adipocytokine with potential implications in metabolic diseases. The expression of resistin in Sertoli and Leydig cells indicates its role in the control of testicular functions [105]. Resistin regulates Leydig cell steroidogenesis and proliferation [106] and increases the synthesis of testosterone [105]. However, seminal resistin concentrations have been shown to negatively correlate with sperm motility and vitality [107]. Resistin has been demonstrated as an inflammation marker, and seminal resistin levels have been shown to positively correlate with the proinflammatory mediators such as elastase, IL-6 [108], and TNF-α [107]. In the present study, the administration of either sunflower oil or omega-3 significantly reduced the intratesticular levels of resistin, as well as TNF-α, IL-1β, IL-6, and NF-κB.

Chemerin is a new adipokine implicated in the regulation of energy metabolism. Chemerin receptors are existent in the testis of rats and humans, and chemerin has been shown to regulate the process of gonadal steroidogenesis in males [12, 109]. In the present study, the administration of sunflower oil or omega-3 significantly reduced the intratesticular concentrations of chemerin. Seminal chemerin concentrations are negatively associated with sperm motility and positively associated with sperm concentration [11].

Visfatin has been recently identified as a novel regulator of the HPG [110] and impacts spermatogenesis [111]. It is present in Leydig cells, spermatocytes, and spermatozoa [12] and has been shown to stimulate steroidogenesis and elevate the production of testosterone in rat cultured Leydig cells [112]. In addition, visfatin mediates inflammatory responses in monocytes via stimulation of proinflammatory and anti-inflammatory cytokines [113]. In this study, the reduced intratesticular levels of visfatin may have partially contributed to the changes observed in proinflammatory cytokines following sunflower oil and omega-3 administration as visfatin has been reported primarily as a proinflammatory marker by increasing the levels of IL-1β, IL-6, and TNF-α [114, 115].

Vaspin, a member of the serine protease inhibitor family, was found in the epididymal adipose tissue [116]. Human seminal plasma levels of vaspin are positively correlated with sperm DNA fragmentation and negatively correlated with ejaculate volume [11]. Vaspin exerts its anti-inflammatory effects via suppression of TNF-α- and IL-1β-induced activation of NF-κB [117, 118]. The intratesticular levels of vaspin in this study were repressed after either sunflower oil or omega-3 administration.

5. Conclusions

The present study revealed for the first time the potential effects of omega-3 and omega-6 PUFAs on the levels of various adipokines in the male reproductive system. Both omega-3 and omega-6 PUFAs negatively influence the male reproductive function via inhibition of the kisspeptin-GnRH signaling pathway. The consumption of omega-3 and omega-6 PUFAs triggers anti-inflammatory properties via upregulation of apelin, adiponectin, irisin, and IL-10 and downregulation of leptin, resistin, visfatin, prostaglandins, and NF-κB and its downstream elements (IL-1β, IL-6, and TNF-α). Moreover, both omega-3 and omega-6 PUFAs ameliorate the testicular antioxidant status by scavenging ROS via increasing the levels of enzymes in the endogenous antioxidant system (SOD, CAT, and GPx).

Data Availability

Data is contained within the article.

Ethical Approval

The study was approved by the Institutional Animal Care and Use Committee of the Faculty of Veterinary Medicine, Zagazig University (Permit Number: ZU-IACUC/2/F/103/2020).

Conflicts of Interest

The author declares no conflict of interest.

Authors' Contributions

AM designed the study, performed the experiments, analyzed the results, and wrote the manuscript.

Acknowledgments

The author would like to thank the staff members of the molecular biology and biotechnology unit at the Zagazig University for their assistance.

Supplementary Materials

Figure S1: graphical abstract showing the effects of omega-3 and omega-6 on testicular levels of adipocytokines, antioxidant status, cytokines, and serum levels of reproductive hormones. *(Supplementary Materials)*

References

[1] J. Orsavova, L. Misurcova, J. V. Ambrozova, R. Vicha, and J. Mlcek, "Fatty acids composition of vegetable oils and its contribution to dietary energy intake and dependence of cardiovascular mortality on dietary intake of fatty acids," *International Journal of Molecular Sciences*, vol. 16, no. 12, pp. 12871–12890, 2015.

[2] S. Fischer, "Dietary polyunsaturated fatty acids and eicosanoid formation in humans," *Advances in Lipid Research*, vol. 23, pp. 169–198, 1989.

[3] A. P. Simopoulos, "The importance of the ratio of omega-6/omega-3 essential fatty acids," *Biomedicine & Pharmacotherapy*, vol. 56, no. 8, pp. 365–379, 2002.

[4] R. S. Khan, A. Chokshi, K. Drosatos et al., "Fish oil selectively improves heart function in a mouse model of lipid-induced

cardiomyopathy," *Journal of Cardiovascular Pharmacology*, vol. 61, no. 4, pp. 345–354, 2013.

[5] G. C. Shearer, O. V. Savinova, and W. S. Harris, "Fish oil – how does it reduce plasma triglycerides?," *Biochimica et Biophysica Acta*, vol. 1821, no. 5, pp. 843–851, 2012.

[6] M. Mazza, M. Pomponi, L. Janiri, P. Bria, and S. Mazza, "Omega-3 fatty acids and antioxidants in neurological and psychiatric diseases: an overview," *Progress in Neuro-Psychopharmacology and Biological Psychiatry*, vol. 31, no. 1, pp. 12–26, 2007.

[7] A. Agarwal and L. H. Sekhon, "Oxidative stress and antioxidants for idiopathic oligoasthenoteratospermia: is it justified?," *Indian Journal of Urology: IJU: Journal of the Urological Society of India*, vol. 27, no. 1, article 78437, pp. 74–85, 2011.

[8] A. Bhattacharya, D. Sun, M. Rahman, and G. Fernandes, "Different ratios of eicosapentaenoic and docosahexaenoic omega-3 fatty acids in commercial fish oils differentially alter pro-inflammatory cytokines in peritoneal macrophages from C57BL/6 female mice," *The Journal of Nutritional Biochemistry*, vol. 18, no. 1, pp. 23–30, 2007.

[9] M. W. A. el husseny, M. Mamdouh, S. Shaban et al., "Adipokines: potential therapeutic targets for vascular dysfunction in type II diabetes mellitus and obesity," *Journal of Diabetes Research*, vol. 2017, Article ID 8095926, 11 pages, 2017.

[10] B. Antuna-Puente, B. Feve, S. Fellahi, and J. P. Bastard, "Adipokines : le chainon manquant entre insulinoresistance et obesite," *Diabetes & Metabolism*, vol. 34, no. 1, pp. 2–11, 2008.

[11] S. Thomas, D. Kratzsch, M. Schaab et al., "Seminal plasma adipokine levels are correlated with functional characteristics of spermatozoa," *Fertility and Sterility*, vol. 99, no. 5, pp. 1256–1263.e3, 2013.

[12] J. Dupont, X. Pollet-Villard, M. Reverchon, N. Mellouk, and R. Levy, "Adipokines in human reproduction," *Hormone Molecular Biology and Clinical Investigation*, vol. 24, no. 1, pp. 11–24, 2015.

[13] Y. Elfassy, J. P. Bastard, C. McAvoy, S. Fellahi, J. Dupont, and R. Levy, "Adipokines in semen: physiopathology and effects on spermatozoas," *International Journal of Endocrinology*, vol. 2018, Article ID 3906490, 11 pages, 2018.

[14] M. Wilkinson, R. Brown, S. A. Imran, and E. Ur, "Adipokine gene expression in brain and pituitary gland," *Neuroendocrinology*, vol. 86, no. 3, pp. 191–209, 2007.

[15] K. P. Maruska and R. D. Fernald, "Social regulation of gene expression in the hypothalamic-pituitary-gonadal axis," *Physiology (Bethesda)*, vol. 26, no. 6, pp. 412–423, 2011.

[16] H. M. Scott, J. I. Mason, and R. M. Sharpe, "Steroidogenesis in the fetal testis and its susceptibility to disruption by exogenous compounds," *Endocrine Reviews*, vol. 30, no. 7, pp. 883–925, 2009.

[17] M. F. R. Hassanien, "Plant sterols and tocols profile of vegetable oils consumed in Egypt," *International Journal of Food Properties*, vol. 16, no. 3, pp. 574–585, 2013.

[18] A. Nordoy, "Is there a rational use for n-3 fatty acids (fish oils) in clinical medicine?," *Drugs*, vol. 42, no. 3, pp. 331–342, 1991.

[19] T. P. Vahl, Y. M. Ulrich-Lai, M. M. Ostrander et al., "Comparative analysis of ACTH and corticosterone sampling methods in rats," *American Journal of Physiology-Endocrinology and Metabolism*, vol. 289, no. 5, pp. E823–E828, 2005.

[20] A. Moustafa, "Changes in nitric oxide, carbon monoxide, hydrogen sulfide and male reproductive hormones in response to chronic restraint stress in rats," *Free Radical Biology and Medicine*, vol. 162, pp. 353–366, 2021.

[21] S. Wang, G. Wang, B. E. Barton, T. F. Murphy, and H. F. Huang, "Impaired sperm function after spinal cord injury in the rat is associated with altered cyclic adenosine monophosphate signaling," *Journal of Andrology*, vol. 26, no. 5, pp. 592–600, 2005.

[22] A. Moustafa, "Effect of light-dark cycle misalignment on the hypothalamic-pituitary-gonadal axis, testicular oxidative stress, and expression of clock genes in adult male rats," *International Journal of Endocrinology*, vol. 2020, Article ID 1426846, 17 pages, 2020.

[23] G. W. Robb, R. P. Amann, and G. J. Killian, "Daily sperm production and epididymal sperm reserves of pubertal and adult rats," *Journal of Reproduction and Fertility*, vol. 54, no. 1, pp. 103–107, 1978.

[24] A. J. Wyrobek and W. R. Bruce, "Chemical induction of sperm abnormalities in mice," *Proceedings of the National Academy of Sciences*, vol. 72, no. 11, pp. 4425–4429, 1975.

[25] S. K. Suvarna, C. Layton, and J. D. Bancroft, *Bancroft's theory and practice of histological techniques*, Churchill Livingstone Elsevier, Oxford, 2013.

[26] D. G. Fuhrich, B. A. Lessey, and R. F. Savaris, "Comparison of HSCORE assessment of endometrial beta3 integrin subunit expression with digital HSCORE using computerized image analysis (ImageJ)," *Analytical and Quantitative Cytopathology and Histopathology*, vol. 35, no. 4, pp. 210–216, 2013.

[27] Z. Shi, H. Zhang, Y. Liu, M. Xu, and J. Dai, "Alterations in gene expression and testosterone synthesis in the testes of male rats exposed to perfluorododecanoic acid," *Toxicological Sciences*, vol. 98, no. 1, pp. 206–215, 2007.

[28] A. J. Travis and G. S. Kopf, "The role of cholesterol efflux in regulating the fertilization potential of mammalian spermatozoa," *The journal of Clinical Investigation*, vol. 110, no. 6, pp. 731–736, 2002.

[29] H. Tavilani, M. Doosti, I. Nourmohammadi et al., "Lipid composition of spermatozoa in normozoospermic and asthenozoospermic males," *Prostaglandins, Leukotrienes and Essential Fatty Acids*, vol. 77, no. 1, pp. 45–50, 2007.

[30] R. Wall, R. P. Ross, G. F. Fitzgerald, and C. Stanton, "Fatty acids from fish: the anti-inflammatory potential of long-chain omega-3 fatty acids," *Nutrition Reviews*, vol. 68, no. 5, pp. 280–289, 2010.

[31] O. Adam, G. Wolfram, and N. Zollner, "Influence of dietary linoleic acid intake with different fat intakes on arachidonic acid concentrations in plasma and platelet lipids and eicosanoid biosynthesis in female volunteers," *Annals of Nutrition and Metabolism*, vol. 47, no. 1, pp. 31–36, 2003.

[32] Y. Angela Liou and S. M. Innis, "Dietary linoleic acid has no effect on arachidonic acid, but increases n-6 eicosadienoic acid, and lowers dihomo-γ-linolenic and eicosapentaenoic acid in plasma of adult men," *Prostaglandins, Leukotrienes and Essential Fatty Acids*, vol. 80, no. 4, pp. 201–206, 2009.

[33] P. Yaqoob, H. S. Pala, M. Cortina-Borja, E. A. Newsholme, and P. C. Calder, "Encapsulated fish oil enriched in alpha-tocopherol alters plasma phospholipid and mononuclear cell fatty acid compositions but not mononuclear cell functions,"

European journal of Clinical Investigation, vol. 30, no. 3, pp. 260–274, 2000.

[34] R. A. Siddiqui, K. A. Harvey, and G. P. Zaloga, "Modulation of enzymatic activities by n-3 polyunsaturated fatty acids to support cardiovascular Health," *The Journal of Nutritional biochemistry*, vol. 19, no. 7, pp. 417–437, 2008.

[35] P. Yaqoob and P. Calder, "Effects of dietary lipid manipulation upon inflammatory mediator production by murine macrophages," *Cellular Immunology*, vol. 163, no. 1, pp. 120–128, 1995.

[36] J. Bautista-Ortega, D. E. Goeger, and G. Cherian, "Egg yolk omega-6 and omega-3 fatty acids modify tissue lipid components, antioxidant status, and ex vivo eicosanoid production in chick cardiac tissue," *Poultry Science*, vol. 88, no. 6, pp. 1167–1175, 2009.

[37] Y. Guo, S. Chen, Z. Xia, and J. Yuan, "Effects of different types of polyunsaturated fatty acids on immune function and PGE_2 synthesis by peripheral blood leukocytes of laying hens," *Animal Feed Science and Technology*, vol. 116, no. 3-4, pp. 249–258, 2004.

[38] D. S. Kelley, P. C. Taylor, G. J. Nelson et al., "Docosahexaenoic acid ingestion inhibits natural killer cell activity and production of inflammatory mediators in young healthy men," *Lipids*, vol. 34, no. 4, pp. 317–324, 1999.

[39] S. Elzanaty, J. Malm, and A. Giwercman, "Duration of sexual abstinence: epididymal and accessory sex gland secretions and their relationship to sperm motility," *Human Reproduction*, vol. 20, no. 1, pp. 221–225, 2005.

[40] D. C. Wathes, D. R. Abayasekara, and R. J. Aitken, "Polyunsaturated fatty acids in male and female reproduction," *Biology of Reproduction*, vol. 77, no. 2, pp. 190–201, 2007.

[41] P. Wysocki and J. Strzeżek, "Molecular forms of acid phosphatase of boar seminal plasma," *Animal Science Papers and Reports*, vol. 18, no. 2, pp. 99–106, 2000.

[42] A. Zöpfgen, F. Priem, F. Sudhoff et al., "Relationship between semen quality and the seminal plasma components carnitine, alpha-glucosidase, fructose, citrate and granulocyte elastase in infertile men compared with a normal population," *Human Reproduction*, vol. 15, no. 4, pp. 840–845, 2000.

[43] S. Elzanaty, J. Richthoff, J. Malm, and A. Giwercman, "The impact of epididymal and accessory sex gland function on sperm motility," *Human Reproduction*, vol. 17, no. 11, pp. 2904–2911, 2002.

[44] L. Lemmens, S. Kos, C. Beijer et al., "Predictive value of sperm morphology and progressively motile sperm count for pregnancy outcomes in intrauterine insemination," *Fertility and sterility*, vol. 105, no. 6, pp. 1462–1468, 2016.

[45] Y. Lin, X. Cheng, J. Mao et al., "Effects of different dietary n-6/n-3 polyunsaturated fatty acid ratios on boar reproduction," *Lipids in Health and Disease*, vol. 15, no. 1, p. 31, 2016.

[46] A. Salas-Huetos, N. Rosique-Esteban, N. Becerra-Tomas, B. Vizmanos, M. Bullo, and J. Salas-Salvado, "The effect of nutrients and dietary supplements on sperm quality parameters: a systematic review and meta-analysis of randomized clinical trials," *Advances in Nutrition*, vol. 9, no. 6, pp. 833–848, 2018.

[47] T. K. Jensen, L. Priskorn, S. A. Holmboe et al., "Associations of fish oil supplement use with testicular function in young men," *JAMA Netw Open*, vol. 3, no. 1, article e1919462, 2020.

[48] A. Risso, F. J. Pellegrino, A. E. Relling, and Y. Corrada, "Effect of long-term fish oil supplementation on semen quality and serum testosterone concentrations in male dogs," *International Journal of Fertility & Sterility*, vol. 10, no. 2, pp. 223–231, 2016.

[49] J. A. Rooke, C. C. Shao, and B. K. Speake, "Effects of feeding tuna oil on the lipid composition of pig spermatozoa and in vitro characteristics of semen," *Reproduction*, vol. 121, no. 2, pp. 315–322, 2001.

[50] C. A. Castellano, I. Audet, J. L. Bailey, P. Y. Chouinard, J. P. Laforest, and J. J. Matte, "Effect of dietary n-3 fatty acids (fish oils) on boar reproduction and semen quality," *Journal of Animal Science*, vol. 88, no. 7, pp. 2346–2355, 2010.

[51] M. Yeste, X. Barrera, D. Coll, and S. Bonet, "The effects on boar sperm quality of dietary supplementation with omega-3 polyunsaturated fatty acids differ among porcine breeds," *Theriogenology*, vol. 76, no. 1, pp. 184–196, 2011.

[52] N. de Roux, E. Genin, J. C. Carel, F. Matsuda, J. L. Chaussain, and E. Milgrom, "Hypogonadotropic hypogonadism due to loss of function of the KiSS1-derived peptide receptor GPR54," *Proceedings of the National Academy of Sciences*, vol. 100, no. 19, pp. 10972–10976, 2003.

[53] S. B. Seminara, S. Messager, E. E. Chatzidaki et al., "TheGPR54Gene as a regulator of puberty," *New England Journal of Medicine*, vol. 349, no. 17, pp. 1614–1627, 2003.

[54] E. Sebokova, M. L. Garg, A. Wierzbicki, A. B. Thomson, and M. T. Clandinin, "Alteration of the lipid composition of rat testicular plasma membranes by dietary (*n*-3) fatty acids changes the responsiveness of Leydig cells and testosterone synthesis," *The Journal of Nutrition*, vol. 120, no. 6, pp. 610–618, 1990.

[55] C. Nagata, N. Takatsuka, N. Kawakami, and H. Shimizu, "Relationships between types of fat consumed and serum estrogen and androgen concentrations in Japanese men," *Nutrition and Cancer*, vol. 38, no. 2, pp. 163–167, 2000.

[56] C. A. Castellano, I. Audet, J. P. Laforest, J. J. Matte, and M. Suh, "Fish oil diets alter the phospholipid balance, fatty acid composition, and steroid hormone concentrations in testes of adult pigs," *Theriogenology*, vol. 76, no. 6, pp. 1134–1145, 2011.

[57] D. M. Stocco, X. Wang, Y. Jo, and P. R. Manna, "Multiple signaling pathways regulating steroidogenesis and steroidogenic acute regulatory protein expression: more complicated than we thought," *Molecular Endocrinology*, vol. 19, no. 11, pp. 2647–2659, 2005.

[58] E. R. Simpson, C. Clyne, G. Rubin et al., "Aromatase–a brief overview," *Annual Review of Physiology*, vol. 64, no. 1, pp. 93–127, 2002.

[59] E. Haug and K. M. Gautvik, "Effects of sex steroids on prolactin secreting rat pituitary cells in culture," *Endocrinology*, vol. 99, no. 6, pp. 1482–1489, 1976.

[60] M. E. Lieberman, R. A. Maurer, and J. Gorski, "Estrogen control of prolactin synthesis in vitro," *Proceedings of the National Academy of Sciences*, vol. 75, no. 12, pp. 5946–5949, 1978.

[61] J. A. Chowen, S. Gonzalez-Parra, L. M. Garcia-Segura, and J. Argente, "Sexually dimorphic interaction of insulin-like growth factor (IGF)-I and sex steroids in lactotrophs," *Journal of Neuroendocrinology*, vol. 10, no. 7, pp. 493–502, 1998.

[62] A. Bartke, H. Klemcke, and K. Matt, "Effects of physiological and abnormally elevated prolactin levels on the pituitary-testicular axis," *Medical Biology*, vol. 63, no. 5-6, pp. 264–272, 1986.

[63] L. Milenkovic, G. D'Angelo, P. A. Kelly, and R. I. Weiner, "Inhibition of gonadotropin hormone-releasing hormone release by prolactin from GT1 neuronal cell lines through prolactin receptors," *Proceedings of the National Academy of Sciences*, vol. 91, no. 4, pp. 1244–1247, 1994.

[64] C. Sonigo, J. Bouilly, N. Carré et al., "Hyperprolactinemia-induced ovarian acyclicity is reversed by kisspeptin administration," *The Journal of Clinical Investigation*, vol. 122, no. 10, pp. 3791–3795, 2012.

[65] L. H. Burgess and R. J. Handa, "Hormonal regulation of androgen receptor mRNA in the brain and anterior pituitary gland of the male rat," *Molecular Brain Research*, vol. 19, no. 1-2, pp. 31–38, 1993.

[66] M. D. McAbee and L. L. DonCarlos, "Regulation of androgen receptor messenger ribonucleic acid expression in the developing rat forebrain," *Endocrinology*, vol. 140, no. 4, pp. 1807–1814, 1999.

[67] V. E. Quarmby, W. G. Yarbrough, D. B. Lubahn, F. S. French, and E. M. Wilson, "Autologous down-regulation of androgen receptor messenger ribonucleic acid," *Molecular Endocrinology*, vol. 4, no. 1, pp. 22–28, 1990.

[68] L. X. Shan, M. C. Rodriguez, and O. A. Janne, "Regulation of androgen receptor protein and mRNA concentrations by androgens in rat ventral prostate and seminal vesicles and in human hepatoma cells," *Molecular Endocrinology*, vol. 4, no. 11, pp. 1636–1646, 1990.

[69] R. J. Handa, C. E. Roselli, L. Horton, and J. A. Resko, "The quantitative distribution of cytosolic androgen receptors in microdissected areas of the male rat brain: effects of estrogen treatment," *Endocrinology*, vol. 121, no. 1, pp. 233–240, 1987.

[70] J. S. Barañao, M. Tesone, R. M. Oliveira-filho et al., "Effects of prolactin on prostate androgen receptors in male rats," *Journal of Ândrology*, vol. 3, no. 5, pp. 281–288, 1982.

[71] E. Reiter, P. Bonnet, B. Sente et al., "Growth hormone and prolactin stimulate androgen receptor, insulin-like growth factor-I (IGF-I) and IGF-I receptor levels in the prostate of immature rats," *Molecular and Cellular Endocrinology*, vol. 88, no. 1-3, pp. 77–87, 1992.

[72] C. Garcia, W. Friedrichs, O. Tolstykh, and S. Ruparel, "Regulation of androgen receptor expression by omega-3 fatty acids," vol. 68, 9 Supplement, pp. 4674–4674, 1992.

[73] A. Somogyi, K. Rosta, P. Pusztai, Z. Tulassay, and G. Nagy, "Antioxidant measurements," *Physiological Measurement*, vol. 28, no. 4, pp. R41–R55, 2007.

[74] A. L. Risso, F. J. Pellegrino, Y. Corrada et al., "Effect of fish oil and vitamin E on sperm lipid peroxidation in dogs," *Journal of Nutritional Science*, vol. 6, p. e48, 2017.

[75] A. Ferramosca, N. Moscatelli, M. Di Giacomo, and V. Zara, "Dietary fatty acids influence sperm quality and function," *Andrology*, vol. 5, no. 3, pp. 423–430, 2017.

[76] J. S. Aprioku, "Pharmacology of free radicals and the impact of reactive oxygen species on the testis," *Journal of Reproduction & Infertility*, vol. 14, no. 4, pp. 158–172, 2013.

[77] N. Wang, H. Liang, and K. Zen, "Molecular mechanisms that influence the macrophage M1-M2 polarization balance," *Frontiers in Immunology*, vol. 5, p. 614, 2014.

[78] G. Gloire, S. Legrand-Poels, and J. Piette, "NF-κB activation by reactive oxygen species: Fifteen years later," *Biochemical Pharmacology*, vol. 72, no. 11, pp. 1493–1505, 2006.

[79] S. Sakon, X. Xue, M. Takekawa et al., "NF-kappaB inhibits TNF-induced accumulation of ROS that mediate prolonged MAPK activation and necrotic cell death," *The EMBO Journal*, vol. 22, no. 15, pp. 3898–3909, 2003.

[80] K. N. Schmidt, E. B. Traenckner, B. Meier, and P. A. Baeuerle, "Induction of Oxidative Stress by Okadaic Acid Is Required for Activation of Transcription Factor NF-κB," *Journal of Biological Chemistry*, vol. 270, no. 45, pp. 27136–27142, 1995.

[81] L. Flohe, R. Brigelius-Flohe, C. Saliou, M. G. Traber, and L. Packer, "Redox regulation of NF-kappa B activation," *Free Radical Biology and Medicine*, vol. 22, no. 6, pp. 1115–1126, 1997.

[82] A. Bowie and L. A. J. O'Neill, "Oxidative stress and nuclear factor-κB activation: A reassessment of the evidence in the light of recent discoveries," *Biochemical Pharmacology*, vol. 59, no. 1, pp. 13–23, 2000.

[83] S. Sandal, S. Tekin, F. B. Seker et al., "The effects of intracerebroventricular infusion of apelin-13 on reproductive function in male rats," *Neuroscience Letters*, vol. 602, pp. 133–138, 2015.

[84] S. Tekin, Y. Erden, S. Sandal et al., "Effects of apelin on reproductive functions: relationship with feeding behavior and energy metabolism," *Archives of Physiology and Biochemistry*, vol. 123, no. 1, pp. 9–15, 2017.

[85] M. Soliman and M. Arafah, "Apelin protect against multiple organ injury following hemorrhagic shock and decrease the inflammatory response," *International Journal of Applied and Basic Medical Research*, vol. 5, no. 3, article 165377, pp. 195–199, 2015.

[86] A. Than, X. Zhang, M. K. Leow, C. L. Poh, S. K. Chong, and P. Chen, "Apelin Attenuates Oxidative Stress in Human Adipocytes," *Journal of Biological Chemistry*, vol. 289, no. 6, pp. 3763–3774, 2014.

[87] K. Higuchi, T. Masaki, K. Gotoh et al., "Apelin, an APJ receptor ligand, regulates body adiposity and favors the messenger ribonucleic acid expression of uncoupling proteins in mice," *Endocrinology*, vol. 148, no. 6, pp. 2690–2697, 2007.

[88] L. Wu, B. Xu, W. Fan, X. Zhu, G. Wang, and A. Zhang, "Adiponectin protects Leydig cells against proinflammatory cytokines by suppressing the nuclear factor-κB signaling pathway," *The FEBS journal*, vol. 280, no. 16, pp. 3920–3927, 2013.

[89] J. E. Caminos, R. Nogueiras, F. Gaytan et al., "Novel expression and direct effects of adiponectin in the rat testis," *Endocrinology*, vol. 149, no. 7, pp. 3390–3402, 2008.

[90] M. Choubey, A. Ranjan, P. S. Bora, F. Baltazar, L. J. Martin, and A. Krishna, "Role of adiponectin as a modulator of testicular function during aging in mice," *Biochimica et Biophysica Acta-Molecular Basis of Disease*, vol. 1865, no. 2, pp. 413–427, 2019.

[91] M. Lu, Q. Tang, J. M. Olefsky, P. L. Mellon, and N. J. Webster, "Adiponectin activates adenosine monophosphate-activated protein kinase and decreases luteinizing hormone secretion in LbetaT2 gonadotropes," *Molecular Endocrinology*, vol. 22, no. 3, pp. 760–771, 2008.

[92] F. Rodriguez-Pacheco, A. J. Martinez-Fuentes, S. Tovar et al., "Regulation of pituitary cell function by adiponectin," *Endocrinology*, vol. 148, no. 1, pp. 401–410, 2007.

[93] J. P. Wen, C. Liu, W. K. Bi et al., "Adiponectin inhibits KISS1 gene transcription through AMPK and specificity protein-1 in the hypothalamic GT1-7 neurons," *The Journal of Endocrinology*, vol. 214, no. 2, pp. 177–189, 2012.

[94] A. Pfaehler, M. K. Nanjappa, E. S. Coleman et al., "Regulation of adiponectin secretion by soy isoflavones has implication for endocrine function of the testis," *Toxicology Letters*, vol. 209, no. 1, pp. 78–85, 2012.

[95] R. H. Ibrahim and N. F. El-Malkey, "Role of irisin administration in modulating testicular function in adult obese albino rats," *QJM: An International Journal of Medicine*, vol. 111, supplement 1, 2018.

[96] A. I. Mazur-Bialy, E. Pochec, and M. Zarawski, "Anti-inflammatory properties of irisin, mediator of physical activity, are connected with TLR4/MyD88 signaling pathway activation," *International Journal of Molecular Sciences*, vol. 18, no. 4, p. 701, 2017.

[97] M. Caprio, A. M. Isidori, A. R. Carta, C. Moretti, M. L. Dufau, and A. Fabbri, "Expression of functional leptin receptors in rodent Leydig cells," *Endocrinology*, vol. 140, no. 11, pp. 4939–4947, 1999.

[98] M. Tena-Sempere and M. L. Barreiro, "Leptin in male reproduction: the testis paradigm," *Molecular and Cellular Endocrinology*, vol. 188, no. 1-2, pp. 9–13, 2002.

[99] M. A. Sanchez-Garrido and M. Tena-Sempere, "Metabolic control of puberty: roles of leptin and kisspeptins," *Hormones and Behavior*, vol. 64, no. 2, pp. 187–194, 2013.

[100] M. Caprio, E. Fabbrini, G. Ricci et al., "Ontogenesis of leptin receptor in rat Leydig cells," *Biology of Reproduction*, vol. 68, no. 4, pp. 1199–1207, 2003.

[101] M. Herrid, T. O'Shea, and J. R. McFarlane, "Ontogeny of leptin and its receptor expression in mouse testis during the postnatal period," *Molecular Reproduction and Development: Incorporating Gamete Research*, vol. 75, no. 5, pp. 874–880, 2008.

[102] V. Rago, S. Aquila, C. Guido, and A. Carpino, "Leptin and its receptor are expressed in the testis and in the epididymis of young and adult pigs," *The Anatomical Record: Advances in Integrative Anatomy and Evolutionary Biology: Advances in Integrative Anatomy and Evolutionary Biology*, vol. 292, no. 5, pp. 736–745, 2009.

[103] F. A. Almabhouh, K. Osman, I. Siti Fatimah, G. Sergey, J. Gnanou, and H. J. Singh, "Effects of leptin on sperm count and morphology in Sprague-Dawley rats and their reversibility following a 6-week recovery period," *Andrologia*, vol. 47, no. 7, pp. 751–758, 2015.

[104] M. Alves, T. Jesus, M. Sousa, E. Goldberg, B. Silva, and P. Oliveira, "Male fertility and obesity: are ghrelin, leptin and glucagon-like peptide-1 pharmacologically relevant?," *Current Pharmaceutical Design*, vol. 22, no. 7, pp. 783–791, 2016.

[105] R. Nogueiras, M. L. Barreiro, J. E. Caminos et al., "Novel expression of resistin in rat testis: functional role and regulation by nutritional status and hormonal factors," *Journal of Cell Science*, vol. 117, no. 15, pp. 3247–3257, 2004.

[106] P. Roumaud and L. J. Martin, "Roles of leptin, adiponectin and resistin in the transcriptional regulation of steroidogenic genes contributing to decreased Leydig cells function in obesity," *Hormone Molecular Biology and Clinical Investigation*, vol. 24, no. 1, pp. 25–45, 2015.

[107] E. Moretti, G. Collodel, L. Mazzi, M. Campagna, F. Iacoponi, and N. Figura, "Resistin, interleukin-6, tumor necrosis factor-alpha, and human semen parameters in the presence of leukocytospermia, smoking habit, and varicocele," *Fertility and Sterility*, vol. 102, no. 2, pp. 354–360, 2014.

[108] J. Kratzsch, U. Paasch, S. Grunewald, M. A. Mueller, J. Thiery, and H. J. Glander, "Resistin correlates with elastase and interleukin-6 in human seminal plasma," *Reproductive BioMedicine Online*, vol. 16, no. 2, pp. 283–288, 2008.

[109] L. Li, P. Ma, C. Huang et al., "Expression of chemerin and its receptors in rat testes and its action on testosterone secretion," *The Journal of Endocrinology*, vol. 220, no. 2, pp. 155–163, 2014.

[110] M. Diot, M. Reverchon, C. Rame, Y. Baumard, and J. Dupont, "Expression and effect of NAMPT (visfatin) on progesterone secretion in hen granulosa cells," *Reproduction*, vol. 150, no. 1, pp. 53–63, 2015.

[111] V. Syriou, D. Papanikolaou, A. Kozyraki, and D. G. Goulis, "Cytokines and male infertility," *European Cytokine Network*, vol. 29, no. 3, pp. 73–82, 2018.

[112] W. Hameed, I. Yousaf, R. Latif, and M. Aslam, "Effect of visfatin on testicular steroidogenesis in purified Leydig cells," *Journal of Ayub Medical College Abbottabad*, vol. 24, no. 3-4, pp. 62–64, 2012.

[113] G. V. Dedoussis, A. Kapiri, A. Samara et al., "Visfatin: the link between inflammation and childhood obesity," *Diabetes Care*, vol. 32, no. 6, p. e71, 2009.

[114] T. Luk, Z. Malam, and J. C. Marshall, "Pre-B cell colony-enhancing factor (PBEF)/visfatin: a novel mediator of innate immunity," *Journal of Leukocyte Biology*, vol. 83, no. 4, pp. 804–816, 2008.

[115] A. R. Moschen, A. Kaser, B. Enrich et al., "Visfatin, an adipocytokine with proinflammatory and immunomodulating properties," *The Journal of Immunology*, vol. 178, no. 3, pp. 1748–1758, 2007.

[116] K. Hida, J. Wada, J. Eguchi et al., "Visceral adipose tissue-derived serine protease inhibitor: a unique insulin-sensitizing adipocytokine in obesity," *Proceedings of the National Academy of Sciences*, vol. 102, no. 30, pp. 10610–10615, 2005.

[117] S. Liu, Y. Dong, T. Wang et al., "Vaspin inhibited proinflammatory cytokine induced activation of nuclear factor-kappa B and its downstream molecules in human endothelial EA.hy926 cells," *Diabetes Research and Clinical Practice*, vol. 103, no. 3, pp. 482–488, 2014.

[118] K. Zieger, J. Weiner, K. Krause et al., "Vaspin suppresses cytokine-induced inflammation in 3T3-L1 adipocytes via inhibition of NFκB pathway," *Molecular and Cellular Endocrinology*, vol. 460, pp. 181–188, 2018.

Hindawi
Oxidative Medicine and Cellular Longevity
Volume 2021, Article ID 6698482, 17 pages
https://doi.org/10.1155/2021/6698482

Research Article

Deferasirox, an Iron-Chelating Agent, Improves Testicular Morphometric and Sperm Functional Parameters in a Rat Model of Varicocele

M. Rahmani,[1] **M. Tavalaee**,[1] **M. Hosseini**,[1] **A. Eskandari**,[1] **E. Shaygannia**,[1] **N. Sadeghi**,[1] **M. N. Nazem**,[2] **P. Gharagozloo**,[3] **J. R. Drevet**,[4] **and M. H. Nasr-Esfahani**[1,5]

[1]*Department of Animal Biotechnology, Reproductive Biomedicine Research Center, Royan Institute for Biotechnology, ACECR, Isfahan, Iran*
[2]*Department of Basic Science, School of Veterinary Medicine, Shahid Bahonar University of Kerman, Kerman, Iran*
[3]*CellOxess LLC, 830 Bear Tavern Road, Ewing NJ 08628, USA*
[4]*GReD Institute, Faculty of Medicine, INSERM-CNRS-Université Clermont Auvergne, France*
[5]*Isfahan Fertility and Infertility Center, Isfahan, Iran*

Correspondence should be addressed to J. R. Drevet; joel.drevet@uca.fr and M. H. Nasr-Esfahani; nasr.royan@gmail.com

Received 1 November 2020; Revised 17 March 2021; Accepted 26 March 2021; Published 9 April 2021

Academic Editor: Yi Fang

Varicocele is characterized by testicular dysfunction that originates from hyperthermia and hypoxia, leading to defects in testicular tissue and altered spermatozoa structure and function. The varicocele testis is characterized by the presence of intracellular iron deposits that contribute to the associated oxidative stress. Therefore, we tested the hypothesis that administration of an iron-chelating agent, such as deferasirox (DFX), could potentially mitigate the consequences of varicocele on testicular tissue and spermatozoa. Using a well-established rat model of varicocele (VCL), we show that treatment with DFX partially improved the structure and function of the testis and spermatozoa. In particular, sperm motility was markedly restored whereas abnormal sperm morphology was only partially improved. No significant improvement in sperm count was observed that could be associated with the proapoptotic response observed following iron chelation treatment. No reduction in oxidative damage to spermatozoa was observed since lipid peroxidation and DNA integrity were not modified. This was suggested to be a result of increased oxidative stress. Finally, we also saw no indication of attenuation of the endoplasmic reticulum/unfolded protein (ER/UPR) stress response that we recently found associated with the VCL testis in rats.

1. Introduction

Dilatation of the testicular pampiniform plexus associated with spermatic vein valve disorder is commonly referred to as varicocele (VCL) [1]. Epidemiological data indicate that VCL is present in 15–20% of the male population and is associated with reduced spermatozoa quality. Varicocele has a multifaceted etiology mainly related to increased testicular temperature and oxidative stress [2]. Although various molecular pathways are thought to be associated with VCL, including hormonal disorders, hypoxia, germ cell apoptosis, and disruption of the testis blood testicular barrier [1, 2], more research is needed to further our molecular understanding of this syndrome and how to improve patient treatment.

One logical approach to reduce the detrimental impact of VCL on testis structure and function would be to try to reduce the associated oxidative stress. We propose that control of iron homeostasis in the VCL testis could be a pertinent approach. Iron is one of the essential nutrients necessary for spermatogenesis. It is transferred to the testis through the circulation and is stored in testicular cells as

ferritin, transferrin, and other storage proteins that comprise the "iron shuttle protein system" [3]. Iron imbalance has been shown to act as a double-edged sword in the reproductive tract [4] as iron deficiency hinders spermatogenesis, while excessive iron deposition can induce sterility. In VCL, it was reported that free iron is deposited in the testicles due to cell lysis following hyperthermia [5]. In addition, it is known that free radicals created by iron accumulation attack iron-containing cells and proteins, resulting in the release and deposition of iron in tissues [6–8]. In this respect, several studies have clearly shown an increase in testicular iron deposits in infertile patients with VCL as well as in rats with induced VCL [5, 9–11]. Iron is involved in the formation of the most toxic form of oxygenated radicals, the hydroxyl radical, following the classical Fenton and Haber–Weiss reactions [12]. As such, it is a major contributor to the oxidative stress that accompanies VCL. In addition to the testicular and spermatozoa oxidative damage that accompanies VCL, we recently used an induced model of VCL in a rat model to demonstrate that the endoplasmic reticulum/unfolded protein (UPR/ER) stress response [13, 14] is part of the VCL testis response. We showed that the classical mediators of the UPR/ER stress response (mainly the IRE1 pathway) were involved [15] confirming earlier reported data [16, 17]. The VCL testis ER response was shown to lead to germ cell apoptosis that may partially account for reduced spermatogenesis and sperm quality in VCL rats.

Deferasirox (DFX) is an orally absorbed iron chelator. It is a lipophilic molecule with a strong affinity for ferric iron (Fe^{3+}) [18, 19] and has a bioavailability of approximately 70% with a long half-life facilitating its use (single daily oral administration). Two molecules of DFX can form a complex with ferric iron (Fe-[DFX]), to reduce iron overload in the body and prevent further iron deposition [18]. In this respect, Miao et al. (2020) demonstrated that DFX can prevent the Fenton reaction and the associated overproduction of reactive oxygen species (ROS) [20]. Our approach to investigate the effect of DFX in the VCL rat model is based on previous studies showing excess iron in the male reproductive tissue of infertile individuals and, in particular, VCL patients [9–11]. As a catalyst, iron plays a central role in the Fenton reaction that accompanies oxidative bursts, with lipid peroxidation as the main consequence of ROS overproduction [4, 21]. In addition, ROS, in particular H_2O_2, damages iron-containing proteins leading to the release of iron into tissues [4, 6–8]. Since VCL is significantly associated with increased ROS and oxidative stress [22], we wanted to test whether a molecule such as DFX could reduce the deleterious effects of VCL, particularly with regard to the testicular ER/UPR response induced by VCL and its associated prooxidative and proapoptotic facets.

2. Materials and Methods

The mouse phospho-JNK monoclonal antibody (#9255) and the mouse CHOP monoclonal antibody (#2895) were supplied by Cell Signaling Technology (Danvers, MA, USA). The anti-GPX4 monoclonal antibody (#ab125066, EPNCIR144) was provided by Abcam (Cambridge, MA, USA). Goat-rabbit horseradish peroxidase (HRP) IgG (#Sc-2301), goat-mouse HRP IgG (#P0447), and mouse anti-β-actin (#A2228) antibodies were purchased from Santa Cruz (CA, USA), Dako (Carpinteria, CA, USA), and Sigma (St. Louis, MO, USA), respectively. The dyes acridine orange (AO) and chromomycin A3 (CMA3) were obtained from Sigma (St. Louis, MO, USA). Deferasirox (DFX) dispersible tablets (OSVERAL®, each tablet containing 250 mg DFX) were purchased from OSVE Pharmaceutical Co. (Tehran, Iran).

2.1. Experimental Design. This study was approved by the ethics committee of the Royan Institute (IR. ACECR.-ROYAN.REC.1397.224). Thirty male Wistar rats (7–8 weeks, 180–220 grams) were obtained from the Royan Institute of Biotechnology (Isfahan, Iran). They were fed and maintained in accordance with the guidelines of the Ethics Committee of the Institute for Laboratory Animal Research. As shown in Figure 1, the rats were divided into three groups: the VCL group ($n = 10$), in which rats were administered water for 8 weeks beginning two months after surgical induction of VCL; the VCL-DFX group ($n = 10$), in which rats were administered 2 mg/kg DFX by gavage in place of water; and a final control group ($n = 10$), in which rats did not undergo any surgery or gavage. The DFX dose was defined on the basis of human doses converted for use in a rat model [19, 23]. Sham-operated animals were not included in this experiment as previous data have shown that there were no differences with control animals for the evaluated parameters [24]. A DFX alone group of animals was not included as DFX was only used to counteract iron overload induced by VCL and was never intended to be administered alone.

All surgeries were performed under sterile conditions. In brief, each rat was anaesthetized with an intraperitoneal injection of ketamine (75 mg/kg) and xylazine (2.5 mg/kg). After shaving the abdominal region, a polyvidone-iodine antiseptic was administered to the skin and an incision was made from the midline of the abdomen (xyphoid) to around the pubis in order to visualize the left renal vein, the left kidney, and the adrenal vein. Next, the inferior vena cava and the left renal vein were located by careful dissection. A 4-0 silk thread was placed and tied on the left renal vein near the branch of the inferior vena cava. The operation was carried out according to the protocol of Gholirad et al. [5]. It should be noted that this study is a continuation of our recent study published by Hosseini et al. [15] and that our animal model of VCL was verified on the basis of reduced semen parameters, histological findings, and functional semen tests [15, 25, 26].

2.2. Tissue and Spermatozoa Collection. All groups were sacrificed after 4 months. The final weight of each rat was recorded. The left testicular volume was determined according to Archimedes' principle by submerging the testicle in water. The left testicle was then divided into three portions: two portions were fixed in Bouin solution for histopathological evaluation and determination of iron content. The remaining portion was exposed to nitrogen vapour and then stored at -70°C prior to molecular analyses (protein and gene expression). The left cauda epididymides were recovered for

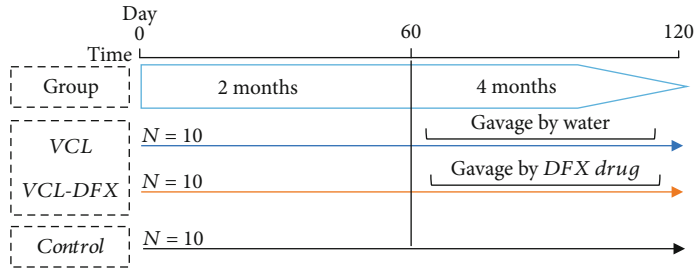

Figure 1: Flowchart of the different experimental sets ($n = 10$ each). VCL was induced surgically on day 0 in groups VCL and VCL-DFX. After 2 months, the VCL animals were given water while the VCL-DFX animals were given DFX (2 mg/kg) for 2 more months. Only one group of rats was used as controls to avoid excessive animal use as we demonstrated earlier that there was no difference between control and sham-operated animals for the parameters monitored [24].

the evaluation of sperm function. The tissues were dilacerated and incubated for 30 min at 37°C in VitaSperm medium (Inoclon, Iran). The following sperm parameters were evaluated: motility, concentration, morphology, nuclear DNA damage, membrane lipid peroxidation, and histone content.

2.3. Histological and Iron Assessment of Testicular Tissues. The fixed tissues were embedded in paraffin and sectioned (10 μm). Sections were dewaxed, rehydrated, and stained with haematoxylin. The mean percentage of spermatogenesis (spermatogenesis index (SI)), meiotic index (MI), and Johnson's score in the seminiferous tubules were evaluated using an Olympus microscope (×40 magnification) and Dino Capture 2 imaging software (AnMo Electronics Corp., Torrance, CA, USA). For SI evaluation, the percentage of seminal tubules containing spermatozoa was defined [26]. For MI, the ratio between the number of round spermatids and primary spermatocytes was evaluated [27]. The degree of histopathological damage in tissue sections was determined according to Johnson's classification score [28]. In short, 100 different seminiferous tubules were randomly evaluated and each tubule was awarded a score between zero and ten. Finally, Johnson's total score was expressed as a percentage.

The free iron content was measured by the Prussian blue staining method (Perl's staining), which evaluates the Fe^{3+} (ferric iron) content. In brief, sections of dewaxed tissue were treated with a mixed solution (2% hydrochloric acid and 2% potassium ferrocyanide, ratio 1 : 1, $v : v$) for 20 min at room temperature. The sections were then washed with tap water and treated with rapid red (NovaUltra; IHC WORLD, LLC, Woodstock, MD, USA) for 5 min. Finally, the sections were dehydrated with successive washes in water, alcohol, and xylene [5, 29–32]. The images were captured using an Olympus BX51 microscope (×100 magnification), and the number of seminiferous tubules containing Fe^{3+} deposits was evaluated using ImageJ software.

2.4. Sperm Mobility, Concentration, Morphology, and Lipid Peroxidation. To determine sperm mobility, 10 μl of the sperm suspensions extracted from the cauda epididymides was placed on a slide and then evaluated under a light microscope (CX31 OLYMPUS; ×40 magnification). Two hundred spermatozoa were observed from random microscopic fields, and mean motility was recorded. A Makler chamber was used to determine sperm concentration, which was presented as millions of cells *per* ml.

Sperm morphology was evaluated by staining 20 μl of washed sperm with 40 μl eosin at room temperature. After 5 min, 60 μl of nigrosine dye was added. Smears were prepared with 20 μl of the preparation [15]. Two hundred spermatozoa on each slide were randomly evaluated on an optical microscope (CX31 OLYMPUS, magnification ×100), and the total percentage of abnormal forms was determined.

The BODIPY® 581/591 C11 test was used to assess sperm membrane lipid peroxidation. The procedure was based on the protocol described by Aitken et al. [21]: two million washed spermatozoa were exposed to the BODIPY C11 probe at a final concentration of 5 mM/ml for 30 min at 37°C. A positive control was performed for each sample by adding H_2O_2 to the sample. The samples were then washed twice with PBS 1x to remove the unbound BODIPY C11 probe (500 g for 5 min). Finally, a flow cytometer FACSCalibur (Becton Dickinson, San Jose, CA, USA) was used to assess lipid peroxidation. The percentage of BODIPY-positive spermatozoa was recorded for each sample.

2.5. Sperm DNA Damage and Nuclear Integrity. The acridine orange (AO) test, which uses a cationic fluorescent dye, was performed to detect damage to sperm DNA. In brief, a smear of washed sperm was prepared on a slide and fixed with Carnoy's solution at 4°C. The slides were then stained with AO in citrate-phosphate buffer (80 ml 0.1 M citric acid+5 ml 0.3 M NaH_2PO_4, pH 2.5). The slides were washed with PBS 1x. Two hundred sperm were counted on each slide using a fluorescent microscope (B-383LD2 OPTIKA). Spermatozoa with a red or orange nucleus (see supplementary figure 1) were considered to show DNA damage [25].

The aniline blue (AB) test was used to assess the level of compaction of the spermatic nucleus. Aniline blue is an acid dye that interacts with lysine-rich histones. In brief, washed sperm cells were spread on slides, and after drying at room temperature, the slides were fixed with 3% glutaraldehyde [25]. Slides were stained with aniline blue (5% aqueous) in 4% ethanoic acid (5 min) and then washed with PBS 1x. A light microscope (×100 magnification, CX31 OLYMPUS, Japan) was used to randomly count 200 sperm cells in different fields for each slide. The percentage of spermatozoa with dark blue nuclei was noted and considered to be sperm cells

exhibiting abnormal chromatin packaging (see supplementary figure 1).

Chromomycin A3 (CMA3) was used to evaluate the sperm nuclear protamine content. Washed spermatozoa were fixed with Carnoy's solution (methyl alcohol : ethanoic acid (3 : 1; $v : v$)) and stored at 4°C for 5 min. Then, 20 μl of fixed spermatozoa solution was spread on slides and left to dry at room temperature. The slides were stained for 90 min with 150 μl CMA3 solution (0.25 mg/ml CMA3 (St. Louis, MO, USA) in McIlvaine buffer containing 7 ml 0.1 M citric acid+33 ml 0.2 M $Na_2HPO_47H_2O$, pH 7.0, 10 mmol/l $MgCl_2$). The slides were then rinsed in PBS 1x and covered with a cover slip. A fluorescent microscope (OPTIKA, CX31 OLYMPUS, Japan) was used to randomly count 200 spermatozoa in different fields. The percentage of spermatozoa with CMA3-labelled nuclei was noted (×100 magnification).

2.6. Isolation of Testicular RNA and qRT-PCR. In brief, 50 mg of tissue from each testicle was homogenized with 1 ml of TRIZOL (Invitrogen Co., USA) for 5 min at 25°C. The nucleic acids were then extracted by centrifugation according to the supplier's recommendation. The RNA concentration was evaluated by NanoDrop using the A260/A280 ratio. The quality of the extracted RNA was confirmed by 1% agarose gel electrophoresis and observation of the 28S and 18S ribosomal RNA bands. A DNase treatment was performed (Fermentas, 1 μg RNA, 0.5 μl RNA inhibitor, 1 μl DNase1, 2 μl buffer, and 15.5 μl sterile water), and the RNAs were transformed into cDNA using a reverse transcription kit according to the manufacturer's protocol (Takara). Finally, a quantitative SYBR® Green RT-qPCR was performed using a thermal cycler (Applied Biosystems; ABi) in a total volume of 10 μl containing 2.8 μl H_2O, 1 μl cDNA, 1 μl specific primers, 0.2 μl ROX, and 5 μl SYBR® Green. The CT comparison method ($\Delta\Delta$CT) was used, and normalization to the GAPDH gene was performed. The primers were designed by Beacon Designer 7 and are shown in Table 1.

2.7. Western Blotting. In brief, total proteins were extracted from the testes after homogenization in a lysis buffer [15]. The protein concentration was evaluated by Bradford's test, and 30 μg protein/sample was evaluated by 12% SDS-PAGE and then transferred to polyvinylidene difluoride (PVDF) membranes by wet transfer. The membranes were then blocked (for p-JNK and GPX4, 5% NFDM/TBST; for CHOP, 5% BSA/TBST; and for β-actin, 5% skim milk) and incubated overnight at 4°C with the primary antibodies according to the protocols of the respective suppliers and the following dilutions: anti-phospho-JNK monoclonal (1 : 1000), anti GPX4 monoclonal (1 : 200), and anti-CHOP/GADD153 monoclonal (1 : 2000). The membranes were then washed (3x, 15 min at 25°C) in 1x PBS to remove unbound antibodies prior to incubation with the secondary antibodies: anti-goat, anti-rabbit, or anti-mouse IgG antibodies conjugated to HRP (2 h at room temperature). Finally, observation of the protein bands was performed using an enhanced chemiluminescence system (ECL, Santa Cruz, USA) following the manufacturer's instructions. Protein band normalization was conducted using β-actin as an internal control.

2.8. Statistical and Image Analyses. Statistical analyses were performed using IBM SPSS Statistics 25.0 software, and graphics were designed using GraphPad Prism (version 8.00). Densitometric analyses of the western blots were performed using ImageJ software (version 1.42q). The data were reported as mean ± SEM. One-way ANOVA (Tukey's post hoc test) was used to compare more than two groups (control, VCL, and VCL-DFX groups), and $p < 0.05$ was considered significant.

3. Results

3.1. Effects of DFX on Body Weight, Testicular Volume, and Testicular Morphometric Parameters in VCL Rats. The average body weight on the day of sacrifice and left testicular volume were compared among the 3 treatment groups. The results showed that unlike the mean body weight, which was similar across the groups (control, 342.89 ± 14.77; VCL, 356.21 ± 7.36; and VCL-DFX, 367.41 ± 7.91 in g), the mean volume of the left testicle was significantly lower in the VCL group than in the control group (in cm^3, respectively, 1.10 ± 0.12 versus 1.48 ± 0.09; $p = 0.04$). In contrast, this parameter was significantly increased in the VCL-DFX group (1.44 ± 0.07 cm^3) compared with the VCL group ($p = 0.04$) and approached the value of the control group. When testicular morphometric parameters were evaluated among groups, we observed that the mean mitotic index, percentage of spermatogenesis, and Johnson's score were significantly ($p < 0.05$) lower in the VCL group compared with the control group and that these parameters approached the control group levels ($p < 0.05$) in DFX-treated VCL rats (Figures 2(a)–2(c)). No significant difference was observed between the VCL-DFX group and the control group ($p > 0.05$).

Varicocele-induced histopathological damages to the testes, such as wide interstitial space, increased irregular basement membranes, the presence of vacuole-like structures, increased cell debris in the lumen of the seminiferous tubules, and loss of germ cells, were higher in the VCL group than in the control group. In contrast, these multiple alterations were markedly less pronounced when VCL rats were treated with DFX (Figures 2(e)–2(j)).

3.2. Effect of DFX on Testicular Free Iron in VCL Rats. The impact of iron chelation by DFX was evaluated via Perl's staining. As shown in Figures 2(k)–2(m), the VCL group showed an excessive accumulation of iron in the seminiferous tubules. In contrast, the VCL-DFX group showed a significant ($p < 0.05$) decrease in Perl's staining compared with the VCL group (Figure 2(d)).

3.3. Effect of DFX on Sperm Parameters in VCL Rats. As expected from previous work, Figure 3 shows that both sperm motility (Figure 3(a)) and sperm concentration (Figure 3(b)) were significantly lower in the VCL group compared with the control group. Also as expected, the percentage of spermatozoa exhibiting abnormal morphologies was

Table 1: List of primers used for real-time RT-PCR analysis.

Gene	Primer sequence (5′-3′)	GenBank no.	Amplicon size (bp)
Grp78	*F TAACAATCAAGGTCTACGAAGG* *R CCATTCACATCTATCTCAAAGGT*	NM_013083.2	193
Splice xbp-1	*F CTGAGTCCGCAGCAGG* *R CTTGTCCAGAATGCCCAAAAGG*	NM_001271731.1	119
Unspliced xbp-1	*F GTCCGCAGCACTCAGACTAC* *R CTGGGGAAGGACATTTGAAAAAC*	NM_001004210.2	178
Nrf2	*F TGCCATTAGTCAGTCGCTC* *R GTGCCTTCAGTGTGCTTC*	NM_031789.2	99
Bcl-2	*F ACTTCTCTCGTCGCTACCGTC* *R AAGAGTTCCTCCACCACCGT*	NM_016993.1	106
Bax	*F GGATCGAGCAGAGAGGATGG* *R ACACTCGCTCAGCTTCTTGG*	NM_017059.2	91
Bak	*F CAGAGAGGTGGTTGGGTGG* *R GTGGGTTGGGGAGAGGTTTAG*	NM_053812.1	181
Bim	*F CACAAACCCCAAGTCCTCC* *R AGTCTCATTGAACTCGTCTCC*	NM_171988.2	152
Caspase-3	*F CGGTATTGAGACAGACAGTGGAAC* *R GCGGTAGAGTAAGCATACAGGAAG*	NM_012922.2	90
p53	*F CCGACTATACCACTATCCACTAC* *R CACAAACACGAACCTCAAAGC*	NM_030989.3	147
GAPDH	*F TGCCGCCTGGAGAAACC* *R TGAAGTCGCAGGAGACAACC*	NM_017008.4	121

significantly increased in the VCL group compared with the control group (Figure 3(c1)). Administration of DFX to VCL animals (VCL-DFX group) restored motility and decreased the percentage of morphologically abnormal spermatozoa, restoring these parameters to the level of control animals (Figures 3(a) and 3(c1)). In contrast, DFX supplementation did not significantly improve spermatozoa concentration (Figure 3(b)).

It should be noted that a more detailed examination of the different types of sperm morphological abnormalities including abnormal head/neck junctions (any abnormality affecting the site of attachment of the sperm head with the sperm midpiece) and abnormal sperm tails (any abnormalities affecting flagellar structure encompassing the sperm midpiece region containing mitochondria and the flagella) revealed that all abnormal morphologies were increased in the VCL group. Only the percentage of sperm cells showing abnormalities in the tail region was not restored to the control level in the DFX-treated VCL group, whereas all other abnormal morphologies were reduced (Figures 3(c2)–3(c4)).

Other classical VCL-associated spermatozoa alterations were monitored, and in agreement with previously reported data, spermatozoa from VCL animals showed a significant increase in lipid peroxidation (as revealed by the BODIPY C11 test), an increase in DNA/nucleus damage and immaturity as shown by the AO test and higher levels of persistent histones compared with spermatozoa from control animals (Figures 3(d)–3(f)). Treatment with DFX only partially restored the integrity of the sperm nucleus of the VCL animals via a decrease in persistent histone content (Figure 3(e)). Treatment with DFX did not reduce the level of sperm lipid peroxidation or the extent of the DNA damage that was likely associated with the characteristic oxidative stress associated with VCL (Figures 3(d) and 3(f)).

3.4. Effect of DFX Effect on the VCL-Induced Testis ER/UPR Response. In order to analyze the effect of DFX on the VCL-induced testis ER/UPR response, we first had to compare the 2-month and 4-month post-VCL induction observations with regard to testicular and spermatozoa parameters. This was necessary because although we had previously reported the ER/UPR status in rat testis 2 months postsurgery [15], we had no information concerning the ER/UPR status 4 months following VCL induction. Since VCL is a chronic condition with progressive oxidative stress leading to cumulative testicular destruction and germ cell apoptosis, we questioned whether the kinetics of the testis ER/UPR response might be different at this later time point.

3.4.1. Evaluation of VCL-Induced Testicular and Spermatozoa Damage 4 Months Post-VCL Induction. Figure 4 illustrates that 4 months post-VCL induction, gross anatomical parameters in the rat (body weight and testicular volume) were similar to those of 2-month VCL animals. Furthermore, although sperm concentration and motility were similar to those of 2-month VCL animals, sperm lipid peroxidation was significantly increased in animals after 4 months. In addition, Figure 4 shows that the deleterious effect on sperm nuclear integrity was exacerbated after 4 months of VCL as revealed by increased AB staining in the 4-month VCL group when compared with the 2-month VCL group. This is in accord with increased oxidative stress damage provoking nuclear decondensation and is supported by the similar elevated

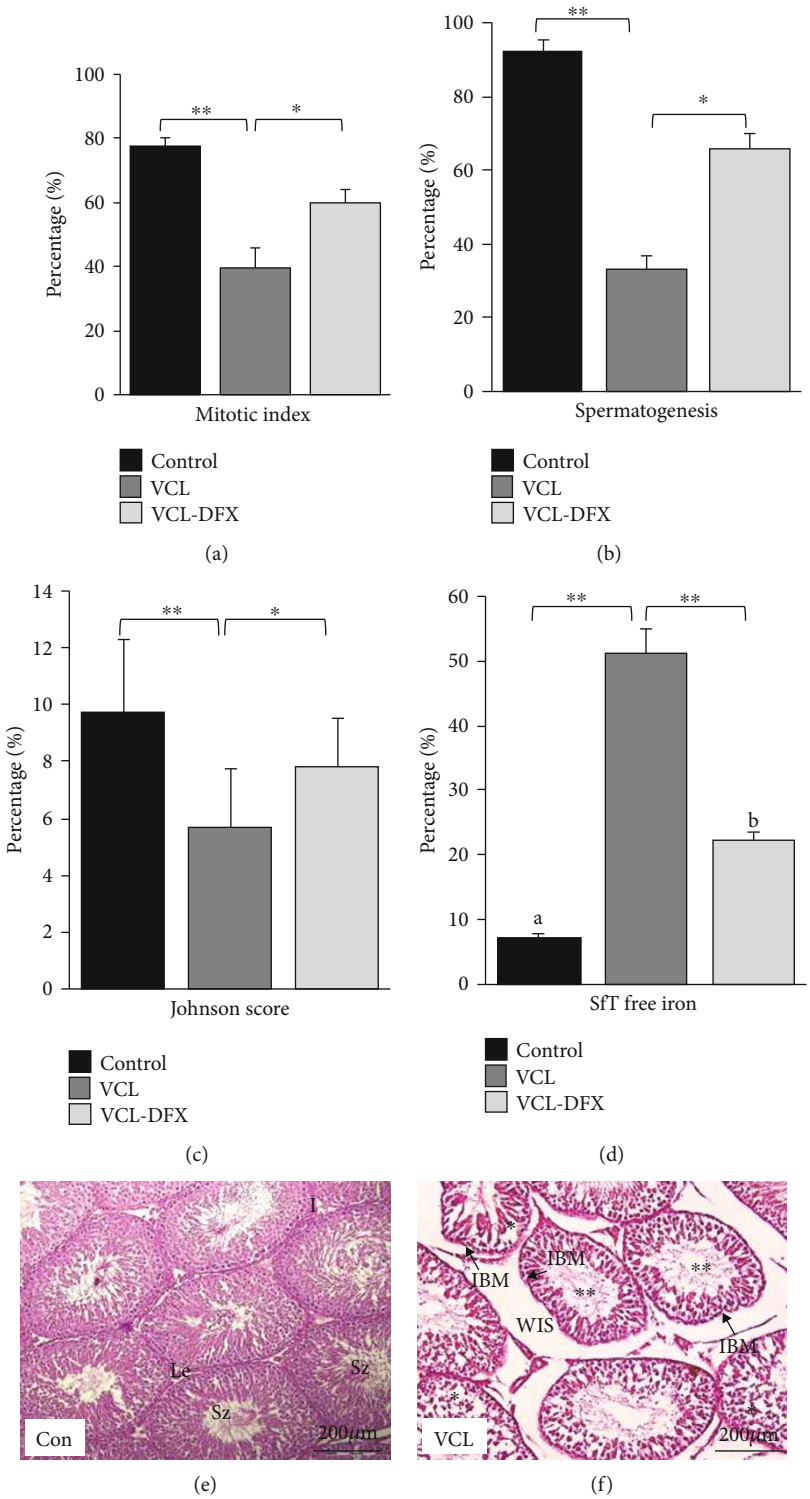

Figure 2: Continued.

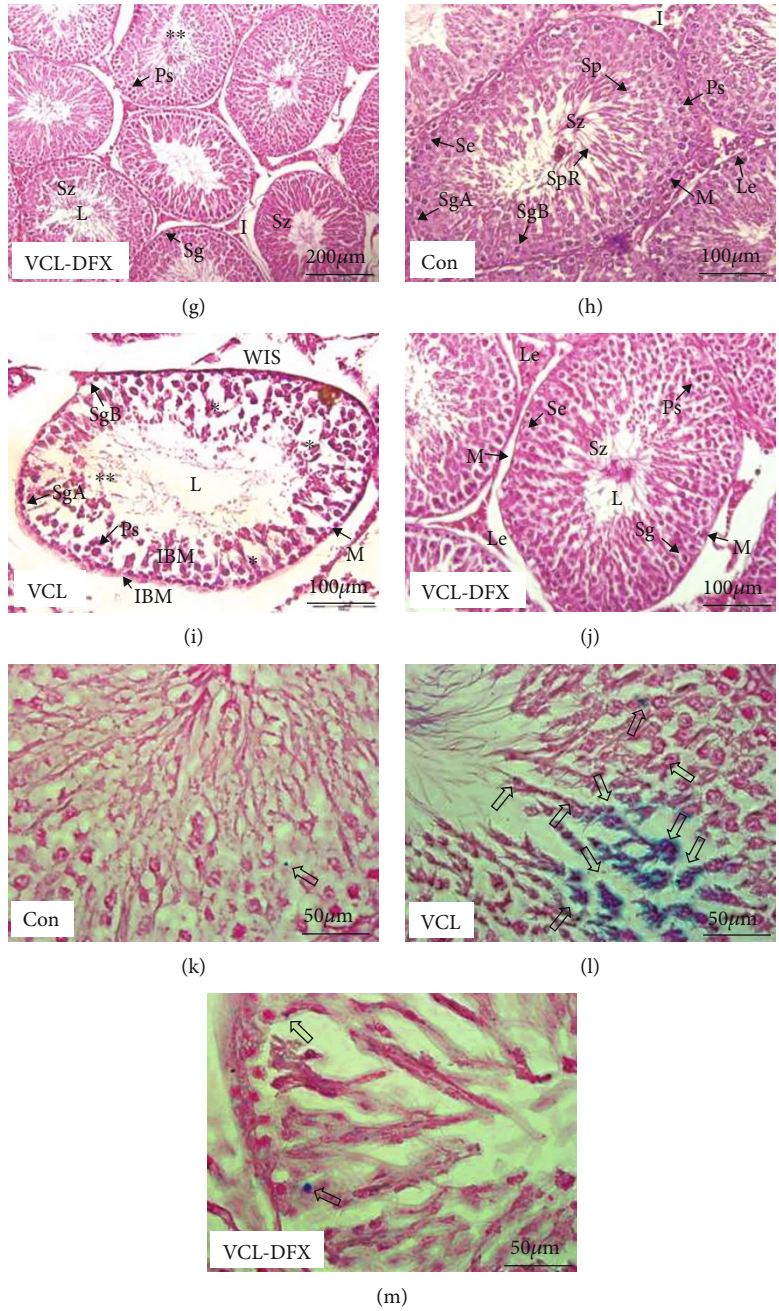

Figure 2: VCL-induced testicular histological damage and free iron content decrease after DFX administration. (a) Mean mitotic index. (b) Mean spermatogenesis index. (c) Mean Johnson score. (d) Mean free iron level from SfTs (seminiferous tubules). (e–g) Representative haematoxylin/eosin-stained testis section (Con = control; VCL and VCL-DFX) at 2 different magnifications: ×20 (e–g) and ×40 (h–j). (k–m) Representative iron accumulation in stained testis sections (Con = control; VCL and VCL-DFX), ×100 magnification. Le: Leydig cells; Se: Sertoli cell; SgA: spermatogonia type A; SgB: spermatogonia type B; Ps: primary spermatocyte; Sp: secondary spermatocyte; I: interstitial space; M: myoid cell; Sz: spermatozoa; WIS: wide interstitial space; IBM: irregular basal membranes; vacuole-like structures and loss of compactness (∗), degraded cells or tubules with minimal spermatozoa content (∗∗), and blue spots show iron accumulation (⇨). Mean ± SEM; $^{*}p < 0.05$, $^{**}p < 0.01$, and $^{***}p < 0.001$; a vs. b ($p = 0.04$) represents significant difference in the three experimental groups.

nuclear protamine deficiencies observed for the two time points (Figure 4(c2)).

Of note is that sperm DNA damage in the control animals also showed a significant increase upon aging. Abnormal sperm morphology was also more pronounced in 4-month VCL animals than it was in 2-month VCL animals, whereas this was not observed for age-matched control animals. Finally, testis iron content was significantly higher in 4-month VCL rats than it was in 2-month VCL rats.

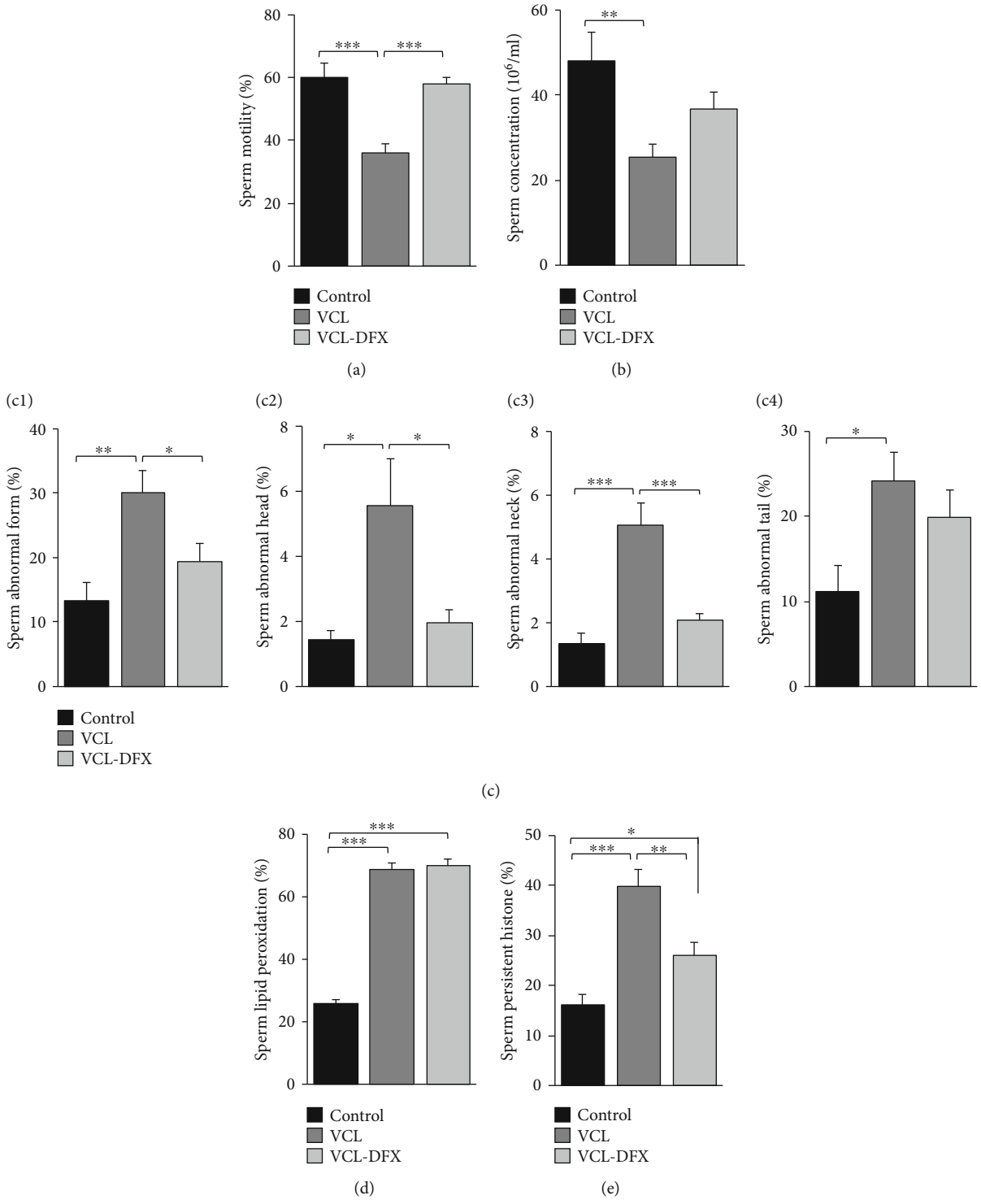

Figure 3: Continued.

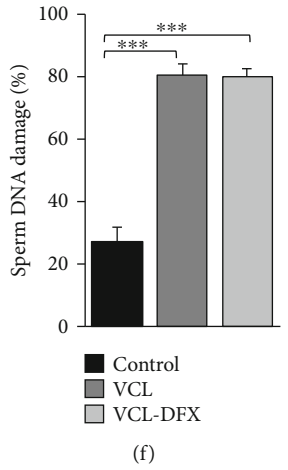

Figure 3: DFX administration improves spermatozoa function and integrity in VCL-induced rats: (a) spermatozoa motility, (b) spermatozoa concentration (10^6/ml), (c1) spermatozoa abnormal morphology, (c2–c4) detailed spermatozoa abnormal morphology (c2: head, c3: neck, and c4: tail), (d) spermatozoa lipid peroxidation, (e) spermatozoa persistent histone content, and (f) spermatozoa DNA damage. Data are presented as mean ± SEM. $^{*}p < 0.05$, $^{**}p < 0.01$, and $^{***}p < 0.001$ show significant difference between the three experimental groups: control, VCL, and VCL-DFX (VCL rats supplemented with DFX).

3.4.2. Evaluation of the ER/UPR Testicular Response 4 Months following VCL Induction. With regard to ER/UPR status, it appeared that the testis response 4 months post-VCL was strikingly distinct from that observed in 2-month VCL animals. Similar to observations made in 2-month VCL animals, the very first mediator of the ER/UPR stress pathway, the testis chaperone Bip/HSPA5/GRP78, was not elevated in 4-month VCL animals. In contrast to activation of the late ER/UPR phase pathway IRE-1/XBP1s/pJUNK observed in the testis after 2 months of VCL [15], none of the 3 classical ER/UPR pathways were found to be activated in the testis after 4 months of VCL (supplementary figures 1 and 2). Only the mitochondrial proapoptotic signals appeared to be elevated as evidenced by increased accumulation of Bim mRNA and a reduction in Bcl-2 mRNA (supplementary figures 1 and 2). Furthermore, it is interesting to note that testicular accumulation of the antiapoptotic Bcl-2 mRNA was found to be lower 4 months post-VCL induction than it was in age-matched control animals (supplementary figures 1 and 2). However, this was not coupled with increased testicular Bax/Bak mRNA accumulation, nor with increased caspase-3 protein content (supplementary figures 1 and 2). In contrast, Bax and Bak steady-state mRNA levels were lower in the 4-month VCL testis than they were in the 2-month VCL testis. With respect to activation of the testis antioxidant response that accompanies both the VCL and ER/UPR stress responses, we show that there was no difference in Nrf2 mRNA accumulation between controls or VCL animals regardless of the duration of VCL (supplementary figure 2). However, a significant reduction in NRF2 testis protein content was observed in the testis of animals after 4 months post-VCL induction (supplementary figures 1 and 2). NRF2 testis protein content was also reduced in 4-month VCL animals when compared with age-matched control animals (supplementary figures 1 and 2). In agreement with the decreased NRF2 testis protein content, testis GPX4 protein content (the corresponding gene is a well-known target of NRF2 *trans*-acting factor) was also reduced in 4-month VCL animals (supplementary figures 1 and 2).

3.5. Does 2 Months of DFX Supplementation Modify the Testis ER/UPR Response in 4-Month VCL Animals? As shown in Figure 5(a), DFX supplementation for 2 months led to a surprisingly significant increase in testicular Bip/HSPA5/Grp78 mRNA, the first mediator of the ER/UPR response. We next examined the ER/UPR downstream pathways and found that DFX supplementation had no effect on the testicular IRE-1/XBP1s/pJUNK pathway as neither Xbp1s mRNA nor the pJUNK protein *was upregulated* (Figures 5(b) and 5(c)). Similarly, DFX supplementation had no effect on the PERK/CHOP ER/UPR pathway as the CHOP testis content was unchanged in all of the animal groups monitored (Figure 6(c)). However, downstream of these ER/UPR membranous players, we found that DFX supplementation provoked increased accumulation of proapoptotic effector mRNAs such as Bim and Bak and the antiapoptotic effector Bcl-2 (Figure 5(d)). Supplementation with DFX appeared to drive the testis further towards apoptosis as evidenced by the increased steady-state level of caspase-3 mRNA (Figure 5(e)) as well as by the increased accumulation of p53 mRNA (Figure 5(f)).

With regard to the antioxidant response that is a component of the ER/UPR and VCL testis response, we show that DFX supplementation provoked a significant increase in NRF2 mRNA accumulation (Figure 6(a)). The DFX-induced overexpression of NRF2 in the testis was further confirmed by the observation that the GPX4 protein was significantly increased in VCL-DFX testes (Figure 6(b)).

4. Discussion

An extensive literature review on the etiology of VCL revealed that ROS play a central role in mediating deleterious

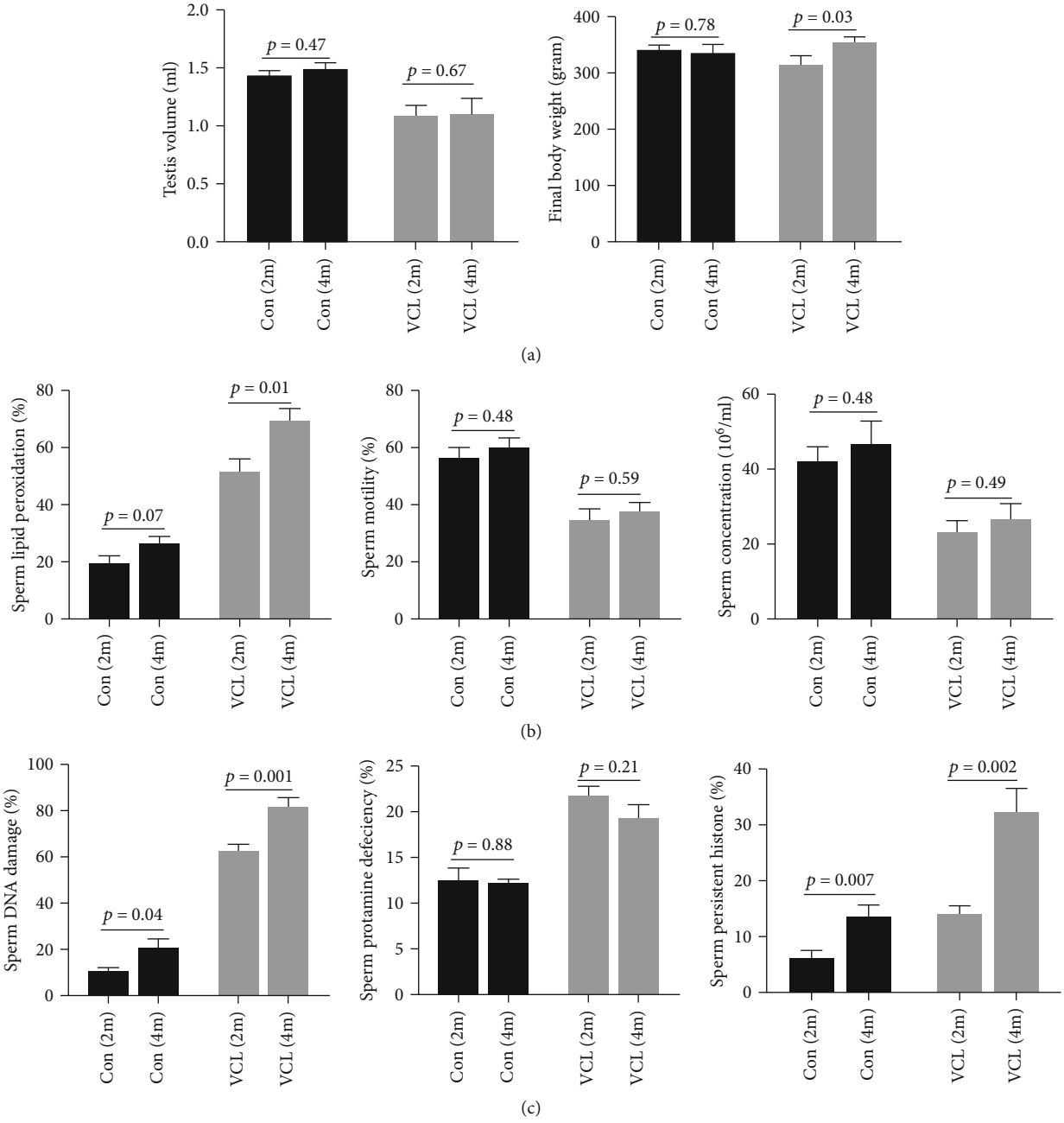

Figure 4: Continued.

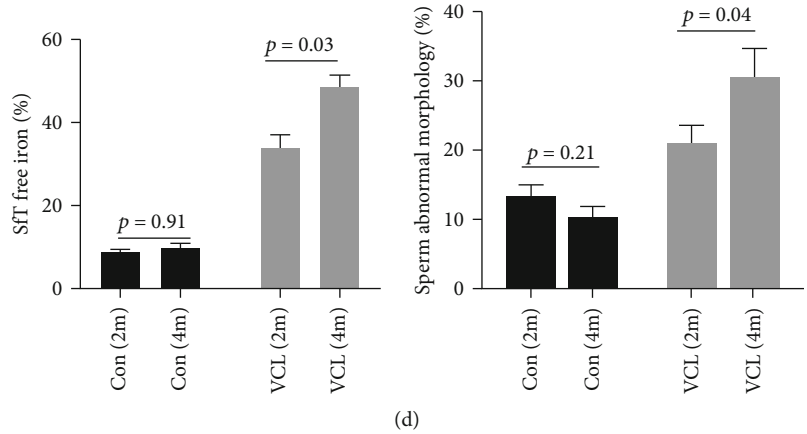

Figure 4: Changes over time for rat anatomical parameters, sperm parameters, and testicular iron content in control and VCL groups. Gross anatomical parameters including (a1) mean final body weight and (a2) mean left testicular volume. Selected semen parameters including (b1) spermatozoa concentration in million/ml, (b2) percentage motile cells, and (b3) percentage of spermatozoa showing lipid peroxidation. Sperm chromatin compaction status with more specifically (c1) percentage of persistent histone, (c2) percentage of protamine-deficient cells, and (c3) percentage of sperm nuclear DNA damage. (d1) Abnormal sperm morphology. (d2) Free iron content of seminiferous tubules (SfTs) in the control (2 *vs.* 4 months) and varicocele (2 *vs.* 4 months) animals. The data represent the mean ± SEM, and an independent *t*-test was performed between two groups. A p value < 0.05 is considered significant.

effects on the testis and germ cells [1, 22]. Seminiferous tubules are composed of Sertoli cells rich in endoplasmic reticulum and mitochondrial [33] organelles known to store a significant amount of iron [34]. It has been shown that testicular iron storage is increased in VCL [5, 9–11, 24–26]. As excess intracellular iron can become toxic due to its ability to accelerate the production of ROS via the classical Fenton/-Haber–Weiss reactions, we tested whether the administration of an iron chelator, DFX, could improve sperm parameters and reduce VCL-induced damage in an animal model of surgically induced VCL.

We show that DFX treatment can decrease testicular free iron overload, protect the testicular tissue from VCL-induced damage, and improve certain sperm parameters (motility and morphology). However, we also show that DFX treatment did not significantly improve spermatozoa concentration measured in cauda epididymis even though the testicular mitotic index and Johnson score were significantly increased. In addition, although DFX treatment significantly decreased the nuclear persistent histone content of VCL spermatozoa, showing an improvement in nuclear quality, this was not accompanied by a decrease in sperm DNA damage.

Of note is that while DFX treatment of VCL animals significantly reduced the percentage of spermatozoa with abnormal morphology, its ameliorative effect was shown to be concentrated on the sperm head and neck, but not on the sperm tail regions. Our initial assumption was that by chelating VCL-mediated testicular iron overload, the iron-induced ROS damage to germ cells could be significantly diminished. This was not fully supported as cauda spermatozoa alterations that are intimately linked to oxidative stress (a high level of lipid peroxidation and nuclear damage) were still observed in VCL-DFX-treated animals. However, it is interesting to note that DFX treatment of VCL animals did succeed in restoring spermatozoa mobility and reducing the proportion of spermatozoa presenting with abnormal head morphology, two parameters that are also closely linked with the impact of oxidative stress on sperm function [35, 36].

One limitation of our study was that based on observations from previously reported treatments, only a single dose of DFX was administered [37, 38]. At this point, we do not know whether other doses could have been more beneficial. Although this awaits additional research, we believe it is rather unlikely because, with the dose administered, we observed beneficial effects (to testicular tissue structures and some functional sperm parameters) in combination with aggravating effects (increased oxidative stress). A question that would merit further investigation is whether or not DFX-chelated iron is removed from the VCL testis. DFX is normally expected to increase renal excretion of iron, but it is possible that due to the specific vascular context of the VCL testis, the removal of chelated iron is limited. If this is indeed the case, it may explain the observed increase in oxidative stress as it has been suggested that chelated iron may contribute to oxidative damage to the same extent as free iron.

Since these conflicting results could be attributed to the dose and duration of DFX treatment administered to the VCL animals used in this study [39–41], we decided to conduct a deeper investigation into the homeostasis of the VCL-DFX-treated testis. We recently reported that the endoplasmic reticulum/unfolded protein response (ER/UPR response), in which oxidative stress is a major player, is likely to be involved in the VCL testis [15]. Therefore, this response was monitored in the testes of the different groups of animals used in the present study. Because we had never evaluated the ER/UPR response of the VCL testis 4 months following surgically induced VCL, it was necessary to monitor the former and compare it to our recent report in which the testis ER/UPR response was analyzed 2 months post-VCL induction [15]. Similar to the observation made 2

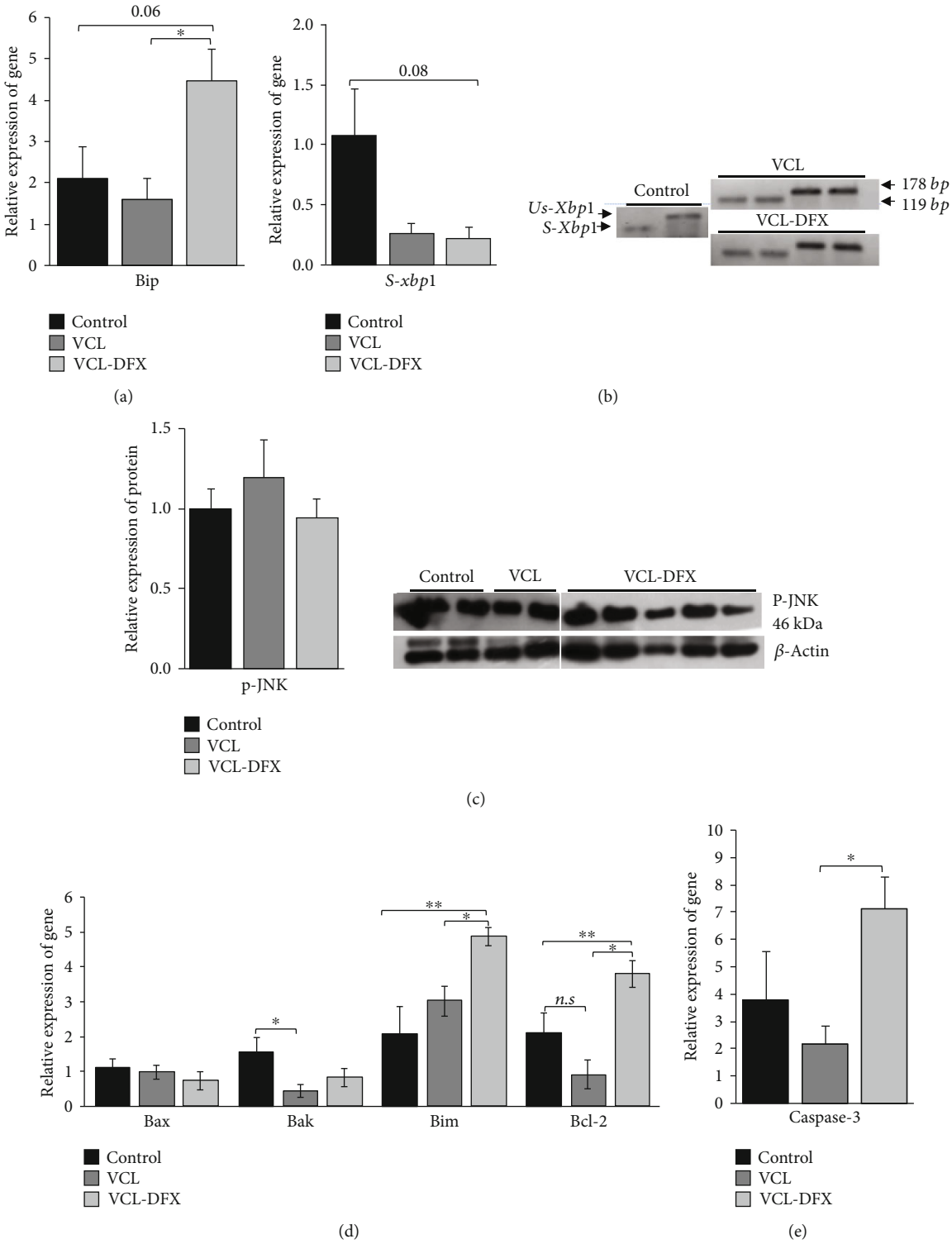

Figure 5: Continued.

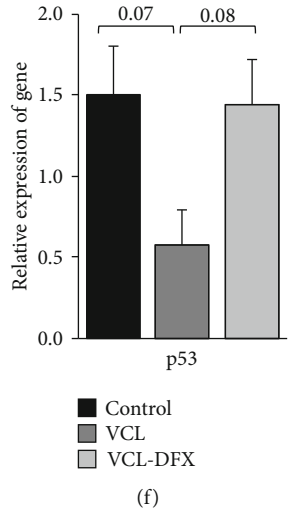

Figure 5: Impacts of DFX chelation on Bip/HspA5/Grp78 transcript and UPR/IRE-1-mediated apoptosis in varicocelized testis: (a) relative accumulation of Bip mRNA; (b1) relative accumulation of s-xbp1 mRNA; (b2) detection of uns-Xbp1 (178 bp band) and s-Xbp1 (119 bp band) mRNA by RT-PCR (2.5% agarose gels); (c1) p-JNK protein content evaluated by western blot (c2); (d) relative mRNA accumulation of mitochondrial-mediated apoptosis markers (Bax, Bak), proapoptosis mediator (Bim), and antiapoptosis mediator (Bcl-2); (e, f) relative mRNA accumulation of caspase-3 and p53 as mediators of programmed cell death. The relative accumulation of mRNA and proteins was normalized to the GAPDH transcript and β-actin antibody, respectively. Data are presented as mean ± SEM. $^{*}p < 0.05$ and $^{**}p < 0.01$, significant difference between study groups: VCL (varicocele), VCL-DFX (varicocelized rats under DFX treatment), and control groups.

months post-VCL induction, the Bip/HSPA5/GRP78 chaperone testis content, the very first mediator of the ER/UPR [13, 15] stress pathway, was not increased at the 4-month time point. In contrast with our previous observation that the late ER/UPR sensor pathway, IRE-1/XBP1s/pJUNK, was activated in the testis after 2 months post-VCL induction, none of the 3 membrane sensor pathways (including PERK, ATF6, and IRE1) were activated in the 4-month VCL testis [15]. Only the mitochondrial-associated apoptotic pathway (as evidenced by increased Bim and decreased Bcl-2 mRNA content), one end point of the ER/UPR pathways, was elevated in the 4-month VCL testis. However, this activation was to a lesser extent when compared with the 2-month VCL testis since neither Bax/Bak nor caspase-3 was found upregulated [15]. Finally, we monitored the testis antioxidant response that accompanies VCL and the ER/UPR response and found that contrary to observations from the 2-month VCL testis [15], the NRF2 protein content and the protein content of one of its known target antioxidant genes (GPX4) were reduced in the 4-month VCL testis. Altogether, these observations suggest that the ER/UPR pathways are no longer activated 4 months after surgically induced VCL. This may be unsurprising as new equilibria are likely to be reached in such a chronic stress-type situation. These observations are consistent with previous studies showing that excess iron and/or oxidative stress not only led to the accumulation of unassembled proteins in the ER but also resulted in reduced Bip/HSPA5/GRP78 expression over time [42–44]. Accordingly, reports of chronic VCL in humans have shown that Bip expression is reduced and is associated with reduced semen quality [45]. Recent studies also revealed an association between compromised sperm maturation and motility with reduced Bip expression in rats in addition to infertile individuals with idiopathic asthenozoospermia [46–49].

In this context, it was surprising to observe that DFX treatment boosted the testis ER/UPR response as evidenced by increased accumulation of the Bip/HSPA5/GRP78 ER chaperone. This event was not associated with any evidence of activation of the downstream ER/UPR membranous sensors (PERK and IRE-1; see Hosseini et al. [15]). However, we recorded a clear increase in apoptotic players (Bim, Bak, caspase-3, and p53) and an increase in the antioxidant response (increased levels of NRF2 mRNA and GPX4 protein in the DFX-treated VCL testis). These data suggest that although DFX was able to limit iron overload-mediated ROS damage to testicular tissue, spermatogenetic function, and sperm cells, this was in parallel with activation of the ER/UPR pathways leading to a proapoptotic response. This provides a likely explanation as to why DFX treatment was unable to restore spermatozoa concentrations to control levels. In addition, it is interesting to note that Bip was immunolocalized to the sperm head and neck compartments, but not to the tail region [48, 49]. This concurs with our observation that DFX treatment, which provoked an increase in Bip content, restored the abnormal head and neck sperm phenotypes, but not the abnormal sperm tail phenotypes. As Bip is involved in protein folding, this may also explain why after DFX stimulation of testicular Bip content we recorded an improved histone to protamine exchange in late differentiating germ cells, a process that requires marked protamine synthesis and ER maturation events [50]. We should point out that our observations contradict earlier reports, which have shown that DFX decreases cellular apoptosis via the

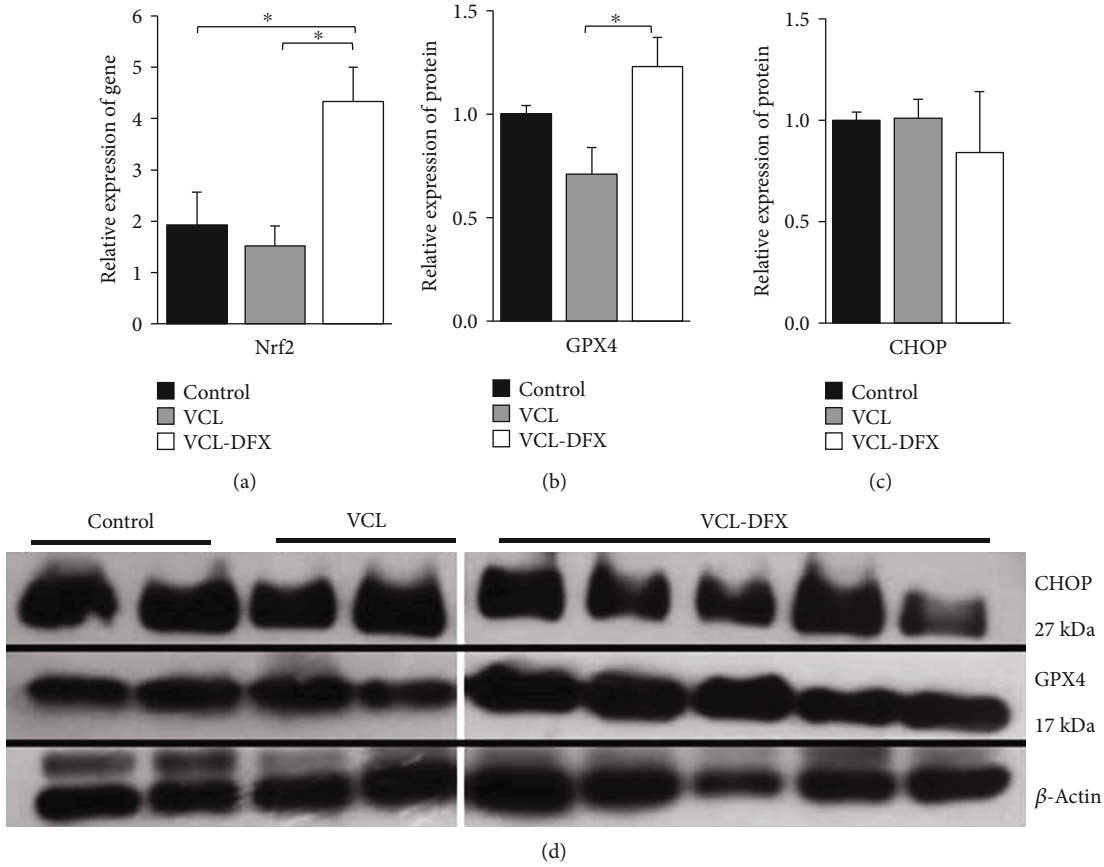

Figure 6: DFX treatment activates the PERK/Nrf2/ARE ER/UPR pathway, but not the PERK/CHOP pathway in the testis of varicocelized rat. (a) Relative accumulation of the Nrf2 transcript. (b) Relative accumulation of the GPX4 protein. (c) Relative accumulation of the CHOP protein. (d) Representative western blots showing the detection of GPX4 and CHOP proteins. The relative accumulation of mRNA and proteins was normalized to the GAPDH transcript and β-actin antibody, respectively. Data are shown as mean ± SEM. $^*p < 0.05$ showed significant difference between study groups: VCL (varicocele), VCL-DFX (varicocelized rats under DFX treatment), and control groups.

inhibition of P-JNK signaling and mitochondrial-dependent cell death [20, 51].

Moreover, our data suggest that DFX treatment provoked a testis antioxidant response as evidenced by the upregulation of NRF2 and one of its targets, GPX4, the stability of which was shown to be associated with the ability of the latter to bind Bip [52]. It is difficult to ascertain whether this antioxidant response is secondary to the activation of the ER/UPR stress pathway PERK [53] or the result of DFX-induced oxidative stress. Since there was no evidence that the PERK/CHOP pathway was triggered, because neither PERK nor CHOP was upregulated in the DFX-treated testis samples, we made the assumption that we had observed DFX-associated oxidative stress. Regardless of the origin, this oxidative stress may explain the increased level of spermatozoa lipid peroxidation and nuclear damage recorded in the DFX-treated VCL animals. This may also explain the inability of DFX to diminish abnormal sperm tail morphology that could originate from oxidative damage to this sperm mitochondrial-associated compartment. Nevertheless, this could contradict with the observation that DFX treatment improved spermatozoa motility in 4-month VCL animals. However, abnormal sperm midpiece organization may be unrelated to mitochondrial energy efficiency. DFX may help to remove iron overload from sperm mitochondria, which has been associated with low ATP generation and alteration of sperm motility as well as with increased ROS generation [4, 54–58]. It is of interest to note that in agreement with our observations, Perera et al. reported that an increase in sperm DNA damage was recorded upon initiation of iron chelation therapy in β-thalassemic patients with iron overload [59].

In conclusion, DFX treatment of surgically induced VCL rats provokes a dual response marked by an increase in testicular proapoptotic markers (Bim, caspase-3, and p53) associated with an increase of antiapoptotic and antioxidant markers (Bcl-2, NRF2, GPX4, and Bip). This is in agreement with previous reports that have shown iron chelation leads to increased p53 expression acting as the "guardian of the genome" together with increased caspase-3 expression in order to restore cell homeostasis [60, 61]. It remains to be determined whether the antioxidant response is mediated by the ER/UPR stress pathways or inherent to DFX. Altogether, the data reported herein show that the iron chelation therapeutic strategy partially restored VCL-induced damage to testicular tissue and sperm function. It will be interesting to test whether coadministration of antioxidants with iron chelators could

provide added benefit to the treatment of VCL. This may be possible as we and others recently reported that antioxidant administration could partially improve VCL tissue and cell alterations in animal models as well as in humans [25, 62, 63]. Such treatment combinations (i.e., iron chelation+antioxidant) have shown therapeutic value in other disease situations [64–66].

Abbreviations

VCL: Varicocele
ER: Endoplasmic reticulum
UPR: Unfolded protein response
PERK: Protein kinase R- (PKR-) like endoplasmic reticulum kinase
ATF6: Activating transcription factor 6
IRE1: Inositol-requiring enzyme 1
DFX: Deferasirox
GRP78: 78 kDa glucose-regulated protein
XBP1: X-box binding protein 1
p-JNK: Phosphorylated JNK
CHOP: C/EBP homologous protein
GPX4: Glutathione peroxidase 4
Nrf2: Nuclear factor erythroid 2-related factor 2
PBS: Phosphate-buffered saline.

Data Availability

Data are available on request.

Conflicts of Interest

None of the authors have a conflict of interest to disclose.

Authors' Contributions

M.H.N.E. and M.T. are responsible for study design, data analysis and interpretation, manuscript writing, and final approval of the manuscript. J.R.D. was responsible for data analysis and interpretation, manuscript writing, and final manuscript approval. M.R., M.H., A.E., E.Sh., and N.S. were responsible for varicocele induction model, sperm functional tests, real-time PCR, and western blot technique. N.N. was responsible for testicular iron evaluation.

Acknowledgments

This study was supported by the Royan Institute (Iran). We would like to express our gratitude to the staff of the Animal Biotechnology Department of the Royan Institute for their full support. In addition, our thanks go to Ms. M. Kelly who professionally edited the manuscript for English syntax and grammar.

Supplementary Materials

Supplementary Figure S1: comparison of time-dependent changes in relative levels of left testicular mRNA/protein content of players involved in the mitochondria and ER/UPR survival/death pathways in control and VCL animals. A1–A4: relative mRNA abundance of markers of the mitochondria proapoptotic (Bax, Bim, and Bak) and antiapoptotic (Bcl-2) responses. B1, B3: relative mRNA abundance of markers of the ER/UPR response (Bip/Grp78 and PERK/Nrf2). B2: relative caspase-3 mRNA abundance. C1–C4: relative CHOP protein content, p-JNK, NRF2, and GPX4 markers. In each analysis, 2-month *vs*. 4-month VCL animals were compared with control animals. The data are presented as mean ± SEM, and an independent t -test was performed between two groups. A p value < 0.05 is considered significant. Supplementary Figure S2: in a surgically induced varicocele model in rats, it was shown that the testis ER/UPR stress pathways were triggered as a result of the hyperthermia, hypoxia, and oxidative stress generated [15]. Among the three main membrane sensors of ER stress that can be mobilized in ER/UPR responses, we had previously shown that after 2 months of VCL, the late pathway IRE1/XBP1s/pJNK was the most prominent, itself triggering the expected proapoptotic and prooxidative responses [15], as revealed by the increased expression of NRF2 and caspase-3. After 4 months of VCL, the testicular response was different, with no involvement of any of the 3 ER membrane sensors. Only a proapoptotic response was revealed, as suggested by the decrease in the antiapoptotic factor Bcl-2 and the increase in the proapoptotic factor Bim. *(Supplementary Materials)*

References

[1] N. Sofikitis, S. Stavrou, S. Skouros, F. Dimitriadis, P. Tsounapi, and A. Takenaka, "Mysteries, facts, and fiction in varicocele pathophysiology and treatment," *European Urology Supplements*, vol. 13, no. 4, pp. 89–99, 2014.

[2] S. W. Leslie, H. Sajjad, and L. E. Siref, *Varicocele*, StatPearls, Treasure Island, FL, USA, 2021.

[3] S. R. Sylvester and M. D. Griswold, "The testicular iron shuttle: a "Nurse" function of the Sertoli cells," *Journal of Andrology*, vol. 15, no. 5, pp. 381–385, 1994.

[4] E. Tvrda, R. Peer, S. C. Sikka, and A. Agarwal, "Iron and copper in male reproduction: a double-edged sword," *Journal of Assisted Reproduction and Genetics*, vol. 32, no. 1, pp. 3–16, 2015.

[5] S. Gholirad, M. Razi, and H. Hassani Bafrani, "Tracing of zinc and iron in experimentally induced varicocele: correlation with oxidative, nitrosative and carbonyl stress," *Andrologia*, vol. 49, no. 6, article e12687, 2017.

[6] N. Bresgen and P. M. Eckl, "Oxidative stress and the homeodynamics of iron metabolism," *Biomolecules*, vol. 5, no. 2, pp. 808–847, 2015.

[7] R. Gozzelino and M. P. Soares, "Coupling heme and iron metabolism via ferritin H chain," *Antioxidants & Redox Signaling*, vol. 20, no. 11, pp. 1754–1769, 2014.

[8] C. U. Carlsen, J. K. Møller, and L. H. Skibsted, "Heme-iron in lipid oxidation," *Coordination Chemistry Reviews*, vol. 249, no. 3-4, pp. 485–498, 2005.

[9] B. Aydemir, A. R. Kiziler, I. Onaran, B. Alici, H. Ozkara, and M. C. Akyolcu, "Impact of Cu and Fe concentrations on oxidative damage in male infertility," *Biological Trace Element Research*, vol. 112, no. 3, pp. 193–204, 2006.

[10] G. Collodel, F. Nerucci, C. Signorini, F. Iacoponi, and E. Moretti, "Associations between biochemical components

of human semen with seminal conditions," *Systems Biology in Reproductive Medicine*, vol. 65, no. 2, pp. 155–163, 2019.

[11] G. Collodel, C. Signorini, F. Nerucci, L. Gambera, F. Iacoponi, and E. Moretti, "Semen biochemical components in varicocele, leukocytospermia, and idiopathic infertility," *Reproductive Sciences*, vol. 28, pp. 91–101, 2021.

[12] J. P. Kehrer, "The Haber-Weiss reaction and mechanisms of toxicity," *Toxicology*, vol. 149, no. 1, pp. 43–50, 2000.

[13] C. Hetz and F. R. Papa, "The unfolded protein response and cell fate control," *Molecular Cell*, vol. 69, no. 2, pp. 169–181, 2018.

[14] Y.-L. Ji, H. Wang, C. Zhang et al., "N-acetylcysteine protects against cadmium-induced germ cell apoptosis by inhibiting endoplasmic reticulum stress in testes," *Asian Journal of Andrology*, vol. 15, no. 2, pp. 290–296, 2013.

[15] M. Hosseini, E. Shaygannia, M. Rahmani et al., "Endoplasmic reticulum stress (ER stress) and unfolded protein response (UPR) occur in a rat varicocele testis model," *Oxidative Medicine and Cellular Longevity.*, vol. 2020, article 5909306, pp. 1–11, 2020.

[16] K. K. Soni, L. T. Zhang, B. R. Choi et al., "Protective effect of MOTILIPERM in varicocele-induced oxidative injury in rat testis by activating phosphorylated inositol requiring kinase 1α (p-IRE1α) and phosphorylated c-Jun N-terminal kinase (p-JNK) pathways," *Pharmaceutical Biology*, vol. 56, no. 1, pp. 94–103, 2018.

[17] K. K. Karna, B. R. Choi, J. H. You et al., "The ameliorative effect of monotropein, astragalin, and spiraeoside on oxidative stress, endoplasmic reticulum stress, and mitochondrial signaling pathway in varicocelized rats," *BMC Complementary and Alternative Medicine*, vol. 19, no. 1, p. 333, 2019.

[18] A. Taher and M. D. Cappellini, "Update on the use of deferasirox in the management of iron overload," *Therapeutics and Clinical Risk Management*, vol. 5, p. 857, 2009.

[19] E. Poggiali, E. Cassinerio, L. Zanaboni, and M. D. Cappellini, "An update on iron chelation therapy," *Blood Transfusion*, vol. 10, no. 4, pp. 411–422, 2012.

[20] J. Miao, M. Xu, Y. Kuang et al., "Deferasirox protects against hydrogen peroxide-induced cell apoptosis by inhibiting ubiquitination and degradation of $p21^{WAF1/CIP1}$," *Biochemical and Biophysical Research Communications*, vol. 524, no. 3, pp. 736–743, 2020.

[21] R. J. Aitken, J. K. Wingate, G. N. De Iuliis, and E. A. McLaughlin, "Analysis of lipid peroxidation in human spermatozoa using BODIPY C11," *MHR: Basic science of reproductive medicine*, vol. 13, no. 4, pp. 203–211, 2007.

[22] A. Agarwal, A. Hamada, and S. C. Esteves, "Insight into oxidative stress in varicocele-associated male infertility: part 1," *Nature Reviews Urology*, vol. 9, no. 12, pp. 678–690, 2012.

[23] J.-W. Shin, I.-C. Seol, and C.-G. Son, "Interpretation of animal dose and human equivalent dose for drug development," 대한한의학회지, vol. 31, no. 3, pp. 1–7, 2010.

[24] P. Mohammadi, H. Hassani-Bafrani, M. Tavalaee, M. Dattilo, and M. H. Nasr-Esfahani, "One-carbon cycle support rescues sperm damage in experimentally induced varicocoele in rats," *BJU international*, vol. 122, no. 3, pp. 480–489, 2018.

[25] E. Shaygannia, M. Tavalaee, G. R. Akhavanfarid, M. Rahimi, M. Dattilo, and M. H. Nasr-Esfahani, "Alpha-lipoic acid improves the testicular dysfunction in rats induced by varicocele," *Andrologia*, vol. 50, no. 9, article e13085, 2018.

[26] N. Sadeghi, N. Erfani-Majd, M. Tavalaee, M. R. Tabandeh, J. R. Drevet, and M. H. Nasr-Esfahani, "Signs of ROS-associated autophagy in testis and sperm in a rat model of varicocele," *Oxidative Medicine and Cellular Longevity*, vol. 2020, Article ID 5140383, 11 pages, 2020.

[27] R. Kheirandish, N. Askari, and H. Babaei, "Zinc therapy improves deleterious effects of chronic copper administration on mice testes: histopathological evaluation," *Andrologia*, vol. 46, no. 2, pp. 80–85, 2014.

[28] S. G. Johnsen, "Testicular biopsy score count – a method for registration of spermatogenesis in human testes: normal values and results in 335 hypogonadal males," *Hormone Research in Paediatrics*, vol. 1, no. 1, pp. 2–25, 1970.

[29] S. Yesil, N. Sungu, A. Kilicarslan et al., "Exenatide reduces oxidative stress and cell death in testis in iron overload rat model," *Experimental and Therapeutic Medicine*, vol. 16, no. 6, pp. 4349–4356, 2018.

[30] F. Pilo, G. Caocci, A. A. DiTucci, V. Serreli, E. Angelucci, and G. La Nasa, "Perl's stain grade in the bone marrow aspirate correlates with overall survival in low risk myelodysplastic patients," *Blood*, vol. 132, article 5517, Supplement 1, 2018.

[31] S. Han, Q. Tang, R. Chen, Y. Li, J. Shu, and X. Zhang, "Hepatic iron overload is associated with hepatocyte apoptosis during *Clonorchis sinensis* infection," *BMC Infectious Diseases*, vol. 17, no. 1, p. 531, 2017.

[32] A. J. Ghio, V. L. Roggli, J. M. Soukup, J. H. Richards, S. H. Randell, and M. S. Muhlebach, "Iron accumulates in the lavage and explanted lungs of cystic fibrosis patients," *Journal of Cystic Fibrosis*, vol. 12, no. 4, pp. 390–398, 2013.

[33] W. Vogl, K. Lyon, A. Adams, M. Piva, and V. Nassour, "The endoplasmic reticulum, calcium signaling and junction turnover in Sertoli cells," *Reproduction*, vol. 155, no. 2, pp. R93–R104, 2018.

[34] C. Andreini, V. Putignano, A. Rosato, and L. Banci, "The human iron-proteome," *Metallomics*, vol. 10, no. 9, pp. 1223–1231, 2018.

[35] J. R. Drevet and R. J. Aitken, "Oxidation of sperm nucleus in mammals: a physiological necessity to some extent with adverse impacts on oocyte and offspring," *Antioxidants*, vol. 9, no. 2, p. 95, 2020.

[36] R. J. Aitken and J. R. Drevet, "The importance of oxidative stress in determining the functionality of mammalian spermatozoa: a two-edged sword," *Antioxidants*, vol. 9, no. 2, p. 111, 2020.

[37] H. Nick, P. Acklin, R. Lattmann et al., "Development of tridentate iron chelators: from desferrithiocin to ICL670," *Current Medicinal Chemistry*, vol. 10, no. 12, pp. 1065–1076, 2003.

[38] H. E. VanOrden and T. M. Hagemann, "Deferasirox—an oral agent for chronic iron overload," *Annals of Pharmacotherapy*, vol. 40, no. 6, pp. 1110–1117, 2006.

[39] M.-Y. Lu, T.-H. Lin, P.-H. Chiang et al., "Deferasirox–iron complex formation ratio as an indicator of long-term chelation efficacy in β-thalassemia major," *Therapeutic Drug Monitoring*, vol. 39, no. 2, pp. 185–191, 2017.

[40] M. D. Cappellini and A. Taher, "Long-term experience with deferasirox (ICL670), a once-daily oral iron chelator, in the treatment of transfusional iron overload," *Expert Opinion on Pharmacotherapy*, vol. 9, no. 13, pp. 2391–2402, 2008.

[41] Y. Aydinok, S. Unal, Y. Oymak et al., "Observational study comparing long-term safety and efficacy of deferasirox with desferrioxamine therapy in chelation-naïve children with

transfusional iron overload," *European Journal of Haematology*, vol. 88, no. 5, pp. 431–438, 2012.

[42] A. Faye, G. Ramey, M. Foretz, and S. Vaulont, "Haptoglobin is degraded by iron in C57BL/6 mice: a possible link with endoplasmic reticulum stress," *Blood Cells, Molecules, and Diseases*, vol. 39, no. 3, pp. 229–237, 2007.

[43] J.-H. Kim, S.-J. Park, T.-S. Kim et al., "Testicular hyperthermia induces unfolded protein response signaling activation in spermatocyte," *Biochemical and Biophysical Research Communications*, vol. 434, no. 4, pp. 861–866, 2013.

[44] M. Vitale, A. Bakunts, A. Orsi et al., "Inadequate BiP availability defines endoplasmic reticulum stress," *eLife*, vol. 8, article e41168, 2019.

[45] H. Hosseinifar, H. Gourabi, G. H. Salekdeh et al., "Study of sperm protein profile in men with and without varicocele using two-dimensional gel electrophoresis," *Urology*, vol. 81, no. 2, pp. 293–300, 2013.

[46] S. Shen, J. Wang, J. Liang, and D. He, "Comparative proteomic study between human normal motility sperm and idiopathic asthenozoospermia," *World Journal of Urology*, vol. 31, no. 6, pp. 1395–1401, 2013.

[47] H. Qin, R. Wang, X. Pang, Y. Wei, F. Yang, and J. Wang, "Association of GRP78 promoter polymorphisms and serum GRP78 level with risk of asthenozoospermia," *Journal of Assisted Reproduction and Genetics*, vol. 35, no. 12, pp. 2223–2231, 2018.

[48] V. Lobo, P. Rao, R. Gajbhiye, V. Kulkarni, and P. Parte, "Glucose regulated protein 78 phosphorylation in sperm undergoes dynamic changes during maturation," *PLoS One*, vol. 10, no. 11, article e0141858, 2015.

[49] V. Lobo and P. Parte, "Membrane-bound glucose regulated protein 78 interacts with alpha-2-macroglobulin to promote actin reorganization in sperm during epididymal maturation," *MHR: Basic science of reproductive medicine*, vol. 25, no. 3, pp. 137–155, 2019.

[50] I. Nagamori, K. Yomogida, M. Ikawa, M. Okabe, N. Yabuta, and H. Nojima, "The testes-specific bZip type transcription factor Tisp40 plays a role in ER stress responses and chromatin packaging during spermiogenesis," *Genes to Cells*, vol. 11, no. 10, pp. 1161–1171, 2006.

[51] R. M. Al-Rousan, S. Paturi, J. P. Laurino et al., "Deferasirox removes cardiac iron and attenuates oxidative stress in the iron-overloaded gerbil," *American Journal of Hematology*, vol. 84, no. 9, pp. 565–570, 2009.

[52] S. Zhu, Q. Zhang, X. Sun et al., "HSPA5 regulates ferroptotic cell death in cancer cells," *Cancer Research*, vol. 77, no. 8, pp. 2064–2077, 2017.

[53] G. Zhang, W. Yang, F. Jiang et al., "PERK regulates Nrf2/ARE antioxidant pathway against dibutyl phthalate-induced mitochondrial damage and apoptosis dependent of reactive oxygen species in mouse spermatocyte-derived cells," *Toxicology Letters*, vol. 308, pp. 24–33, 2019.

[54] M. Gumińska, T. Kedryna, A. Laszczka et al., "Changes in ATP level and iron-induced ultra-weak photon emission in bull spermatozoa, caused by membrane peroxidation during thermal stress," *Acta Biochimica Polonica*, vol. 44, no. 1, pp. 131–138, 1997.

[55] Z. Kňažická, J. Lukáčová, E. Tvrdá et al., "In vitro assessment of iron effect on the spermatozoa motility parameters," *Journal of Microbiology, Biotechnology and Food Sciences*, vol. 2, pp. 414–425, 2012.

[56] A. Kwiatkowski, G. Ryckewaert, P. J. Tchofo et al., "Long-term improvement under deferiprone in a case of neurodegeneration with brain iron accumulation," *Parkinsonism & Related Disorders*, vol. 18, no. 1, pp. 110–112, 2012.

[57] O. Kakhlon, W. Breuer, A. Munnich, and Z. I. Cabantchik, "Iron redistribution as a therapeutic strategy for treating diseases of localized iron accumulation," *Canadian Journal of Physiology and Pharmacology*, vol. 88, no. 3, pp. 187–196, 2010.

[58] D. M. Ward and S. M. Cloonan, "Mitochondrial iron in human health and disease," *Annual Review of Physiology*, vol. 81, no. 1, pp. 453–482, 2019.

[59] D. Perera, A. Pizzey, A. Campbell et al., "Sperm DNA damage in potentially fertile homozygous β-thalassaemia patients with iron overload," *Human Reproduction*, vol. 17, no. 7, pp. 1820–1825, 2002.

[60] J. Shen, X. Sheng, Z. Chang et al., "Iron metabolism regulates p53 signaling through direct heme-p53 interaction and modulation of p53 localization, stability, and function," *Cell Reports*, vol. 7, no. 1, pp. 180–193, 2014.

[61] B. T. Greene, J. Thorburn, M. C. Willingham et al., "Activation of caspase pathways during iron chelator-mediated apoptosis*," *Journal of Biological Chemistry*, vol. 277, no. 28, pp. 25568–25575, 2002.

[62] H. Garg and R. Kumar, "An update on the role of medical treatment including antioxidant therapy in varicocele," *Asian Journal of Andrology*, vol. 18, no. 2, pp. 222–228, 2016.

[63] B. Abbasi, N. Molavi, M. Tavalaee, H. Abbasi, and M. H. Nasr-Esfahani, "Alpha-lipoic acid improves sperm motility in infertile men after varicocelectomy: a triple-blind randomized controlled trial," *Reproductive BioMedicine Online*, vol. 41, no. 6, pp. 1084–1091, 2020.

[64] S. Wongjaikam, S. Kumfu, J. Khamseekaew et al., "Combined iron chelator and antioxidant exerted greater efficacy on cardioprotection than monotherapy in iron-overloaded rats," *PLoS One*, vol. 11, no. 7, article e0159414, 2016.

[65] J. Sripetchwandee, S. Wongjaikam, W. Krintratun, N. Chattipakorn, and S. C. Chattipakorn, "A combination of an iron chelator with an antioxidant effectively diminishes the dendritic loss, tau-hyperphosphorylation, amyloids-β accumulation and brain mitochondrial dynamic disruption in rats with chronic iron-overload," *Neuroscience*, vol. 332, pp. 191–202, 2016.

[66] S. Wongjaikam, S. Kumfu, J. Khamseekaew, S. C. Chattipakorn, and N. Chattipakorn, "Restoring the impaired cardiac calcium homeostasis and cardiac function in iron overload rats by the combined deferiprone and N-acetyl cysteine," *Scientific Reports*, vol. 7, no. 1, p. 44460, 2017.

Hindawi
Oxidative Medicine and Cellular Longevity
Volume 2021, Article ID 6612796, 7 pages
https://doi.org/10.1155/2021/6612796

Review Article

Research Progress on the Relationship between Obesity-Inflammation-Aromatase Axis and Male Infertility

Liu Yuxin,[1] Lin Chen,[2] Luo Xiaoxia,[1] Luo Yue,[1] Lai Junjie,[1] Li Youzhu,[3] Zhou Huiliang,[2] and Liu Qicai[2]

[1]*School of Medical Technology and Engineering, Fujian Medical University, China*
[2]*Center of Reproductive Medicine, The First Affiliated Hospital of Fujian Medical University, China*
[3]*Center of Reproductive Medicine, The First Affiliated Hospital of Xiamen University, China*

Correspondence should be addressed to Li Youzhu; liyouzhu2006@sina.com, Zhou Huiliang; zhllq@sina.com, and Liu Qicai; lqc673673673@163.com

Liu Yuxin and Lin Chen contributed equally to this work.

Received 23 November 2020; Revised 4 January 2021; Accepted 30 January 2021; Published 8 February 2021

Academic Editor: Keren Cheng

Aromatase is a key enzyme in the transformation of androgen into estrogen. Its high expression will destroy the hormonal balance in the male body, and the excessive transformation of androgen into estrogen in the body will further damage the spermatogenic function of the testis, affect the normal development of the sperm, and cause spermatogenic disturbance. Adipose tissue has a high expression of aromatase and shows high enzymatic activity and ability to convert estrogen. Adipose tissue is the most estrogen-producing nongonadal tissue in the body because of its large size, accounting for about 20% of the body mass in healthy adults. PPARγ is recognized as the key adipose differentiation in the transcriptional regulation of the transcription factor. In the process of adipocyte differentiation, PPARγ regulate the expression of aromatase. The increase of aromatase is associated with the inflammatory response in adipose tissue caused by obesity. After obesity, the increase of proinflammatory factors in adipocytes will lead to enhanced transcription of the CYP19 gene encoding aromatase in adipocytes, which in turn will lead to increased expression of aromatase in adipocytes. This article reviews the regulation of male sterility from the angle of the "obesity-inflammation-aromatase" axis.

1. Introduction

The World Health Organization predicts that infertility will become the third chronic disease after tumors and cardiovascular and cerebrovascular diseases in the 21st century, with up to 15% of the world's population suffering from infertility, about half of which is caused by male factors [1]. In China, there are nearly 20 million couples suffering from fertility difficulties, among which the infertility caused by the male accounts for about 30%, while in the male infertility patients, the semen quality problem is as high as 90% [2, 3].

There are many causes for male infertility, among which endocrine disorder is an important factor. Up to 70% of infertile men have endocrine dysfunction, such as metabolic syndrome characterized by insulin resistance and obesity. Obesity is the main cause of hypogonadism at present, which associates with impaired gonadal function in males [4]. The fertility of men depends on a certain number and high quality sperm. Spermatogenesis and maturation are a highly complex process involving the fine regulation of sex hormones, testis, Sertoli cells, and epididymal fluid. However, in recent years, it has gradually revealed the fact that obesity affects men's reproductive potential. Too much fat can lead to changes in hormone levels and promote chronic inflammation of the genital tract. High fat content in the scrotal region can also lead to increased scrotal temperature. All of these consequences of obesity destroy the testicular and epididymal microenvironment, which is crucial for sperm production

and maturation [5–7]. In recent years, obesity caused by unhealthy lifestyle and social-psychological factors has become a research hotspot. Therefore, clarifying the relationship between obesity and infertility has become the key to research breakthroughs. The purpose of this review is to explore the relationship between the abnormal aromatase axis caused by obesity and male infertility.

2. Obese and Inflammation

2.1. Related Inflammatory Factors and Chemokines in Obesity. Obesity is a "low-grade chronic inflammatory state" caused by multiple factors [8]. In the state of obesity, lipid deposition leads to the enlargement of adipocyte volume. When adipocyte hypertrophy exceeds its own limit, apoptosis will occur. Necrotic adipocytes secrete various inflammatory factors and chemokines, such as ICAM and VCAM-1. So that the monocyte-macrophages proliferate and migrate to the adipose tissue and have a unique structure, that is, CLSs gather around necrotic fat cells [9]. Adipocytes release more fatty acids and endotoxins, which activate macrophages to transform into M1 macrophages that promote inflammation, and then activate the NF-κB pathway, which significantly increases the release of proinflammatory factors such as TNF-α, IL-6, and IL-1β, while anti-inflammatory factors are reduced. In addition, hypertrophic adipocytes can also change intracellular signal transduction, increase the expression of proinflammatory cytokines, and ultimately cause chronic inflammation [10].

2.2. M1 Macrophage Infiltration under Obesity. The proportion of macrophages in normal adipose tissue to total cells is only 10%, while in obese tissues, this proportion can be as high as 50%, and the increase is mainly M1 macrophages that secrete proinflammatory factors [11]. The accumulation and infiltration of ATMs cause aseptic inflammation and break the balance between M1 macrophages and M2 macrophages, resulting in the polarization of M2 macrophages secreting anti-inflammatory factors towards M1 macrophages secreting proinflammatory factors [12]. Then, M1 macrophages will secrete a large amount of proinflammatory factors. This causes the obese people to gradually change from a "low-grade chronic inflammation state" locally to the whole body, thus forming a vicious circle [13, 14].

2.3. Tissue Hypoxia and Chronic Inflammation Caused by Obesity. Local hypoxia in adipose tissue is also one of the mechanisms of chronic inflammation, and this local hypoxia is caused by insufficient blood flow supply due to the rapid growth of adipose tissue [15]. In the case of low oxygen content, the cell itself has a defense mechanism to adapt to this hypoxic environment. This cell's defense response to hypoxia is achieved through the activation of specific transcription factors, including: HIF-1α, GLUT1, HO-1, PDK1, and VEGF, which increase the expression of factors produced by local hypoxia. It further recruits macrophages to infiltrate adipose tissue, leaving the body in a state of low-grade inflammatory response [16].

2.4. Oxidative Stress in Obesity. In the case of a high-carbohydrate or high-fat diet, excessive glucose and fatty acids generate pyruvate, CoA, and other reducing metabolites. Then, the above-mentioned substrates enter the mitochondria for oxidation, which enhances the activity of the mitochondrial respiratory chain and increases single electron transfer and ROS production [17]. Due to the chronic low-level inflammatory response in obese patients, inflammation activates a variety of immune cells to produce a large number of free radicals, aggravating oxidative stress. Oxidative stress further aggravates cell oxidative damage and accelerates cell senescence. Senescent adipocytes recruit macrophages, release a variety of proinflammatory cytokines, and promote inflammation [18].

3. Body Inflammation and Expression of Aromatase

3.1. The Biological Activity of Aromatase. Aromatase belongs to the cytochrome P450 superfamily, which is encoded by the CYP19A1 gene located on chromosome 15 (15q21). The entire CYP19 gene is 123 kb, of which about 30 kb containing 9 exons (II-X) that encode the aromatase protein and 93 kb containing untranslated first exons that are controlled in a tissue-specific manner. There are a variety of tissue-specific promoters in the 5′-end nontranslational region, including PI.1, PI.2a, PI.8, PI.4, PI.5, PI.7, PI.f, PI.2, PI.6, PI.3, and PII [19]. The promoter selectively splices the nontranslational area (5-UTR) of its own exons I 5′ side onto the splice site (AG/GACT) at the 38 kb upstream of the translation initiation site (ATG) on exon II (Figure 1) [20, 21]. The regulatory factors of CYP19 gene include cis-acting factors such as CRE together with ER, and trans-acting factors such as growth factor together with TBP.

Aromatase is composed of two proteins, NADPH cytochrome P450 and specific cell P450 aromatase. The former provides reductive equivalent $NADPH+H^+$ and electron transfer for hydroxylation catalyzed by P450arom, while the latter provides steroid hormone binding sites for catalytic synthesis of estrogen [22]. Aromatase is a key enzyme in the synthesis of estrogen, which can catalyze the irreversible conversion of testosterone and androstenedione into estrogen, which plays an important role in the life activities of normal individuals. Due to alternative use of multiple promoters, the transcription level of CYP19 and the activity of aromatase in different tissues are different. In humans, aromatase is expressed in many cells and tissues, including Leydig cells, Sertoli cells, granulocytes, luteal cells, placental cells, neurons, fibroblasts, vascular smooth muscle cells, preadipocytes, chondrocytes, and osteoblasts, etc. [23, 24].

A natural mutation in the male aromatase gene may lead to testicular abnormalities, endocrine disorders, and altered sperm parameters. Increased aromatase activity can lead to decreased testosterone levels, which is one of the mechanisms leading to male hypogonadism. AI can inhibit aromatase activity, correct the condition of "low androgen and high estrogens," and improve the spermatogenic function of testis. More and more attention has been paid to the use of AI in the treatment of spermatogenesis dysfunction. AI is especially suitable for patients with spermatogenesis dysfunction with low androgen level and high estrogen level (quantified by T/E_2 ratio, which is currently considered as low limit of 10)

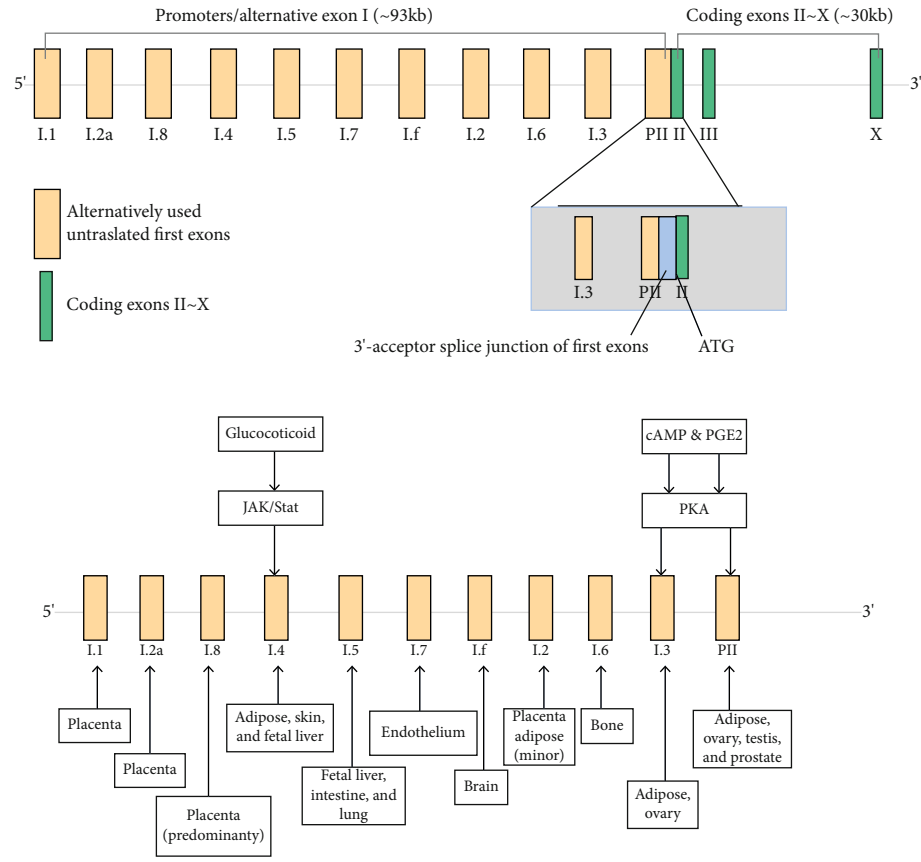

Figure 1: Encoding CYP19A1 gene structure of aromatase.

[25]. Although clinicians have attached increased importance to the therapeutic effect of AI on spermatogenic disorders, more in-depth studies are needed in terms of their applicable population and mechanism of action.

3.2. Inflammatory State Induces the Expression of Aromatase. Obesity is now accepted as a low-grade, chronic, and systemic inflammatory disease, which is predominantly characterized by an increase of M1 macrophages and the inflammatory mediators in adipose tissue [26, 27]. And the obesity-associated adipose tissue inflammation leads to increased CYP19A1 expression in males, which leads to excessive aromatase in obese men. The CYP19 gene contains several cis-regulatory elements [28, 29], of which the CRE is the major regulator. The cAMP activates the downstream cAMP-dependent protein kinase that is also called PKA and causes CREB phosphorylation, thereby coupling CRE latterly. The formation of the cAMP/PKA/CREB signaling pathway leads to subsequent signal transduction and upregulation of aromatase expression. Discovery showed that insulin concentration and sensitivity could interfere with various signal pathways, which were mainly based on the cAMP-dependent signaling pathway, thus affecting the expression of CYP19. The high expression of proinflammatory mediators such as PGE2, TNF-α, and IL-6 in M1 macrophages can induce the expression of aromatase in preadipocytes by amplifying the inflammatory effect. And the significant regulatory effect of PGE2 on CYP19 is worthy of attention. The PGT removes PGE2 from the extracellular milieu and delivers it to the cytoplasm. Thereby, PGE2 activates the CAMP/PKA/CREB pathway through binding to EP2 and EP4, thus resulting in enhanced interaction between CREB, p300, and aromatase promoter I.3/II [30]. Moreover, PGE2 decreases the amounts of BRCA1, a repressor of aromatase transcription, which reduced interaction between BRCA1 and the aromatase promoter I.3/II. In conclusion, CYP19 transcription and aromatase activity are enhanced ultimately (Figure 2).

Meanwhile, the results of Kotha Subbaramaiah showed that M1 macrophages infiltrated in adipose and breast tissues of obese mice, with increased content of inflammatory mediators and aromatase. These results suggest that the expression of the CYP19 gene may be influenced by proinflammatory mediators, which may in turn change the aromatase content and activity in obese mice. Collectively, these findings suggest that obesity-induced inflammation interfering with the cAMP-dominated signal transduction pathway through secondary IR and related inflammatory factors, stimulating CYP19 transcription and elevating the aromatase level.

In recent years, the biological effects of EGCG and TGR5 on improving obesity have attracted much attention. It has been found that EGCG administration can improve the interference of nutritional obesity on insulin signal, reduce the accumulation of lipids in liver tissue, and interfere with the TLR4-mediated inflammatory response pathway and the key molecule of insulin signal pathway in liver tissue, thus balancing the redox state, relieving inflammation [31–33]. Additionally, EGCG can also make the composition of its

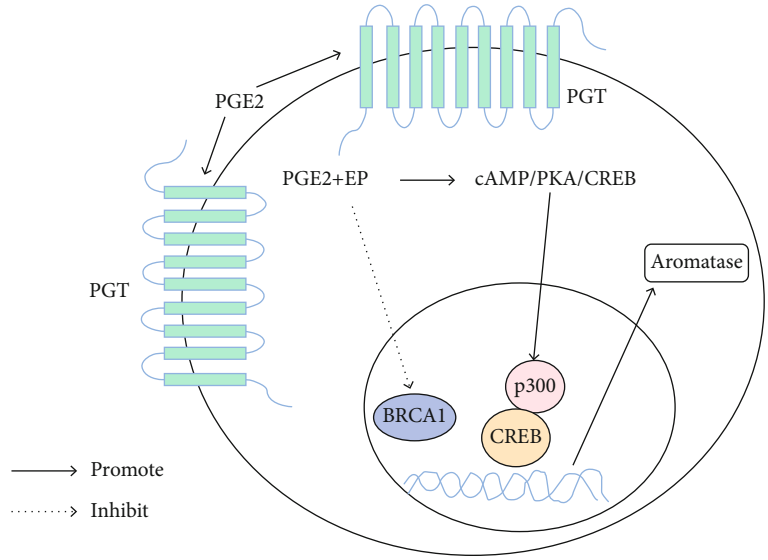

Figure 2: Signal transduction pathway of aromatase expression regulated by PGE2 through PGT. PGT is a trans-membrane domain transporter that carries extracellular PGE2 into cytoplasm, which activates the CAMP/PKA/CREB pathway by binding to its receptors EP2 and EP4, thus resulting in enhanced interaction between CREB, p300, and aromatase promoter I.3/II. PGE2 also decreased the amounts of BRCA1 and inhibited the interaction of BRCA1 and aromatase promoter I.3/II; then, CYP19 transcription and aromatase activity are enhanced ultimately.

intestinal microbiota significantly change and LPS into the blood reduce, thus reducing endotoxemia, alleviating IR and improving low-grade, chronic obesity-associated inflammation. The findings of Hassan et al. showed that EGCG could improve the male infertility with the EGCG administration, suggesting that EGCG could improve the sterility of male rats by ameliorating inflammation, thereby affecting the expression of aromatase [34]. Furthermore, TGR5 has been found to have anti-inflammatory effects by inhibiting NF-κB, thus inhibiting proinflammatory cytokine production. The mice with the TGR5 gene knocked out showed severe hyperlipidemia, steatosis, IR, and inflammation.

PPARs are members of the nuclear receptor superfamily and have three subtypes, PPARα, PPARβ/δ, and PPARγ, which have the properties of anti-inflammation, anti-TLR4 inflammatory response pathway, and anti-NF-κB [35, 36]. PPARs are found in many tissues, such as the liver, heart, skeletal muscle, and brown adipose tissue. The localization of PPARs in mouse testis by Gang Wang et al. showed that PPARα was mainly located in the nucleus of Leydig cells and PPARβ/δ mainly in Sertoli cells, while PPARγ mainly distributed in the nucleus of the sperm cell. It has been found that the activation of PPARs may regulate the expression of aromatase directly or indirectly by regulating the transcription of NF-κB, ROS enzyme-relevant genes, and RNA metabolism together with anti-inflammatory and antioxidative pathways [37].

4. Aromatase Expression Disorder and Male Infertility

4.1. Aromatase Overexpression Leads to Hormone Disorder. Aromatase, as a rate-limiting enzyme for the irreversible conversion of androgens to estrogens, leads to the overconversion of androgens to estrogen in men, resulting in a high concentration of estrogen and low concentration of androgens, when its activity increases. Although estrogen has always been regarded as a typical female hormone, more and more studies show that estrogen not only maintains a certain amount in the male body but also plays an important role in male reproduction in recent years. Therefore, the balance between estrogen and androgen is an important part of male fertility, and the aromatase expression will be particularly important in this balance. Excessive estrogen inhibits the release of FSH and LH by inhibiting the HPG axis, thereby further reducing androgen levels. Spermatogenesis proceeds with the rigorous regulation of the above hormones. So when the balance of these hormones is disturbed, it will bring a negative effect on spermatogenesis. Therefore, the high expression of aromatase can disrupt the hormone balance in the male body, hinder the process of spermatogenesis, and lead to male infertility. In recent years, AI administration has received extensive attention in the field of male infertility. It can correct the condition of "low androgen level and high estrogen level" and then improve the spermatogenic function of the testis. It also relieves estrogen's negative feedback inhibition of the HPG axis, which in turn promotes the release of FSH and LH from the pituitary gland (Figure 3) [25].

4.2. The Receptor Sensitivity of Estrogen Is Enhanced in the State of High Expression. Studies have shown that when estrogen levels in male rats are elevated, the expression of estrogen receptors ERα and ERβ in sperm cells is increased. This suggests that with increased levels of estrogen, its sensitivity is also increased, which is also detrimental to spermatogenesis [38].

4.3. Damage of Leydig Cells Induced by Overexpression of Aromatase. There are two types of macrophages in the testis.

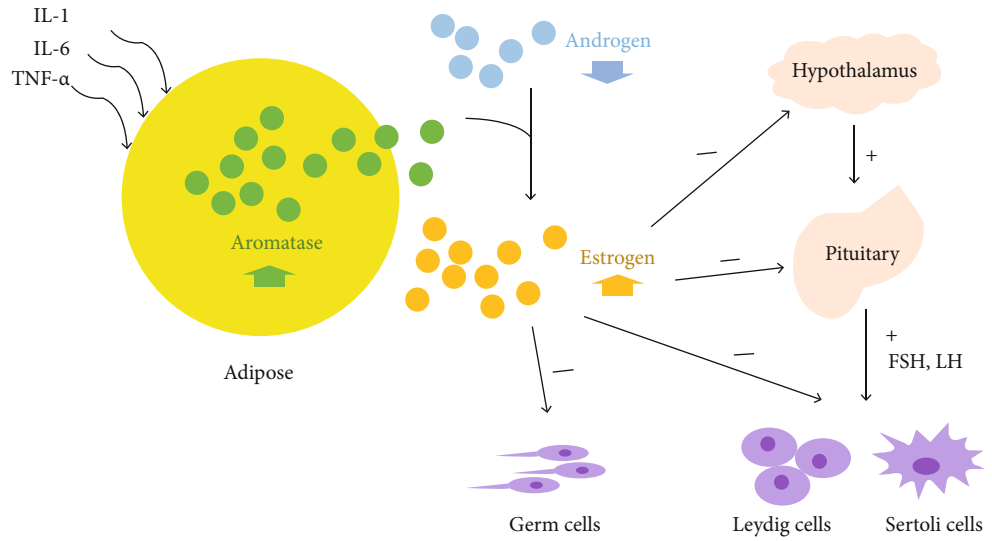

Figure 3: Effect of aromatase axis disorder on spermatogenic system. During inflammation, the secretion of proinflammatory factors such as IL-1, IL-6, and TNF-α increases the expression of aromatase in adipose tissue. The high expression of aromatase makes androgens irreversibly converted into estrogens, breaking the balance between male and female hormones. That is, the body androgen level drops and the estrogen level rises. Therefore, on the one hand, it can directly regulate the testicular stromal cells so that spermatogenesis cannot proceed normally. On the other hand, the HPG axis is inhibited by inhibiting the release of FSH and LH as well as Leydig and Sertoli cells, thus hindering the process of spermatogenesis.

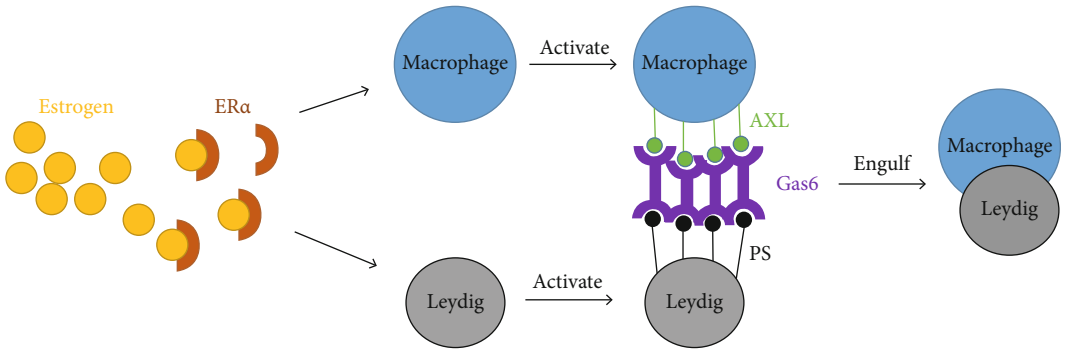

Figure 4: Mechanism of the estrogen-induced phagocytosis of Leydig cells by macrophages. Estrogen acts on macrophages and Leydig cells through estrogen receptor ER. In Leydig cells, estrogen activates its cell surface overexpression of phospholipid amino acid, PS, and growth specificity gene 6, Gas6. Through the Gas6, the PS molecules bind to AXL, one of the TAM receptor tyrosine kinase subfamily, which are overexpressed by macrophages after the estrogen stimulation. Namely, the PS molecules are an "eat me" signal to attract the macrophage cell to engulf the Leydig cells.

One is macrophage ED1$^+$ that moves from the peripheral blood to testicular tissue. This type of macrophage increases during chronic inflammation of the testis. The other is macrophage ED2$^+$, which is testis tissue-resident. It is less active and produces lower levels of inflammatory factors than the peritoneal macrophages. Under physiological conditions, the macrophages in testis can express IL-1, IL-6, TNF-α, and other major inflammatory factors, regulating the function of the testis.

In the male reproductive system, Leydig cells are important sites for aromatase to realize its biological activity. In animal experiments and clinical patients, we can find that when aromatase is overexpressed, excess estrogen causes macrophage activation in Leydig cells, which in turn are devoured by adjacent macrophages. This results in damage to the blood-testosterone barrier in the end. Apparently, it will adversely affect spermatogenesis and storage, thereby impairing male fertility [39, 40].

In addition, studies have shown an increase in the number of macrophages in azoospermia patients. Overexpression of aromatase and high levels of estrogen in testis activate the testis macrophages. At the same time, the Leydig cells are also activated and release specific molecules, making macrophages through the AXL-Gas6-PS pathway engulf the Leydig cells. Again, it will damage the blood-testosterone barrier and induce male sterility. The mechanism of the estrogen-induced "eat me" signaling in Leydig cells is illustrated below (Figure 4).

5. Prospects

In conclusion, the obesity-inflammation-aromatase axis severely impairs male fertility and causes male infertility. Although some studies have found that the intervention of EGCG and TGR5 can improve the body's inflammatory state to a certain extent, thereby improving infertility, we should realize that obesity not only leads to male infertility from this aspect of the "obesity-inflammation-aromatase axis" but also causes male infertility from obesity-induced leptin resistance and oxidative stress damage, etc. [4, 41]. In addition, we should be aware that male infertility is not caused solely by obesity and, where necessary, consider obesity as a common or synergistic factor in infertility, as well as other etiological factors.

Abbreviations

AI: Aromatase inhibitor
ATMs: Adipose tissue macrophage
cAMP: Cyclic adenosine monophosphate
CLSs: Crown-like structures
CoA: Coenzyme A
CRE: Cyclic adenosine monophosphate- (cAMP-) response element
CREB: CRE binding protein
CYP: Cytochrome P450 proteins
EGCG: Epigallocatechin-3-gallate
ER: Estrogen receptor
GLUT1: Glucose transporter-1
HIF-1α: Hypoxia inducible factor-1α
HO-1: Heme oxygenase-1
IR: Insulin resistance
ICAM: Intercellular adhesion molecule
LPS: Lipopolysaccharide
PDK1: Pyruvate dehydrogenase kinase-1
PGT: Prostaglandin transporter
PKA: Protein kinase A
PPARγ: Peroxisome proliferator-activated receptor γ
ROS: Reactive oxygen species
TBP: TATA binding protein
TGR5: G protein coupled bile acid receptor 5
TLR4: Toll-like receptor 4
VCAM-1: Vascular cell adhesion molecule-1
VEGF: Vascular endothelial growth factor.

Conflicts of Interest

The authors have no competing interests to declare.

Authors' Contributions

Liu Yuxin and Lin Chen contributed equally to this work.

Acknowledgments

This work was supported by the National Nature Science Foundation of China (No. 81871293), Undergraduate Innovation and Entrepreneurship Training Program (1020-11000501), Xiamen Medical and Health Guidance Project (No. 3502Z20209267), and Youth Fund of Fujian Provincial Department of Health (2019-1-41 and 2019-1-46).

References

[1] M. O. Strasser and J. M. Dupree, "Care delivery for male infertility: the present and future," *The Urologic Clinics of North America*, vol. 47, no. 2, pp. 193–204, 2020.

[2] Y. Liu and Z. Ding, "Obesity, a serious etiologic factor for male subfertility in modern society," *Reproduction*, vol. 154, no. 4, pp. R123–R131, 2017.

[3] W. N. Li, M. M. Jia, Y. Q. Peng, R. Ding, L. Q. Fan, and G. Liu, "Semen quality pattern and age threshold: a retrospective cross-sectional study of 71,623 infertile men in China, between 2011 and 2017," *Reproductive Biology and Endocrinology*, vol. 17, no. 1, p. 107, 2019.

[4] D. F. Carrageta, P. F. Oliveira, M. G. Alves, and M. P. Monteiro, "Obesity and male hypogonadism: tales of a vicious cycle," *Obesity Reviews*, vol. 20, no. 8, pp. 1148–1158, 2019.

[5] Y.-J. Won, B.-k. Kim, Y.-K. Shin et al., "Pectinase-treated Panax ginseng extract (GINST) rescues testicular dysfunction in aged rats via redox-modulating proteins," *Experimental Gerontology*, vol. 53, pp. 57–66, 2014.

[6] S. Tanrıkulu-Küçük, C. Başaran-Küçükgergin, M. Seyithanoğlu et al., "Effect of dietary curcumin and capsaicin on testicular and hepatic oxidant - antioxidant status in rats fed a high-fat diet," *Applied Physiology, Nutrition, and Metabolism*, vol. 44, no. 7, pp. 774–782, 2019.

[7] Y. F. Jia, Q. Feng, Z. Y. Ge et al., "Obesity impairs male fertility through long-term effects on spermatogenesis," *BMC Urology*, vol. 18, no. 1, p. 42, 2018.

[8] C. Li, M. M. Xu, K. Wang, A. J. Adler, A. T. Vella, and B. Zhou, "Macrophage polarization and meta-inflammation," *Translational Research*, vol. 191, pp. 29–44, 2018.

[9] B. F. Zamarron, T. A. Mergian, K. W. Cho et al., "Macrophage proliferation sustains adipose tissue inflammation in formerly obese mice," *Diabetes*, vol. 66, pp. 392–406, 2016.

[10] L. Mao, D. Hochstetter, L. Yao et al., "Green tea polyphenol (−)-epigallocatechin gallate (EGCG) attenuates neuroinflammation in palmitic acid-stimulated BV-2 microglia and high-fat diet-induced obese mice," *International Journal of Molecular Sciences*, vol. 20, no. 20, p. 5081, 2019.

[11] Y. Y. Jing, F. Wu, D. Li, L. Yang, Q. Li, and R. Li, "Metformin improves obesity-associated inflammation by altering macrophages polarization," *Molecular and Cellular Endocrinology*, vol. 461, pp. 256–264, 2018.

[12] H. L. Caslin, M. Bhanot, W. R. Bolus, and A. H. Hasty, "Adipose tissue macrophages: unique polarization and bioenergetics in obesity," *Immunological Reviews*, vol. 295, no. 1, pp. 101–113, 2020.

[13] D. Z. Chen, H. J. Zhao, X. Gao et al., "Subcutaneous administration of α-GalCer activates iNKT10 cells to promote M2 macrophage polarization and ameliorates chronic inflammation of obese adipose tissue," *International Immunopharmacology*, vol. 77, p. 105948, 2019.

[14] Y. J. Baek, M. N. Lee, D. Y. Wu, and M. Pae, "Luteolin reduces adipose tissue macrophage inflammation and insulin resistance in postmenopausal obese mice," *The Journal of Nutritional Biochemistry*, vol. 71, pp. 72–81, 2019.

[15] A. Engin, "Adipose tissue hypoxia in obesity and its impact on preadipocytes and macrophages: hypoxia hypothesis,"

Advances in Experimental Medicine and Biology, vol. 960, pp. 305–326, 2017.

[16] P. Trayhurn, "Hypoxia and adipose tissue function and dysfunction in obesity," *Physiological Reviews*, vol. 93, no. 1, pp. 1–21, 2013.

[17] Z. Zhang, T. Zhang, R. Feng, H. Huang, T. Xia, and C. Sun, "circARF3 Alleviates Mitophagy-Mediated Inflammation by Targeting miR-103/TRAF3 in Mouse Adipose Tissue," *Molecular Therapy - Nucleic Acids*, vol. 14, pp. 192–203, 2019.

[18] L. K. Heilbronn and L. V. Campbell, "Adipose tissue macrophages, low grade inflammation and insulin resistance in human obesity," *Current Pharmaceutical Design*, vol. 14, no. 12, pp. 1225–1230, 2008.

[19] M. Demura, S. Reierstad, J. E. Innes, and S. E. Bulun, "Novel promoter I.8 and promoter usage in the CYP19 (aromatase) gene," *Reproductive Sciences*, vol. 15, no. 10, pp. 1044–1053, 2008.

[20] S. Zhang, Q. Chen, X. Lin, M. Chen, and Q. Liu, "A review of adropin as the medium of dialogue between energy regulation and immune regulation," *Oxidative Medicine and Cellular Longevity*, vol. 2020, Article ID 3947806, 7 pages, 2020.

[21] M. Shozu, K. Murakami, and M. Inoue, "Aromatase and leiomyoma of the uterus," *Seminars in Reproductive Medicine*, vol. 22, no. 1, pp. 51–60, 2004.

[22] J. Frasor, J. M. Danes, B. Komm, K. C. N. Chang, C. R. Lyttle, and B. S. Katzenellenbogen, "Profiling of estrogen up- and down-regulated gene expression in human breast cancer cells: insights into gene networks and pathways underlying estrogenic control of proliferation and cell phenotype," *Endocrinology*, vol. 144, no. 10, pp. 4562–4574, 2003.

[23] B. R. Winters and T. J. Walsh, "The epidemiology of male infertility," *The Urologic Clinics of North America*, vol. 41, no. 1, pp. 195–204, 2014.

[24] J. T. Sanderson, "The steroid hormone biosynthesis pathway as a target for endocrine-disrupting chemicals," *Toxicological Sciences*, vol. 94, no. 1, pp. 3–21, 2006.

[25] X. Xu, M. Sun, J. Ye et al., "The effect of aromatase on the reproductive function of obese males," *Hormone and Metabolic Research*, vol. 49, no. 8, pp. 572–579, 2017.

[26] B. C. Lee and J. Lee, "Cellular and molecular players in adipose tissue inflammation in the development of obesity-induced insulin resistance," *Biochimica et Biophysica Acta (BBA) - Molecular Basis of Disease*, vol. 1842, no. 3, pp. 446–462, 2014.

[27] A. M. Cardoso, M. G. Alves, P. P. Mathur, P. F. Oliveira, J. E. Cavaco, and L. Rato, "Obesogens and male fertility," *Obesity Reviews*, vol. 18, no. 1, pp. 109–125, 2017.

[28] K. Zhu, S. Li, J. S. Liu, Y. Hong, Z. J. Chen, and Y. du, "Role of RAB5A in FSHR-mediated signal transduction in human granulosa cells," *Reproduction*, vol. 155, no. 6, pp. 505–514, 2018.

[29] M. Xie, M. L. Li, J. Zhou et al., "Brain-derived neurotrophic factor promotes human granulosa-like tumor cell steroidogenesis and proliferation by activating the FSH receptor-mediated signaling pathway," *Scientific Reports*, vol. 7, no. 1, p. 180, 2017.

[30] K. Subbaramaiah, C. A. Hudis, and A. J. Dannenberg, "The prostaglandin transporter regulates adipogenesis and aromatase transcription," *Cancer Prevention Research*, vol. 4, no. 2, pp. 194–206, 2011.

[31] Z. Yang, M. Z. Zhu, Y. B. Zhang et al., "Coadministration of epigallocatechin-3-gallate (EGCG) and caffeine in low dose ameliorates obesity and nonalcoholic fatty liver disease in obese rats," *Phytotherapy Research*, vol. 33, no. 4, pp. 1019–1026, 2019.

[32] S. Bao, Y. Cao, C. Fan et al., "Epigallocatechin gallate improves insulin signaling by decreasing toll-like receptor 4 (TLR4) activity in adipose tissues of high-fat diet rats," *Molecular Nutrition & Food Research*, vol. 58, no. 4, pp. 677–686, 2014.

[33] R. Wu, Y. Yao, Q. Jiang et al., "Epigallocatechin gallate targets FTO and inhibits adipogenesis in an mRNA m^6A-YTHDF2-dependent manner," *International Journal of Obesity*, vol. 42, no. 7, pp. 1378–1388, 2018.

[34] E. Hassan, K. Kahilo, T. Kamal, M. Hassan, and M. Saleh Elgawish, "The protective effect of epigallocatechin-3-gallate on testicular oxidative stress in lead-induced toxicity mediated by Cyp19 gene/estradiol level," *Toxicology*, vol. 422, pp. 76–83, 2019.

[35] B. Grygiel-Górniak, "Peroxisome proliferator-activated receptors and their ligands: nutritional and clinical implications–a review," *Nutrition Journal*, vol. 13, no. 1, p. 17, 2014.

[36] A. Z. Mirza, I. I. Althagafi, and H. Shamshad, "Role of PPAR receptor in different diseases and their ligands: physiological importance and clinical implications," *European Journal of Medicinal Chemistry*, vol. 166, pp. 502–513, 2019.

[37] G. Wang, S. Cheng, S. Zhang, Y. Zhu, Y. Xiao, and L. Ju, "LPS impairs steroidogenesis and ROS metabolism and induces PPAR transcriptional activity to disturb estrogen/androgen receptor expression in testicular cells," *Molecular Biology Reports*, vol. 47, no. 2, pp. 1045–1056, 2020.

[38] M. Verderame, V. Migliaccio, and R. Scudiero, "Role of estrogen receptors, P450 aromatase, PCNA and p53 in high-fat-induced impairment of spermatogenesis in rats," *Comptes Rendus Biologies*, vol. 341, no. 7-8, pp. 371–379, 2018.

[39] M. C. Lardone, F. Argandoña, M. Flórez et al., "Overexpression of CYP19A1 aromatase in Leydig cells is associated with steroidogenic dysfunction in subjects with Sertoli cell-only syndrome," *Andrology*, vol. 5, no. 1, pp. 41–48, 2017.

[40] X. Li, H. Li, L. Jia, X. Li, and N. Rahman, "Oestrogen action and male fertility: experimental and clinical findings," *Cellular and Molecular Life Sciences*, vol. 72, no. 20, pp. 3915–3930, 2015.

[41] N. M. Lainez and D. Coss, "Obesity, neuroinflammation, and reproductive function," *Endocrinology*, vol. 160, no. 11, pp. 2719–2736, 2019.